University of Florida
Civil and Coastal Engineering

UF

University of Florida
Civil and Coastal Engineering

Final Report **June 2013**

Key Royale Bridge Five Year Evaluation

Principal investigator:
H. R. Hamilton

Research assistants:
James McCall
Yen-Chih Tsai
Stefan Szyniszewski
Edward Roske
Chris Ferraro

Department of Civil and Coastal Engineering
University of Florida
P.O. Box 116580
Gainesville, Florida 32611

Sponsor:
Florida Department of Transportation (FDOT)
Michael Bergin–Project Manager

Contract:
UF Project No. 00094203
FDOT Contract No. BDK75 977-52

Disclaimer

The opinions, findings, and conclusions expressed in this publication are those of the authors and not necessarily those of the State of Florida Department of Transportation.

SI* (MODERN METRIC) CONVERSION FACTORS

*APPROXIMATE CONVERSIONS **TO** SI UNITS*

SYMBOL	WHEN YOU KNOW	MULTIPLY BY	TO FIND	SYMBOL
LENGTH				
in	inches	25.4	millimeters	mm
ft	feet	0.305	meters	m
yd	yards	0.914	meters	m
mi	miles	1.61	kilometers	km
AREA				
in^2	square inches	645.2	square millimeters	mm^2
ft^2	square feet	0.093	square meters	m^2
yd^2	square yard	0.836	square meters	m^2
ac	acres	0.405	hectares	ha
mi^2	square miles	2.59	square kilometers	km^2
VOLUME				
fl oz	fluid ounces	29.57	milliliters	mL
gal	gallons	3.785	liters	L
ft^3	cubic feet	0.028	cubic meters	m^3
yd^3	cubic yards	0.765	cubic meters	m^3
NOTE: volumes greater than 1000 L shall be shown in m^3				
MASS				
oz	ounces	28.35	grams	g
lb	pounds	0.454	kilograms	kg
T	short tons (2000 lb)	0.907	megagrams	Mg (or "t")
TEMPERATURE (exact degrees)				
^oF	Fahrenheit	5(F-32)/9 or (F-32)/1.8	Celsius	^oC
ILLUMINATION				
fc	foot-candles	10.76	lux	lx
fl	foot-Lamberts	3.426	candela/m^2	cd/m^2
FORCE and PRESSURE or STRESS				
kip	1000 pound force	4.45	kilonewtons	kN
lbf	pound force	4.45	newtons	N
lbf/in^2	pound force per square	6.89	kilopascals	kPa

*SI is the symbol for the International System of Units. Appropriate rounding should be made to comply with Section 4 of ASTM E380.

SI* (MODERN METRIC) CONVERSION FACTORS

*APPROXIMATE CONVERSIONS **FROM** SI UNITS*

SYMBOL	WHEN YOU KNOW	MULTIPLY BY	TO FIND	SYMBOL
LENGTH				
mm	millimeters	0.039	inches	in
m	meters	3.28	feet	ft
m	meters	1.09	yards	yd
km	kilometers	0.621	miles	mi
AREA				
mm^2	square millimeters	0.0016	square inches	in^2
m^2	square meters	10.764	square feet	ft^2
m^2	square meters	1.195	square yards	yd^2
ha	hectares	2.47	acres	ac
km^2	square kilometers	0.386	square miles	mi^2
VOLUME				
mL	milliliters	0.034	fluid ounces	fl oz
L	liters	0.264	gallons	gal
m^3	cubic meters	35.314	cubic feet	ft^3
m^3	cubic meters	1.307	cubic yards	yd^3
MASS				
g	grams	0.035	ounces	oz
kg	kilograms	2.202	pounds	lb
Mg (or "t")	megagrams (or "metric	1.103	short tons (2000 lb)	T
TEMPERATURE (exact degrees)				
^oC	Celsius	1.8C+32	Fahrenheit	^oF
ILLUMINATION				
lx	lux	0.0929	foot-candles	fc
cd/m^2	candela/m^2	0.2919	foot-Lamberts	fl
FORCE and PRESSURE or STRESS				
kN	kilonewtons	0.225	1000 pound force	kip
N	newtons	0.225	pound force	lbf
kPa	kilopascals	0.145	pound force per square inch	lbf/in^2

*SI is the symbol for the International System of Units. Appropriate rounding should be made to comply with Section 4 of ASTM E380.

Technical Report Documentation Page

1. Report No.	2. Government Accession No.	3. Recipient's Catalog No.

4. Title and Subtitle	5. Report Date
Key Royale Bridge Five Year Evaluation	June 2013
	6. Performing Organization Code

7. Author(s)	8. Performing Organization Report No.
McCall, J., Tsai, Y. C, Szyniszewski, S., Roske, E., Ferraro, C., and Hamilton, H. R.	00094203

9. Performing Organization Name and Address	10. Work Unit No. (TRAIS)
University of Florida Department of Civil & Coastal Engineering P.O. Box 116580 Gainesville, FL 32611-6580	11. Contract or Grant No. BDK75 977-52

12. Sponsoring Agency Name and Address	13. Type of Report and Period Covered
Florida Department of Transportation Research Management Center 605 Suwannee Street, MS 30 Tallahassee, FL 32301-8064	Final Report
	14. Sponsoring Agency Code

15. Supplementary Notes

16. Abstract

This report describes the design, construction, instrumentation, and five-year evaluation of the Key Royale Bridge substructure. The primary focus was the evaluation of the implementation of highly reactive supplementary cementitious materials (SCM) into the construction of the bridge piles. Four different SCM were used to create six different concrete mixtures; these were then used to construct the bridge and fender piles. This allowed monitoring under realistic exposure conditions in real time rather than performing accelerated corrosion testing in laboratory conditions. Corrosion sensors were embedded in the bridge piles for periodic monitoring; five years after placement, none of the remaining operable sensors indicated the presence of corrosion. Removable fender piles were also installed with the same mixtures as were used on the bridge piles and will be removed after 15-20 years of seawater exposure to be examined for ingress of chlorides and corrosion damage. Coring was performed on the fender piles to evaluate chloride ingress after 5 years of exposure. In addition, durability segments were constructed using the same concrete and prestressing strand as the fender piles. These segments were hung from the fender piles for consistent exposure conditions and instrumented with corrosion sensors and temperature sensors for long-term corrosion monitoring, although none of the remaining operable sensors indicate the presence of corrosion. These segments will be cored in the future for evaluating the chloride ion penetration and concrete hydration over time.

Data gathered during the five years since the bridge was erected indicate that corrosion has not yet initiated in either bridge or fender piles. Electrical measurements were taken at selected intervals to assess the condition of the prestressing steel in the piles. Half-cell potential measurements of the pile prestressing steel were taken using a copper copper-sulfate reference electrode and indicated a very low probability that corrosion was occurring in the prestressing steel. As noted previously, embedded sensors in the bridge and fender piles provided no indication of corrosion activity.

17. Key Word	18. Distribution Statement
corrosion sensors, pozzolans, durability, piles, supplementary cementitious materials, corrosion potential	No restrictions. This document is available to the public through the National Technical Information Service, Springfield, VA, 22161

19. Security Classif. (of this report)	20. Security Classif. (of this page)	21. No. of Pages	22. Price
Unclassified	Unclassified	309	

Form DOT F 1700.7 (8-72) Reproduction of completed page authorized

Acknowledgments

The authors would like to acknowledge the Federal Highway Administration Innovative Bridge Research and Construction Program for providing funding for this project. The authors would also like to express their gratitude to FDOT District Two, Cone and Graham, Dura-Stress Inc., Smart Structures Inc., and all the SCM suppliers, Civil & Marine, Inc., Boral Material Technologies, Micron 3, Inc., Grace, and Burgess Pigment Co., for their time and effort to make this research successful.

Authors would like to thank Ivan Lasa, Mario Paredes, Dennis Baldi, Ron Simmons, Jason Burchfield, Matthew Duncan, Richard Nalli III, Elizabeth Miller, and Richard DeLorenzo from the Florida Department of Transportation for their assistance and knowledge on taking corrosion readings and laboratory testing. We would also like to acknowledge the graduate students, undergraduate students, and faculty from the University of Florida for the contribution of their time and knowledge in the laboratory and in the field. They include Chuck Broward, Robert Gomez, Gustavo Llanos, Nathan Van Etten, Abraham Alende, and Enrique Vivas.

Executive Summary

This report describes the design, construction, instrumentation, and five-year evaluation of the Key Royale Bridge substructure. The primary focus was the evaluation of the implementation of highly reactive supplementary cementitious materials (SCM) into the construction of bridge piles. Four different SCM were used to create six different concrete mixtures; these were then used to construct the bridge and fender piles. This allowed monitoring under realistic exposure conditions in real time rather than performing accelerated corrosion testing in laboratory conditions. Corrosion sensors were embedded in the bridge piles for periodic monitoring; five years after placement, none of the remaining operable sensors indicated the presence of corrosion. Removable fender piles were also installed with the same mixtures and will be removed after 15-20 years of seawater exposure to be examined for ingress of chlorides and corrosion damage. Coring was performed on the fender piles to evaluate chloride ingress after 5 years of exposure. In addition, durability segments were constructed using the same concrete and prestressing strand as the fender piles. These segments were hung from the fender piles for consistent exposure conditions and instrumented with corrosion sensors and temperature sensors for long-term corrosion monitoring, although none of the remaining operable sensors indicate the presence of corrosion. These segments will be cored in the future for evaluating the chloride ion penetration and concrete hydration over time.

Data gathered during the five years since the bridge was erected indicate that corrosion has not yet initiated in either bridge or fender piles. Electrical measurements were taken at selected intervals to assess the condition of the prestressing steel in the piles. Half-cell potential measurements of the pile prestressing steel were taken using a copper copper-sulfate reference electrode and indicated a very low probability that corrosion was occurring in the prestressing steel. As noted previously, embedded sensors in the bridge and fender piles provided no indication of corrosion activity.

Table of Contents

Disclaimer ii

Acknowledgments vi

Executive Summary vii

List of Figures x

List of Tables xiii

1 Introduction 14

2 Literature Review 15
- 2.1 Corrosion Overview 15
- 2.2 Corrosion Mechanism 16
- 2.3 Mechanisms of Chloride Penetration 18
- 2.4 Environmental Effects on Chloride Penetration 20
- 2.5 Tests for Evaluating Durability 21
- 2.6 Effect of Cement and SCM on Concrete Properties 36
- 2.7 Effects of Ternary Blends on Concrete Performance 52

3 Project Chronology 63

4 Structure Description 65

5 Concrete Mixture Designs 70

6 Pile Design and Construction 74
- 6.1 Design 74
- 6.2 Pile Production and Material Sampling 75
- 6.3 Curing, Prestress Transfer, and Transportation 77
- 6.4 Sampling 80
- 6.5 Pile Installation 86

7 Pile Instrumentation 89
- 7.1 Overview 89
- 7.2 Corrosion Sensors 89
- 7.3 Covermeter 92

8 Durability Segment 93
- 8.1 Design and Construction 94
- 8.2 Corrosion Instrumentation 97
- 8.3 Temperature Instrumentation 99

9 Corrosion Potential 100
- 9.1 Measurement of Corrosion Potentials in Prestressing Strand 100
- 9.2 Corrosion Potential of Pile Electrodes 107
- 9.3 Corrosion Potential of Durability Segment Electrodes 115
- 9.4 Evaluation of Internal Electrode Function 125
- 9.5 Electrical Current Measurement 130

10 Surface Resistivity 134

11 Chloride Diffusion 137
- 11.1 Selection of Coring Locations 137

11.2 Results of chloride analysis 137
12 Summary and Conclusions 143
13 Future Inspection Plan 144
14 References 146
Appendix A–Pile Construction 155
Appendix B–Material Testing Data 193
Appendix C–Durability Segment 215
Appendix D–Covermeter Data 218
Appendix E–Bridge Pile Corrosion Data 230
Appendix F–Durability Segment Corrosion Data 249
Appendix G–Chloride Profile Data 253
Appendix H–Application of Epoxy Protection at Fender Pile Coring Site 274
Appendix I–Long-Term Monitoring Plan for Key Royale Bridge 278
Appendix J–Key Royale Bridge Inspection Report 292

List of Figures

Figure 1–Service life model for concrete in a corrosive environment 16
Figure 2–Chloride exposure zones of a typical bridge substructure 20
Figure 3–Wenner linear four-probe array and display 22
Figure 4–Four-point Wenner probe test setup 23
Figure 5–Half-cell potential map of the four faces of a Turtle River Bridge pile (Moser et al., 2010) 30
Figure 6–Overlay of damage profile on half-cell potential map for beam MS3 (Naito et al., 2010) 31
Figure 7–Probability of corrosion for prestressing steels based on half-cell potential 31
Figure 8–Compilation of the average corrosion potential of tested piles (Cannon et al., 2006) 32
Figure 9–Correlation of half-cell potential and chloride level 35
Figure 10–Key Royale Drive Bridge was selected for this project. 66
Figure 11–Bridge foundation plan showing bridge and fender pile layout 67
Figure 12–Cross-section of bridge during the phase I construction on August 2006 67
Figure 13–Cross-section of bridge during the phase I construction on August 2006 68
Figure 14–Cross-section of bridge during the phase II construction on December 2006 68
Figure 15–Cross-section of completed bridge on May 2007 69
Figure 16–Spiral ties spacing for 18-in. and 24-in. piles 74
Figure 17–Cross-section of 24-in. square piles 75
Figure 18–Cross-section of 18-in. square piles 75
Figure 19–18-in. fender pile with stressed prestressed strands in place 76
Figure 20–Pile casting at precast yard 77
Figure 21–Lifting loops were inserted into the fresh concrete after screeding 77
Figure 22–Moist curing at precast yard 78
Figure 23–Flame cutting of lifting loop after the pile was removed from the casting bed. 79
Figure 24–An epoxy was applied to the area for corrosion protection. 79
Figure 25–Pilgrim EM 5-2 epoxy was used to provide corrosion protection. 80
Figure 26–Molded cylinders and beams were used to sample the concrete from each representative mixture 81
Figure 27–Sample segment with debonded strands from which cores were taken (a) side view (b) top view 81
Figure 28–Compressive strength of all mixtures at 28, 91, and 365 days 83
Figure 29–Surface resistivity of all mixtures at 28, 91, and 365 days 85
Figure 30–RMT of all mixtures at 56, 91, and 182 days 86
Figure 31–Pile installation for piles in bents 3 and 4 (not to scale) 87
Figure 32–Pile driving 87
Figure 33–Pile being lifted into position for driving 88
Figure 34–Location of corrosion sensors 90
Figure 35–#3 steel electrode with 2-in. length of the electrode exposed 90
Figure 36–¼ -in. diameter titanium electrode with 2-in. length of the electrode exposed 91
Figure 37–Wired corrosion sensors (top-titanium, bottom-steel) 91
Figure 38–Protection of the wires in the electrical box 91
Figure 39–Cross-sectional view of 24-in. pile with strand nomenclature and layout 92
Figure 40–Durability segment after installation on the pile 93
Figure 41–Durability segments were attached to the fender piles 94
Figure 42–Durability segment and sample segment construction 95
Figure 43–Sample segment and durability segment were divided by a plywood sheet 95
Figure 44–Sample segment and durability segments after concrete had been poured 95
Figure 45–Sample segment and durability segment with prestressing strands exposed 96
Figure 46–Concrete and prestressing strands were chipped and cut below the concrete surface. 97

Figure 47–The top of durability segment after application of epoxy to protect strands 97
Figure 48–Instrumentation in the durability segment 98
Figure 49–Cross-sectional view of durability segment with instrumentation..... 99
Figure 50–Thermocouples grip system..... 99
Figure 51–Fluke 85 series III digital multimeter was used to take corrosion readings 101
Figure 52–Copper copper-sulfate reference electrode showing method to provide electrical conductivity between external electrode and concrete..... 101
Figure 53–External electrode ready to use on the concrete surface..... 102
Figure 54–Surface resistivity and external potentials measuring locations (see Table 21 for "A" dimensions) 105
Figure 55–The orientation of pile surface upon which potential readings were taken 105
Figure 56–Typical plot of pile prestressing steel half-cell potentials (UFA)..... 106
Figure 57–Location of electrical measurements along pile face..... 106
Figure 58–Creation of normalized and averaged prestress half-cell potentials for each SCM and each measurement date..... 107
Figure 59–Change in normalized and averaged prestress half-cell potentials 107
Figure 60–The orientation of box and electrodes for each mixture 108
Figure 61–Location of corrosion probes relative to the bottom of pile cap in the 24-in. piles..... 109
Figure 62–Mapping of electrodes and wires in the electrical box by color of wire and inlets 110
Figure 63–Surface electrode contact location when measuring the external corrosion potential of each individual electrode..... 110
Figure 64–Half-cell potentials of layer 1 steel electrodes for bents 3 (a) and 4 (b) for each pile type..... 112
Figure 65–Half-cell potentials of layer 2 steel electrodes for bents 3 (a) and 4 (b) for each pile type..... 112
Figure 66–Half-cell potentials of layer 1 titanium electrodes for bents 3 (a) and 4 (b) for each pile type113
Figure 67–Half-cell potentials of layer 2 titanium electrodes for bents 3 (a) and 4 (b) for each pile type113
Figure 68–Potential difference between layer 1 titanium and steel electrodes for instrumented piles in bents (a)3 and (b)4..... 114
Figure 69–Potential difference between layer 2 titanium and steel electrodes for instrumented piles in bents (a)3 and (b)4..... 115
Figure 70–Two short wires were used to connect the steel electrodes 116
Figure 71–Durability segment attachment locations relative to fender piles..... 116
Figure 72–Location and mapping of wires and electrodes in the durability segments 117
Figure 73–Potential readings–external electrode contact locations (see Table 27 for dimension "A")... 118
Figure 74–Half-cell potentials of layer 1 steel electrodes..... 120
Figure 75–Half-cell potentials of layer 2 steel electrodes..... 120
Figure 76–Half-cell potentials of layer 2 steel electrodes with the CSE dipped in seawater..... 121
Figure 77–Half-cell potentials of layer 3 steel electrodes..... 121
Figure 78–Half-cell potentials of layer 3 steel electrodes with the CSE dipped in seawater..... 122
Figure 79–Half-cell potentials of layer 1 titanium electrodes..... 122
Figure 80–Half-cell potentials of layer 2 titanium electrodes..... 123
Figure 81–Half-cell potentials of layer 3 titanium electrodes..... 123
Figure 82–Potential difference between layer 1 titanium and steel electrodes for durability segments... 124
Figure 83–Potential difference between layer 2 titanium and steel electrodes for durability segments... 125
Figure 84–Potential difference between layer 3 titanium and steel electrodes for durability segments... 125
Figure 85–Electrical resistance was measured using Nilsson model 400 soil resistance meter 127
Figure 86–Resistance between S1 and S2 electrodes for (a) bent 3 piles (b) bent 4 piles..... 127
Figure 87–Resistance between S1 and T1 electrodes for (a) bent 3 piles (b) bent 4 piles..... 128
Figure 88–Resistance between S2 and T2 electrodes for (a) bent 3 piles (b) bent 4 piles..... 128
Figure 89–Resistance between durability segment electrodes (a) S1 and S2 (b) S1 and S3 129
Figure 90–Resistance between durability segment electrodes (a) S2 and S3 (b) S1 and T1 129
Figure 91–Resistance between durability segment electrodes (a) S2 and T2 (b) S3 and T3 130

Figure 92–Electrical current flow between S1 and S2 electrodes in bent 3 and bent 4 piles..... 131
Figure 93–Electrical current flow between S1 and S2 electrodes in durability segments 132
Figure 94–Electrical current flow between S1 and S3 electrodes in durability segments 132
Figure 95–Electrical current flow between S2 and S3 electrodes in durability segments 133
Figure 96–Wenner linear four-probe array and display 134
Figure 97–Surface resistivity readings were taken on the bridge piles. 135
Figure 98–Surface resistivity in bridge piles measured at increasing ages 136
Figure 99–Typical locations of 2-in. diameter cores taken from fender piles 137
Figure 100–Diffusion coefficients and coring locations 139
Figure 101–Coring locations and averaged measured chloride content at more than ¾" depth 139
Figure 102–Coring locations and average measured chloride content at more than ¾" depth (excluding CEM) 140

List of Tables

Table 1–Measured electrical resistivities of typical aggregates used for concrete (Monfore, 1968) 25
Table 2–Correlation between RCP and SR results 4-inch (102-mm) diameter by 8-inch (204-mm) concrete cylinders (Chini et al., 2003) 26
Table 3–Chloride diffusion coefficients from cores taken at Key Royale Bridge in 2008 (Presuel-Moreno 2010) 34
Table 4–Typical oxides and their shorthand notations 36
Table 5–Typical chemical compounds and their shorthand notations 37
Table 6–Typical chemical compositions and properties of ASTM Type I to V cements 38
Table 7–Cube strength of fly ash concrete normalized by control strength (Jones et al., 2006) 43
Table 8–Percent increase in compressive strength when fly ash is replaced by ultrafine fly ash 44
Table 9–Slag activity index (ASTM C 989) 44
Table 10–Summary of SCM effect on concrete properties 52
Table 11–Summary of ternary blend concrete mixture characteristics 62
Table 12–Timeline for Key Royale Bridge activity 64
Table 13–Mixture designs considered in preliminary laboratory testing 70
Table 14–Notation used to denote six mixtures used in bridge piles 72
Table 15–Construction phases and associated mixture designs to be implemented 72
Table 16–Mixture designs selected for use in CEM, UFA, and FA piles 72
Table 17–Mixture designs selected for use in SF, MET, and BFS piles 73
Table 18–Pile casting schedule 76
Table 19–Summary of number and types of samples taken from each mixture (18-in. fender pile) 81
Table 20–Summary of number and types of samples taken from each mixture (24-in. bridge pile) 82
Table 21–Summary of types of sample used in each test 82
Table 22–Modulus of rupture, compressive strength, and coefficient at 28 days 84
Table 23–Distance from MGL to bottom of pile cap (inches) 103
Table 24–“A” dimension for surface resistivity and external potential measurements (inches) 105
Table 25–Location of corrosion electrodes in 24-in. FA and UFA piles 109
Table 26–Location of corrosion electrodes in 24-in. SF, BFS, and MET piles 109
Table 27–External electrodes measuring locations (*See Figure 73 for details) 118
Table 28–Distance from top of durability segment to marine growth line and high tide mark (in) 118
Table 29–Diffusion coefficients for fender pile 1 (CEM) 140
Table 30–Diffusion coefficients for fender pile 2 (UFA) 140
Table 31–Diffusion coefficients for fender pile 3 (FA) 141
Table 32–Diffusion coefficients for fender pile 4 (SF) 141
Table 33–Diffusion coefficients for fender pile 5 (BFS) 141
Table 34–Diffusion coefficients for fender pile 6 (MET) 142

1 Introduction

To ensure the longest possible service life from bridges constructed in a marine environment, supplementary cementitious materials (SCM) are typically used for concrete piles placed in the splash zone of a marine environment. The splash zone is the vertical distance from 4 feet below mean low water (MLW) to 12 feet above mean high water (MHW). A number of new highly reactive SCM have been used in recent years to protect against the aggressive nature of the marine environment.

Innovative Bridge Research and Construction (IBRC) funding (project #FL-2004-01) was secured by the Florida Department of Transportation (FDOT) to aid in constructing and instrumenting a bridge in coastal waters that contained several of the relatively new highly reactive SCMs. Key Royale Drive Bridge in Sarasota, FL was selected as the test bed for the implementation of these SCM. This report documents the bridge construction process along with data from the initial evaluation and further evaluation at the 5-year mark following construction.

This report was written to be used for several purposes. First, the report describes the state-of-the-art theory and experimental research regarding corrosion in concrete. Properties and experimental results of concrete specimens containing varying levels of cement replacement with SCM are provided, as is a description of the process by which mixture designs and cement replacement levels were chosen for the Key Royale Bridge. The design of the embedded electrodes within the piles was experimental; observations contained within this document may be used to improve the design of these sensors for future projects. Concrete fender piles were used in the Key Royale Bridge that will be removed and tested in the future. Information in this report will be useful in evaluating the performance of these piles under destructive testing. Finally, the information contained within this report will be useful for the FDOT to evaluate guidelines regarding the use of SCM in extremely aggressive environments. This will lead to bridges that cost less to build and last longer.

2 Literature Review

2.1 Corrosion Overview

Corrosion results in significant maintenance and serviceability problems in highway bridges. The U.S. Federal Highway Administration (FHWA) released the results of a 2-year study in 2002 that concluded that the corrosion costs the U.S. $276 billion per year (Koch et al. 2006), or 3.1% of the Gross Domestic Product (GDP). This works out to be approximately $970 per person, based on census figures from July 1, 2001. The cost of weather-related disasters (hurricanes, tornadoes, tropical storms, floods, fires, droughts, and freezes), which receive much greater public attention, is about $17 billion. Corrosion in national infrastructure alone accounts for $22.6 billion in annual expenses. Measures that reduce this figure are of vital importance.

The state of Florida has a particular need to improve corrosion performance of infrastructure components. Florida has approximately 5,500 bridges in the FDOT inventory, of which two thirds are exposed to salt water (Sagüés 2001). The state has implemented a 75-year design service life, which is a substantial increase in the lifespan of many bridges. As an example, the Bryant Patton Bridge connecting St. George Island to the mainland had to be replaced after only 40 years in service. The cost of this replacement was $74 million (District 3 Update).

The concept of design service life has been proposed for new structures built by FDOT; this incorporates the expected length of time that a structure will remain in service. As summarized by Smith and Virmani (2000), the service life model for reinforced concrete structures has two stages – initiation and propagation. The initiation time is the length of time from construction until the onset of rapid corrosion. Once begun, corrosion proceeds in a manner controlled by corrosion process kinetics until cracking and spalling occur. Figure 1 is a graphical representation of the service life model.

Sohanghpurwala (2006) is a manual that establishes the state-of-the-art modeling for service life design. Three steps in developing this model as it applies to a specific structure have been proposed. First, the condition of reinforced concrete bridge structural elements subjected to corrosion-induced deterioration must be assessed. Second, the remaining service life of such elements must be predicted. Finally, the service life extension resulting from alternative maintenance and repair options must be quantified. The primary focus of the present research

project is to formulate a protocol for assessing the condition of the Key Royale Bridge, thus fulfilling part of the first step in developing a service life model.

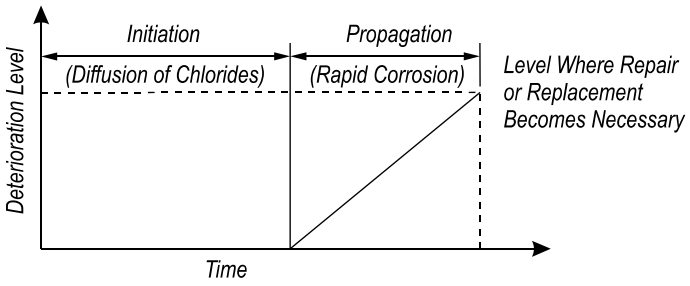

Figure 1–Service life model for concrete in a corrosive environment

2.2 Corrosion Mechanism

Corrosion of steel in concrete is an electrochemical process involving the transfer of electrons from one species to another (ACI 222R-01). This transfer process occurs in two half-cell reactions: the liberation of electrons from iron atoms in the reinforcing and the acceptance of electrons by oxygen or hydroxide molecules in solution. The most likely anodic (electron donating) half-cell reactions are given by Equation 1 through Equation 4.

$Fe \rightarrow Fe^{++} + 2e^{-}$ Equation 1

$2\,Fe^{++} + 4OH^{-} \rightarrow 2Fe(OH)_2$ Equation 2

$2Fe(OH)2 + 1/2O2 \rightarrow 2FeOOH + H2O$ Equation 3

$Fe + OH- + H2O \rightarrow HFeO2- + H2$ Equation 4

The most likely cathodic (electron accepting) half-cell reactions are given by Equation 5 and Equation 6.

$2H_2O + O_2 + 4e^{-} \rightarrow 4OH^{-}$ Equation 5

$2H^{+} + 2e^{-} \rightarrow H_2$ Equation 6

Investigating Equation 1 through Equation 6, the presence of water and oxygen is a requirement for corrosion to occur in steel but is not sufficient to drive the reaction. Concrete piles in water become saturated long before corrosion initiates and, especially in the tidal zone and the splash zone, oxygen is present. Despite this, corrosion does not occur immediately. The mechanism protecting steel from corrosion under these conditions is passivation, which is the presence of a film of iron oxide that builds up on the surface of steel in a solution with a sufficiently high hydroxide concentration. This layer, usually a single molecule thick, occupies potential reaction sites on the surface of the steel and reduces the rate of reaction to insignificant levels (ACI 222R-01). If the passive layer is disturbed, the corrosion rate increases exponentially. This occurs as iron atoms are exposed to the oxidizing effects of the solution without a protective cover to protect it. An increase in the reaction rate will cause section loss in either reinforcement or prestressing steel, reducing the load-carrying capacity of the member. Prevention of depassivation is a primary goal of corrosion prevention in reinforced and prestressed concrete.

Depassivation of the reinforcing steel leads directly to corrosion when water and oxygen are present. Two primary methods of depassivation include carbonation and chloride penetration. The passive layer depends upon a high pH in the pore solution, typically 13 to 13.5 in sound concrete (ACI 222R-01). Carbon dioxide may react with calcium hydroxide, reducing alkalinity. This loss of alkalinity leads to a reduction in pH of the pore solution, causing depassivation of reinforcing steel. Carbonation advances slowly in sound concrete, making it less of a factor in corrosion than chloride penetration. When chloride concentration reaches a certain point, reinforcement is depassivated and rapid corrosion may initiate. This concentration is referred to as the threshold chloride concentration.

Attempts to establish a threshold concentration of chloride to initiate corrosion have been stymied by the variability of this threshold due to atmospheric conditions, moisture content, oxygen concentration, pH, and the composition of the concrete (Smith and Virmani 2000). A general observation is that the concentration of chloride must be greater than 1.2 lb/yd^3 and the ratio of chloride ions to hydroxyl ions must be greater than 0.6.

Sagüés et al. (2001) undertook a study of 13 Florida bridges to improve corrosion forecasting models. The effect of small cracks (~0.15 mm) that sometimes extended to the waterline was studied. These cracks often extended to the depth of the reinforcing, although no

conspicuous corrosion was occurring. Substantial chloride penetration, however, was noted at these locations. The analysis predicts that even narrow cracks allow for chloride ingress, and that cracks that terminate a short distance from the surface may allow for even more severe chloride buildup than cracks that extend deep into the structure.

Sagüés et al. (2001) created a model for predicting the onset of corrosion in concrete. This model addresses the combined tidal and splash-evaporation zone, extending from the high tide level (HT) to 6 ft. above the high tide level (AHT), concentrating on the worst-case elevation within that range. The model included input options for sound or cracked concrete. For sound concrete, inputs include surface chloride concentration, the threshold chloride concentration, the concrete cover, the geometric condition (i.e. 2 or 3 way corners, flat face, rounded face, etc.), and reinforcement diameter. At locations where the crack extends to the reinforcing, the model conservatively estimates that the time to initiation is zero. The implication of this assumption is that transportation officials must design and implement repair procedures to repair local corrosion that may occur at cracks substantially earlier than would be predicted by other factors.

2.3 Mechanisms of Chloride Penetration

Stanish et al. (1997) summarize the mechanisms of chloride ion transport as capillary absorption, permeation by hydrostatic pressure, and diffusion. Diffusion is the movement of chloride ions under a concentration gradient, requiring a continuous liquid phase and a chloride ion concentration gradient. Permeation is the penetration of water containing chloride ions caused by a hydraulic head applied to one surface of a concrete structure. Permeation is uncommon in highway structures as it relies upon a hydraulic head. Absorption occurs due to wetting and drying cycles. When water containing chloride ions contacts dry concrete, capillary suction brings the water into the structure. The chloride ions are deposited when the structure dries again. Since the depth of concrete subject to this wet-dry cycle is limited, absorption will not cause chloride ions to reach the depth of the reinforcing except in the case of poor concrete quality with shallow reinforcement.

It is generally agreed that diffusion is the most important transport mechanism that can cause chlorides to penetrate concrete to the depth of the reinforcing (Stanish et al. 1997, Costa and Appleton 1998, Smith and Virmani 2000,Sohanghpurwala 2006). Diffusion may be modeled using Fick's Second Law, given in Equation 7. In this equation, C is the concentration

of a species, t is time, x is a coordinate along an axis parallel to the gradient of species C, and D_{eff} is the effective diffusion coefficient. A solution to this equation is given by Equation 8, with C_0 as the initial concentration of chloride in the concrete and *erf* as the error function. The effective diffusion coefficient is the primary method by which chloride diffusion may be compared between different specimens.

$$\frac{\partial C}{\partial t} = D_{eff}\frac{\partial^2 C}{\partial x^2} \qquad \text{Equation 7}$$

$$\frac{C(x,t)}{C_0} = 1 - \text{erf}\left(\frac{x}{\sqrt{4D_{eff}t}}\right) \qquad \text{Equation 8}$$

Properties of the concrete affect the chloride diffusion rate. Construction practices, age, and materials used have an influence, as does the pore structure within the concrete. The older the concrete, the more highly developed will be the pore structure, reducing the diffusion rate. High temperature casting will create concrete more resistant to chloride penetration at early ages but with a decreased resistance to chloride penetration at later ages when compared with low temperature cast concrete. Chloride binding to the cement matrix surfaces reduces the rate of diffusion by removing chloride from the pore solution. The effect of chloride binding continues to be an influence until chloride binding sites have been occupied and steady state conditions have been reached.

As summarized by Smith and Virmani (2000), the chloride diffusion rate may be lowered by reducing the water to cementitious material (w/cm) ratio of the concrete, adding pozzolanic materials to the concrete, adding polymer modifiers to the concrete, and improving aggregate gradation. Other factors influencing diffusion of chloride ions in concrete include the surface charge on the hydrated cement paste, the formation of porous transition zones at the aggregate/cement paste interface, and microcracking.

Sagüés et al. (2001) noted that reinforcement acts as a barrier to prevent further migration of chlorides. The result of this is that the buildup of chloride ions at reinforcing layers occurs more quickly than simple one-dimensional models. The results of this study were to propose a derating factor that could be applied to estimate the reduction in time to corrosion initiation. The

derating factor can range from 0.9 (for substantial cover) to 0.6, indicating that it may be substantial.

Costa and Appleton (1998) indicate that the use of Fick's second law to simulate the chloride concentrations within the concrete for each time step is a good approximation, but that it is impossible to predict long-term chloride penetration due to the time-dependence of the diffusion coefficient and surface chloride concentration. Exposure to chlorides causes an increase in surface concentration, while the continued hydration and pozzolanic reactions within the cement matrix leads to a decrease in diffusion coefficient.

2.4 Environmental Effects on Chloride Penetration

Concrete placed in a marine environment are categorized based on location. The portion of the element located under the mean low tide level is referred to as the submerged zone and is constantly exposed to seawater. Between the mean low tide and mean high tide levels is the tidal zone, which experiences cyclical wetting and drying caused by the changing tides. Above the tidal zone is the splash zone, which is the portion of the element that experiences wave action and is only occasionally wetted. Above the splash zone is the atmospheric zone, which comes in contact with sea spray and precipitation but is not in direct contact with seawater. The relative locations of these zones are illustrated in Figure 2.

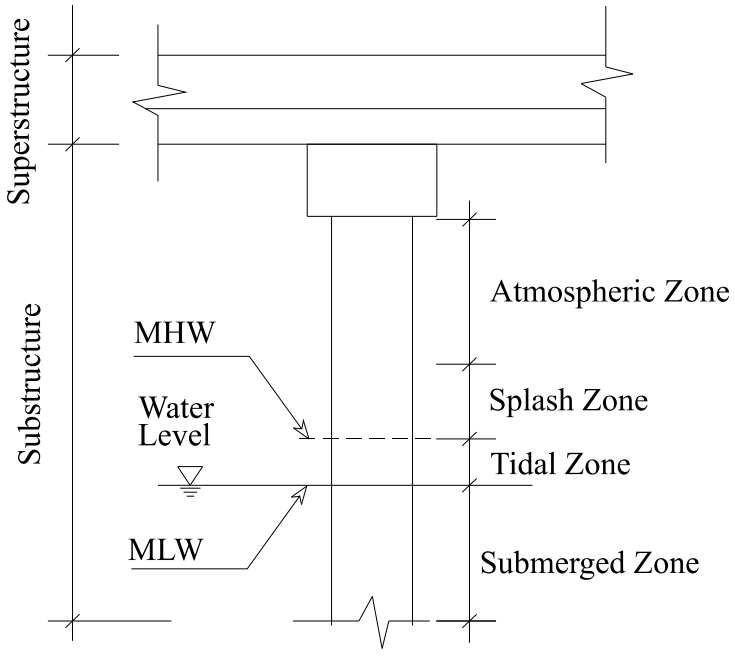

Figure 2–Chloride exposure zones of a typical bridge substructure

Costa and Appleton (1998) tested several concrete structures placed in a marine environment. For this project, fifty-four panels measuring 1.0 x 0.5 x 0.12 m were cast, cured, and coated except for the top surface with epoxy paint. The panels were exposed to a marine environment in an estuary. Panels were placed in five exposure conditions, including spray zone, tidal zone, atmospheric zone, and two locations where the panels were exposed to cycles of atmospheric and estuary environments. Chloride levels were determined by obtaining dust samples at 5 mm depth increments taken from two adjacent holes using a 20 mm diameter drilling tool. Dust samples were then processed to determine the total chloride content using a chloride ion selective electrode. The highest chloride penetration rates were observed in the tidal zone, followed by the spray zone. For this project, the spray zone was defined as the transition between the splash and atmospheric zone. The atmospheric zone showed much less penetration. Furthermore, the surface chloride content of the concrete was found to be influenced by exposure conditions but not by the quality of the concrete. This content increases with time.

Sandberg et al. (1998) placed samples with 50 different concrete qualities (differing w/c, scm) on a pontoon in Sweden. These samples had atmospheric zones, splash zones, and submerged zones. Cores were taken and chloride profiles were produced at 7 or 12 months, 2 years, and 5 years exposure. Samples included ternary blends incorporating fly ash and silica fume. Samples were taken from 100-mm diameter cylinders and ground in increments of 1 mm. Pulverized samples were analyzed for total chloride content using AASHTO T260-A. Diffusion coefficients were calculated from the results and then compared to one another by mix design and exposure conditions. As expected, diffusion coefficients were greatest in the submerged zone followed by the splash zone.

2.5 Tests for Evaluating Durability

2.5.1 Surface Resistivity Test using the Four-Point Wenner Probe

Concrete electrical conductivity is directly related to the permeability of fluids and the diffusivity of ions through a porous material (Whiting and Mohamad 2003). As a result, the electrical resistivity can be used as an indirect measure of the ease in which chlorides ions can penetrate concrete (Hooton et al. 2001).

Two procedures have been developed to determine the electrical resistivity of concrete. The first method involves passing a direct current through a concrete specimen placed between

two electrodes. The concrete resistance between the two electrodes is measured. The actual resistance measured by this method can be reduced by an unknown amount due to polarization at the probe contact interface. The second method solves the polarization problem by passing an alternating current (AC) through the sample. A convenient tool to measure using this method is the four-point Wenner Probe resistivity meter (Hooton et al. 2001). The set up utilizes four equally spaced surface contacts, where a small alternating current is passed through the concrete sample between the outer pair of contacts. A digital voltmeter is used to measure the potential difference between the two inner electrodes, obtaining the resistance from the ratio of voltage to current (see Figure 4). This resistance is then used to calculate resistivity of the section. A typical Wenner linear four-probe array is illustrated in Figure 3.

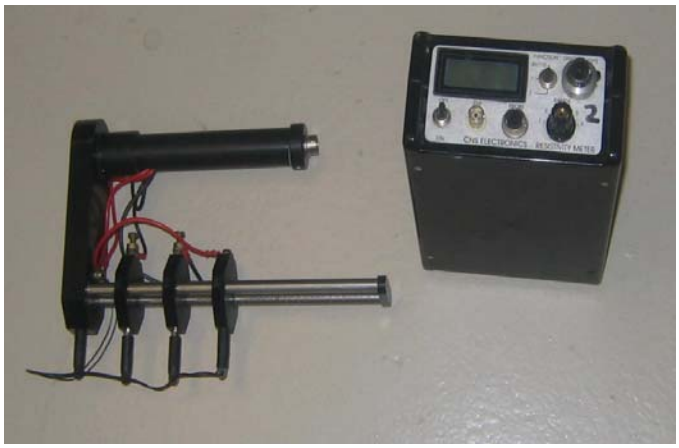

Figure 3–Wenner linear four-probe array and display

The resistivity ρ of a prismatic section of length L and section area A is given by Equation 9, where R is the resistance of the specimen calculated by dividing the potential V by the applied current I. The resistivity ρ for a concrete cylinder can be calculated by the formula provided in Equation 10, where d is the cylinder diameter and L its length (Morris et al. 1996).

$$\rho = \frac{A.R}{L} \rho = \qquad \text{Equation 9}$$

$$\rho = \left(\frac{\pi . d^2}{4}\right)\frac{1}{L}\cdot\left(\frac{V}{I}\right) \qquad \text{Equation 10}$$

Assuming that the concrete cylinder has homogeneous semi-infinite geometry (the dimensions of the element are large in comparison to the probe spacing), and the probe depth is far less than the probe spacing, the concrete cylinder resistivity ρ is given by Equation 11, where a is the electrode spacing (see Figure 4).

$$\rho = (2.\pi.a)\cdot\left(\frac{V}{I}\right) \qquad \text{Equation 11}$$

The non-destructive nature, speed, and ease of use make the Wenner Probe technique a promising alternative test to characterize concrete permeability.

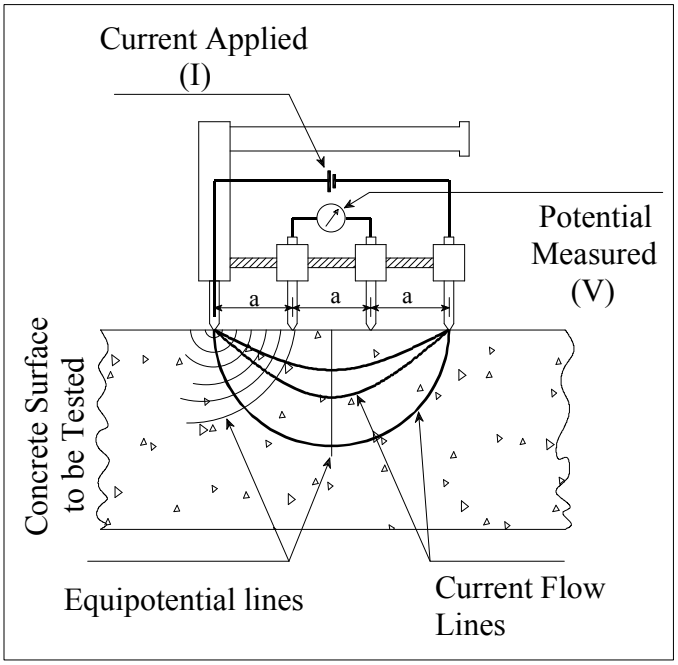

Figure 4–Four-point Wenner probe test setup

Results from Wenner Probe testing can vary significantly with changes in the degree of saturation or conductivity of the concrete. Techniques to achieve more uniform saturation, such as vacuum saturation or submerging in water overnight, can be performed in the laboratory.

However, the laboratory pre-saturation procedure still presents some inconsistencies. The known conductivity of the added solution changes when mixed with the ions (mainly alkali hydroxides) still present in the concrete pores after the drying process (Hooton, Thomas and Stanish 2001). To overcome this problem, Streicher and Alexander (1995) suggested the use of a high conductivity solution, for example 5 M NaCl, to saturate the sample so that the change in conductivity from the ions remaining in the concrete is insignificant.

Use of the Wenner Probe on concrete in the field presents further complications. The test can give misleading results when used on field samples with pore solution of unknown conductivity. Therefore, the pore solution must be removed from the sample to determine its resistivity or the sample must be pre-saturated with a known conductivity solution (Hooton, Thomas and Stanish 2001). Moreover, pre-saturation of the concrete requires that the sample be first dried to prevent dilution of the saturation solution. Some *in situ* drying techniques, however, can cause microcracks to form in the pore structure of the concrete, resulting in an increase in diffusivity. Another possible problem with the *in situ* readings is that reinforcing steel can cause a "short circuit" path and give a misleadingly low reading. The readings should be taken at right-angles to the steel rather than along the reinforcing length to minimize this error (Broomfield and Millard 2002). Hooton, Thomas and Stanish (2001) have suggested that because of these problems, the Wenner probe should only be used in the laboratory, on either laboratory-cast specimens or on cores taken from the structure without steel.

The test probe spacing is critical to obtaining accurate measurements of surface resistivity (SR). The Wenner resistivity technique assumes that the material measured is homogeneous (Chini et al., 2003). In addition, the electrical resistivity of the concrete is mainly governed by the cement paste microstructure (Whiting and Mohamad 2003). It depends upon the capillary pore size, pore system complexity and moisture content. Changes in aggregate type, however, can influence the electrical resistivity of concrete. Monfore (1968) measured the electrical resistivity of several aggregates typically used in concrete by themselves (see Table 1). The resistivity of a concrete blend containing granite aggregate was higher than a blend containing limestone (Whiting and Mohamad 2003). Moreover, other research (Hughes, Soleit and Brierly 1985) showed that as the aggregate content increased, the electrical resistance of the concrete also increased. Gowers and Millard (1999) determined that the minimum probe spacing should be 1.5 times the maximum aggregate size, or ¼ the depth of the specimen, to improve reading

accuracy. Morris et al. (1996) suggest averaging multiple readings taken with varying internal probe spacings. Another reasonable technique is to average multiple readings in different locations of the concrete surface. In the case of test cylinders, the readings can be made in four locations at 90-degree increments to minimized variability induced by the presence of a single aggregate particle interfering with the readings (Chini et al. 2003).

Morris et al. (1996) evaluated the use of SR by testing the ends and sides of cylinder specimens to determine the best method of performing SR testing and whether or not SR could be used on the flat end of samples (for use with cylinder slices, for example). Taking measurements at multiple tangential locations on the cylinder surface was recommended to reduce variability caused by the non-homogeneity of concrete. The variance of the measurements was not affected by the size or type of aggregate used in the concrete blend.

Table 1–Measured electrical resistivities of typical aggregates used for concrete (Monfore, 1968)

Type of Aggregate	Resistivity (ohm-cm)
Sandstone	18,000
Limestone	30,000
Marble	290,000
Granite	880,000

Polder (2001) provided a RILEM TC-154 technical recommendation covering the use of SR on site for various purposes. While resistivity mapping does not show whether steel is actively corroding, it can be used to locate areas of strongest corrosion activity. It is noted that under laboratory conditions the resistivity may be influenced by 3% for saturated concrete and 5% for dry concrete for every degree K that the temperature changes. Because of this, the temperature of the concrete should be measured and an adjustment applied. Alternating current is utilized for 4-point probing to prevent polarization of the ions within the pore solution, which will cause false measurements. Erroneous readings may occur if the probe is used near reinforcement. A compromise between avoiding reinforcement and reducing non-homogeneity effects must be made when determining the spacing of the probes. Close probe spacing avoids problems caused by embedded reinforcement but will exacerbate errors due to nonhomogeneous concrete. Coefficients of variation may be high, with 20% in the lab and 25% in the field considered normal.

Chini et al. (2003) evaluated the possible replacement of the widely used electrical RCP test (AASHTO T277, ASTM C1202) by the simple non-destructive surface resistivity test. The research program correlated results from the two tests from a wide population of more than 500 sample sets. The samples were collected from actual job sites of concrete pours at the state of Florida. The tests were compared over the entire sample population regardless of concrete class or admixture present to evaluate the strength of the relationship between procedures. The two tests showed a strong relationship. The levels of agreement (R^2) values reported were as high as 0.95 for samples tested at 28 days and 0.93 for samples tested at 91 days. Finally, a rating table to aid the interpretation of the surface resistivity results was proposed (see Table 2) based on the previous permeability ranges provided in the standard RCP test.

Table 2–Correlation between RCP and SR results 4-inch (102-mm) diameter by 8-inch (204-mm) concrete cylinders (Chini et al., 2003)

Chloride Ion Permeability	RCP Test Charge (Coulombs)	Surface Resistivity Test	
		28-Day Test (kΩ-cm)	91-Day Test (kΩ-cm)
High	> 4,000	< 12	< 11
Moderate	2,000 - 4,000	12 -21	11 -19
Low	1,000 - 2,000	21 – 37	19 – 37
Very Low	100 - 1,000	37 – 254	37 – 295
Negligible	< 100	> 254	> 295

In Florida, SR is conducted according to FM 5-578, which is the standard used by the Florida Department of Transportation. This test is applicable to concretes containing supplemental cementitious materials, including fly ash, blast furnace slag, silica fume, or metakaolin. The method is not applicable to cores, however, as they may be contaminated by chloride. In this method, a Wenner 4-probe array is used along the side of 4 in. x 8 in. sample cylinders to measure resistance. Duplicate measurements are taken at 90 degree increments at the center of the side and are then averaged. The test is not a direct test of permeability; the test measures the extent to which the pores in the concrete microstructure are interconnected. A low permeability concrete offers higher resistance since micropores are more likely to be discontinuous. This test is simple, inexpensive, and has a single operator coefficient of variation of only 8.2%. This test has largely replaced the rapid chloride permeability (RCP) test for use with the FDOT.

Presuel-Moreno et al. (2010) performed laboratory and field experiments to evaluate the use of SR for bridge structures. Laboratory samples featured a w/c of 0.4, with some containing fly ash and/or reinforcement. Samples were rectangular prisms (12 in. x 12 in. x 6 in.), with cylinders (4 in x 8 in.) used as references. Cover was 2 in. SR was measured on the top of the rectangular prisms using two different Wenner probe spacings. Measurements were taken in a series of patterns, with the probe held parallel, perpendicular, or at a 45-degree angle to reinforcing bars present. The objective was to evaluate the effect of reinforcing on the SR measurements for a flat "infinite" surface. Some samples underwent cyclic ponding with seawater to mimic field conditions. Cylinder SRs were measured per the Florida test standard (FM5-578).

Presuel-Moreno et al. (2010) discovered that the SR of the portland cement cylinders increased in a linear pattern when stored in lab temperature and relative humidity (RH) after 60 days. Upon relocation to 95% humidity, SR values dropped exponentially to a third of what they had been previously. Samples stored at 95% RH or in the fog room displayed SR that increased with time, with similar SR to that of the sample reintroduced to high humidity after laboratory temperature and relative humidity. No significant difference in results for different probe spacings was noted. The pattern was repeated for the cylinders with fly ash, albeit with continued increase in resistivity caused by pozzolanic reaction.

Rectangular specimens responded to environmental changes similar to those of the cylinders. Results from samples with no bars indicated that the position and orientation of the Wenner probe had little influence on the measurement. The closer probe spacing indicated a higher peak resistivity than the wider probe spacing when samples were stored at laboratory temperature and RH. This was thought to be caused by surface drying. The spread between the maximum and minimum SR values was also higher for the wider probe spacing, suggesting that resistivity is not constant throughout the depth of a concrete object. As with the cylinders, fly ash increased the rate at which samples developed resistivity, with a plateau at 500 days.

Presuel-Moreno et al. (2010) performed SR measurements on bridges throughout Florida, chosen to represent a variety of bridge ages and environments. At each bridge, initial measurements were taken followed up by measurements at 24 and 48 hours. The measurements at 24 and 48 hours were conducted using containers to apply water to the concrete surface. All SR measurements were temperature corrected. It was observed that the resistivity increased with

elevation above the water line during the initial set of measurements. Conditioning reduced the SR, confirming that resistivity drops as moisture content increases. There was no significant difference between different Wenner probe spacings. Factors that affected SR measurements included concrete moisture, air temperature, weather (rain), water temperature, tidal cycle, and the prevailing wind direction.

Cores were taken during these investigations (Presuel-Moreno 2010), stored in high humidity conditions in the lab, and tested with SR. Cores were monitored for weight gain (moisture absorption). SR measurements dropped initially as the cores gained moisture content but stabilized following saturation. Data from core weight gain indicates that it would take at least 10 days to saturate in situ concrete, which is impractical. SR readings from the field were about three times higher than SR readings from the lab.

Of specific interest, Presuel-Moreno et al. (2010) conducted SR testing on the Key Royale Bridge; measurements indicate that the blast furnace slag piles had the lowest SR, with fly ash, ultrafine fly ash, and silica fume being higher. The metakaolin piles had the highest SR.

Chini et al. (2003) determined that the type of coarse aggregate and w/c ratio did not influence the consistency of the SR testing. Also noted was that it would be inappropriate to compare data obtained from testing cylinders to on-site measurements.

Roske et al. (2008) determined that SCM significantly increases the surface resistivity of ternary concrete blends when compared with control specimens. Ternary blends included portland cement, fly ash, and a third ingredient chosen from silica fume, ultrafine fly ash, metakaolin, and blast furnace slag. The ternary mixes containing silica fume had the highest SR values, followed by ultrafine fly ash, metakaolin, and blast furnace slag.

Research performed by Van Etten et al. (2009) indicated that a ternary blend containing fly ash and silica fume had the highest SR values after 28 days. The increase in SR for this blend slowed down as the early reacting silica fume was consumed, leaving the fly ash alone to continue pozzolanic reactions. The SR of the ternary blends containing fly ash and blast furnace slag increased more quickly than the fly ash and silica fume ternary blend at higher ages, although this rate of increase was not sufficient for the blast furnace slag ternary blend to overtake the silica fume ternary blend in terms of SR performance.

2.5.2 Electrical Potentials

Half-cell potential (HCP) measurements are used to assess the corrosion condition of reinforcement in a structure. Further uses include determining locations for performing destructive testing, evaluating the corrosion states of reinforcement after repair work, and designing the anode layout of cathodic protection systems. Corroding steel in chloride contaminated concrete shows potentials ranging from -0.6 to -0.4 V using a copper-copper-sulfate reference electrode (CSE), depending on the presence of carbonation, oxygen availability, and moisture content of the concrete.

ASTM publishes a standard, ASTM C 876, which discusses the use and analysis of half-cell potential mapping with a CSE. Recommended test apparatus, test method, and restrictions on the use of the test are also presented. One of the difficulties in obtaining stable measurements is to provide sufficient moisture content within the concrete; this is typically accomplished with a wetting solution applied at the time of testing. Interpretation guidelines are provided in the standard; a measurement less than -350 mV indicates a 90% probability that corrosion is occurring while a measurement greater than -200 mV indicates a 90% probability that corrosion is not occurring. Measurements between -350 mV and -200 mV are inconclusive.

Elsener (2003) produced a RILEM recommendation (TC 154-EMC) for the use of half-cell potential mapping to evaluate in situ concrete structures for corrosion. Elsener recommends that the potential values included in ASTM C876 should not be used as absolute criteria to determine the condition of steel in concrete. Changes in moisture content of the concrete can lead to changes in the potential readings; a negative shift of 100 mV was observed after a dry bridge deck became wet after rain, for example. This indicates that the potential gradient (spatial variation of potential fields), not the absolute potential, is an indicator of corroding reinforcing.

Moser et al. (2010) took half-cell potential measurements between pile surfaces and prestressing steel using CSE and a voltmeter. These piles had been removed from the Turtle River Bridge for testing as part of a Georgia Department of Transportation study. The CSE used a sponge soaked in mild detergent as a conductor. Measurements were taken at one foot intervals along the length of the piles. A map of the potential measurements taken at one pile is given in Figure 5. Areas of the pile near the high tide mark had potentials below -500 mV, serving as confirmation of the corrosion in the pile observed upon visual inspection. Two faces

of the pile had potentials below -500 mV, suggesting that substantial areas of the pile below the water surface were experiencing corrosion.

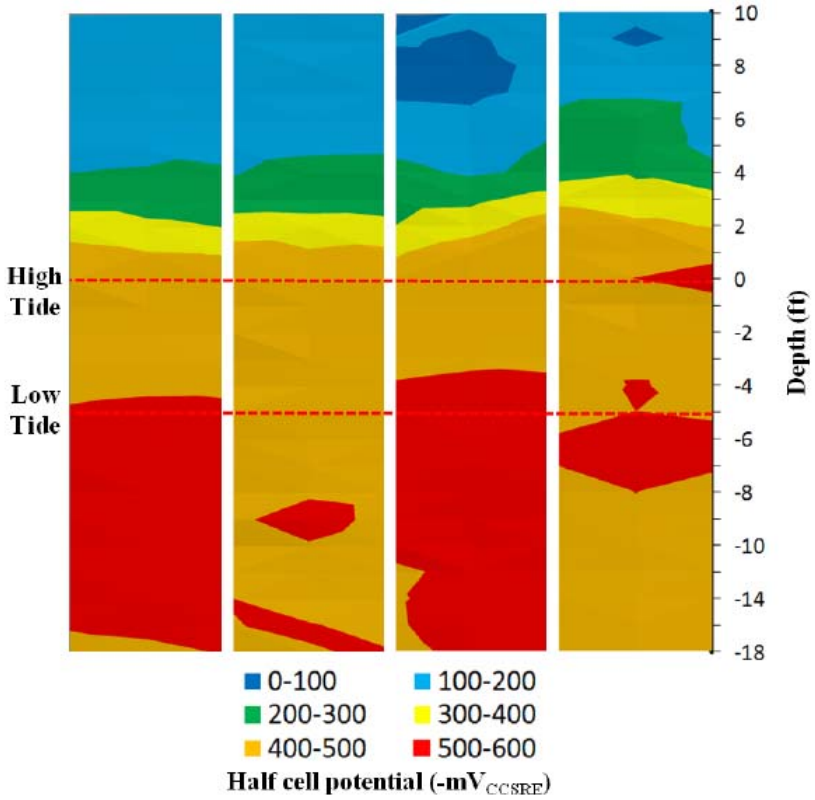

Figure 5–Half-cell potential map of the four faces of a Turtle River Bridge pile (Moser et al., 2010)

Naito et al. (2010) performed half-cell potential mapping as part of their investigation into in situ measurement techniques. Decommissioned corroded prestressed box sections were transferred to a laboratory for testing. Soaking with sprinklers or burlap was done in lieu of using a detergent sponge to provide sufficient moisture to take measurements. An example of the results obtained is Figure 6; areas shaded red indicate sufficient negative potential (below -350 mV) for corrosion to be likely (over 90% probability).

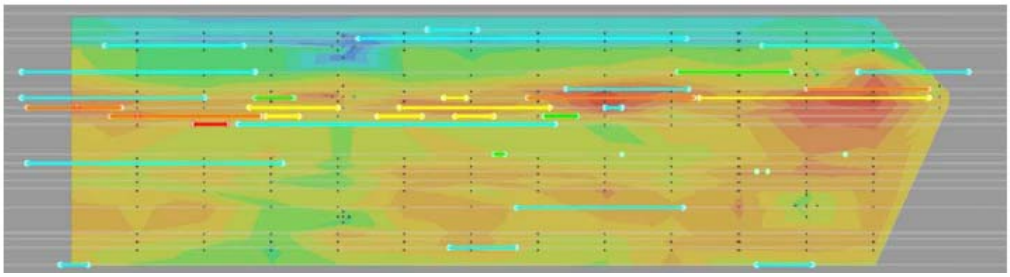

Figure 6–Overlay of damage profile on half-cell potential map for beam MS3 (Naito et al., 2010)

Such plots were correlated with damage observed in test specimens. Some severe corrosion was not detected by HCP, although this corrosion was localized to a short piece of one tendon. Elsewhere, low HCP occurred at the same locations as severe corrosion, usually near cracks. A statistical correlation between the amount of corrosion in a prestressing location (on a 1 to 5 scale) with the corresponding half-cell measurement was conducted. A table was produced (Figure 7) that refined the table given in ASTM C876. In this table, DI refers to the damage index, a value of zero indicates the absence of visible corrosion.

Table 7-3: Probability of Corrosion for Prestressing Steels Based on Half-Cell Potential	
Half-Cell Potential	Probability of Corrosion (DI > 0)
Greater than -0.20 V	3.7%
Between -0.20 V and -0.25 V	9.0%
Between -0.25 V and -0.30 V	18.6%
Between -0.30 V and -0.35 V	26.5%
Less than -0.35 V	45.5%

Figure 7–Probability of corrosion for prestressing steels based on half-cell potential

Cannon et al. (2006) performed potential mapping on corroded piles that were pulled from service as part of a bridge replacement project. This bridge was in a bay adjacent to the Gulf of Mexico, roughly the same environment as the Key Royale Bridge. The potential mapping was then compared with the results of flexural testing. Potential mapping was performed prior to pile removal, guaranteeing an in situ evaluation that eliminated any possible errors due to the handling and desiccation of the piles. Figure 8 below summarizes the results of the potential testing for several piles; plots feature the averaged potentials for all four faces. One pile, 40-3J, had potentials indicating the likely presence of corrosion extending more than five

feet above the mean water height. When flexural testing was performed, the pile was found to have only 31% of its calculated capacity remaining, indicating substantial degradation of the prestressing strand. Substantial corrosion was observed on the prestressing strand when the concrete cover was removed. Conversely, pile 44-2 has only one reading below -350 mV, which occurred near the water line. This pile retained at least 100% of its calculated capacity, indicating that corrosion was not influencing the prestressing strand. The relationship between the measured corrosion potential and flexural capacity was linear and quite strong (R-squared of 0.92). The relationship indicates that if readings drop below -350 mV at one foot above MHW then the pile retains 100% of its flexural capacity. This capacity drops to 68% when the readings below -350 mV extend to 3 feet above the water line and to 32% at 5 feet.

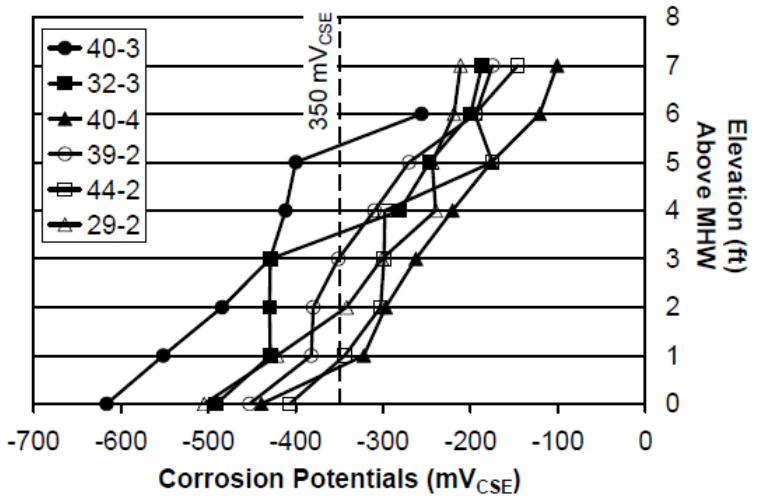

Figure 8–Compilation of the average corrosion potential of tested piles (Cannon et al., 2006)

Assouli et al. (2008) reviewed the factors that can lead to the incorrect interpretation of half-cell potential measurements. They indicate that the absolute values provided in ASTM C876 that indicate the presence or absence of corrosion can be incorrect depending on the moisture content, chloride content, temperature, carbonation, and concrete cover thickness.

Francois et al. (1993) investigated the correlation between active corrosion of reinforcement and external electrode potential measurements. The total voltage potential measured by the electrode is a function of three potentials; that of the steel reinforcing, that of the reference electrode, and that of the junction between the reference electrode and the steel reinforcing. The total potential is measured as the potential of the reference minus that of the

steel plus that of the junction. Since the potential of the reference electrode is constant, any change in the measured voltage will reflect a change in the junction or steel potentials. The junction potential is a function of the interface between the reference electrode solution (copper sulfate) and the wetting liquid (seawater for this project) and the interface between the wetting liquid and the concrete interstitial solution, with the latter a function of the amount of moisture present in the pore space. This was confirmed by observing that the potentials measured for a laboratory specimen that had been exposed to a salt fog increased from -600 mV to -100 mV in five days when relative humidity was decreased from 100% to 40%. These sample had been in salt fog for eight years; as corrosion was assumed to have not changed during five days relative to eight years, this change reflects the change in the junction potential caused by the loss of wetting liquid.

2.5.3 Chloride Content and Diffusion Coefficient

In Florida, chloride content is measured using FM 5-516, which is the standard test protocol for the Florida Department of Transportation. This test method is designed for chloride contents lower than 100 ppm although it will accurately measure chloride concentrations up to 625 ppm. The samples to be tested are pulverized and boiled in nitric acid, causing both pore solution chloride and adsorbed chloride to be liberated. Titration with silver nitrate is used in conjunction with a pH/mV meter to determine chloride content with the assistance of a computer program. The concentrations of chloride for different layers within a sample are fitted to a curve based on Fick's second law; the coefficient of diffusion results from this fitting. A higher coefficient indicates that chloride more readily diffuses through a sample.

Presuel-Moreno et al. (2010) reports chloride profiles from cores taken from bridges throughout Florida. A nominal 2-in. diameter drill bit was used to take cores from locations near where SR measurements were taken. Cores were between 2 in. and 6 in. long, depending on the reinforcing depth. A total of 315 cores from about 80 pile structures were taken. Cores were taken at two elevations above the marine growth. The slices were of increasing thickness, with 0.4 cm for the outermost slice and 0.7 cm for the fourth and subsequent slices. These slices were analyzed in accordance with FM5-516. One of the bridges investigated as part of this research was the Key Royale Bridge. Table 3 lists the diffusion coefficients obtained from these cores; "Pile type" refers to the supplemental cementitious materials used for constructing the piles. These included piles with fly ash (FA), ultrafine fly ash (UFA), silica fume (SF), blast furnace

slag (BFS), metakaolin (MET), and without supplemental cementitious materials (CEM). Of special significance for the present research was the diffusion coefficient obtained from the CEM pile. Cores from this pile were indistinguishable from those taken from piles containing supplemental cementitious materials. This pattern would be repeated during the present research; five of the eight CEM cores had diffusion coefficients that were indistinguishable from those of the piles containing supplemental cementitious materials. A combination of well-graded and ground cement clinker and a low water to cement ratio (0.30) may explain these results.

Table 3–Chloride diffusion coefficients from cores taken at Key Royale Bridge in 2008 (Presuel-Moreno 2010)

Distance above MGL (in)	Pile type	D_{app} (x 10^{-12} m^2/s)
5	CEM	0.22
-3	CEM	0.24
-3	CEM	0.23
4	UFA	0.21
4	UFA	0.09
-6	UFA	0.13
5	FA	0.14
5	FA	0.31
-7	FA	0.36
5	SF	0.25
-5	SF	0.29
-5	SF	0.34
4	BFS	0.09
-5	BFS	0.16
-5	BFS	0.95
6	MET	0.29
6	MET	0.39
-5	MET	0.80

Sagüés et al. (2001) took cores from tidal and splash elevation zones using a 2-in. core bit. The structures were investigated for cracks; cores were taken from locations with cracks and adjacent to those locations to serve as a baseline comparison. Even though the cracks were thin, levels of chloride beyond the theoretical threshold level were observed, especially in the splash zone. Despite this, indications of corrosion were not observed at the crack locations.

2.5.4 Comparative Analysis of Different Measurement Methods

Presuel-Moreno et al. (2010) compared wet resistivity (SR) with the diffusion coefficient (as measured using BD) for 80 different bridge structures in Florida. Three relationship

equations were proposed, with the best fitting encompassing only those structures built in the previous 30 years. The R-squared value for this equation was 0.67.

Chini et al. (2003) compared results obtained from RCP with those obtained by SR. The correlation between the two was significant, with R-squared values of 0.9481 at the 28-day test and 0.9321 at the 91-day test. This correlation is based on the entire set of samples from this project. Based on this finding, SR is a suitable replacement for RCP.

Moser et al. (2010) recorded half-cell potentials and correlated them with chloride content taken from 0.5-in. diameter plugs at identical locations. This was done with several box beams removed from a decommissioned structure. A correlation between these two measurements did occur, although R-squared was only 0.26, indicating a loose correlation at best. Figure 9 illustrates the data fit for this project.

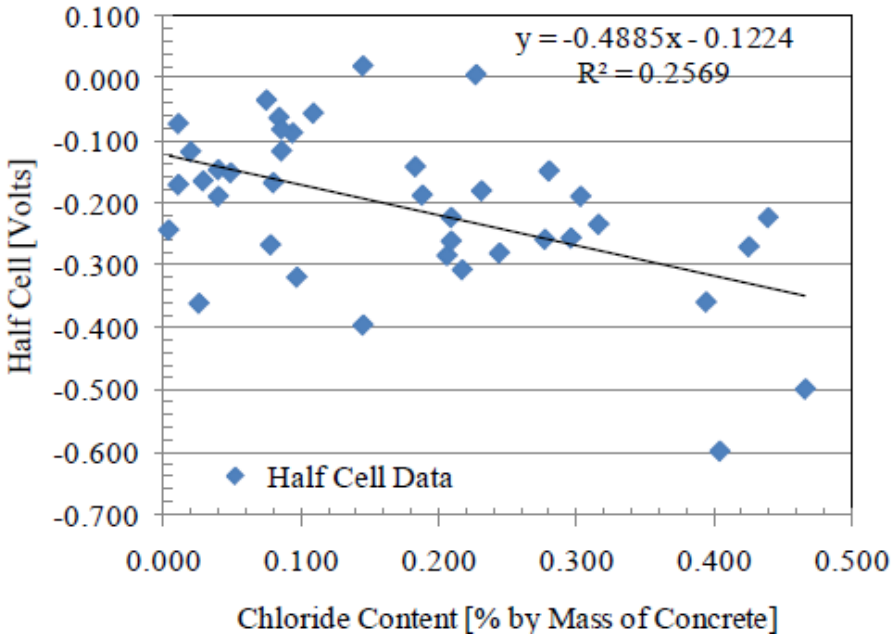

Figure 9–Correlation of half-cell potential and chloride level

Vivas et al. (2007) conducted research to evaluate the use of RCP, rapid migration (RMT) and impressed current (IC) tests to determine the resistance of concrete to chloride intrusion. These test methods, which utilize electric fields to accelerate chloride penetration, were compared with bulk diffusion BD and AASHTO T259, which use diffusion as the only mechanism of chloride penetration. Of particular interest was the evaluation of the electrical tests for analyzing concretes with different admixtures. Some mixes featured pozzolans like fly

ash and silica fume; one mix had calcium nitrate corrosion inhibitors. The BD and T259 tests were conducted with a 364 day chloride exposure period, with chloride contents at different penetration depths plotted and an apparent diffusion coefficient obtained from Fick's Second Law. Correlations between the RMT test and the long term tests were equal to or slightly better than those obtained by RCP and SR testing, with RMT testing being less affected by the presence of supplementary cementitious materials. Also, 91 days was determined to be the optimum sample age for using SR, RMT, or RCP testing to predict the results of 364-day bulk diffusion test.

2.6 Effect of Cement and SCM on Concrete Properties

2.6.1 Portland Cement Unhydrated Chemistry

Portland cement is hydraulic cement which is typically produced by initially heating limestone with clay in a kiln at 2500 to 2900°F to produce clinker (Mindess et al. 2003). The clinker is then ground to a specific fineness. Small amounts of gypsum are interground with the clinker to control the hydration rate of the finished cement product.

Shorthand notation used to represent the actual chemical formulas for oxides found in cements and SCM are shown in Table 4. Chemical compounds that are the major constituents in cement are formed from these oxides in the calcining process of cement manufacturing. The chemical name, chemical formula and shorthand notation for the five most abundant compounds are found in Table 5.

Table 4–Typical oxides and their shorthand notations

Common Name	**Chemical Formula**	**Shorthand Notation**
Lime	CaO	C
Silica	SiO_2	S
Alumina	Al_2O_3	A
Ferric Oxide	Fe_2O_3	F
Magnesia	MgO	M
Potassium Oxide	K_2O	K
Sodium Oxide	Na_2O	N
Sulfur Trioxide	SO_3	$\hat{S}$
Carbon Dioxide	CO_2	$\hat{C}$
Water	H_2O	H

Table 5–Typical chemical compounds and their shorthand notations

Chemical Name	Chemical Formula	Shorthand Notation
Tricalcium Silicate	$3CaO \cdot SiO_2$	C_3S
Dicalcium Silicate	$2CaO \cdot SiO_2$	C_2S
Tricalcium Aluminate	$3CaO \cdot Al_2O_3$	C_3A
Tetracalcium Aluminoferrite	$4CaO \cdot Al_2O_3 \cdot Fe_2O_3$	C_4AF
Calcium Sulfate Dihydrate (gypsum)	$CaSO_4 \cdot 2H_2O$	$C\hat{S}H_2$

Portland cement is produced with a specific composition and fineness to ensure a satisfactory performance for a particular application, such as high early strength or low heat of hydration. ASTM classifies cements so that a more consistent product is available. These standardized cements are designated ASTM Types I, II, III, IV, and V.

ASTM Type I is a general purpose cement with average strength gain and heat of hydration. If a more specialized application, such as sulfate resistance or high early strength development, is needed, a different type should be selected. Type V cements was developed to combat sulfate attack. Sulfate attack involves the hydration products formed from C_3A. Therefore, lowering the percentage of C_3A will serve to increase the sulfate resistance of cement. Type III cement was developed to create a high early strength concrete. This was accomplished by increasing the proportions of C_3S or, more effectively, grinding the cement finer. However, much heat is generated during the hydration process because of the increase surface area of C_3S. Therefore, this cement cannot be used where high temperatures create adverse effects, such as in mass concrete, where thermal cracking can become a problem. It is for this reason that Type IV was created. Type IV cement was developed to create a low heat of hydration product. The proportions of the highly exothermic compounds, C_3A and C_3S, were reduced. However, there are problems associated with this cement also. Because of the lower C_3S composition, this cement has a slow strength gain; therefore, a Type II cement was developed. The C_3S proportion remains the same, while C_3A is slightly lowered. This cement has a better strength development, as well as being fairly sulfate resistant. Table 6 was recreated from Mindess (et al., 2003), detailing typical chemical compositions and properties of ASTM Types I to V cements.

Table 6–Typical chemical compositions and properties of ASTM Type I to V cements

	I	II	III	IV	V
C_3S	55	55	55	42	55
C_2S	18	19	17	32	22
C_3A	10	6	10	4	4
C_4AF	8	11	8	15	12
$C\hat{S}H_2$	6	5	6	4	4
Fineness (m^2/kg)	365	375	550	340	380

2.6.2 Portland Cement Hydration

The hydration of the calcium silicates in portland cement produces calcium silicate hydrate and calcium hydroxide. The C_3S and C_2S reactions are very similar, with the only difference being the quantity of calcium hydroxide (CH) formed. The following equations provide a summary of the primary reactions with some of the intermediate reactions omitted for clarity.

$$2C_3S + 11H \rightarrow C_3S_2H_8 + 3CH \qquad \text{Equation 1}$$

$$2C_2S + 9H \rightarrow C_3S_2H_8 + CH \qquad \text{Equation 2}$$

The composition of this calcium silicate hydrate product can vary widely—typically in water content. Presented here, the product is in its saturated state. In contrast, CH has a fixed composition.

Hydration of C_3A occurs in the presence of sulfate ions supplied by the dissolution of gypsum. These ions react with C_3A to form a calcium sulfoaluminate hydrate, or more commonly, ettringite:

$$C_3A + 3C\hat{S}H_2 + 26H \rightarrow C_6A\hat{S}_3H_{32} \qquad \text{Equation 3}$$

The ettringite can transform to a different form of calcium sulfoaluminate hydrate if the sulfate is consumed before the C_3A is completely hydrated as indicated in the following equation:

$$2C_3A + C_6A\hat{S}_3H_{32} + 4H \rightarrow 3C_4A\hat{S}H_{12} \qquad \text{Equation 4}$$

This form is called monosulfoaluminate. If a new source of sulfate ions comes in contact with this product, ettringite can be reformed:

$$C_4A\hat{S}H_{12} + 2C\hat{S}H_2 + 16H \rightarrow C_6A\hat{S}_3H_{32} \qquad \text{Equation 5}$$

2.6.3 Pozzolanic Reaction Overview

Pozzolans are not cementitious, but rather amorphous silica which will react with CH and water to form a cementitious product, C-S-H:

$$CH + S + H \rightarrow \text{C-S-H} \qquad \text{Equation 6}$$

If the silica content in the pozzolan is very high, a secondary reaction will occur:

$$C_3S + 2S + 10.5H \rightarrow 3[CSH_{3.5}] \qquad \text{Equation 7}$$

When the pozzolan has large quantity of reactive alumina, the CH will react with alumina to form a calcium aluminate hydrate (C-A-H):

$$CH + A + H \rightarrow \text{C-A-H} \qquad \text{Equation 8}$$

Other compounds besides C-A-H may form depending on the composition of the pozzolan such as C_2AH, C_2ASH_8, or monosulfoaluminate.

2.6.4 Fly Ash

Fly ash is precipitated from the exhaust gases of a coal burning power station. The majority of particles are spherical, glassy, either hollow or solid, and have a high fineness. Particle diameter typically ranges from 1 μm to 100 μm with specific surface area ranging from 250 to 600 m^2/kg (Neville 1995). The main components in the composition of fly ash are oxides of silicon, aluminum, iron, and calcium. The varying calcium content in fly ash composition led to the creation of ASTM C 618. This standard created two classes of fly ash—Class C and Class F. ASTM C 618 requires a Class F fly ash to be composed of a minimum of 70% silicon oxide (SiO_2) plus aluminum oxide (Al_2O_3) plus iron oxide (Fe_2O_3), while a Class C has a minimum of 50%. Derived from the burning of subbituminous coal or lignite, Class C fly ash has a high lime (CaO) content. Because of this, it is also slightly cementitious. Use of Class C fly ash may cause high water demand, early stiffening, and rapid setting. Class F fly ash is derived from the burning of bituminous coal or anthracite. Its calcium content is lower than a Class C fly ash.

Because fly ash is a pozzolan, the silica and alumina will react with CH to form a cementitious compound, C-S-H and C-A-H, respectively. The reactions depend on the breakdown and dissolution of silica and alumina by the hydroxide ions and heat generated by the hydration of portland cement. The glass material in fly ash is only broken down when the pH value of the pore water is at least 13.2 (Neville 1995). In other words, the fly ash will consume CH and form a hydration product as long as enough CH is present in the pore solution and there is sufficient void space present for the hydration product to occupy.

Fly ash influences the properties of a fresh concrete in a variety of ways. Workability, bleeding, and time of setting are all affected by the addition of fly ash. For the most part, the changes caused by the addition of fly ash are due to the shape and size of the particles and its chemical composition.

A reduction in water demand and an increase is workability is attributed to the spherical shape, electrical charge, and small size of the particles. The particle shape reduces the interparticle friction within the mixture, effectively increasing the workability. This also allows for a reduction in water to keep the same workability for a concrete mixture. Neville (1995) indicates that another mechanism of fly ash may be dominant in decreasing the water demand. The finer fly ash particle may become electrically charged and cover the surface of the cement particles. This deflocculates the cement particles, thus reducing the water demand for a given

workability. Another benefit of fly ash is the small particle size, which allows them to pack between the cement particles. This is known as particle packing; it reduces bleeding, lowers the mean size of the capillary pores, and can reduce water requirements (Mindess et al. 2003).

The composition of fly ash also extends setting times and decreases the overall heat liberated during hydration. Delayed setting times are ascribed to the slow pozzolanic reactions of fly ash. As mentioned above, the glassy fraction of fly ash will only breakdown when sufficient hydroxide ions are present in the pore solution. This process takes place only after a certain amount of portland cement hydration has taken place (Neville 1995). A consequence of the delay in the cement hydration is the slow pattern of heat evolution. Much of the heat is generated during the early stages of hydration of the C_3S and C_3A within the paste. The delayed setting time allows the concrete to slowly liberate the heat generated. In addition, when fly ash is used as a cement replacement, smaller quantities of the high heat generating compounds, C_3S and C_3A, are present. Therefore, the overall heat of hydration is reduced.

Fly ash influences the properties of a hardened concrete in a variety of ways. Compressive strength and rate of strength gain, modulus of elasticity, permeability, sulfate resistance, and drying shrinkage are all affected by the addition of fly ash. For the most part, the changes due to the addition of fly ash are because of the shape, size, and chemical composition of the particles.

The rate of strength gain is reduced by the addition of a Class F fly ash. As mentioned above, the pozzolanic reactions of fly ash depend on a high pH pores solution. Because this takes time to occur, the early hydration of mixtures containing fly ash is slow. Consequently, the early age compressive strengths are low. However, over time, the Class F fly ash will react to produce a stronger concrete than that of the same mixture containing only portland cement (ACI 232.2R-03). Conversely, Class C fly ash concrete often exhibit higher rate of reaction at early ages, but lower strength gain at late ages when compared to a Class F fly ash concrete (ACI 232.2R-03).

ACI (232.2R-03) has found that the effects of fly ash on the modulus of elasticity are not as significant as the effects on compressive strength. Furthermore, they suggest that cement and aggregate characteristics will have a greater effect on modulus of elasticity that the use of fly ash. Similar to modulus of elasticity, creep strain is more affected by compressive strength than fly ash. Lower compressive strengths result in higher creep strains (ACI 232.2R-03).

The consequence of using the slow reacting fly ash is that the initial permeability is higher than that of the same concrete containing only portland cement (Neville 1995). However, over time the fly ash concrete will develop a very low permeability through pozzolanic reactions (ACI 232.2R-03). CH is susceptible to leaching, leaving voids in which deleterious solution can ingress. However, fly ash chemically combines with CH to form a cementitious product, C-S-H. This action reduces the risk of leaching and further reduces permeability as the pore structure becomes occupied with C-S-H. Consequently, the durability of a concrete exposed to aggressive environments containing sulfates and chlorides is improved because of the reduction in permeability (Neville 1995). In addition, sulfate resistance is further improved through the removal of CH (Mindess et al. 2003).

2.6.5 Ultrafine Fly Ash

Ultrafine fly ash, similar to ordinary fly ash, is precipitated from the exhaust gases of a coal-burning power station. The larger particles are removed through filters or separators, leaving small particles that are spherical, glassy, either hollow or solid in shape, and having a very high fineness. Boral (2003) states that the average particle diameter is 3 μm with a minimum of 50% of particles having a size less than 3.25 microns and a minimum of 90% of particles having a size less than 8.50 microns.

Little research has been conducted on the effects of ultrafine fly ash on the durability and mechanical properties of a concrete. However, estimations of the behavior can be made through comparison with ordinary fly ash based upon chemical composition and particle size. The addition of ultrafine fly ash will influence the properties of a fresh concrete similarly to ordinary fly ash. Differences in workability and bleeding from that of ordinary fly ash are attributed to the smaller average particle size.

The higher surface area of the ultrafine particles increases water demand. Therefore, the addition of ultrafine fly ash reduces workability when compared to ordinary fly ash. However, workability is increased when using ultrafine fly ash as a replacement for portland cement (Boral 2003). Bleeding is also affected by the particle size. The ultrafine fly ash particles will pack between cement grains and aggregate. Consequently, the mixture is more cohesive and a reduction in bleeding is achieved.

Jones et al. (2006) conducted 72-hour heat of hydration experiments on 30% ultrafine fly ash and 30% ordinary fly ash mixtures. Because of the retardation of C_3A hydration, the rate of

heat evolution was impeded by 2 hours and 5 hours for the ordinary fly ash and ultrafine fly ash mixtures, respectively. They have shown that both mixtures lower the total heat of hydration when compared to the control. The ultrafine fly ash mixture showed the lowest total heat until 18 hours. Beyond 18 hours, the ordinary fly ash mixture had the lowest total heat.

Because the mineral composition is the same, ultrafine fly ash will have similar chemical reactions to that of ordinary fly ash. However, because the average particle size of ultrafine fly ash is much smaller, the reactivity will increase. Consequently, the strength and durability on the concrete will be higher at early ages.

Boral (2003) found that there is an increase in strength activity index compared to the control: 107% at seven days and 124% at 28 days. Furthermore, they have conducted compressive strength tests on 8% silica fume, 6% ultrafine fly ash, and 9% ultrafine fly ash mixtures with the following characteristics: w/cm of 0.26 – 0.28, cement = 823 lb/yd^3, and fly ash = 100 lb/yd^3. They have shown that a 6% replacement of ultrafine fly ash has nearly equal compressive strength at 7 and 28 days, and roughly a 5% increase at 91 days when compared to an 8% silica fume concrete. A 9% replacement showed increases over the 8% silica fume concrete of roughly 6%, 8%, and 11% at 7, 28, and 91 days, respectively. Jones (et al. 2006) researched the effects of 15% and 30% replacements of ordinary and ultrafine fly ash at a 0.50 w/cm on cube strength. They found that at 28 days, the control mixture had the highest strength (Table 7). At 90 and 180 days, both ultrafine fly ash mixtures showed higher strength than the control, while both ordinary fly ash mixtures were lower.

Table 7–Cube strength of fly ash concrete normalized by control strength (Jones et al., 2006)

Mixture	Test age		
	28 day	**90 day**	**180 day**
Control	100	100	100
15% Ordinary Fly Ash	75	85	87
30% Ordinary Fly Ash	54	30	64
15% Ultrafine Fly Ash	96	116	110
30% Ultrafine Fly Ash	87	102	104

At each age, the ultrafine fly ash mixtures showed an improvement in compressive strength over the ordinary fly ash (Table 8). Therefore, it is evident that the decreased particle

size of the ultrafine fly ash increases the strength development at early ages relative to that of ordinary fly ash.

Table 8–Percent increase in compressive strength when fly ash is replaced by ultrafine fly ash

Mixture	Test age		
	28 day	90 day	180 day
15% Ultrafine Fly Ash	27%	36%	39%
30% Ultrafine Fly Ash	61%	45%	64%

Research conducted by Boral (2003) has also shown improvement in concrete mixtures containing ultrafine fly ash in reducing chloride penetration. They measured chloride diffusion coefficients for 8% silica fume, 8% ultrafine fly ash, and 12% ultrafine fly ash mixtures (0.40 w/cm) at 40 days and 2 years. At both ages, the ultrafine fly ash mixtures showed lower coefficients when compared to the control. It appears that the 12% replacement showed slightly better results that the 8% mixture. Neither ultrafine fly ash mixture, however, had lower coefficients than the silica fume mixture.

Jones et al. (2006) researched the effects of 30% replacement of ordinary fly ash and ultrafine fly ash on the total CH content within a mixture. They found that from an age of 3 days to 90 days, the ultrafine fly ash mixtures showed a lower CH content when compared to the ordinary fly ash mixtures. This indicates that ultrafine fly ash is more reactive and has consumed more CH through pozzolanic reactions

2.6.6 Slag

Blast furnace slag is the residue wastes formed from the production or refinement of iron. Slag is removed from the molten metal and rapidly cooled. The raw slag is then dried and ground to a specific fineness so that it can be used as a cement replacement. ASTM C 989 provides three grades for slag based upon its relative strength to a reference mortar made with pure cement (Table 9).

Table 9–Slag activity index (ASTM C 989)

Designation	7 day	28 day
Grade 80	---	75%
Grade 100	75%	95%
Grade 120	95%	115%

Typically, silica, calcium, aluminum, magnesium and oxygen constitute over 95% of the chemical composition of slag (ACI 233R-03). Because of the high lime content, slag is a hydraulic admixture, meaning it will react with water to form a cementitious compound.

Concrete containing slag as a portion of the cementitious materials typically have better workability in the fresh state than that of similar concrete with portland cement alone. This is thought to be due to smooth dense surface of the particles that absorb little water during mixing. This results in better particle dispersion and fluidity of the paste (ACI 233R-03). Bleeding is typically reduced when slag is ground to a high fineness (finer that portland cement) and used as a replacement for portland cement. If the slag particles are larger than those of portland cement, then the rate and amount of bleeding may increase.

The addition of slag in a mixture increases the silica content and decreases the total lime content. Consequently, more C-S-H is produced resulting in a microstructure that is denser than that of a cement only mixture (Neville 1995). However, the rate of strength gain is initially very slow because of the presence of impervious coatings of amorphous silica and alumina on the slag particles (Mindess et al. 2003). These coatings are broken down in a slow process by hydroxyl ions that are released during the hydration of the portland cement (Neville 1995).

ACI (233R-03) has found that when compared with a portland cement only concrete, the use of Grade 120 slag typically reduces the strength at ages before 7 days; at 7 days and later, Grade 120 slag increases strength. Grade 100 slag reduces strength at ages of less than 21 days, while producing equal or greater strength at later ages. Grade 80 slag shows lower strength at ages less than 28 days, and comparable strength at 28 days and later.

Modulus of rupture is generally increased with the addition of slag at ages beyond 7 days (ACI 233R-03). They suggest that the improvement in modulus of rupture is because of an increased density of the paste and improved bond at the aggregate-paste interface. Neville (1995) has stated that the incorporation of slag does not significantly alter the usual relations between compressive strength and modulus of rupture.

The use of slag in concrete that is water cured does not have an effect on early modulus of elasticity. At later ages, however, modulus is increased ACI (233R-03). Conversely, air cured specimens exhibited reductions in modulus, which is attributed to inadequate curing. Because the modulus of elasticity is most dominantly affected by porosity, prolonged moist curing is particularly important in a slag concrete in which the low early hydration results in a

system of capillary pores which allow for the loss of water under dry conditions (Neville 1995). Consequently, hydration is halted, leaving a porous concrete and reduced modulus of elasticity.

This compound adds to the strength of the mix, while also increasing durability by decreasing the interconnectivity of the voids. In addition, the high silica and alumina content promote pozzolanic reactions. The CH produced from cement hydration will be consumed and transformed into more cementitious compounds. These compounds are in the forms of C-S-H or C-A-H, depending on whether the reactive compound was silica or alumina. These new hydration products are denser and more homogenous than that produced by cement hydration alone.

At early ages, the incorporation of slag in a mixture will increase shrinkage; at later ages, however, shrinkage and creep are not adversely affected (Neville 1995). ACI (233R-03) supports the conclusion that there is no significant effect on shrinkage or creep.

The heat of hydration has been found by ACI (233R-03) to be lower in a 75% slag replacement concrete than in a 30% fly ash concrete or cement only concrete. Slag reduced the early rate of heat generation and lowered the peak temperature.

One benefit of the addition of slag into a concrete arises from the denser microstructure of hydrated cement paste in which more of the pore space is filled with C-S-H than in a cement only paste (Neville 1995). As a result, the permeability is decreased. ACI (233R-03) has found that as the slag content increases, the permeability decreases. Consequently, the resistance to sulfate attack is increased. The resistance to sulfate attack is further increased through consumption of CH, the major component in sulfoaluminate corrosion (Mindess et al. 2003). ACI (233R-03) found that 50% blends of slag with a Type I concrete had the same sulfate resistance as a Type V cement concrete. They have found that the use of slag in a well hydrated concrete reduces the penetrability of chloride ions and the depth of carbonation. However, Neville (1995) presents conflicting opinions regarding improvements in depths of carbonation with the addition of slag. Slag can have a detrimental effect at early ages when there is very little CH present in the concrete. Because of the decreased presence, CH cannot react with carbon dioxide to form calcium carbonate in the pores. Consequently, the depth of carbonation is significantly greater than in a concrete containing only cement. Conversely, the reduced permeability of slag concrete at later ages prevents continued increases in depth of carbonation.

2.6.7 Metakaolin

Metakaolin is manufactured by calcining kaolin or kaolinite clays at temperatures between 650 and 800ºC (Vu 2002). This results in a material that is largely composed of highly reactive amorphous aluminosilicates. Mindess (et al. 2003) has reported that the reactive silica and alumina content in metakaolin typically contains about 55% and 35 to 45%, respectively. The particles are plate-like and have an average size of 1 to 2 μm, with a specific surface area of about 15 m^2/g. ACI (232.1R-00) has reported an average size of highly reactive metakaolin to range from 1 to 20 μm. Through pozzolanic reactions, CH will react with both silica and alumina to form a cementitious hydration product. These can be in the form of C-S-H or C-A-H (depending on whether the reactive compound is silica or alumina), which are denser and more homogenous than those produced by cement hydration alone (Mindess et al. 2003).

Zongjin and Ding (2003) have found that a 10% blend of metakaolin reduces the fluidity of the mixture. They have shown that the water demand was increased by roughly 11%, which is attributed to the plate-like particle shape and its tendencies to absorb water. Setting times were shown to decrease by 26% and 36% for initial and final setting times. ACI (232.1R-00) has reported lower adiabatic temperatures for 15 and 30% metakaolin replacements compared to cement only concrete. Conversely, a 10% replacement showed higher temperatures when compared to the control.

ACI (232.1R-00) has shown improvements in compressive strength of 0.3 and 0.4 w/cm concretes with blends of 8 and 12% metakaolin. At ages up to 45 days, each metakaolin mixture showed higher compressive strengths; compressive strength increased as proportion increased and w/cm decreased. Badogiannis et al. (2005) researched the strength development of 0.4 w/cm concrete with metakaolin replacements rates of 10% and 20%. Compressive strength was tested at ages of 1 to 180 days. They have shown that, at these ages, a 10% replacement will increase the compressive strength. However, 20% replacement has shown that the compressive strength was not higher than the control until ages of 7 days and later. In addition, the 20% replacement concrete showed lower compressive strength than the 10% blend at all ages.

Kim et al. (2006) conducted research on metakaolin blends of 5, 10, 15, and 20%. They have shown that there is no significant effect on the flexural strength or splitting tensile strength for replacement levels of 5 to 15%. A slight decrease in strength, however, was noted in the 20% blends at ages less than 28 days.

ACI (232.1R-00) has reported improvements in chloride penetration resistance for both 0.3 and 0.4 w/cm concretes with an 8 and 12% blend of metakaolin. Furthermore, they state that the 12% replacement improved the chloride penetration resistance more than reducing the w/cm from 0.4 to 0.3 in a concrete containing no metakaolin. By reducing the w/cm from 0.4 to 0.36, chloride permeability values for a 10% metakaolin concrete were reduced. Research conducted by Kim et al. (2006) supports the findings by ACI in which increasing metakaolin contents (5 to 20%) reduces chloride ion penetrability at 28, 60, and 90 days. They have also reported on the effects of increasing metakaolin contents on the depth of carbonation, finding that increasing metakaolin content will increase the depth of carbonation at ages of 7, 14, 28, and 56 days. These data suggest that the decreased amount of CH present in the concrete because of the pozzolanic reaction with the additional metakaolin can have a detrimental effect. Because of the decreased presence, CH cannot react with carbon dioxide to form calcium carbonate in the pores (Neville 1995). Consequently, the depth of carbonation is significantly greater in metakaolin concretes than in concretes containing only cement. However, the reduced permeability of metakaolin concrete at later ages prevents continued increases in depth of carbonation.

Justice et al. (2005) compared two different metakaolins (with differing particle sizes) and a silica fume. Test samples included an portland cement blend and three binary blends, each with 8% replacement using one of the three SCMs. Three w/c ratios were used. Durability was one aspect of this study, with RCP testing performed. The blend with finer metakaolin was best at reducing permeability, followed by the blend with the coarser metakaolin and then the silica fume blend. All three were substantially less permeable than the portland cement control. At a w/c of 0.4, the two metakaolin blends passed less than 1000 coulombs while the silica fume blend passed 2000. The control blend passed 5000.

2.6.8 Silica Fume

A by-product of producing silicon metals or ferrosilicon alloys, silica fume is a highly reactive pozzolanic material that is commonly used as a cement replacement in concrete. Escaping gases condense to form a large quantity of highly amorphous silicon dioxide, typically 85 to 98% by weight (ACI 234R-06). Particle size is very small, typically 0.1 to 0.3μm, with a specific surface area of 15 to 25 m^2/g and particles are spherical in shape (Mindess et al. 2003). Silica fume is typically supplied in densified or pelletized form.

Because of the large surface area, silica fume has a higher water demand which must be offset in low w/cm mixtures with a superplasticizer (Neville 1995). However, it was found that the effectiveness of the superplasticizer is enhanced in a silica fume mixture. This is because of spherical shape and small particle size, which allow silica fume particles to pack between cement particles and act as a lubricant (Mindess et al. 2003). An additional benefit of the small silica fume particles packing between cement grains is the reduction in bleeding (Neville 1995). ACI (234R-06) has stated that bleeding is reduced as the content of silica fume is increased because very little free water is available to bleed.

Typically, air entraining admixture in a silica fume concrete must be increased by 125 to 150% over that of similar concrete with cement only (ACI 234R-06). This has been attributed to the high surface area of the particle (Neville 1995).

ACI (234R-06) indicates that there is no significant delay in setting time. However, they have shown that there is an increase in heat of hydration. Peak temperatures increase with higher contents of silica fume because of its interactions with C_3S. Silica fume tends to accelerate the exothermic hydration of C3S (Kurdowski and Nocum-Wezelik 1983); consequently, more CH is produced. In turn, this action starts the pozzolanic reaction with the silica fume, which further increases the concrete temperature. They have also suggested, however, that the total heat is somewhat decreased as the increase in silica fume dosage.

The effect of silica fume on the hardened properties is directly a function of the pore structure, cement paste-aggregate transition zone, and chemical composition (ACI 234R-06). As hydration continues, the pore structure becomes more homogenous and capillary pores sizes are reduced and become disconnected (Neville 1995). However, ACI (234R-06) has found that total porosity is largely unaffected by silica fume at all w/cm.

The cement paste-aggregate zone, or interfacial transition zone (ITZ), is composed of less C-S-H, has a higher localized w/cm and permeability, and contains large crystals of CH and ettringite. Silica fume greatly improves the ITZ by eliminating large pores and making the structure more homogeneous. This eliminates the growth of CH or transforming the already present CH to C-S-H by pozzolanic reaction. Furthermore, the rheological properties of a fresh concrete are improved by reducing internal bleed because the small size of the silica fume particles allow it to pack between cement particles and aggregate. (Mindess et al. (2003))

ACI (234R-06) indicates that concretes made with silica fume exhibit higher compressive strengths at earlier ages, up to 28 days with minimal contribution to compressive strength after 28 days. Neville (1995) indicates that the behavior of silica fume beyond the age of 3 months depends upon moisture conditions. In wet cured conditions, the silica fume concrete showed only a small increase in compressive strength for up to 3.5 years of age. Conversely, under dry conditions a reduction of strength, typically 12% below the peak at 3 months, was observed. These findings indicate the tendencies of a silica fume concrete to self-desiccate. Therefore, adequate curing is essential for full development of strength.

The trends of the development of compressive strength to flexural and splitting tensile strength of a concrete made with silica fume is similar to that of a cement only concrete (ACI 234R-06). In other words, as compressive strength increases, the tensile strength also increases, but with a decreasing ratio. They have found that a 20% silica fume had a compressive to flexural strength ratio that ranged from 0.13 to 0.15. They have also found splitting tensile strength at various ages to range from 5.8 to 8.2% of the compressive strength.

It has been shown that the use of silica fume reduces water permeability and chloride diffusion rates in concrete. ACI 234R-06 indicates that an 8% substitution in a 0.40 w/cm concrete resulted in a reduction in diffusion coefficient by a factor of seven. Furthermore, addition rates above 8% resulted in little additional improvement to resistance of chloride penetration. Reduced permeability is the primary mechanism in which silica fume increases the resistance to sulfate attack by sodium sulfate (ACI 234R-06). However, an additional increase in sulfate resistance occurs from the pozzolanic reactions with silica fume as there is a large consumption of CH, the major component in sulfoaluminate corrosion (Mindess et al. 2003).

Shekarchi et al. (2009) studied the effect of silica fume addition on chloride diffusion at different ages and w/c ratios. Sample specimens were placed in the Persian Gulf and were immersed except for a brief drying period at low tide. Significant drying did not occur. Samples were prismatic, with four sides sealed and two sides exposed. Testing for chlorides involved use of ASTM C1152 and C 114, part 19. For exposure periods of 3, 9, and 36 months, the diffusion coefficient dropped substantially between 0% and 5% silica fume addition. At 3 months age in the 0.5 w/c ratio, the addition of 12.5% silica fume reduced the diffusion coefficient more than lower replacement levels. For later ages with this w/c ratio and for all other w/c ratios at all

ages, replacement levels of silica fume above 5% were not significantly better than 5% replacement at reducing the coefficient of diffusion.

Chini et al. (2003) performed analysis on more than 500 sample sets drawn from Florida. Sample sets were drawn from several classes of concretes as defined by the FDOT, including Class IV, Class IV drilled shaft, Class V, Class V special, and Class VI. Analysis was performed using RCP and SR testing and indicated that mixtures containing silica fume resists chloride penetration better than those containing blast furnace slag or fly ash.

2.6.9 Summary

In summary, all of the SCM previously described improve mechanical and durability properties of portland cement concrete by virtue of their pozzolanic reactions and their ability to fill the portland cement paste pore structure to increase overall density. This increases the compressive strength and slows the diffusion of harmful ions through the concrete. Table 10 provides a reference table that covers the key aspects of each SCM.

Table 10–Summary of SCM effect on concrete properties

SCM	Replacement[b] (% by weight)	Mean particle size (µm)	Effect on Concrete (compared to concrete with no SCM)		1-Year Bulk Diffusion Coefficient[e] (x 10^{-12} m^2/s)
			Fresh Properties	Hardened Properties	
fly ash	18-22	20-30[a]	-improve workability -reduce water demand -delay set time	-reduce heat of hydration -strength gain delay	5.0
ultrafine fly ash	8-12	1-5[a]	-reduce water demand	-improved early strength gain over fly ash	4.8
slag	25-70	varies	-improve workability -increase water demand -delay set time	-strength gain delay -reduction in heat of hydration -may increase early shrinkage	2.7
metakaolin	8-12	1.4[d]	-increase water demand -reduce bleed -delay set time	-early strength gain	1.1
silica fume	7-9	0.1-0.2[c]	-increase water demand -reduce bleed -reduce segregation -increase in susceptibility to plastic shrinkage cracking	-early strength gain	2.1

[a]American Coal Ash Association (2003)
[b]FDOT Specification (2007)
[c]ACI 234R-06
[d]Manufacturer's information
[e]Vivas et al. (2007).

2.7 Effects of Ternary Blends on Concrete Performance

There are two main reasons to blend SCM (Nehdi 2001). The first is to take advantage of particle packing. The use of a SCM to ensure that particle sizes are well distributed produces an improved density and reduced pore structure. This increases compressive strength and resistance to chloride penetration. The second advantage is the synergistic effect of the chemical reactions that are created when using pozzolanic materials.

Prior research into the use of ternary blends composed of portland cement, fly ash, and blast furnace slag is limited. The majority of research into the use of ternary blends has involved some combination with silica fume (portland cement-silica fume-fly ash or portland cement-

silica fume-blast furnace slag) (Bleszynski et al. 2002, Nehdi and Sumner 2002, Popovics 1993, Long et al. 2002, Shehata and Thomas 2002, Khsn and Lynsdale 2002, Khsn et al. 2000, Thomas et al. 1999, Lane and Ozyildirim 1999, Bágel 1998, Jones et al. 1997, Menendez et al. 2003, Isaia et al. 2003, Domone and Soutsos 1995). Other work includes quaternary blends containing all three of the primary SCM (silica fume, fly ash, and slag) (Nehdi and Sumner 2002). SCMs not commonly used in Florida, such as limestone fillers (Menendez et al. 2003) or rice husk ash (Isaia et al. 2003), have also been considered.

The use of ternary blends in high performance concretes is a relatively unexplored field compared to vast research already conducted on binary blends. Currently, there are no national specifications for optimum mixing proportions of ternary blends. Therefore, finding the optimum proportions of ternary blend concretes is often obtained after the testing of numerous trial mixtures (Erdem and Kirca 2008). However, they reported that after an optimal ternary blend has been found, the use of ternary blends can provide mechanical and durability properties similar to silica fume and portland cement binary blends. In addition to consideration of mixing proportions, it is recommended that ternary blends should be a combination of low and high surface area supplementary cementitious materials, such as fly ash and silica fume (Mehta and Gjoerv 1982).

Roske and Hamilton (2008) studied the permeability of several ternary blends, including blends used in the construction of the Key Royale Bridge. Ternary blends incorporated fly ash and portland cement as two of the three cementitious materials. Tests included mechanical and chloride penetration tests. The rapid migration test method indicated that all of the ternary blends experienced less chloride ion penetration than the control. Of the ternary blends, the silica fume blend showed the best performance, followed closely by metakaolin. Depending on the age at which the test was conducted, either the ultrafine fly ash or blast furnace slag had the least improvement over the controls. All four ternary blends were acceptable for use in extremely aggressive environments at 91 days after concrete placement, although only ternary blends with silica fume or metakaolin were acceptable at 28 days after placement. Table 11 summarizes some of the characteristics of the different ternary blend concrete mixtures used in the present research.

2.7.1 Fly Ash and Silica Fume Ternary Blends

While the addition of fly ash in concrete mixes is common, the reduced early strength in fly ash and portland cement concretes is still a concern. Meanwhile, silica fume has been shown to provide a source of early strength development. However, the use of silica fume in modern concrete blends is limited due to the high costs of silica fume itself and the high quantities of super-plasticizer needed to provide adequate workability. Fortunately, research has shown that the combinations of certain additions may provide more benefits for concrete when compared to the use of a single admixture.

Compressive strengths of concretes containing a combination of portland cement, fly ash, and silica fume are higher at 28 days and later than mixtures containing only portland cement. However, at 3 and 7 days, mixtures containing both fly ash and silica fume produce compressive strengths lower than portland cement only concretes (Khatri and Sirivivatnanon, 1995). The pozzolanic activity of silica fume- fly ash ternary blends, and portland cement only concrete mixtures were measured through the analysis of the free lime content in each mixture. It was discovered that mixtures containing silica fume and fly ash indicated signs of higher pozzolanic activity at 7 and 28 days than portland cement only concretes (Mehta and Gjoerv 1982).

The flexural strength and elastic modulus of ternary blends increase due to the addition of fly ash and silica fume ternary blends. However, all gains in flexural strength and elastic modulus were found to be proportional with the gains found in compressive strength (Khatri and Sirivivatnanon 1995). The inclusion of fly ash on mixtures containing silica fume and portland cement show superior creep characteristics than those of portland cement only concrete (Khatri Sirivivatnanon 1995). The addition of fly ash on silica fume and portland cement concrete mixtures produces decreased specific creep values than portland cement only mixtures due to the increases in compressive strength and modulus of elasticity. The calculated specific creep values for silica fume, fly ash, and portland cement ternary blends still produce values higher than silica fume and portland cement binary blends. Despite the decrease in specific creep created by the addition of silica fume and fly ash in portland cement concrete mixtures, it has been found that the percentage of fly ash added to silica fume and portland cement concrete mixtures does not affect the specific creep values of a mixture (Khatri and Sirivivatnanon 1995).

The combination of fly ash, silica fume and portland cement in ternary blends is an effective means to reduce the 2 year pore expansion of a concrete mix below the 0.04%

benchmark specified in the Standard Concrete Prism Test (Canadian Standards Association A23.2-14A), which is similar to ASTM C1293 (Shehata and Thomas 2002). The decrease in pore expansion seen by the addition of fly ash into silica fume and portland cement concretes has been found to retard the Alkali Silica Reaction that increases the porosity of concrete with time. The combined use of silica fume with portland cement in concrete has been found to produce lower alkalinity levels at early ages, however, silica fume and portland cement binary mixtures release an alkali solution back into the concrete due to secondary reactions (Berube et al. 1998). Increased alkali concentrations in concrete could potentially cause swelling and expansion in the interior concrete, resulting in cracking. The cracking caused by high alkalinity in the concrete would provide less resistance to corrosion (Neville 1995).

Elahi et al. (2009) studied the durability and mechanical effects of using ternary blends. They determined that silica fume increased the long-term strength of ternary blends containing fly ash. Ternary blends with silica fume SF and fly ash had lower chloride diffusion coefficients than blast furnace slag or fly ash binary blends. These ternary blends also had lower chloride diffusion coefficients than any binary blends across a range of SCM replacement levels.

Thomas et al. (1999) studied the permeability of ternary blends containing 8% silica fume and 25% fly ash. Comparisons between portland cement, binary blends with either fly ash or silica fume with portland cement, and ternary blends indicated that the silica fume and fly ash act synergistically to reduce the diffusion coefficient. The silica fume reduces the diffusion coefficient more than the fly ash at an early age, while the fly ash reduces the diffusion coefficient more than the silica fume at later ages.

Sandberg et al. (1998) evaluated chloride diffusion in concrete samples placed on a pontoon structure near the North Sea. The effects of fly ash and silica fume were analyzed, including a comparison with a fly ash- silica fume ternary blend. For a given w/c, 10% silica fume had better performance than 20% fly ash. For ternary blends with 5% silica fume, increasing fly ash from 10% to 17% was sufficient to more than offset an increase in w/c from 0.35 to 0.40.

Van Etten et al. (2009) studied the durability and mechanical characteristics of ternary blends, including mixtures with silica fume and fly ash. Strength gain was inhibited in mixtures with a high fly ash content, as indicated by tests performed on 28-day samples. From RMT analysis, diffusion (migration) coefficients were lowest in ternary blends containing silica fume.

SR testing indicated that ternary blends containing silica fume develop higher resistance at an early age than other ternary blends. This is consistent with a high initial pozzolanic reaction rate from the silica fume caused by the small size and high reactivity of the silica fume particles. Through 365 days, other ternary blends never achieved SR as high as that achieved by the silica fume ternary blend.

Roske et al. (2008) studied the use of highly reactive pozzolans to improve durability in bridge structures. As part of this project, they analyzed the mechanical and durability aspects of several ternary blends, including two blends containing 18% fly ash and 7% or 9% silica fume. Two controls were used; one control was 100% CEM while the other included 18% fly ash. Compressive strength testing indicated that the 3-day compressive strength of the ternary blends was somewhat lower than that of the 18% fly ash control and substantially less than that of the CEM control. The compressive strength at 365 days was nearly identical for both ternary blends and the 18% fly ash control. Surface resistivity increased very rapidly for the ternary blends; both reached higher resistivity values than either control; the higher the silica fume content, the higher the SR values. At 28 days, the ternary blends were in the "Very Low" penetrability category, indicating suitability for use in extremely aggressive environments. This was supported by RMT results indicating that the fly ash- silica fume ternary blends were appropriate for use in extremely aggressive environments at 28 days.

2.7.2 Fly Ash and Slag Ternary Blends

Ternary blends containing fly ash and slag have become increasingly popular as a substitute for silica fume for producing high performance concrete (Li and Zhao 2002). While both blast furnace slag and fly ash are slower reactive supplementary cementitious materials than silica fume, blast furnace slag typically reacts faster than fly ash resulting in higher earlier strengths than fly ash and portland cement binary concretes. Unfortunately, there is a dearth of published research papers that present results of the mechanical and durability properties of fly ash and blast furnace slag ternary blends.

The compressive strength gains seen in fly ash and blast furnace slag ternary blends at early ages (less than 28 days) have been found to be similar to portland cement only concrete. At later testing ages, fly ash and blast furnace slag ternary blends have been found to outperform portland cement only concretes. Unfortunately, fly ash and ternary blends do not reach the compressive strengths of fly ash and portland cement concretes (Li and Zhao 2002). Li and

Zhao also report that fly ash, blast furnace slag, and portland cement ternary blends have higher modulus of elasticity compared to fly ash and portland cement concretes.

The concretes ability to protect against sulfate attack has been found to depend on the permeability performance of the concrete mixture. Ternary blends containing fly ash, blast furnace slag and portland cement have been found to outperform portland cement only and fly ash and portland cement concrete mixtures. The increase in durability performance is a result of the pore refinement and the generation of discontinuities in the pore structure caused by strong pozzolanic reaction (Li and Zhao 2002).

Haque and Chulilung (1990) investigated the use of 'slagment' (65% portland cement, 35% blast furnace slag) to manufacture structural grade concrete; to characterize ternary blends by replacing a portion of the slagment with fly ash; to provide performance data of the slagment and slagment with fly ash under inadequate and non-standard curing conditions; and to explore the effect of specimen size on strength under standard and non-standard curing conditions. Four curing conditions were considered: control; fog curing; 7 days fog curing; and sealed fog curing. The results reported focused on effects on compressive strength, effects of curing, effects of specimen size, and water penetration. It was found that samples cast with slagment increased in strength faster than with portland cement concrete and that replacement of slagment with fly ash decreased strength. Maximum water penetration was observed in mixtures of 65% slagment and 35% fly ash.

Douglas and Pouskouleli 1991 proposed empirical equations and ternary diagrams from which the compressive strength may be predicted for any combination of portland cement, blast furnace slag, and fly ash. Mixtures with 50% portland cement and 50% blast furnace slag mixtures produced higher compressive strengths than 50% portland cement and 50% fly ash. Mixtures with 50% blast furnace slag and 50% fly ash performed better at 28 days and beyond. It was observed from predicted and experimental results that a 66% portland cement, 17% blast furnace slag, 17% fly ash performed better than 100% portland cement after 28 days. It was also observed that a 17% portland cement, 66% blast furnace slag, 17% fly ash mixture performed better than a 17% portland cement, 17% blast furnace slag, 66% fly ash mix, especially at 28 and 91 days.

Domone and Soutsos (1995) studied the effects of fly ash and blast furnace slag on the workability, heat of hydration, and long-term strength of high-strength concretes. Since the high

strength necessitates a lower binder-water ratio, fly ash+blast furnace slag+portland cement and fly ash+ blast furnace slag +portland cement+silica fume mixes were tested at water-binder ratios from 0.20 to 0.38. They found that high-slump mixes can be made with a water-binder ratio down to 0.2. High slump, however, is insufficient for description of workability of high-strength concretes in practice. Heat of hydration thermal effects were reduced through the use of fly ash and blast furnace slag. Long-term strengths of fly ash and blast furnace slag mixtures may not reach that of 100% portland cement mixtures when the water-binder ratio is reduced to 0.26 and below. The addition of silica fume increased the strength of all mixes.

Using seven design points and three cubic polynomial models, Dehuai and Zhaoyuan (1997) established strength predicting equations of mortars with ternary blends by the simplex-centroid design. The simplex-centroid design, introduced by Scheffe in 1958 and later studied for strength effects by Douglas and Stanish, was used with upper and lower bounds of portland cement, blast furnace slag, and fly ash proportions. Five experimental checkpoints were used to verify the precision of the strength-predicting equations. At seven days the compressive strength of mortars with a water-cement ratio of 0.44 was almost proportional to the proportion of portland cement present. blast furnace slag contributed the most to strength gain at both 7 to 28 days and at 28 to 56 days. fly ash and portland cement contributed the least, respectively.

Thomas and Scott (2010) compared the chloride diffusion coefficients of binary blends utilizing fly ash and ternary blends with fly ash and slag. Bulk diffusion was performed on cores taken from samples that had been exposed in the Bay of Fundy for 25 years. Blends tested included 25% fly ash, 20% fly ash with 40% blast furnace slag, and 20% fly ash with 60% blast furnace slag. At a w/c ratio of 0.4, the two ternary blends had almost identical coefficients of diffusion, with the binary blend slightly higher. At a w/c ratio of 0.5, the ternary blend with 60% slag outperformed the other ternary blend.

Van Etten et al. (2009) studied the durability and mechanical characteristics of several ternary blends, including blends with blast furnace slag and fly ash. The seven day compressive strength of concrete blends containing 20% fly ash and blast furnace slag was reduced compared with the portland cement concrete control; the higher the blast furnace slag content, the higher the strength reduction. Early strength gain was likewise inhibited in ternary blends with a high fly ash content, as indicated by tests performed on 28-day samples. From analysis, diffusion (migration) coefficients were lower than portland cement concrete in ternary blends containing

high levels of blast furnace slag but not as low as those containing silica fume. SR testing indicated that resistivity of ternary blends containing silica fume increased more rapidly after a curing period of 28 days than ternary blends with blast furnace slag. After a curing period of 91 days, however, the rate of SR increase in the silica fume ternary blend had slowed to a rate similar to that of the ternary blends containing blast furnace slag. This is consistent with a higher initial pozzolanic reaction rate from the silica fume than the blast furnace slag caused by the smaller size and higher reactivity of the silica fume particles. Through 365 days, however, the blast furnace slag ternary blends never achieved SR as high as that achieved by the silica fume ternary blend.

Roske et al. (2008) studied the use of highly reactive pozzolans to improve durability in bridge structures. As part of this project, mechanical and durability aspects of several ternary blends were evaluated, including three blends containing 18% fly ash and 25%, 30%, or 35% blast furnace slag. Two controls were used; one control was 100% portland cement concrete while the other included 18% fly ash. The 3-day compressive strength of three blast furnace slag ternary blends was significantly lower than that of either of the controls, with higher blast furnace slag content leading to lower compressive strength. Compressive strength testing indicated that the 3-day compressive strength of the ternary blends was less than that of either control; the compressive strength of the ternary blends was very sensitive to the replacement level of the blast furnace slag with a higher level of blast furnace slag replacement producing a lower strength. The compressive strength at 365 days of the ternary blends containing 25% and 30% blast furnace slag was nearly identical to the 18% fly ash control. The ternary blend containing 35% blast furnace slag was significantly weaker than this control at 365 days, although the authors indicate that there were some mixing problems that may have influenced the quality of the concrete and caused errant results. Surface resistivity increased with age; SR values for the ternary blends were higher than those of both controls at all ages. The ternary blend containing 30% blast furnace slag produced the highest SR values. At 28 days, the ternary blends were in the “Low” penetrability category, suggesting that these ternary blends may not have the optimum early age impermeability required for use in extremely aggressive environments. This was supported by RMT results indicating that the fly ash-blast furnace slag ternary blends had not developed sufficient resistance to chloride migration for use in extremely aggressive environments at 28 days.

2.7.3 Fly Ash and Metakaolin Ternary Blends

Research into the use of fly ash and metakaolin ternary blends is not abundant, although some experiments have been done to evaluate the mechanical and durability of such blends. Like silica fume, metakaolin has a high surface area to volume ratio. This allows for higher early strength gain than the use of pozzolans with lower surface area to volume ratios.

Bai et al. (2003) studied the chloride ingress and strength loss in concrete containing different blends with fly ash and metakaolin. They used four different total cement replacement levels (10%, 20%, 30%, and 40%) and exposed test specimens in synthetic seawater for up to 1.5 years. Mechanical testing indicated that the addition of metakaolin reduced the strength loss compared with both the portland cement concrete controls and the portland cement concrete -fly ash binary blends caused by exposure to synthetic sea water. A ternary blend containing 5% metakaolin and 15% fly ash reduced chloride penetration compared with the portland cement concrete control, although the difference between the two was small enough to have possibly been due to experimental variability. At 30% replacement levels, the binary blend with 30% fly ash and the ternary blend with 7.5% metakaolin and 22.5% fly ash experienced similar reductions in chloride penetration compared with the control, an unexpected result. Blends with 30% replacement and containing 2.5% or 5% metakaolin did not reduce chloride ingress as much as two other blends with 30% replacement. At the 40% replacement level, the ternary blend allowed less chloride penetration than the control as expected. For all blends, the higher the cement replacement rate, the lower the chloride penetration.

Vivas et al. (2007) evaluated different test methods designed to rapidly determine the resistance to penetration of chlorides. Several different blends, including a ternary blend containing 20% fly ash and 10% metakaolin cement replacement were evaluated with these methods. RCP tests performed at 364 days indicated that the ternary blend had a coefficient of diffusion (migration) that was about 80% the value of those of binary blends containing 10% silica fume or 20% fly ash, which were similar to one another. The control mixture had a diffusion coefficient that was three times higher than that of the two binary blends.

Roske et al. (2008) studied the use of highly reactive pozzolans to improve durability in bridge structures. As part of this project, they analyzed the mechanical and durability aspects of several ternary blends, including three blends containing 18% fly ash and 8%, 10%, or 12% metakaolin . Two controls were used; one control was 100% portland cement concrete while the

other included 18% fly ash. The 3-day and 365-day compressive strength of the ternary blends were similar to that of the 18% fly ash control, with the high metakaolin content blends exceeding the 18% fly ash control at 365 days. Surface resistivity increased much more rapidly for the ternary blends than either control; the higher the metakaolin content, the higher the SR values. At 28 days, the ternary blends were in the "Low" penetrability category, suggesting that these ternary blends may not have the optimum early age impermeability required for use in extremely aggressive environments. This was supported by RMT results indicating that the fly ash-metakaolin ternary blends were appropriate for use in extremely aggressive environments at 28 days.

2.7.4 Fly Ash and Ultrafine Fly Ash Ternary Blends

Roske et al. (2008) studied the use of highly reactive pozzolans to improve durability in bridge structures. As part of this project, they analyzed the mechanical and durability aspects of several ternary blends, including three blends containing 18% fly ash and 10%, 12%, or 14% ultrafine fly ash. Two controls were used; one control was 100% portland cement concrete while the other included 18% fly ash. Compressive strength testing indicated that the 3-day compressive strengths of the ternary blends were significantly lower than that of either control blend. The 365-day compressive strengths of the ternary blends were similar to that of the 18% fly ash control. Surface resistivity increased very rapidly for the ternary blends, more rapidly than either control. The higher the silica fume content, the higher the 365-day SR values. At 28 days, the ternary blends were in the "Low" penetrability category, suggesting that these ternary blends may not have the optimum early age impermeability required for use in extremely aggressive environments. This was supported by RMT results indicating that the fly ash-ultrafine fly ash ternary blends had not developed sufficient resistance to chloride migration for use in extremely aggressive environments at 28 days.

Table 11–Summary of ternary blend concrete mixture characteristics

Admixtures (with fly ash)	Characteristics
Silica fume	Low compressive strength at less than 7 days Improved creep performance Lower diffusion coefficient than other ternary blend concrete mixtures at early and later ages Chloride penetration resistance at early ages
Blast furnace slag	Low compressive strength at 3 days Higher early strength than fly ash binary blend concretes Improved durability performance relative to fly ash binary blend concretes May not be for use in extremely aggressive environments at 28 days
Metakaolin	Average compressive strength at 28 and 365 days “Low” SR results at 28 days Rapid gain in surface resistivity May not be for use in extremely aggressive environments at 28 days
Ultrafine fly ash	Low compressive strength at 28 days Average compressive strength at 365 days “Low” SR results at 28 days May not for use in extremely aggressive environments at 28 days

3 Project Chronology

Before the bridge was constructed, the FDOT, in conjunction with the University of Florida, evaluated potential concrete mixture designs to maximize durability (Roske et al. 2008). Based upon FDOT mixture requirements and a literature review, several mixture designs similar to those used in the Key Royale Bridge were created that were thought to maximize durability. These mixtures included binary mixtures with portland cement and fly ash as well as ternary blends containing portland cement, fly ash, and either ultrafine fly ash, metakaolin, blast furnace slag, or silica fume. Cement replacement by supplementary cementitious materials was varied for the different test mixture designs. Mixture designs were evaluated using plastic property and mechanical property tests as well as durability tests. The test results were analyzed with a test matrix which included the cost of the supplementary cementitious materials as an added variable. While some of the longer term testing was not completed in time, the results of the test matrix were used by the FDOT to select concrete mixture designs for use in the Key Royale Bridge piles.

FDOT let the contract for the Key Royale Bridge with project ID 199676-1-52-01 in April 2006. As described in this report, piles were driven in two phases to allow vehicular access to Key Royale to continue throughout the construction sequence. The first phase piles were placed in August 2006 followed by the second phase in January 2007. Durability segments were installed in April 2007 with the bridge fully open to traffic shortly thereafter. Fender piles were installed at the same time as the main bridge piles with fender piles at the north side of the bridge installed with the phase I piles and those at the south side of the bridge installed with the phase II piles.

The Key Royale Bridge is expected to serve as a research platform for decades to come. Initial inspections were carried out within the first year of the operation of the bridge. Inspections included measurements that are recorded in this report. Follow-up measurements were taken one month, 13 months, 25 months, and 5 years after these initial measurements (Table 12). Future monitoring and testing protocols are recommended in this report. Measurements are recommended at five-year intervals until the bridge is removed from service. With a design service life of 75 years, the Key Royale Bridge should provide data until at least 2082.

Table 12–Timeline for Key Royale Bridge activity

Date	Event
April 2006	KRB Contract let
August 2006	Phase I piles installed
January 2007	Phase II piles installed
April 2007	Durability segments installed
May 2007 (Initial)	First Measurements
June 2007 (1 month)	Second Measurements
June 2008 (13 month)	Third Measurements
September, November 2011; April 2012 (5 year)	Forth Measurements
September 2017 (10 year)	Future Measurements, remove and core (6) durability segments
September 2022 (15 year)	Future measurements, remove and test (12) fender piles
September 2027; every 5 years after	Future measurements

4 Structure Description

The Key Royale Drive Bridge (FDOT bridge 136502), located on Anna Maria Island in Manatee County, Florida, was selected for the implementation of the highly reactive SCM. The bridge connects Key Royale with Anna Maria Island and is located in a primarily residential area with light vehicle traffic (average daily traffic of 300 vehicles) traveling at low speeds. The body of water spanned, Bimini Bay, is connected to the Gulf of Mexico and is thus a marine environment with chloride levels of 32000 ppm (FDOT Bridge Environmental Data). The superstructure is a five-span continuous slab supported by pile bent substructures (Figure 10). The substructure components include two end bents and four (4) intermediate bents, with five (5) driven precast, pretensioned concrete piles in each bent. Two pile sizes are highlighted in the foundation schematic shown in Figure 11. The 24-in. square piles are the bridge foundation piles while the 18-in. square piles are fender piles that will eventually be pulled and autopsied in the future to determine how well each concrete has resisted chloride intrusion and to assess the remaining flexural capacity of each member.

The contract for the bridge construction was let in April of 2006. Construction was divided into 2 phases outlined in Figure 12 through Figure 15. The phased sequence was required to maintain traffic flow to Key Royale; only Key Royale Drive accesses the island. During phase I (Figure 12 and Figure 13), two lines of piles were installed for the new bridge while traffic flow was maintained on a portion of the previous bridge. During phase II (Figure 14), traffic was rerouted to the completed section of the new bridge while three additional lines of piles are installed. Finally, the completed bridge was opened to traffic (Figure 15).

A series of highly reactive SCMs were employed in the concrete used to produce the piles, including fly ash (FA), ultrafine fly ash (UFA), ground granulated blast furnace slag (BFS), metakaolin (MET), and silica fume (SF). As indicated in Figure 11, each bent contains five piles, each produced with different mixture designs. This created a series of high performance concretes that are exposed to the same severe environment, allowing for a relative comparison of performance over a long period in actual service conditions. Although not required, a fender system was installed using precast, prestressed concrete piles. These fender piles were produced with the same concrete and at the same time as the respective bridge piles. One additional fender pile was produced with no SCMs, using ordinary portland cement as the

sole cementitious material (CEM). Companion “durability segments” were also constructed with same concrete used in the bridge and fender piles. These were hung from the fender piles in the splash zone and were more heavily instrumented than the bridge or fender piles. Details on these segments are covered in Chapter 7.

Extensive material testing was conducted during and after construction of the piles to document the mechanical characteristics of each of the plant produced mixtures. These data are documented in this report for use in evaluating performance of the bridge piles.

Initial readings were taken from the corrosion instrumentation soon after completion of the bridge and are documented in this report. Additional readings were taken at one year and five years following construction. These readings are expected to provide the data against which future readings can be compared.

Figure 10–Key Royale Drive Bridge was selected for this project.

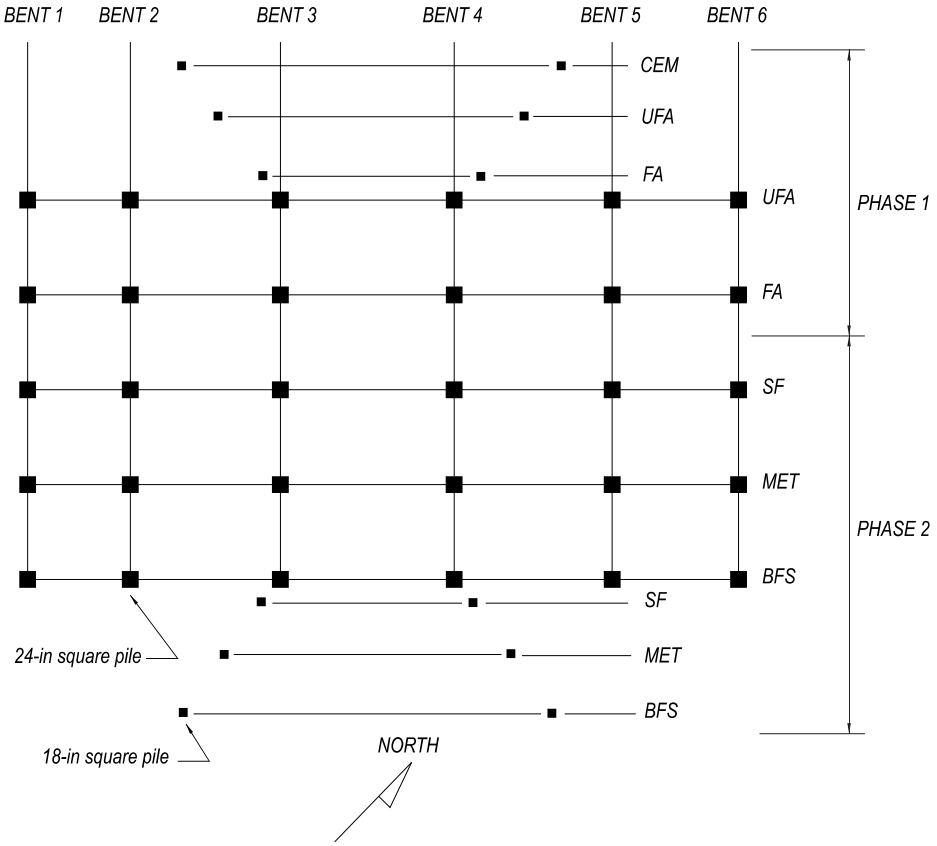

Figure 11–Bridge foundation plan showing bridge and fender pile layout

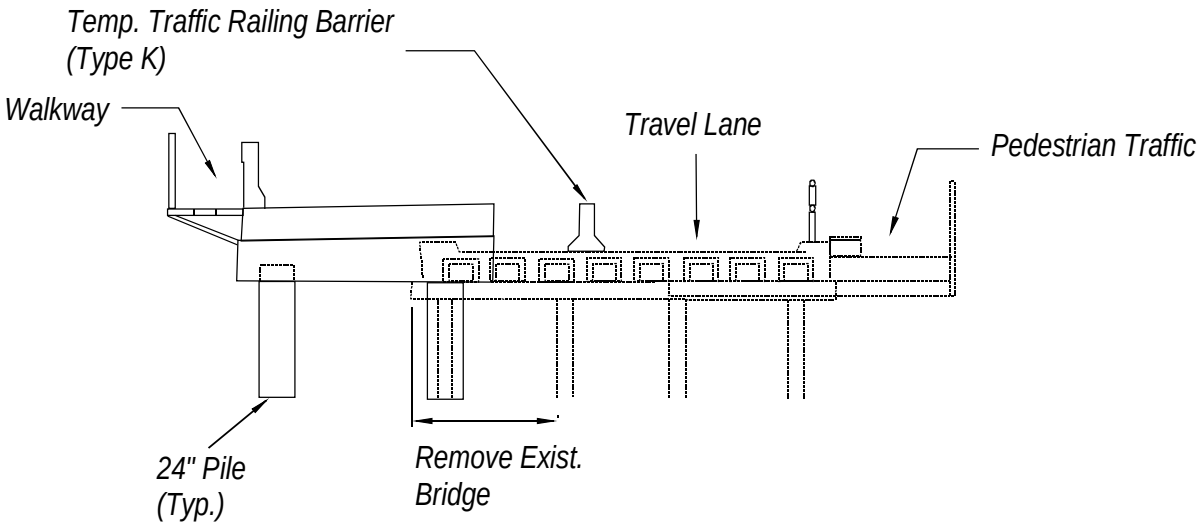

Figure 12–Cross-section of bridge during the phase I construction on August 2006

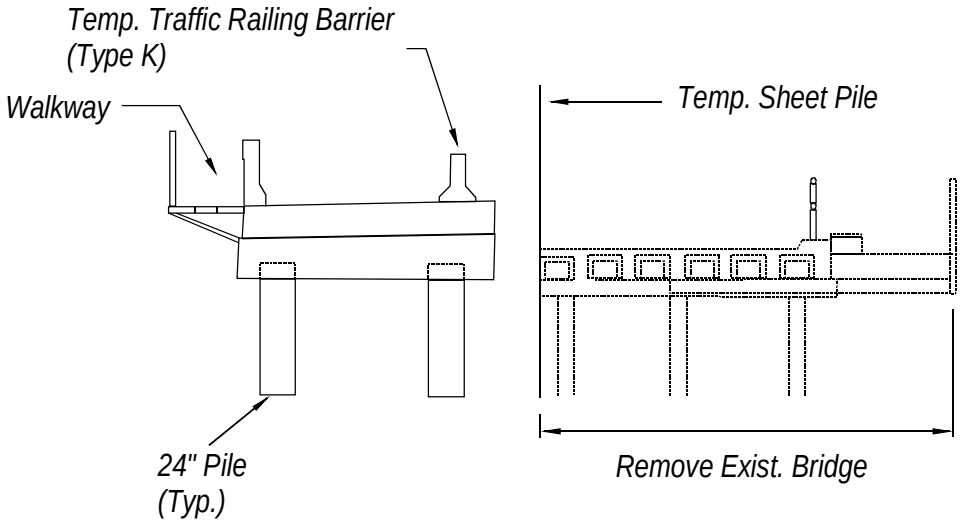

Figure 13–Cross-section of bridge during the phase I construction on August 2006

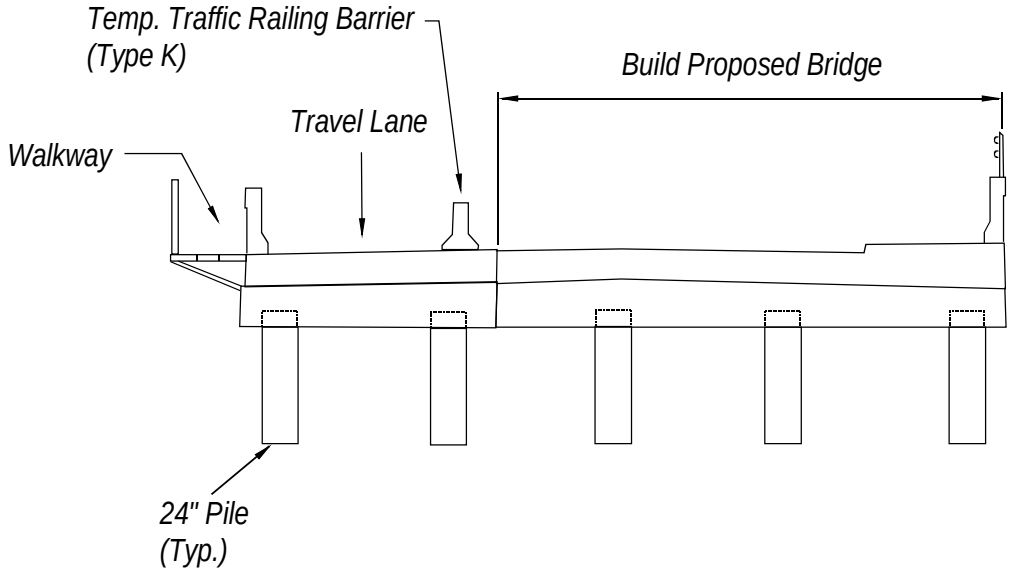

Figure 14–Cross-section of bridge during the phase II construction on December 2006

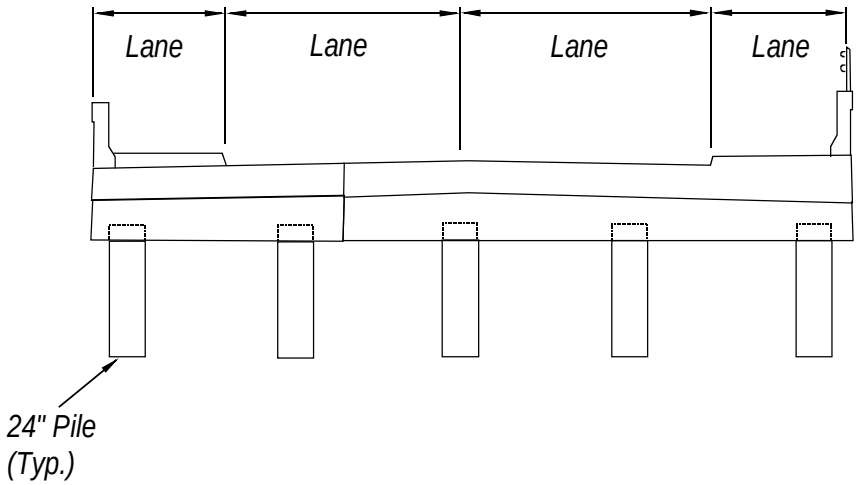

Figure 15–Cross-section of completed bridge on May 2007

5 Concrete Mixture Designs

Thirteen mixture designs containing a variety of highly reactive SCMs were prepared in the FDOT State Materials Office Laboratory. The details of this testing are covered in Roske et al. (2008). The goal was to optimize the mixture proportions to maximize the strength and durability characteristics of concrete. Fly ash (FA), ultrafine fly ash (UFA), ground granulated blast furnace slag (BFS), metakaolin (MET), and silica fume (SF) were all considered (Table 13).

Table 13–Mixture designs considered in preliminary laboratory testing

Mixture Number	Material Quantity (%)					
	Cement	FA	BFS	MET	UFA	SF
1	100	0	0	0	0	0
2	82	18	0	0	0	0
3	57	18	25	0	0	0
4	52	18	30	0	0	0
5	47	18	35	0	0	0
6	74	18	0	8	0	0
7	72	18	0	10	0	0
8	70	18	0	12	0	0
9	72	18	0	0	10	0
10	70	18	0	0	12	0
11	68	18	0	0	14	0
12	75	18	0	0	0	7
13	73	18	0	0	0	9

The laboratory work involved preparing specimens from mixtures with the proportions listed in the table. The following tests were conducted for each mixture series:

- ASTM C 78 – Flexure Strength of Concrete
- ASTM C 157 – Length Change of Hardened Hydraulic-Cement Mortar and Concrete
- ASTM C 642 – Voids in Hardened Concrete
- ASTM C 1012 – Length Change of Hydraulic-Cement Mortars Exposed to a Sulfate Solution
- ASTM C 1585 – Measurement of Rate of Absorption of Water by Hydraulic-Cement Concretes
- FM5-578 - Resistivity as an Electrical Indicator of its Permeability
- NT Build 492 – Rapid Chloride Migration
- Water Permeability
- Modulus of Elasticity

Selection of the final mixture proportions for the bridge piles was based on a decision matrix, which weighted durability, physical properties, and cost. The laboratory tests were divided into two major categories: physical and durability results. The test results were normalized to the results of the tests on the control mixture (Mixture 1). The data were normalized such that ratings that were less than 1.0 were considered an improvement over the control results.

A single rating for each mixture was then compiled. The relative importance of durability and physical results were weighted at 50% and 40%, respectively. The remaining 10% was assigned to cost. The average price per ton of each material was identified and then amassed to determine a normalized cost value.

After the precast supplier had been selected the selected mixture designs were adjusted to accommodate their particular plant practice and typical materials. Final mixture designs used to produce the concrete for the piles are shown in Table 16 and Table 17 with the mixture identifier shown in Table 14. Construction phases with associated mixture designs are presented in Table 15 and Figure 11.

Piles for the Key Royale Bridge were cast in accordance with requirements of the FDOT Structures Design Guidelines (SDG), "current edition". The current edition of the SDG at the time of the Key Royale Bridge project was the January 2005 edition. Class V (Special) concrete was specified for the piles, with minimum cylinder strength of 6,000 psi at 28 days and of 4,000 psi at the time of prestressing force transfer. Silica fume was required in all superstructure piles located within extremely aggressive environments. According to the 2004 edition of the FDOT Standard Specification Section 346, fly ash or slag was a required constituent of all substructure components placed in an extremely aggressive environment. Fly ash was required to be used to replace 18% to 22% of cement by weight while slag was required to be used to replace 50% to 70% of the cement. In cases where silica fume and/or metakaolin were required, the amount of slag substitution dropped to between 50% and 55% of total cementitious materials. Silica fume replacement was specified as being between 7% and 9% by weight while metakaolin replacement was specified as being between 8% and 12% by weight. No guidelines for the use of ultrafine fly ash were provided.

Table 14–Notation used to denote six mixtures used in bridge piles

Designation	SCM
CEM	None
SF	Silica Fume+Fly Ash
MET	Metakaolin+Fly Ash
UFA	Ultrafine fly ash+Fly Ash
BFS	Blast furnace slag+Fly Ash
FA	Fly ash

Table 15–Construction phases and associated mixture designs to be implemented

Pile Label	Phase I			Phase II		
	CEM	UFA	FA	SF	MET	BFS
24-in. Square – 70-ft Long	0	2	2	2	2	2
24-in. Square – 85-ft Long	0	4	4	4	4	4
18-in. Square – 45-ft Long	2	2	2	2	2	2
18-in. Square – 5-ft Long	1	1	1	1	1	1

Table 16–Mixture designs selected for use in CEM, UFA, and FA piles

PHASE I					
Material	Producer	Type	CEM	UFA	FA
Coarse Aggregate	GA-553	#67	1840.0	1840.0	1840.0
Fine Aggregate	36-491	Silica	806.0	806.0	806.0
Cement	Suwannee American	Type II	970.0	670.0	795.0
Fly Ash	ISG	Type F	0.0	175.0	175.0
GGBFS	Civil & Marine	Grade 100	0.0	0.0	0.0
Ultrafine Fly Ash	Boral (Micron3)	Type F	0.0	125.0	0.0
Metakaolin	Optipozz	Type N	0.0	0.0	0.0
Silica Fume	Force 10000D (Grace)	Densified	0.0	0.0	0.0
Water	Local		333.0	333.0	333.0
Air Entr. Admixture	Daravair 1000 (Grace)	AEA	5.0	5.0	5.0
1st Admixture	WRDA 60 (Grace)	Type D	28.6	28.6	28.6
2nd Admixture	ADVA CAST 540 (Grace)	Type F	42.9	42.9	42.9

Table 17–Mixture designs selected for use in SF, MET, and BFS piles

PHASE II					
Material	Producer	Type	SF	MET	BFS
Coarse Aggregate	GA-553	#67	1840.0	1840.0	1840.0
Fine Aggregate	36-491	Silica	806.0	806.0	806.0
Cement	Suwannee American	Type II	715.0	695.0	670.0
Fly Ash	ISG	Type F	175.0	175.0	175.0
GGBFS	Civil & Marine	Grade 100	0.0	0.0	300.0
Ultrafine Fly Ash	Boral (Micron3)	Type F	0.0	0.0	0.0
Metakaolin	Optipozz	Type N	0.0	100.0	0.0
Silica Fume	Force 10000D (Grace)	Densified	80.0	0.0	0.0
Water	Local		333.0	333.0	333.0
Air Entr. Admixture	Daravair 1000 (Grace)	AEA	5.0	5.0	5.0
1st Admixture	WRDA 60 (Grace)	Type D	28.6	28.6	28.6
2nd Admixture	ADVA CAST 540 (Grace)	Type F	42.9	42.9	42.9

6 Pile Design and Construction

6.1 Design

The bridge was designed by Avart Consulting Engineers under the supervision of FDOT District One. Based on the two soil borings taken for this project, the soil is divided into approximately three layers. Soil borings were taken from elevation +10 to elevation -80 (NGVD). The top 40 feet of soil is poorly graded sands and gravelly sands, below which is a 30-foot-deep layer composed of a combination of inorganic clays of high plasticity and fine sands or silt. The bottom 20 feet is all sand-silt mixtures. Pile design was based on standard FDOT drawings from the State Structures Design Office. The selected strand pattern for the 24-in. bridge pile was (20) ½-in. diameter special low relaxation seven-wire strands evenly distributed around the perimeter (Figure 17). The strands were ASTM A416 GR270 with a specified ultimate strength of 270 ksi. The selected strand pattern for the 18-in. fender pile was (12) ½-in. diameter strands evenly distributed around the perimeter (Figure 18). For both pile types, each strand was to be prestressed to 34.0 kips. The design calls for a 1000 psi uniform compression in the pile section after prestress losses and without loads applied. Both piles were designed with 3-in. of clear cover over the spiral ties as required by FDOT for piles in marine environments.

The design concrete strength (f'_c) was 6,000 psi at 28-days with a minimum compressive strength of 4,000 psi at the time of prestress transfer. The required pile lengths were such that splices were not needed. More details on the prestressing information, such as actual stress level, stress pattern, and stress results can be found in Appendix A–Pile Construction.

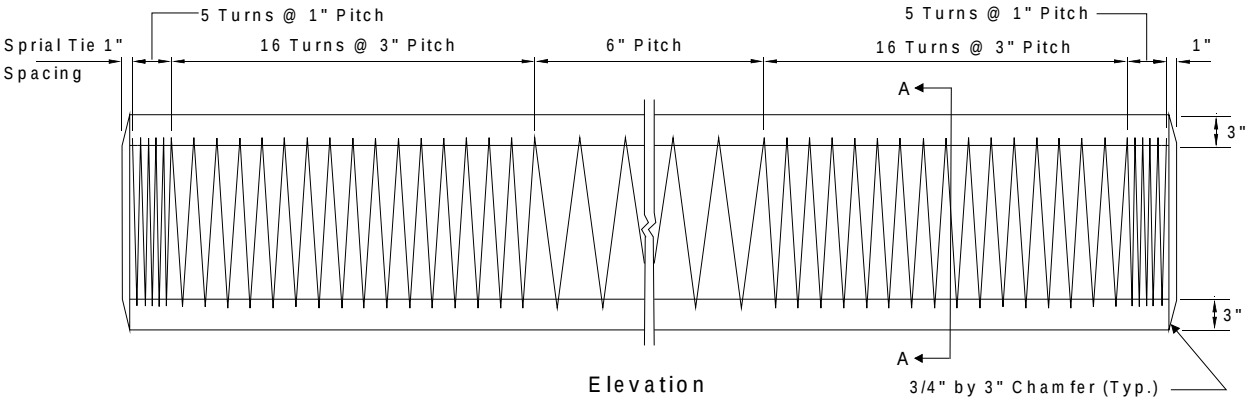

Figure 16–Spiral ties spacing for 18-in. and 24-in. piles

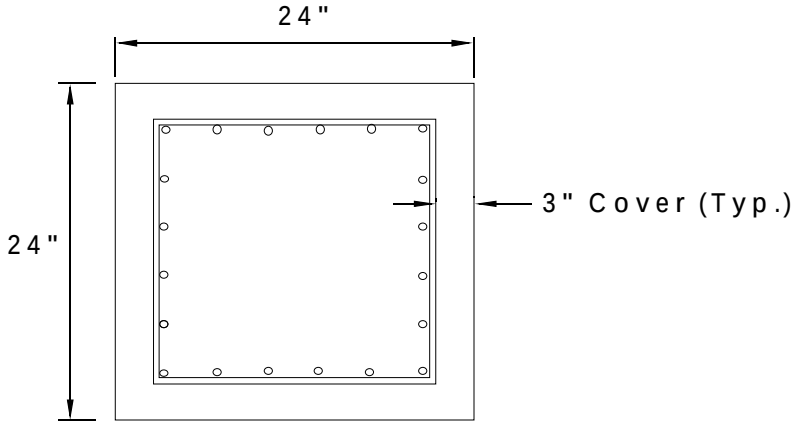

Figure 17–Cross-section of 24-in. square piles

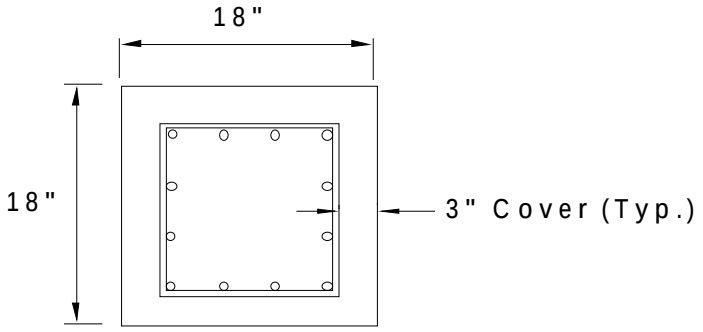

Figure 18–Cross-section of 18-in. square piles

6.2 Pile Production and Material Sampling

Six bridge piles, two fender piles and one durability segment were produced from each mixture. Four of the bridge piles (for the intermediate bents) were 85-ft. long and two of the bridge piles (for the end bents) were 70-ft. long. The fender piles were 45-ft. long. The six piles and single durability segment were cast in a single bed during a single production run of concrete. This ensured that all of the piles contained the same concrete, prestressing strand and were prestressed to the same stress level at transfer. Two additional fender piles and a durability segment created using the concrete mixture without SCM were cast separately.

Prestressing strand was pulled using standard plant practice and according to FDOT specifications (Figure 19). Elongation and force were monitored and recording accordingly. Detailed prestressing logs are included in Appendix A–Pile Construction. The stressing dates for each pile are shown in Table 18. Before casting the piles, corrosion instrumentation was installed. (See Chapter 6.4 for instrumentation plan).

Table 18–Pile casting schedule

Piles	Strands Pulled	Pile Cast
CEM18	6/15/06	6/16/06
UFA24	6/5/06	6/6/06
UFA18	6/8/06	6/9/06
FA24	6/22/06	6/23/06
FA18	6/15/06	6/16/06
SF24	9/28/06	9/29/06
SF18	9/28/06	9/29/06
MET24	10/12/06	10/13/06
MET18	10/12/06	10/13/06
BFS24	10/5/06	10/6/06
BFS18	10/5/06	10/6/06

Figure 19–18-in. fender pile with stressed prestressed strands in place

Piles were cast using concrete buggies with 5 cubic yard capacity (Figure 20). The on-site batch plant mixed a sufficient quantity of concrete for the buggy and discharged for transport. The quantities were documented on a mixture ticket, which are included in the Appendix A–Pile Construction. Typical time from mixture discharge to placement in the forms was approximately 10 minutes. Lifting loops made of bent strand sections were stabbed into the concrete immediately after screeding (Figure 21).

Figure 20–Pile casting at precast yard

Figure 21–Lifting loops were inserted into the fresh concrete after screeding

6.3 Curing, Prestress Transfer, and Transportation

Immediately after the piles were cast, burlap was applied to the exposed surface and a sprinkler maintained moist curing conditions for three days as required by FDOT for piles in a marine environment (Figure 22). When the concrete reached sufficient compressive strength after curing, the strands were torch-cut to transfer the prestress. The piles and segments were then lifted out of the casting bed and placed adjacent to the prestressing bed. The lifting loops were then torch-cut (Figure 23) and Pilgrim EM 5-2 epoxy was applied to the area to provide corrosion protection (Figure 24 and Figure 25). During installation of the lifting loops, a small foam piece was pushed into the concrete around the lifting loops. This allowed the loops to be

cut below the surface of the concrete. The epoxy was then applied to provide protection. These epoxy areas of pile were all cut off after the piles were driven to the final elevation. Previous research (Cannon et al. 2006) has shown this area to be particularly prone to corrosion.

After removal of the lifting loops, the piles were stored at the prestress yard awaiting transportation. The durability segments and sample segments were transported to UF to complete instrumentation and allow sampling.

Figure 22–Moist curing at precast yard

Figure 23–Flame cutting of lifting loop after the pile was removed from the casting bed.

Figure 24–An epoxy was applied to the area for corrosion protection.

Figure 25–Pilgrim EM 5-2 epoxy was used to provide corrosion protection.

6.4 Sampling

Extensive material sampling was conducted to document the mechanical properties of the concrete mixtures used in the pile construction. Molded cylinder and beam samples were obtained from the buggies during the pour as shown in Figure 26. Additional samples were cored from a short segment of concrete that was cast when the piles were cast (Figure 27). This allowed comparison of the molded specimens to the cored specimens. Each sample segment and durability segment was cast using the same concrete as was used to cast the fender piles. Table 19 and Table 21 outline the number and types of samples taken from each mixture for laboratory testing. Appendix B contains the detailed results of the testing that was conducted in accordance with the following standards:

- ASTM C 39 – Compressive Strength of Cylindrical Concrete Specimens
- ASTM C 496 – Splitting Tensile Strength of Cylindrical Concrete Specimens
- ASTM C 78 – Flexural Strength of Concrete
- ASTM C 469 – Static Modulus of Elasticity and Poisson's Ratio of Concrete in Compression
- FM 5-578 - Concrete Resistivity as an Electrical Indicator of its Permeability
- NTBuild 492 – Chloride Migration Coefficient from Non-Steady-State Migration Experiments
- ASTM C 512 – Creep of Concrete in Compression
- ASTM C 642 – Density, Absorption, and Voids in Hardened Concrete

Figure 26–Molded cylinders and beams were used to sample the concrete from each representative mixture

Figure 27–Sample segment with debonded strands from which cores were taken (a) side view (b) top view

Table 19–Summary of number and types of samples taken from each mixture (18-in. fender pile)

Mixture	Type of samples			
	4-in.dia x 8-in. cylinder	6-in.dia x 12-in. cylinder	4-in. x 4-in. x 14-in. square beam	Cored 4-in.dia x 2-in. cylinder from 5 ft sample segment
CEM	18	9	5	8
UFAF	18	9	5	8
FAF	18	9	5	8
SFF	18	9	5	8
BFSF	18	9	5	8
METF	18	9	5	8

Table 20–Summary of number and types of samples
taken from each mixture (24-in. bridge pile)

Mixture	Type of samples
	4-in.dia x 8-in. cylinder
UFA	9
FA	9
SF	9
BFS	9
MET	9

Table 21–Summary of types of sample used in each test

Concrete Property	Type of sample
Compressive strength	4-in.dia x 8-in. cylinder
Split tensile strength	4-in.dia x 8-in. cylinder
Modulus of rupture	4-in. x 4-in. x 14-in. square beam
Modulus of elasticity	4-in.dia x 8-in. cylinder
Surface resistivity	4-in.dia x 8-in. cylinder
RMT	Cored 4-in.dia x 2-in. cylinder from 5 ft sample segment
Creep Coefficient	6-in.dia x 12-in. cylinder
Voids and Absorption	Cored 4-in.dia x 2-in. cylinder from 5 ft sample segment

High early compressive strength is desirable to allow prestress transfer as early as possible and minimize the time piles must spend in the prestressing bed. Furthermore, high early compressive and tensile strengths are needed to prevent pile damage during handling and driving. Figure 28 shows the compressive strength gain curves for all the mixtures in which all of the piles meet the 28-day strength of 6000 psi. All mixtures except MET have higher strength than the CEM mixture at 28 days. SF has the highest strength at this point because of its high reactivity at early ages. At 365 days, all the mixtures have compressive strengths well above that of the CEM mixture, although not enough samples of UFA were available to test at 365 days.

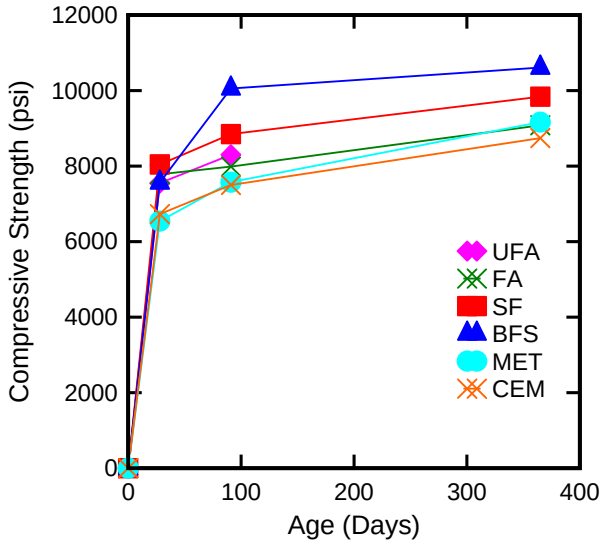

Figure 28–Compressive strength of all mixtures at 28, 91, and 365 days

Beam tests were conducted to determine the modulus of rupture (MOR). ACI (363R-92) has recommended using the following formula as a prediction of the tensile strength of concrete as measured by the MOR from the compressive strength:

$$MOR = 11.7 \times \sqrt{f'_c} \qquad \text{Equation 12}$$

where f'_c is the 28-day compressive strength (psi). Table 22 shows the MOR and compressive strength results for all of the mixtures, along with the calculated coefficients based on the tested 28-day compressive strength. At 28 days, MOR for MET, FA, UFA, and CEM were all less than that suggested by Equation 12. The 28 day MOR for BFS and SF, however, are well above that of the CEM mixture, indicating that these mineral admixtures appear to be reacting more quickly than the others.

Table 22–Modulus of rupture, compressive strength, and coefficient at 28 days

Mixture	28 days		
	f_r	f'_c (psi)	$f_r / \sqrt{f'_c}$
UFA	889	7550	10.2
CEM	893	6730	10.9
FA	857	7780	9.7
SF	1218	8040	13.6
BFS	1262	7560	14.5
MET	933	6540	11.5

Figure 29 shows the increase in surface resistivity with time for all the mixtures. At 28 and 91 days, all mixtures have higher SR values than the CEM mixture. SF and BFS have the highest SR values at this point, indicating the high early reactivity of these admixtures when compared to the others. Note that 365-day results are not available for the UFA samples. It is anticipated, however, based on the early results, that UFA will have SR values comparable to SF and BFS mixtures at 365 days. According to FDOT specifications, when mixtures are prepared for approval the test mixtures that contains SF, MET, and UFA are required to have a SR value equal or higher than 29 kΩ-cm at 28 days. Although field samples are not currently tested for SR it is interesting to note that for these samples taken at the plant site, SF, BFS, and FA have SR value higher than the value required for mixture design approval.

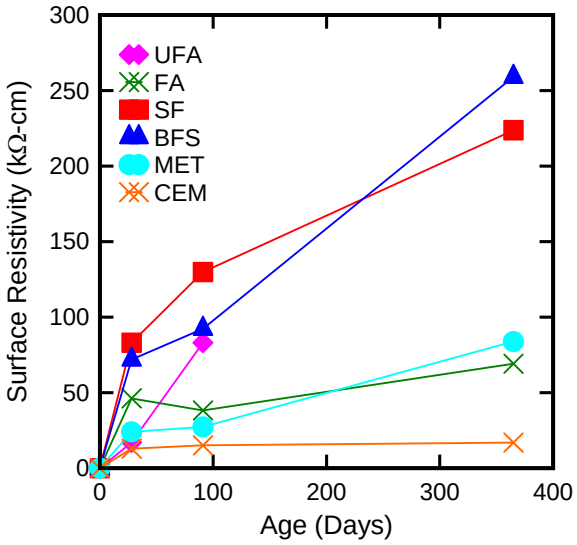

Figure 29–Surface resistivity of all mixtures at 28, 91, and 365 days

The rapid migration test (RMT), another electrical conductivity test, was also conducted on specimens gathered during pile casting. Figure 30 shows the average non-steady-state migration coefficient curves for all mixtures. The coefficient gives an indication of the permeability of the concrete, with a smaller coefficient indicating a less permeable concrete. At 56 days of age, the SF mixture had the highest coefficient; this contradicts previous testing. The CEM mixture should have had the highest coefficient at this time but did not. These results suggest that errors occurred in some of the samples run at 56 days, possibly errors in the voltage setting, sample preparation, or test duration. Results from the 180-day testing indicate that the UFA and BFS had the lowest migration coefficients, followed by SF, MET, and FA. The diffusion coefficient for the FA mixture was significantly higher than those of the ternary blends but lower than that of CEM, which had a much higher coefficient than the other mixtures. The UFA mixture had a very low coefficient, indicating that the pozzolanic reactions continued to reduce pore interconnectedness through 180 days. The results of this testing suggested that the ternary blend mixtures tested, including UFA, BFS, MET, and SF, would resist chloride penetration well with the FA binary blend mixture providing less protection. CEM would provide the least protection of the mixtures tested.

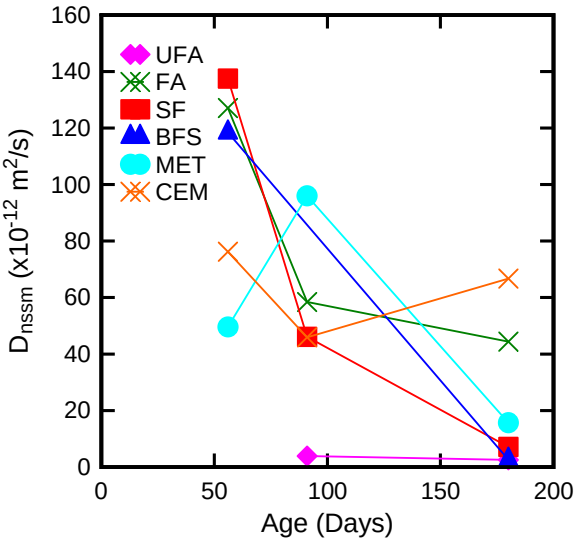

Figure 30–RMT of all mixtures at 56, 91, and 182 days

6.5 Pile Installation

Because residential structures were relatively close to the site, holes were predrilled before piles were placed and driven. For bents 3 and 4, steel casings (42-in. diameter) were installed first using a vibratory hammer (Figure 31). Lead holes were predrilled to elevation -60 ft. using a 32-in. diameter auger drill. Piles were then lowered into the predrilled holes and casing. Some loose soil remained in the casing after auger drilling because soil spilled into the casing during drill retraction so the pile tip did not reach near the bottom of the casing. The piles were then placed in the holes and driven to approximately 1 foot below the bottom of the casing until refusal of the hammer was reached. The final tip elevations of these piles in bent 3 and 4 were at approximately -61 ft.

For the remaining bents, casing and predrilled holes were vibrated and drilled to elevation -30 ft before the piles were placed in the casing. Unlike the piles in bent 3 and 4, piles were driven to about 18 ft below the tip of casing. So, the final tip elevations of these piles were approximately at -48 ft. Top of the piles were cut to desired elevation after the driving.

Pile driving logs were prepared by the contractor, Cone and Graham. The driving logs show the first blow of pile driving started at approximately 7 feet above the tip of casing. The blow count per foot (bpf) in the casing is relatively small compared to the bpf as the pile tip approaches the last 2 feet of the casing. This indicates the hammer was not striking the pile perfectly straight down the casing or the piles were not aligned straight down through the casing.

Consequently, the piles were actually striking against the casing as the piles were driven down to the bottom of casing. When the piles reached the last foot or 2 feet of casing, the piles were driven into the left over soil that was spilled out during the lifting of the auger drill and eventually through the casing into a stiff soil layer. This was verified by the large bpf (over 100) for the last 2 feet of driving in the driving logs.

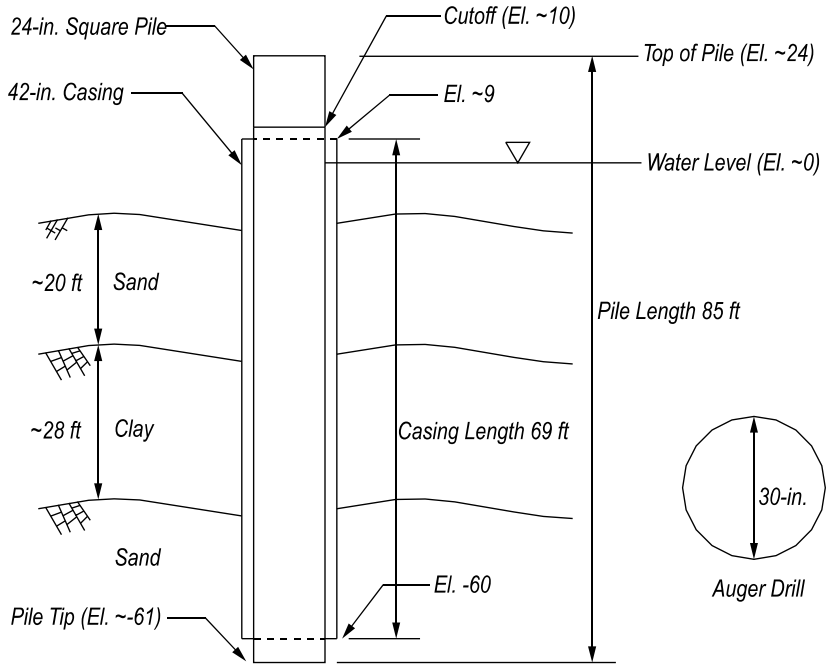

Figure 31–Pile installation for piles in bents 3 and 4 (not to scale)

Figure 32–Pile driving

Figure 33–Pile being lifted into position for driving

7 Pile Instrumentation

7.1 Overview

Accelerated corrosion testing in laboratory conditions is commonly used to evaluate the relative performance of materials and systems under typically unrealistic harsh conditions. The construction of the Key Royale Bridge provides an opportunity to monitor substructure corrosion in a marine environment under realistic exposure conditions and in real time. Instrumentation was designed to be monitored periodically over several years rather than continuously. Electronic measurement systems that take measurements continuously were avoided due to the maintenance needed and unknowns concerning the service life of such systems. Another key element in the plan is that removable elements such as the durability segments and fender piles were included in the construction. These elements can be destructively sampled or even removed without affecting the bridge serviceability.

7.2 Corrosion Sensors

Electrodes were cast into the concrete with wiring arranged in an electrical box at the surface to allow periodic measurements using portable electronic devices. Bridge piles in bent 3 and 4 were instrumented with these corrosion sensors as shown in Figure 34. The corrosion sensors consisted of titanium and steel electrodes (Figure 35 and Figure 36). The steel electrode was fabricated from a short piece of grade 60 reinforcing bar and was intended to measure corrosion potential and serve as the working electrode when measuring corrosion rates. The titanium electrode, fabricated from a titanium core with a mixed metal oxide coating was intended to be the counter electrode for use in measuring corrosion rates of the steel bars. The electrodes were oriented in the same plane as the prestressing strand so that the clear cover was the same as that of the strand (Figure 37) and fixed in place with nonconductive material to ensure no electrical contact with the strands.

Terminals in the electrical junction box were formed by soldering the copper stranded lead wires to stainless steel bolts. The soldered connection was then coated with the Scotch-Kote ™ (Figure 38). Each bolt was covered with a rubber cap to prevent any contacts between the wires that may cause any closed circuit. It is recommended that after each periodical reading, a new layer of Scotch-Kote ™ be placed on the connection to prevent corrosion.

Each pile was instrumented with two sets of corrosion sensors. One set was installed approximately 2 ft above the mean high water level (MHW). The second set was installed 2 ft above the splash zone for comparison. Leads from the corrosion sensors were terminated at an electrical box to allow quick connection to a digital multimeter for measurement. Corrosion sensors were fabricated at UF and installed at the prestress yard by UF personnel. These corrosion sensors underwent quality control (stability of natural potential readings on titanium electrodes) at FDOT State Materials office (SMO) by UF staff. Details of corrosion monitoring are described in subsequent chapters.

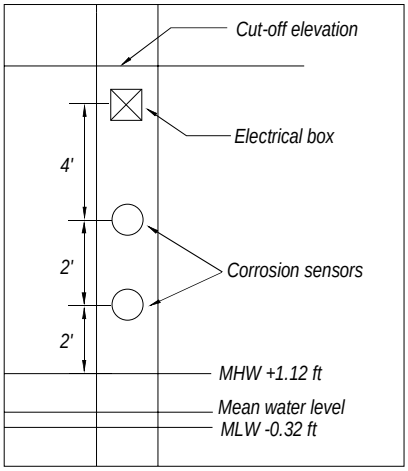

Figure 34–Location of corrosion sensors

Figure 35–#3 steel electrode with 2-in. length of the electrode exposed

Figure 36–¼ -in. diameter titanium electrode with 2-in. length of the electrode exposed

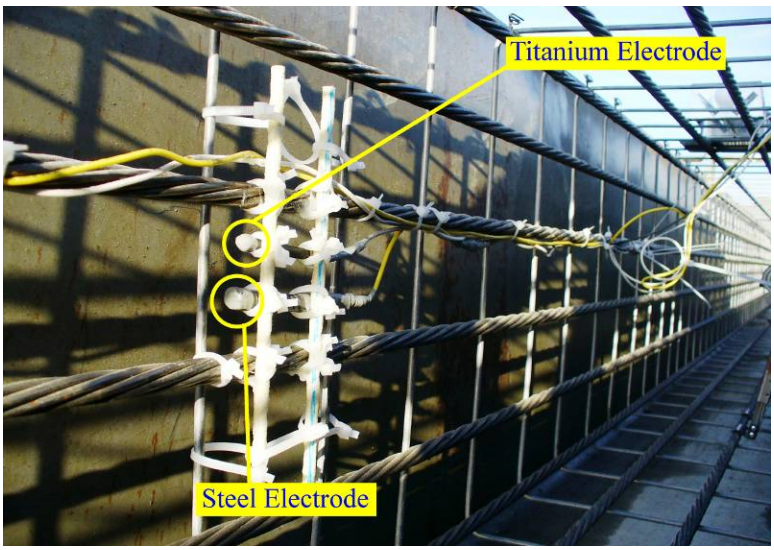

Figure 37–Wired corrosion sensors (top-titanium, bottom-steel)

Figure 38–Protection of the wires in the electrical box

7.3 Covermeter

Covermeter measurements were made after piles were cast to verify the depth of the prestressing strands within the 24-in. piles. A total of five locations were measured for each pile, one at each tip and three locations along the length. The depth of cover at the pile tips were measured with a ruler. The end measurements also provided a location to calibrate the covermeter.

For the 70-ft piles, measurements were taken 15 ft from each end and at the mid-length. For the 85-ft piles, measurements were taken at 20 ft from each end and at mid-length. Each 24-in. pile has a total of 20 strands, requiring a total of 24 depth measurements taken as shown in Figure 39. The covermeter data are included in the appendix.

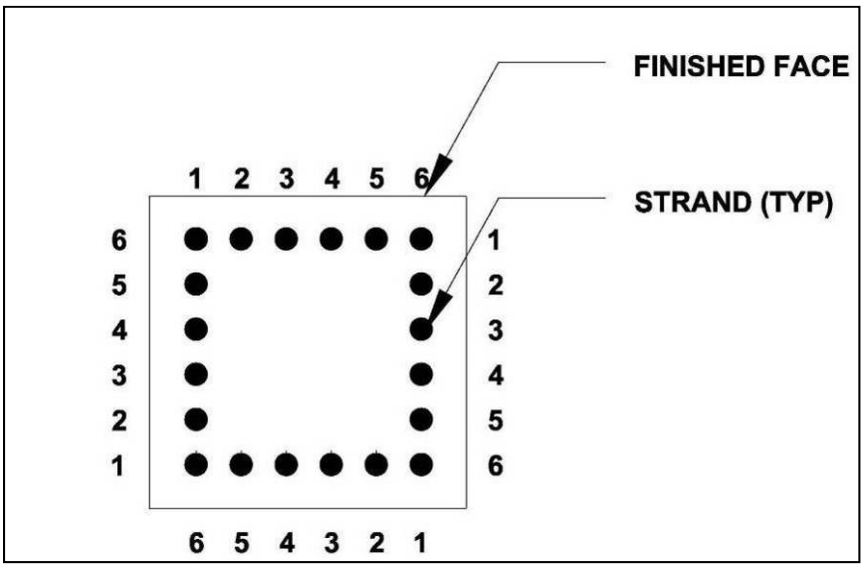

Figure 39–Cross-sectional view of 24-in. pile with strand nomenclature and layout

8 Durability Segment

It was anticipated that the final elevation of the instrumented bridge piles would vary depending on the individual driving conditions. This would result in variation of the final elevation of the corrosion sensors relative to the water line and splash zone. This difference will affect the corrosion readings due to the variation in the exposure conditions at each of the corrosion sensors. To ensure a uniform exposure at the corrosion instrumentation, short slab-shaped concrete sections ("durability segments") were cast at the same time and using the same concrete and prestressing strand as the fender piles. These segments were instrumented with corrosion sensors and temperatures sensors for periodic monitoring.

The segments were installed after construction was completed by clamping and strapping the segments to the fender pile using galvanized plates and stainless steel straps (Figure 41). This enabled precise location of corrosion sensors in the splash zone, where corrosion development is critical for the structure. One segment per mixture was cast. These segments will also eventually be cored for evaluating the chloride ion penetration and concrete hydration over time.

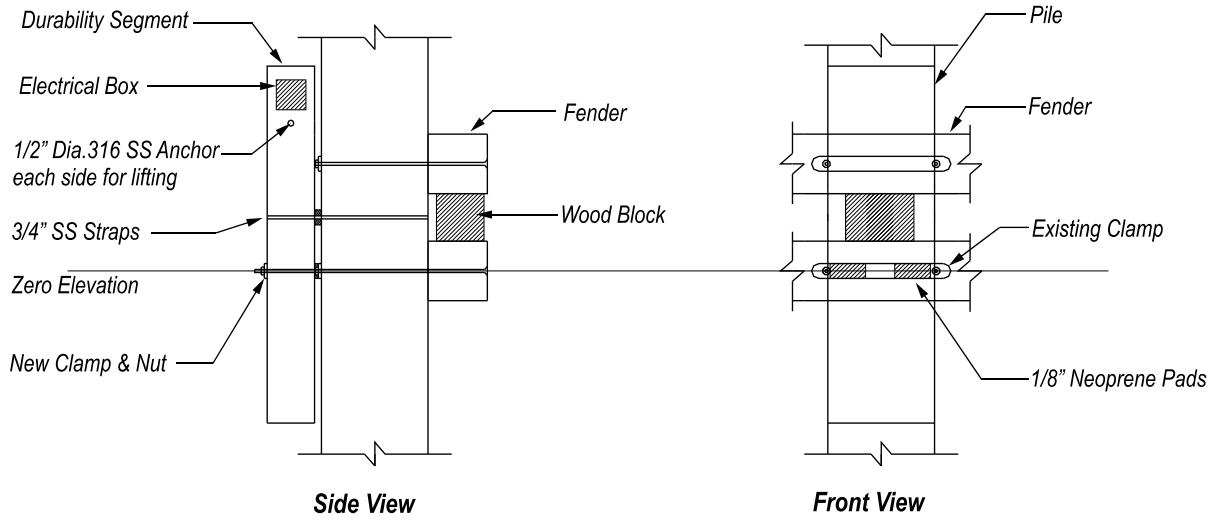

Figure 40–Durability segment after installation on the pile

Figure 41–Durability segments were attached to the fender piles

8.1 Design and Construction

Durability segments were cast with each set of fender piles using the same concrete. In some cases fender piles were also cast simultaneously with the main 24-in. piles. Figure 42 shows the configuration of the segment and how it was arranged in the 18-in. pile casting beds. The segments are approximately 7.5-in. thick leaving the remaining portion of the form to cast concrete that was used to take material samples as described earlier.

The pile casting bed was divided using a 5/8-in. thick plywood sheet (Figure 43). Since sample segments were to be cored for laboratory testing, some strands were debonded to allow removal before coring. Concrete was poured and vibrated in the sample segment first, thus fresh concrete pushed the plywood against the debonded strands (Figure 44). Then, the concrete was placed and vibrated in the durability segment of the casting bed.

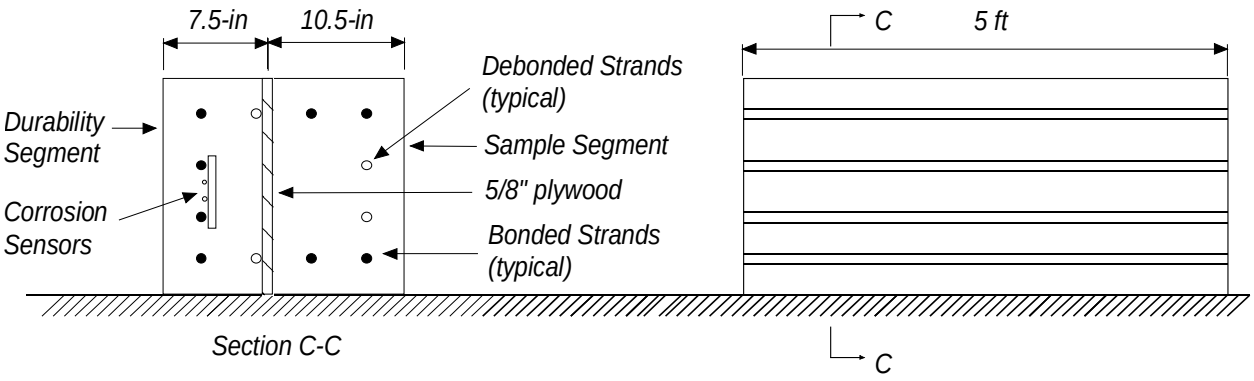

Figure 42–Durability segment and sample segment construction

Figure 43–Sample segment and durability segment were divided by a plywood sheet

Figure 44–Sample segment and durability segments after concrete had been poured

After curing and when the concrete reached sufficient compressive strength, the strands were torch-cut to transfer the prestress. The durability and sample segments were then lifted out of casting bed and placed adjacent to the prestressing bed (Figure 45). The segments were then transported back to UF for testing (The curing condition and lifting method are described in Section 6.3). Eight cores were taken from the each sample segment.

Figure 45–Sample segment and durability segment with prestressing strands exposed

To prevent corrosion of the exposed strands, the ends of the durability segments were repaired (Figure 46). The concrete was chipped out from around the strands below the concrete surface. The strands were then cut as close as possible to the bottom of the depression. The sides were formed and an epoxy fill was placed. Approximately 1-in. of Sikadur 32 high modulus structural epoxy mixed with sand was poured on the end to seal the durability segment (Figure 47).

Figure 46–Concrete and prestressing strands were chipped and cut below the concrete surface.

Figure 47–The top of durability segment after application of epoxy to protect strands

8.2 Corrosion Instrumentation

Three sets of corrosion sensors were installed in each durability segment (Figure 48 and Figure 49). Segments were attached to the fender piles such that central set of probes was in the splash zone. Bottom sensors were placed at the MHW level and top sensors were placed above the splash zone. Corrosion was expected to occur first in the splash zone where the central probes were located. The other probes were expected to perform as references.

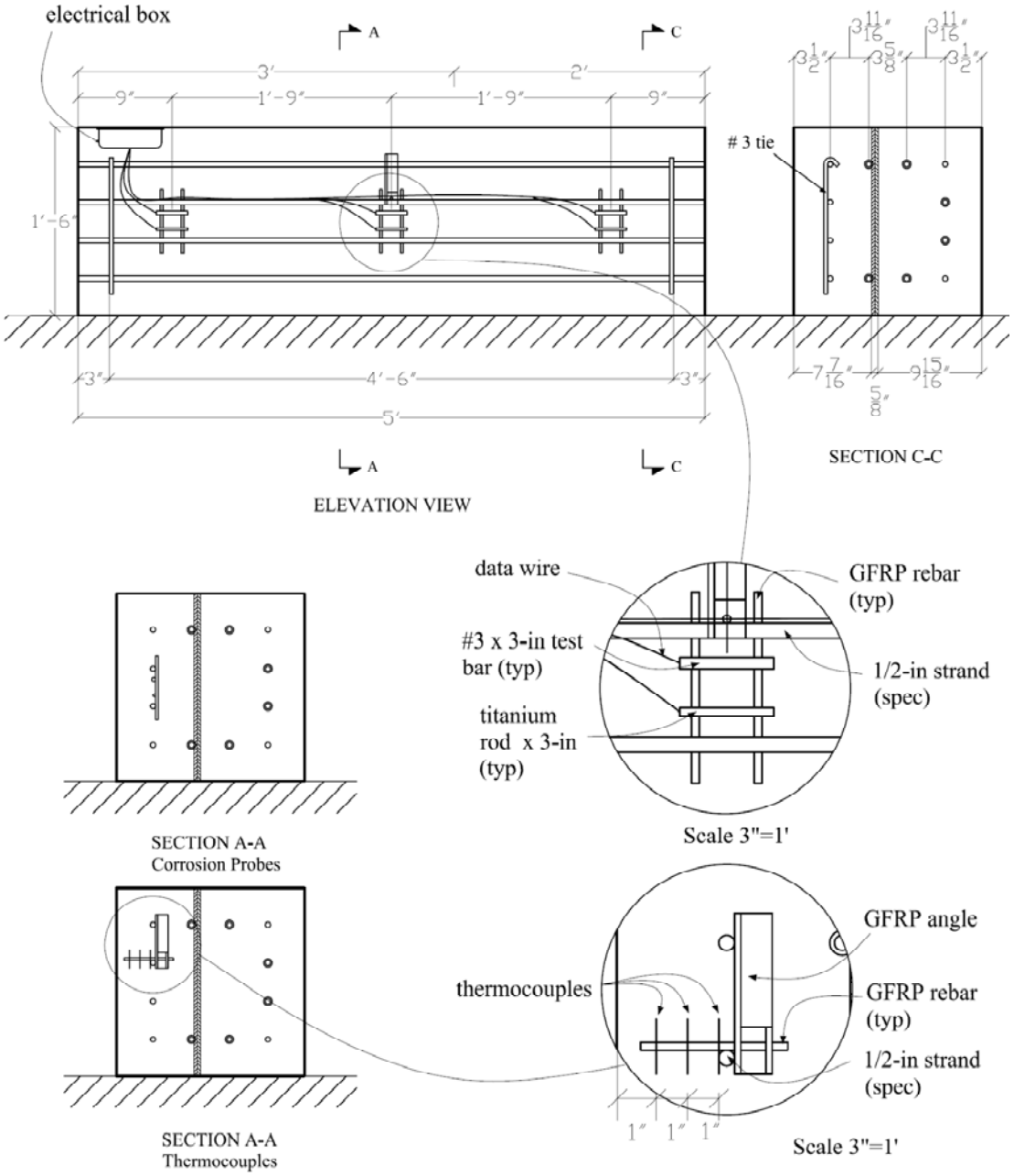

Figure 48–Instrumentation in the durability segment

Figure 49–Cross-sectional view of durability segment with instrumentation

8.3 Temperature Instrumentation

Thermocouples were installed only in the durability segments. They were placed to measure temperature gradient in the cover zone when corrosion is detected. Three thermocouples were placed in the central portion of the segment (Figure 48), which is in the splash zone, where corrosion is expected to be the most intensive. The fixture holds three thermocouples spaced at 1-in. increments from the surface to the reinforcement. Thermocouples were attached to the strands using a cantilever grip shown in Figure 50.

Figure 50–Thermocouples grip system

9 Corrosion Potential

9.1 Measurement of Corrosion Potentials in Prestressing Strand

Measuring the half-cell potentials of the prestressing steel and internal probes provided an indication of the electrical potential of those elements in the Key Royale Bridge. Significant changes in electrical potentials could have indicated that corrosion was occurring.

The measurement of half-cell potentials in the KRB bridge piles was performed over a five-year period. The first measurements were taken soon after the bridge was completed in May 2007. Subsequent measurements were taken in June 2007, June 2008, September 2011, and April 2012. Since no corrosion has been detected as of this writing, future measurements are expected to occur at five-year intervals. The next measurements are anticipated to occur in 2017.

A Fluke 95 Series III digital multimeter was used for taking half-cell potentials. Corrosion potentials of the prestressing strands were measured against a copper-copper-sulfate reference electrode (CSE). The CSE was a Model RE-7 produced by McMiller Co. as seen in Figure 52 and Figure 53. When taking potential measurements using the reference electrode, the lead wire from the reference electrode was connected to the negative (ground) terminal on the multimeter. The wire connected to the prestressing steel was then connected to the positive multimeter terminal.

The CSE was designed to be used in an aqueous solution; the salt bridge located at the electrode tip requires conductive liquid for the electrode to function. This requirement was satisfied in two ways. The first method was to use a sponge soaked in seawater to bear against the concrete surface and transmit charge across the gap between the concrete and the electrode (Figure 52). The second method was to dip the electrode in seawater to moisten the salt bridge. This was effective at producing stable measurements, provided that the salt bridge was rewetted regularly to keep it moist.

Figure 51–Fluke 85 series III digital multimeter was used to take corrosion readings

Figure 52–Copper copper-sulfate reference electrode showing method to provide electrical conductivity between external electrode and concrete

Figure 53–External electrode ready to use on the concrete surface

9.1.1 Measurement Technique

Corrosion potentials of the prestress steel were measured by the method described in ASTM C876 (2009). These potentials were taken with the reference electrode centered in the pile face at 1-ft. intervals (Figure 54). An example of the plots produced by this technique is provided in Figure 56 with Figure 57 demonstrating the significance of the vertical axis of these plots.

Initial measurements were taken on either the north or south face of the piles as indicated in Figure 55 while recent measurements were taken along all four pile faces. This change, while increasing the time required to perform half-cell potential measuring, increases the probability that corrosion initiation will be detected as such corrosion may occur in any of the four pile faces.

The vertical positioning of the CSE along the pile face was altered during the course of this investigation. Initial measurements were taken with the top of marine growth as a reference datum, with the location of the topmost measurement point given in (Table 24). This resulted in the measurement locations being different for each pile. To simplify the procedure and reduce the possibility of error, subsequent measurements were taken with the bottom of the pile cap as the reference datum. This ensured that the first measurement location was always 12-in. from the bottom of the pile cap, with subsequent measurements taken at 12-in. increments below. The distance between the marine growth line (MGL) and the bottom of the pile cap is provided in Table 23.

Table 23–Distance from MGL to bottom of pile cap (inches)

Bent	Pile				
	UFA	FA	SF	MET	BFS
2	79	78.5	84	78.5	79
3	92.5	91	96	90	90
4	96	96	96	96	96
5	79.5	79.5	84	79	78.5

9.1.2 Measurement Analysis

ASTM C876 (2009) provides guidelines for predicting the likelihood of corrosion based on the potential measurement. According to the standard, a potential measurement of greater than -200 mV indicates that there is a greater than 90% probability that no corrosion is occurring at the time of measurement. A potential measurement of less than -350 mV indicates that there is a greater than 90% probability that corrosion was occurring at the time of measurement. A measurement between -200 and -350 mV indicates that corrosion is uncertain. Several caveats apply, however. The temperature at the time of measurement has some effect, although this amount to only 0.5 mV per degree F. A greater influence is the presence of moisture within the pore structure of the piles. Moisture in the concrete causes the potential to drop in value, which explains the low potentials recorded near the MHW. Using the criteria established by ASTM, potentials seemed to indicate that corrosion was occurring near the MHW even though no corrosion was actually occurring. According to previous research (Leelalerkiet et al. 2004), the presence of water at the prestress steel causes excessively negative potentials. Previous experimentation with half-cell potential mapping in a similar environment (Cannon et al. 2006) indicated that the low potentials near the MHW should be discounted. Rather, it is the increasing negativity over time of potential measurements immediately above the splash zone that indicates corrosion is occurring.

The results of the prestress steel monitoring indicate that there is a low probability that any corrosion is occurring in the pile prestress steel. A typical plot of potential as a function of reference electrode position is provided in Figure 56. This plot is produced from measurements taken on the UFA pile; different plots correspond to the measurement dates. For comparison, the vertical positions of the measurements have been normalized so that they occur in 1-ft. increments from the bottom of the pile cap. Potentials are highest near MHW, matching observations in other Florida bridge piles by Cannon et al. (2006). Significantly, the potentials

along the height of the piles have not become more negative over time. If corrosion were occurring, the potentials close to the MHW would become more negative as time proceeds. Changes in the potentials observed over time were most likely caused by environmental conditions; wind driven moisture, tidal conditions, and air temperature differences explain much of the variation. Also, the measurement locations were difficult to repeat to a greater accuracy than one inch. The measurement process involved using a tape measure to mark the proper location, followed by shifting the reference electrode as required to obtain a stable measurement. As observed in Cannon et al. (2006), corrosion would be accompanied by increasingly negative potentials measured in the splash zone region.

A new method of analysis was created to enable the comparison of half-cell potential measurements taken from different piles using the same SCM and measurements taken from different locations along the pile face. The motivation of this analytical method was to reduce half-cell potential measurements taken along a pile face into a single value. This single value can be compared with the single values produced by single measurements to determine whether corrosion had initiated.

The analytical method involved "integrating" the half-cell potentials with respect to the height of the pile and then dividing by the pile height to obtain an "average" potential for the pile (Figure 58). This process is straightforward for measurements conducted using the pile cap as the reference datum. Measurements taken using the marine growth line required adjustment; linear interpolation was used to adjust half-cell potential values to approximate those using the pile cap as the datum. The "average" potentials for all four piles of each mixture were then averaged and plotted with respect to time. This plot is given in Figure 59.

From Figure 59, it is apparent that the half-cell potential measurements are not becoming significantly more negative with time. Between June 2007 and June 2008, the "average" potential increased dramatically as the pile lost moisture to the atmosphere. From June 2008 through September 2011, the "average" potential declined very slightly. Based upon experiences with other structures subjected to a similar monitoring regimen (Cannon et al, 2006), the "average" potential should decline significantly when corrosion has initiated. Corrosion in the prestressing steel is unlikely as of the time of the present research.

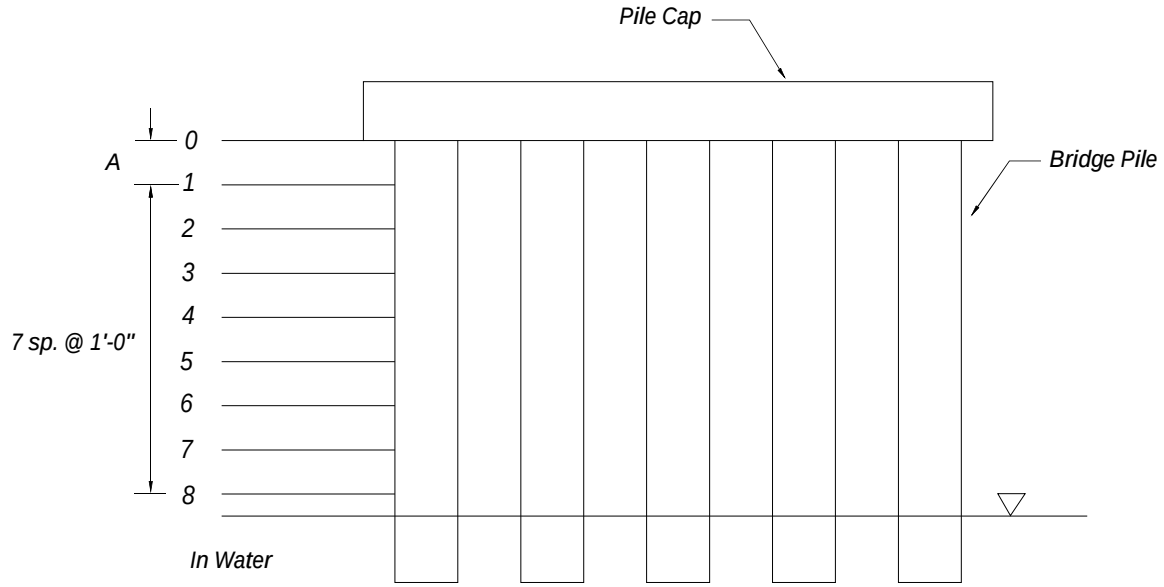

Figure 54–Surface resistivity and external potentials measuring locations (see Table 21 for "A" dimensions)

Table 24–"A" dimension for surface resistivity and external potential measurements (inches)

Bent	Pile				
	UFA	FA	SF	MET	BFS
2	7	6.5	12	6.5	7
3	8.5	7	12	6	6
4	12	12	12	12	12
5	7.5	7.5	12	7	6.5

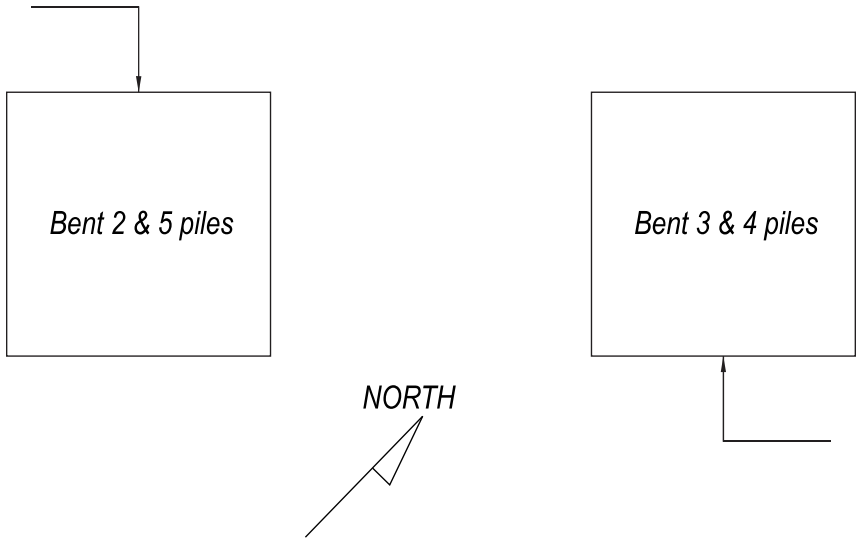

Figure 55–The orientation of pile surface upon which potential readings were taken

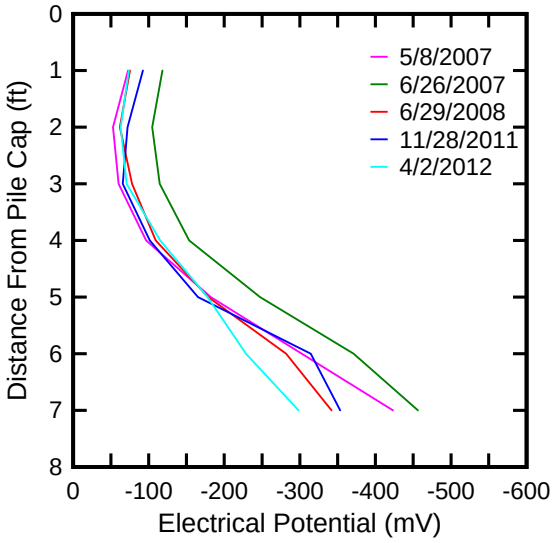

Figure 56–Typical plot of pile prestressing steel half-cell potentials (UFA)

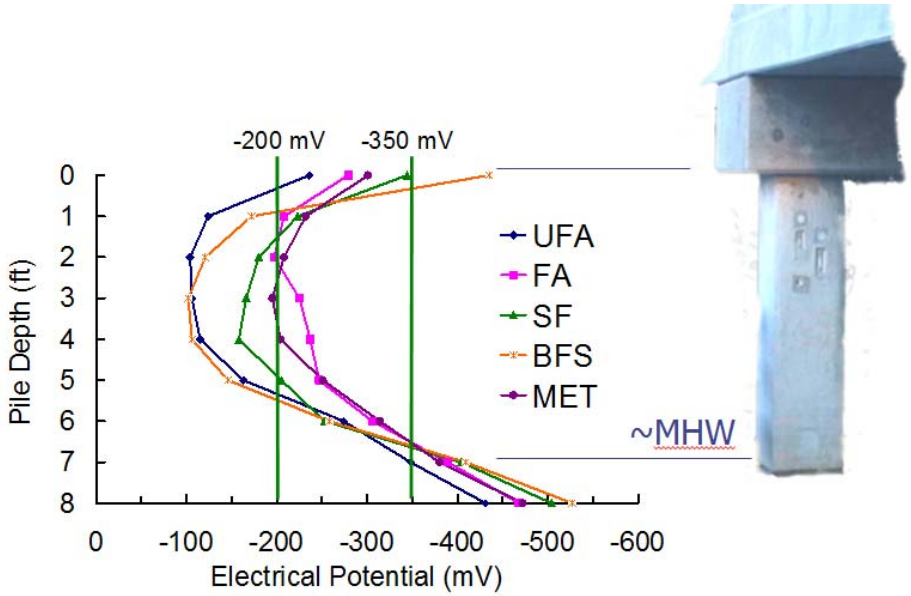

Figure 57–Location of electrical measurements along pile face

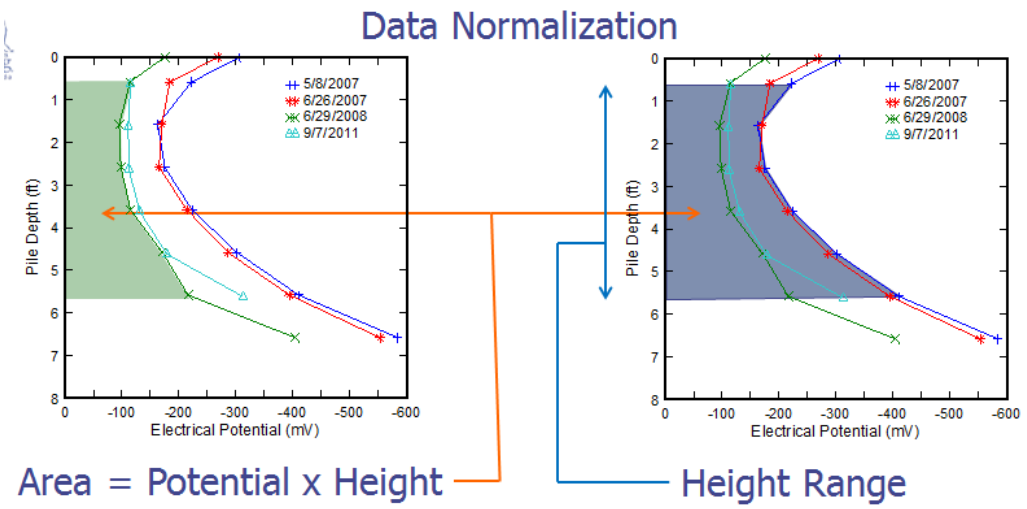

Figure 58–Creation of normalized and averaged prestress half-cell potentials for each SCM and each measurement date

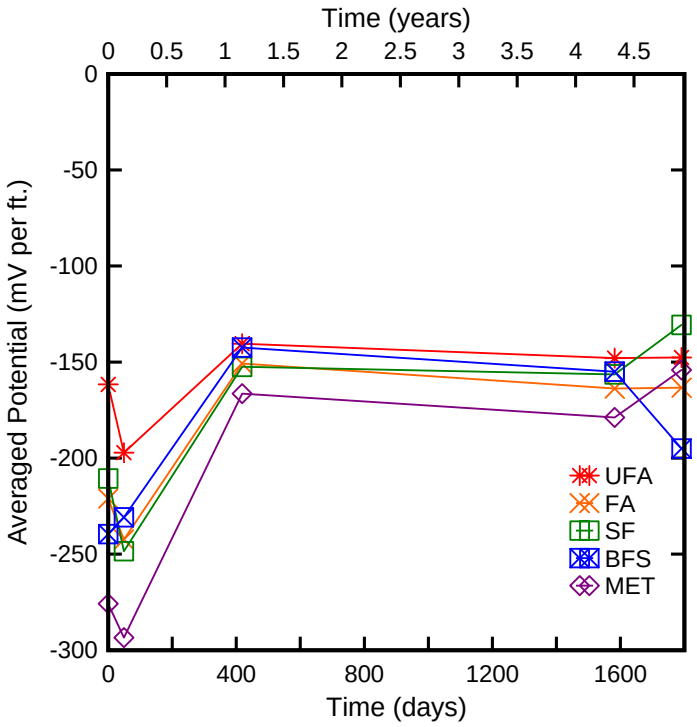

Figure 59–Change in normalized and averaged prestress half-cell potentials

9.2 Corrosion Potential of Pile Electrodes

Electrical potential readings give information about the natural potentials of the internal electrodes. They should remain constant until the onset of corrosion. Once significant change in

potential readings was noted and explanations other than corrosion ruled out, electrical current was to be measured as well.

Figure 60 shows the orientation of the junction box and electrodes for each pile. For the readings on the bridge piles, Figure 61 along with Table 25 and Table 26 show the distance from the bottom of pile cap to each pair of electrodes for each instrumented pile in bent 3 and 4. Figure 62 shows the color coding of the leads used to take measurements. Figure 63 shows the surface electrode contact location to be used when measuring the external corrosion potential of each individual electrode.

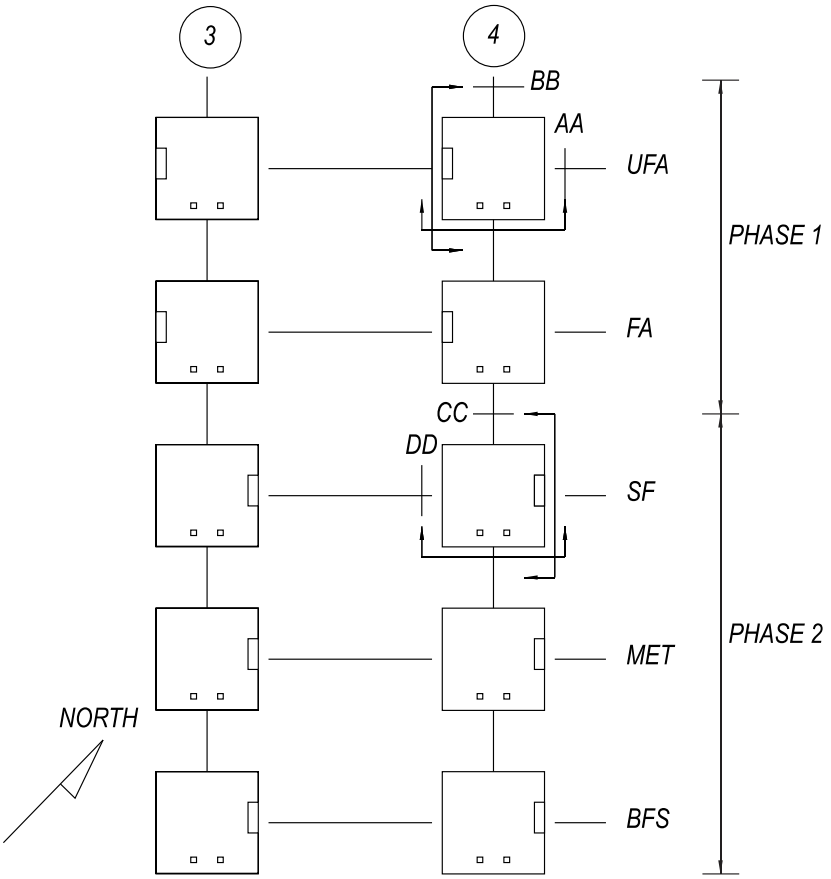

Figure 60–The orientation of box and electrodes for each mixture

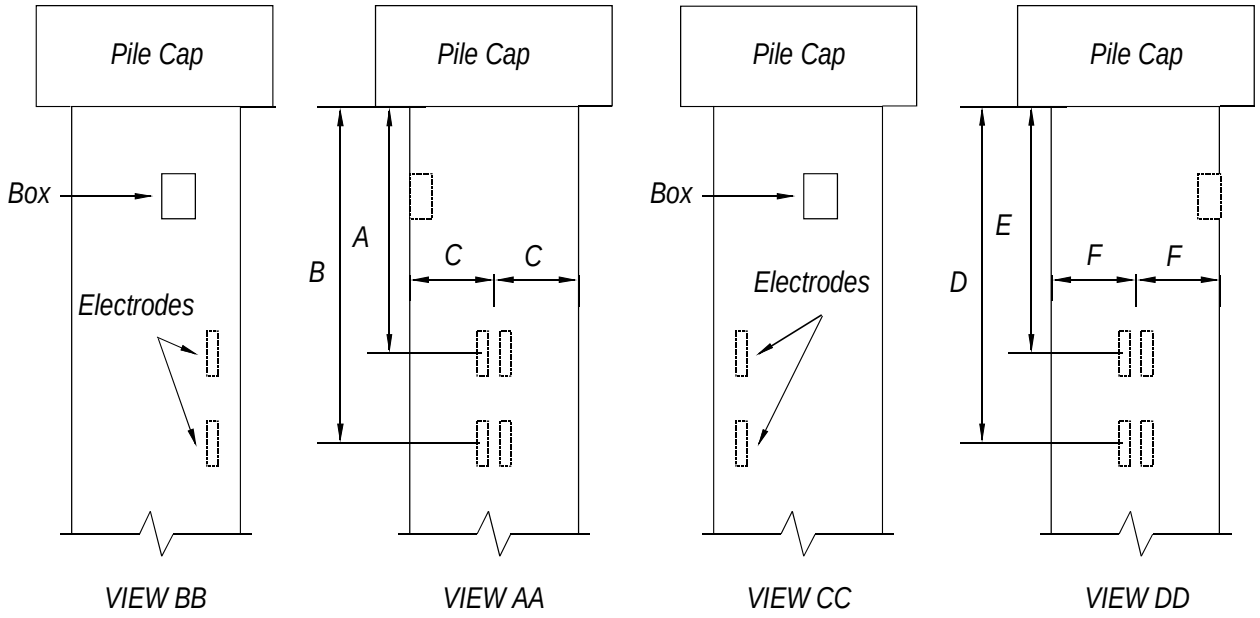

Figure 61–Location of corrosion probes relative to the bottom of pile cap in the 24-in. piles

Table 25–Location of corrosion electrodes in 24-in. FA and UFA piles

	A	B	C
FA3	61.5-in	85.5-in	12-in
UFA3	59-in	83-in	12-in
FA4	53.5-in	77.5-in	12-in
UFA4	55.5-in	79.5-in	12-in

Table 26–Location of corrosion electrodes in 24-in. SF, BFS, and MET piles

	D	E	F
SF3	65-in	89-in	12-in
MET3	48.5-in	72.5-in	12-in
BSF3	60.5-in	84.5-in	12-in
SF4	50-in	74-in	12-in
MET4	56.6-in	80.5-in	12-in
BSF4	56-in	80-in	12-in

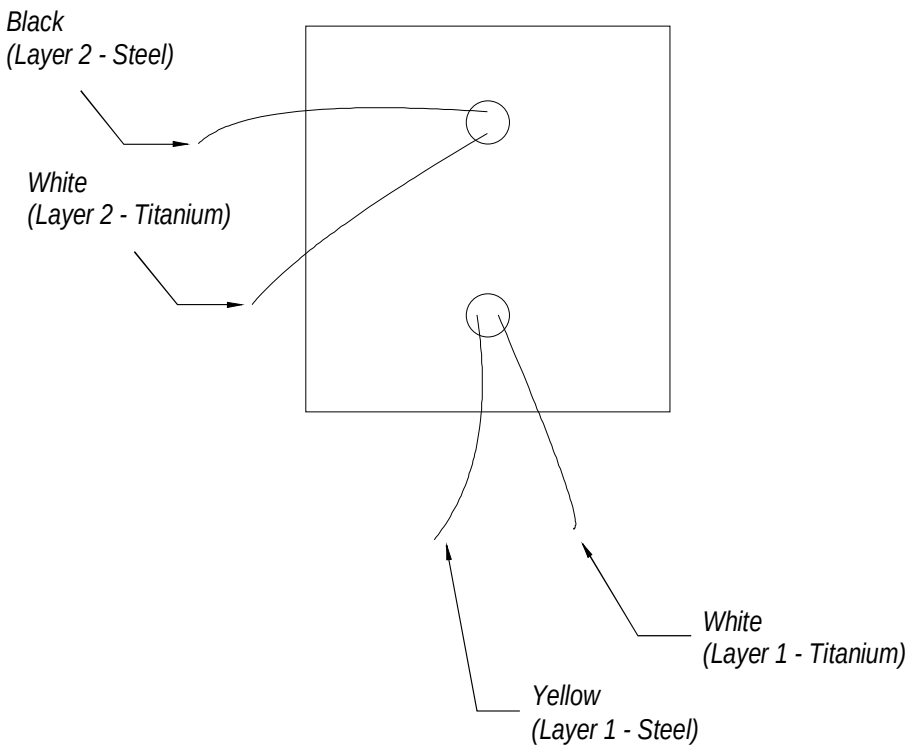

Figure 62–Mapping of electrodes and wires in the electrical box by color of wire and inlets

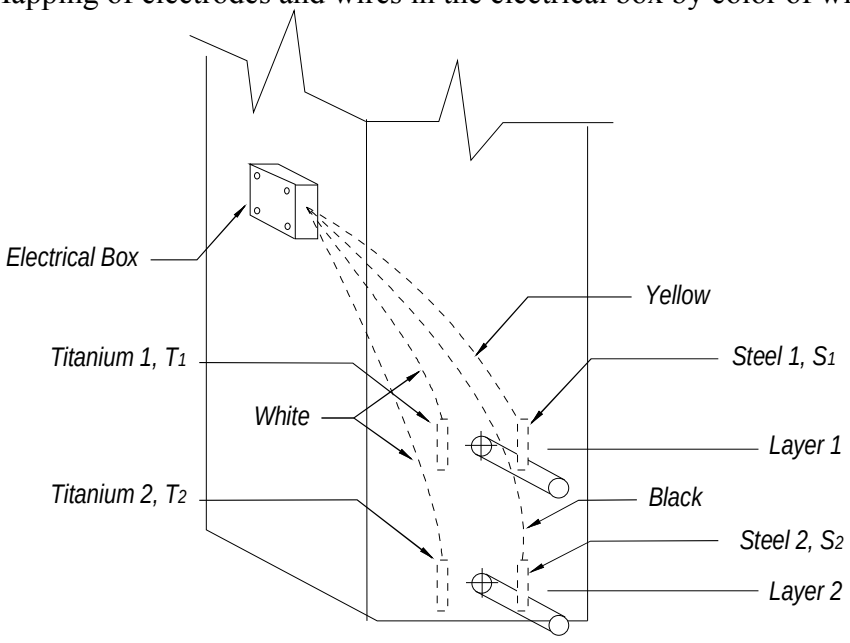

Figure 63–Surface electrode contact location when measuring the external corrosion potential of each individual electrode

Half-cell potential measurements were taken for the electrodes within each of the piles in bents 3 and 4. The measurement technique was similar to that used for measuring half-cell

potentials in the prestress strand discussed previously. The same multimeter and CSE were used; the multimeter was attached to leads for the steel electrodes that were located within the electrical box. When taking potential measurements using the reference electrode, the lead wire from the reference electrode was connected to the negative (ground) terminal on the multimeter. The wire connected to the pile internal electrode was connected to the positive multimeter terminal.

Potential measurements were taken for both steel and titanium electrodes to investigate the presence of corrosion. Potentials that drop significantly between measurements may indicate the onset of oxidation within the probe. Other influences, such as ongoing pozzolanic reactions, cannot be discounted. Figure 64 and Figure 65 indicate that there has been little change in potential over time for the internal steel electrodes. Only the BFS piles had an extremely negative potential, and that was only for the first two measurements (May and June 2007). Other measurements were consistent, with potentials at or above -200 mV. As discussed previously, potentials above -200 mV are consistent with a 90% probability that corrosion is not occurring (ASTM C876 2009). The half-cell potentials for the titanium electrodes indicate a similar pattern. Other than the first two measurements of the BFS pile electrodes, half-cell potentials of the titanium electrodes (Figure 66 and Figure 67) did not change. While no guidance exists for interpreting the potentials within titanium as exists for steel, it is logical to assume that a lack of change in the potentials of the titanium electrodes is indicative of a lack of corrosion.

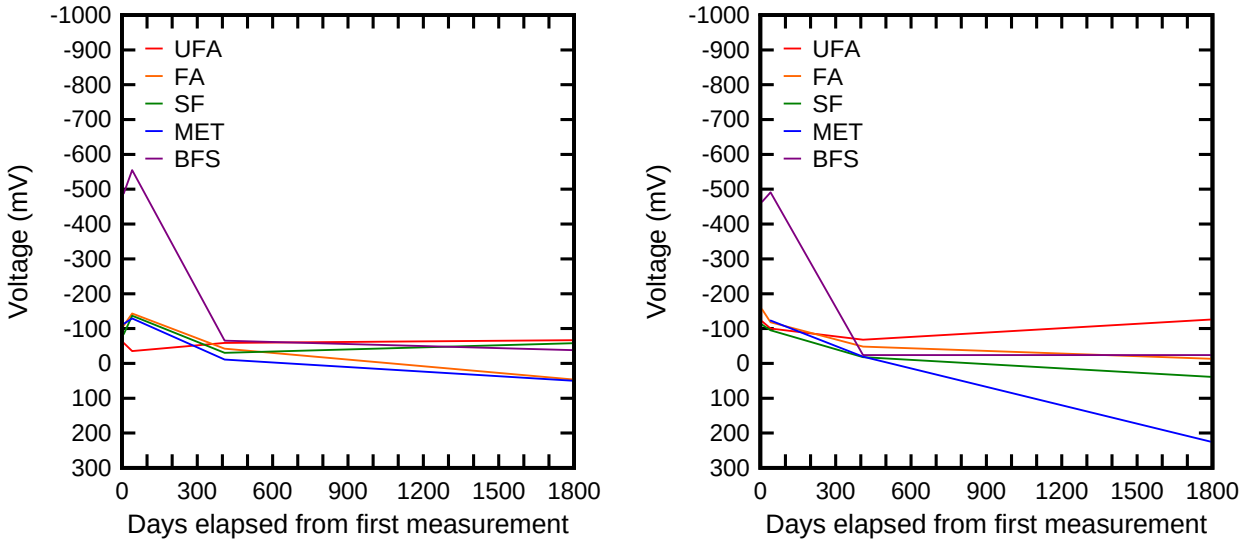

(a) (b)

Figure 64–Half-cell potentials of layer 1 steel electrodes for bents 3 (a) and 4 (b) for each pile type

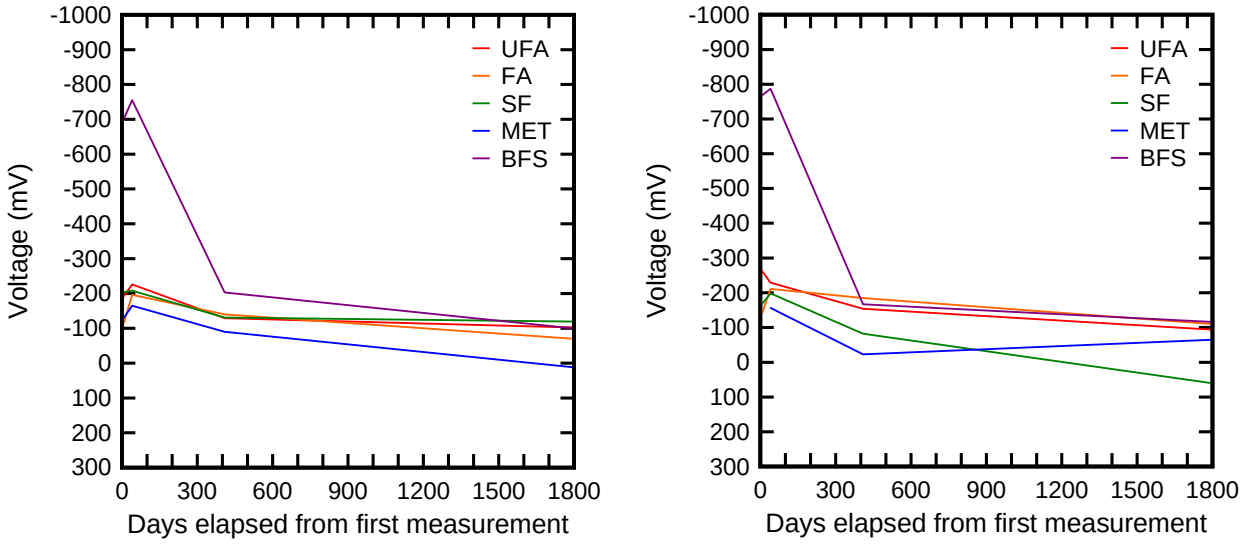

(a) (b)

Figure 65–Half-cell potentials of layer 2 steel electrodes for bents 3 (a) and 4 (b) for each pile type

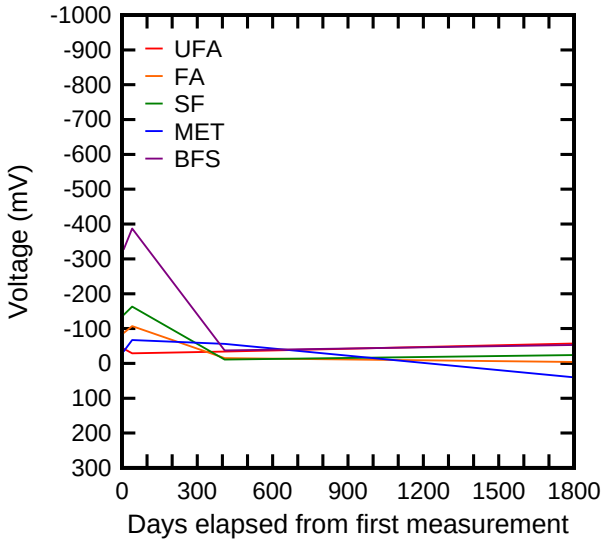

(a)

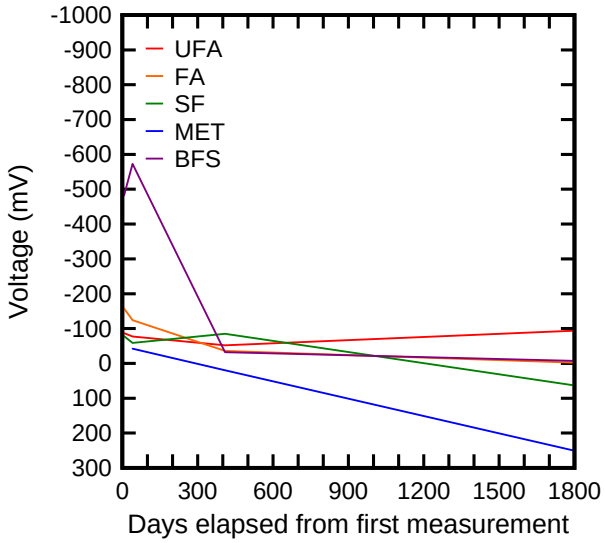

(b)

Figure 66–Half-cell potentials of layer 1 titanium electrodes for bents 3 (a) and 4 (b) for each pile type

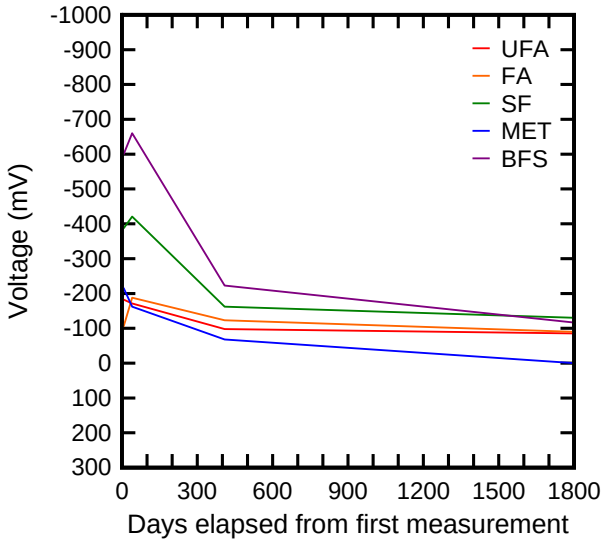

(a)

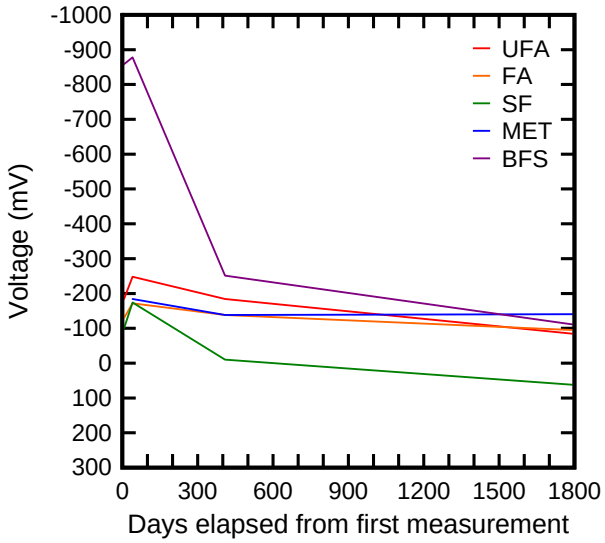

(b)

Figure 67–Half-cell potentials of layer 2 titanium electrodes for bents 3 (a) and 4 (b) for each pile type

Another technique for assessing whether corrosion was occurring in the steel electrodes was to measure the potential difference between the two electrode types on the assumption that the steel electrodes would corrode before the titanium electrodes due to the higher nobility of the

latter. If the steel electrode corroded sacrificially to the titanium electrode, then the difference in potential between the two would change. Potential measurements were taken between steel and titanium electrodes with the Fluke 95 multimeter; the wire from the titanium electrode in the electrical box was connected to the negative terminal while the wire from the steel electrode was connected to the positive terminal of the multimeter. Two measurements were taken at each instrumented pile; one with the upper pair of electrodes (layer 1) and the other with the lower pair of electrodes (layer 2).

Results from measuring the corrosion potential difference between the steel and titanium electrodes indicated that no corrosion had initiated by the time of the most recent testing (April 2012). The voltage differences between the potentials of the two electrodes in layer one and layer two of the instrumented piles are shown in Figure 68 and Figure 69. In each figure, voltage differences between the two electrodes remain consistent during the monitoring period; the absolute value of this difference remains below 100 mV for all measurements.

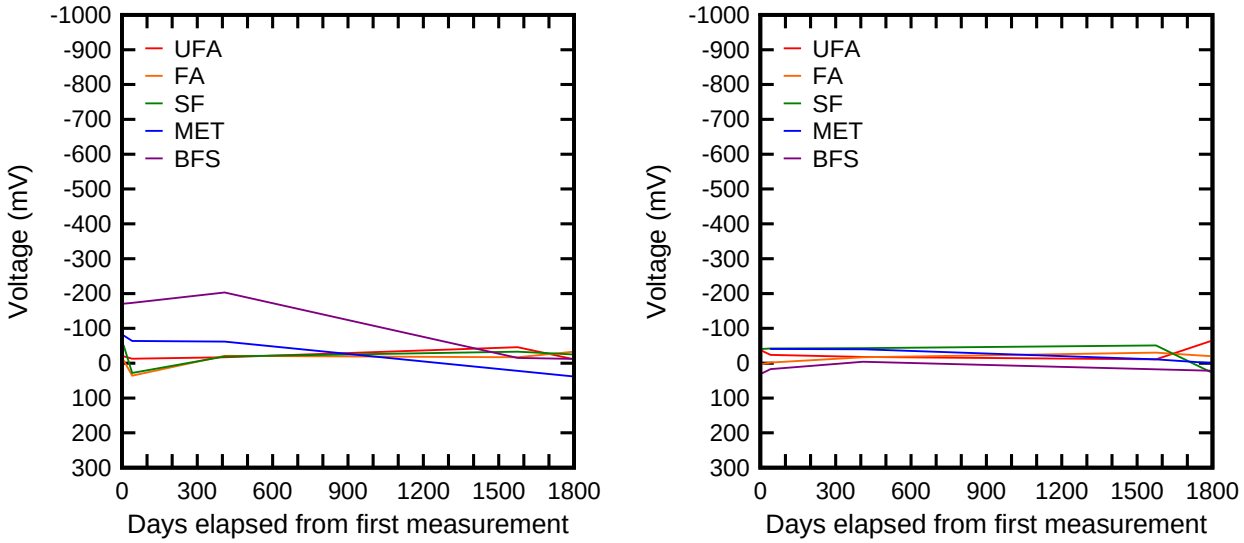

Figure 68–Potential difference between layer 1 titanium and steel electrodes for instrumented piles in bents (a)3 and (b)4

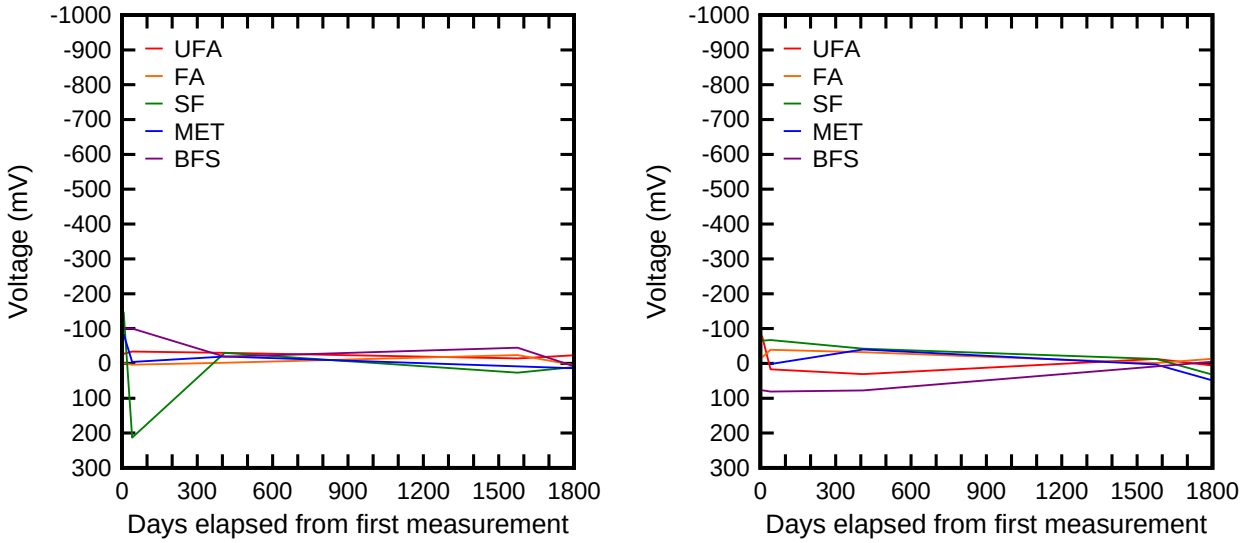

Figure 69–Potential difference between layer 2 titanium and steel electrodes for instrumented piles in bents (a)3 and (b)4

9.3 Corrosion Potential of Durability Segment Electrodes

Durability segments were installed at the Key Royale Bridge to evaluate the durability of six concrete mixture designs by placing internal electrodes within the splash zone and submerged zone. Embedded electrodes within the bent 3 and bent 4 piles could not be precisely located in the splash and submerged zones due to the uncertainty of the pile driving process. The durability segments were equipped with three pairs of electrodes, each containing one steel and one titanium electrode. The process of obtaining and analyzing measurements was similar to that employed on the pile internal electrodes discussed previously.

For the readings on the durability segments, Figure 72 shows the locations of the electrodes and mapping of wires and electrodes. Figure 73 and Table 27 show the contact location of the surface electrode when measuring the external potentials of each electrode. The procedures of taking the external potential readings and potential between electrodes are the same as for the bridge piles described above in the bridge pile section. Before taking the readings, two wires connecting the steel electrodes were removed (Figure 70). Steel electrodes were connected using this wire to ensure consistent rates of corrosion when corrosion occurs. The central and bottom pair of embedded corrosion electrodes were designed to be in the splash

zone, completely submerged in the water. Because the external surface electrode could not be used while submerged, the external potential readings for central and bottom pair of electrodes were taken at water level instead of location of the electrodes. The distance from the top of the segment to the external surface electrode contact locations are shown in Table 27. After measurements were taken, the wires connecting the electrodes together were replaced back in original position.

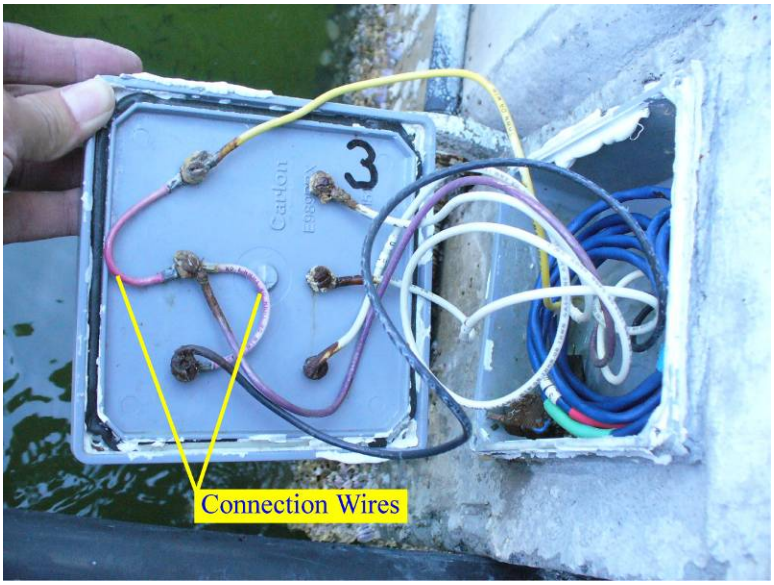

Figure 70–Two short wires were used to connect the steel electrodes

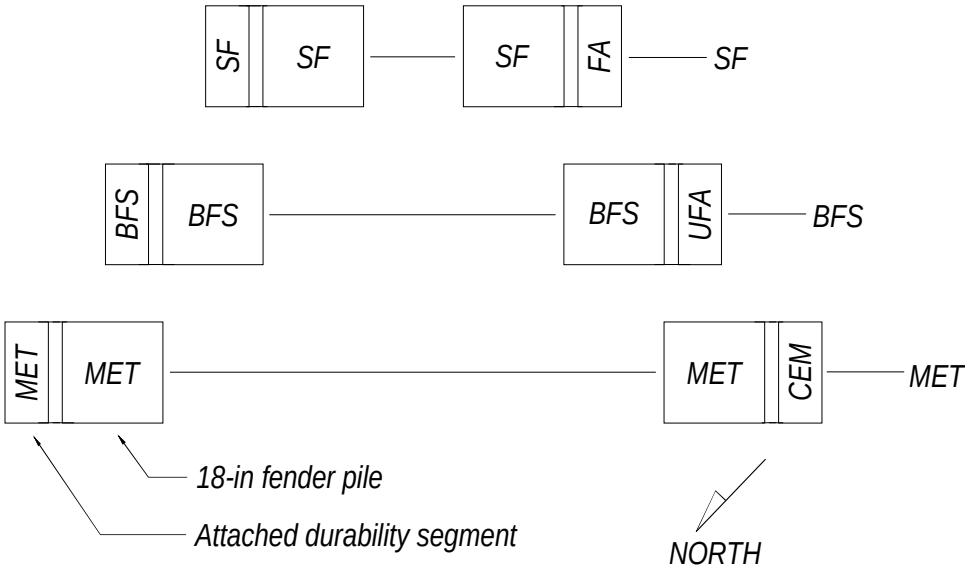

Figure 71–Durability segment attachment locations relative to fender piles

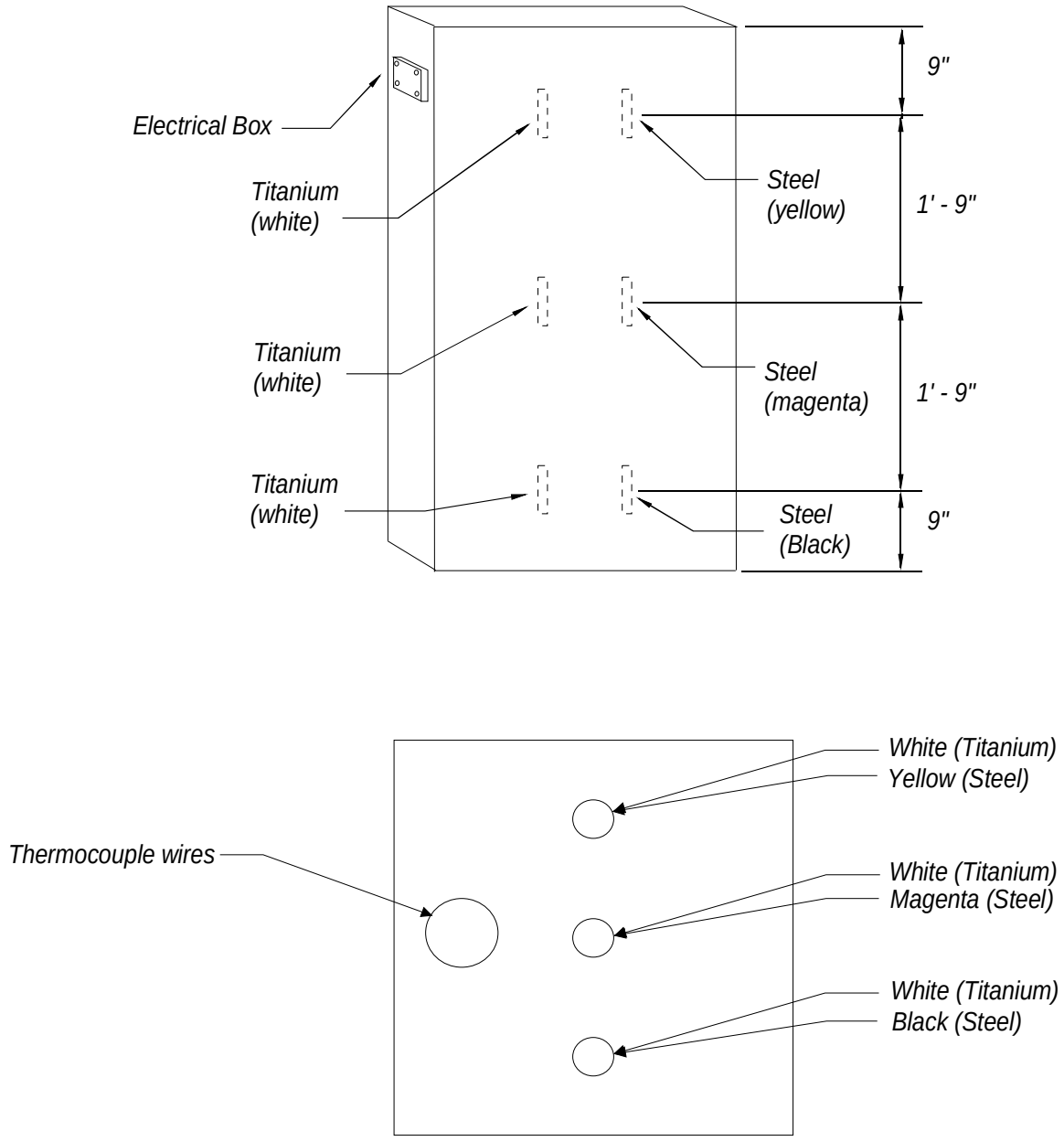

Figure 72–Location and mapping of wires and electrodes in the durability segments

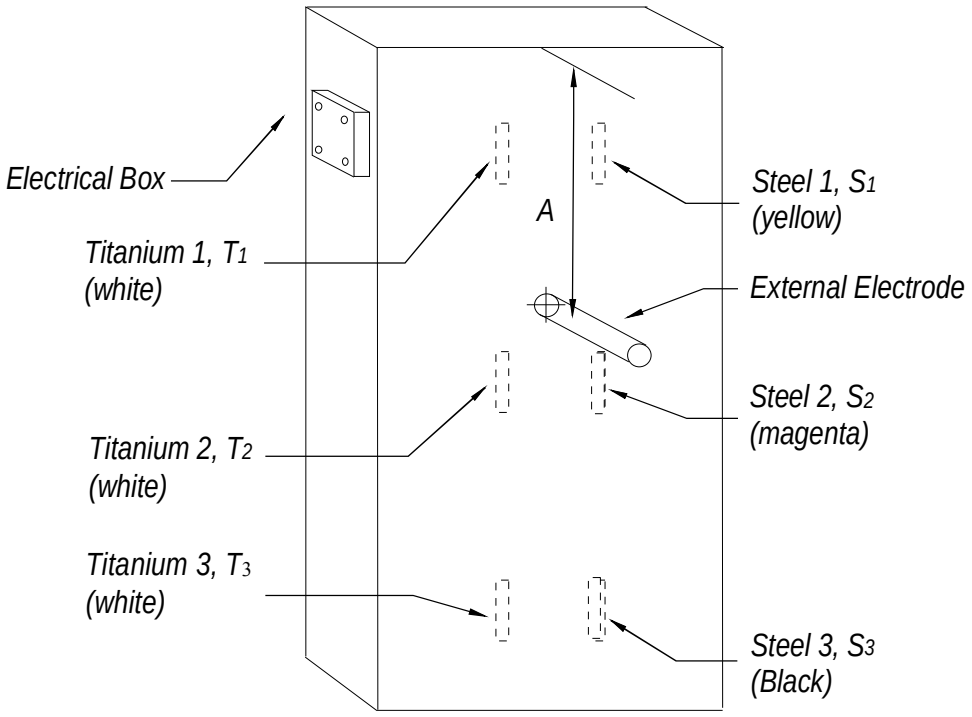

Figure 73–Potential readings–external electrode contact locations
(see Table 27 for dimension "A")

Table 27–External electrodes measuring locations (*See Figure 73 for details)

Mixture	*Distance A (in.) measured from top of the segment					
	S_1 - R	S_2 - R	S_3 - R	T_1 - R	T_2 - R	T_3 - R
CEM	10	16	16	10	16	16
UFA	10	16	16	10	16	16
FA	10	16	16	10	16	16
SF	9	18	18	9	18	18
MET	10	19	19	10	19	19
BFS	10	19	19	10	19	19

Table 28–Distance from top of durability segment to marine growth line and high tide mark (in)

Mixture	Marine Growth	High Tide Mark
CEM	14	12
UFA	14	12
FA	14	12
SF	16	14
BFS	17	15
MET	17	15

Half-cell potential measurements using a CSE were taken for both steel and titanium electrodes. The interpretation of the results of these measurements was similar to that used for evaluating measurements taken from the internal electrodes located within piles in bents 3 and 4.

Half-cell potentials were not as consistent as those taken from the pile electrodes but still indicate that corrosion is not occurring in the steel electrodes. Figure 74 shows the half-cell potential results from the layer 1 steel electrodes. The most recent measurements, obtained in April 2012, indicate that the potentials for all of the steel electrodes were above -200 mV, indicating a 90% probability that corrosion is not occurring (ASTM C876 2009).

Results from the layer 2 steel half-cell potentials are shown in Figure 75. Most of the durability segments are above -200 mV as of the last measurement, indicating a lack of corrosion. The CEM and SF electrodes have potentials that are between -200 and -350 mV, which indicates that corrosion may or may not be occurring. These low potentials may be due to concrete saturation, however; half-cell potential measurements taken with the external electrode in the water (Figure 76) show similar potential levels to those in Figure 75, suggesting that the low potential results for layer 2 electrodes are the result of presence of seawater in the concrete pore structure.

Results from the layer 3 steel half-cell potentials are shown in Figure 77. Most of the durability segments are above -200 mV as of the last measurement, indicating a low probability of corrosion. The CEM, BFS, and SF electrodes have potentials that are between -200 and -350 mV, which indicates that corrosion may or may not be occurring. Again, these low potentials may be due to concrete saturation. Half-cell potential measurements taken with the external electrode in the water (Figure 78) have similar potential levels as those in Figure 77, suggesting that the low potential results for the layer 3 steel electrodes are the result of presence of seawater in the concrete pore structure.

A lack of change in the potentials of the titanium electrodes is indicative of a lack of corrosion. For layer 1 electrodes (Figure 79), the potentials for UFA and BFS have become more positive between June 2008 and April 2012. Potentials for SF, FA, and MET have become slightly more negative, while that of CEM has dropped by 100 mV in this time. The potentials for all layer 1 electrodes are still higher than those from June 2007.

Layer 2 and Layer 3 electrode potentials were difficult to interpret due to the concrete saturation discussed previously. For these electrodes, potentials changed but not consistently.

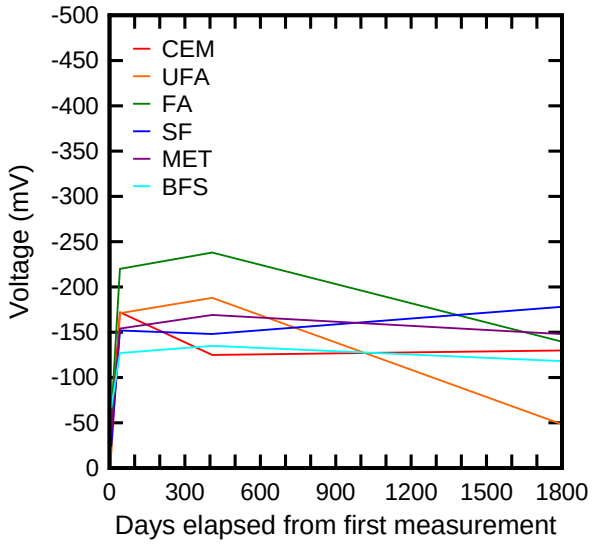

Figure 74–Half-cell potentials of layer 1 steel electrodes

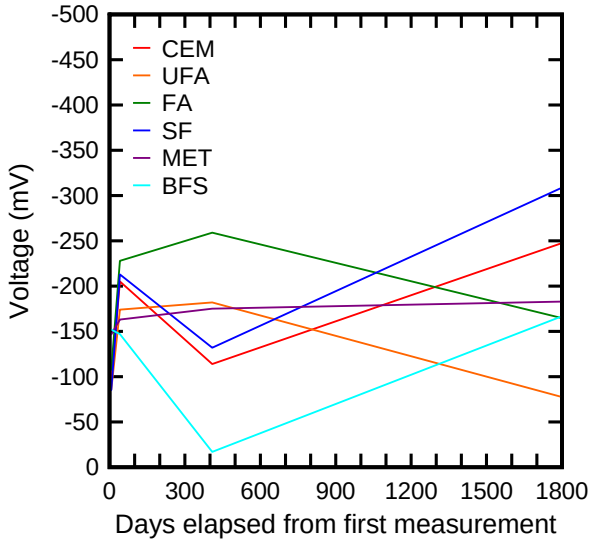

Figure 75–Half-cell potentials of layer 2 steel electrodes

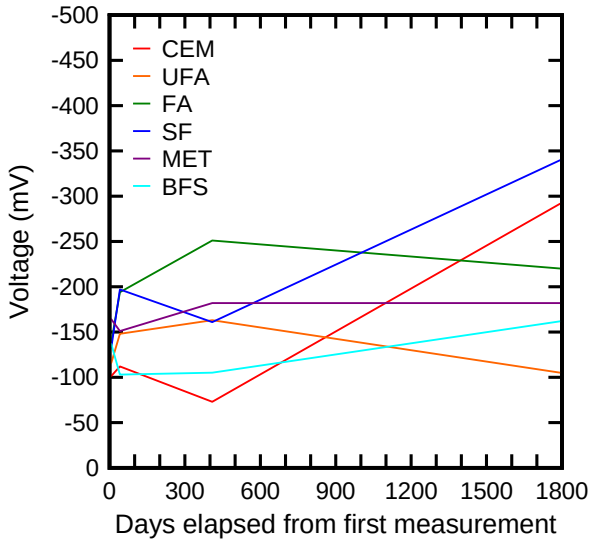

Figure 76–Half-cell potentials of layer 2 steel electrodes with the CSE dipped in seawater

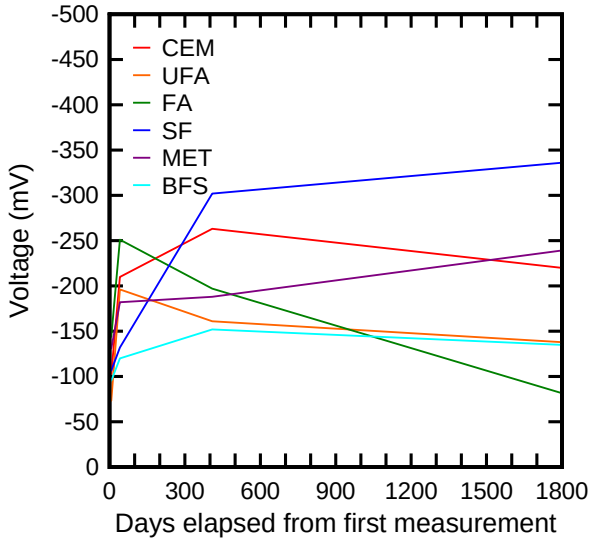

Figure 77–Half-cell potentials of layer 3 steel electrodes

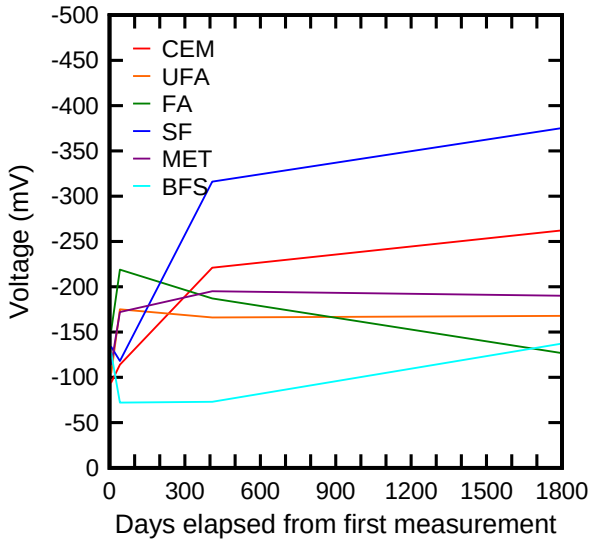

Figure 78–Half-cell potentials of layer 3 steel electrodes with the CSE dipped in seawater

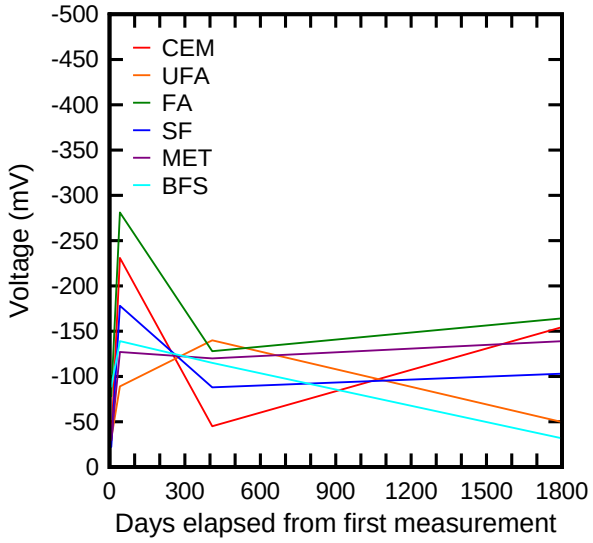

Figure 79–Half-cell potentials of layer 1 titanium electrodes

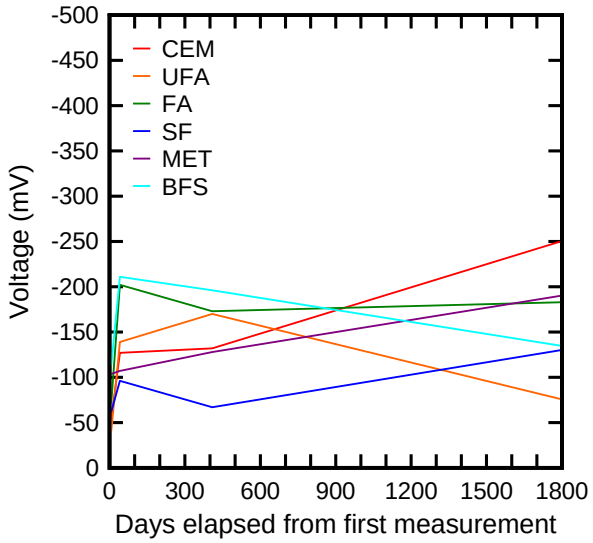

Figure 80–Half-cell potentials of layer 2 titanium electrodes

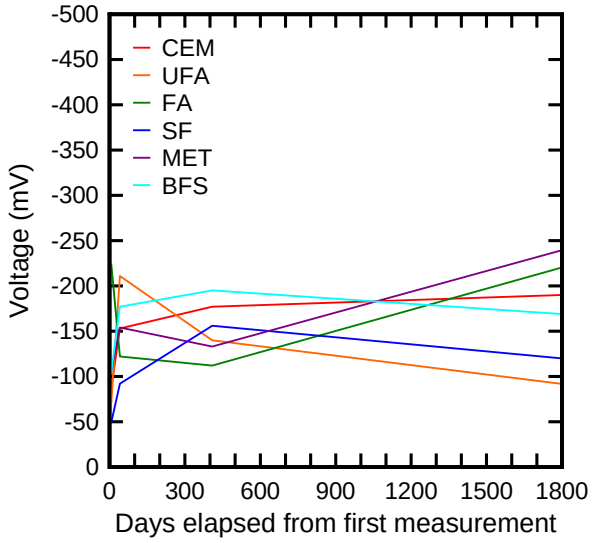

Figure 81–Half-cell potentials of layer 3 titanium electrodes

As was done with electrodes embedded within the pile, the potential differences between the two electrode types were measured on the assumption that the steel electrodes would corrode before the titanium electrodes due to the higher nobility of the latter. If the steel electrode corroded while the titanium electrode remained noble, the difference in potential between the two would change. Potential measurements were taken in a similar manner to those taken for the internal pile electrodes. Three measurements were taken at each durability segments; one with

the upper pair of electrodes (layer 1), the center pair of electrodes (layer 2) and the other with the lower pair of electrodes (layer 3).

Results from measuring the corrosion potential difference between the steel and titanium electrodes indicate that no corrosion had initiated by the time of the most testing (April 2012). The voltage differences between the potentials of the two electrodes in layers one through three of the durability segments are shown in Figure 79, Figure 80, and Figure 81. In each figure, voltage differences between the two electrodes fluctuate but remain consistent during the monitoring period; the absolute value of this fluctuation remains below 150 mV for all measurements with the exception of the layer 2 electrodes in the SF durability segment. Moreover, the potential differences between the titanium and steel electrodes at the May 2007 and April 2012 measurements were within 100 mV, with the exception of the layer 2 BFS durability segment, which was less than 150 mV.

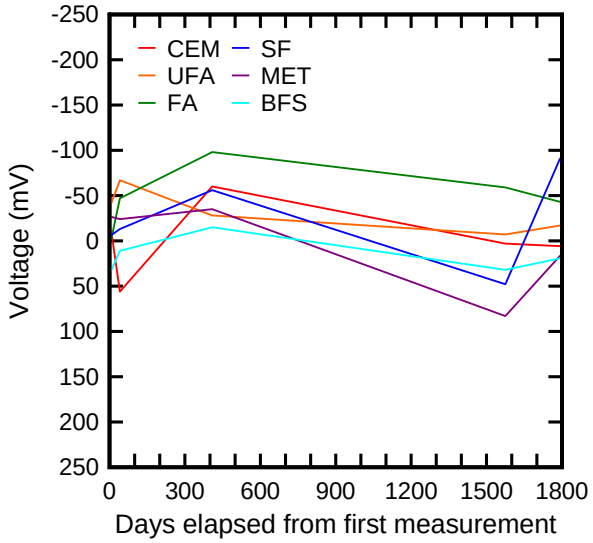

Figure 82–Potential difference between layer 1 titanium and steel electrodes for durability segments

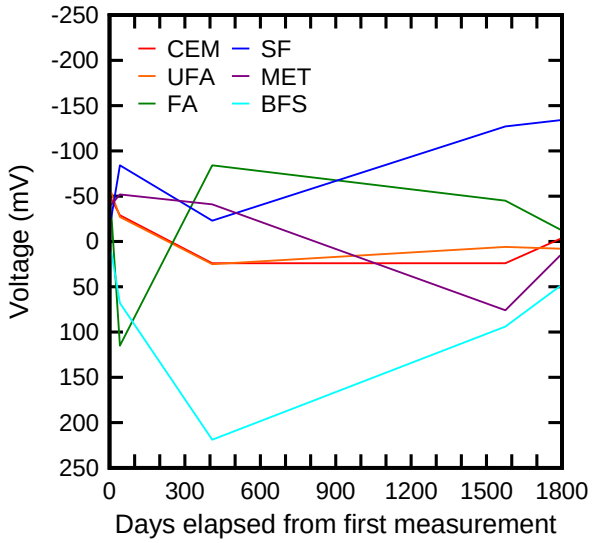

Figure 83–Potential difference between layer 2 titanium and steel electrodes for durability segments

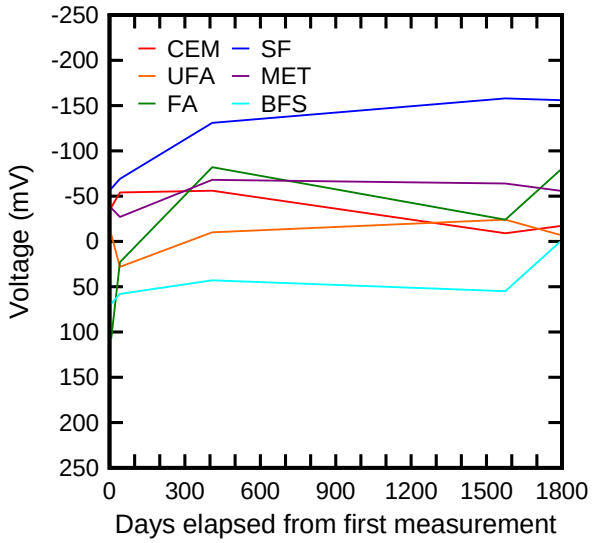

Figure 84–Potential difference between layer 3 titanium and steel electrodes for durability segments

9.4 Evaluation of Internal Electrode Function

Electrical resistance was measured to ensure there was no direct contact between the steel and titanium electrodes at each location. If there had been a path or direct connection, the current or potential readings between the electrodes would be invalid. Electrical resistance was measured using both the Nilsson AC current resistance meter (Figure 85) and the Fluke DC

current multimeter. Initial resistance readings confirmed that there was no electrical continuity between the electrodes. A drop in resistance over time would suggest that chlorides penetrated the concrete, making it more conductive. An increase in resistance would suggest that the wire leads to the internal electrodes were corroding. There was a possibility that ongoing pozzolanic reactions influenced the measured resistance by inducing a voltage in the leads; this merits caution when evaluating the corrosion of the leads using an ohmmeter. The high resistances in the piles containing blast furnace slag, a slow reacting admixture, are suggestive of this.

Measured resistances between electrodes placed in the piles in bent 3 and 4 indicated that corrosion was occurring in some electrodes and that chloride penetration had not increased electrical conductivity through the concrete pore structure. Figure 86 through Figure 88 show the change in resistance between different electrodes over time. Figure 86 shows the change in resistance between the two steel electrodes within each pile in bents 3 and 4, while Figure 87 and Figure 88 show the resistance between the steel and titanium electrodes in the top and bottom layer of those piles, respectively. Resistivity increased between all tested combinations of electrodes, suggesting wire corrosion. Electrodes that had large increases in resistance must be monitored at future site visits. Wiring and/or electrodes installed in the bridge piles may be approaching end-of-life condition and that further analysis using these sensors must be balanced against an evaluation of remaining integrity.

Resistance was also measured between electrodes in the durability segments, as shown in Figure 89 through Figure 91. As with electrodes in the bridge piles, ongoing pozzolanic reactions may influence resistance measurements. From Figure 89 and Figure 90, it is possible that the wires leading to the S2 and S3 electrodes in the SF durability segment have begun to corrode as indicated by an increase in resistance between S1 and S2, S1 and S3, and S2 and S3. At the same time, this increase was not pronounced between S1 and T1 (Figure 90b). Similarly, the resistance caused by the S1 electrode in the MET durability segment has increased. This is shown as resistance increases in Figure 89a, Figure 89b, and Figure 90b, but none in Figure 90a. Corrosion in the leads of the T2 electrode in the UFA durability segment is indicated by high resistance shown in Figure 91a that is indicated shown in Figure 89a or Figure 90a. Corrosion in other electrode leads is minimal as indicated by the stable resistance measurements.

Electrical resistance was also measured to develop a correction factor for electrical current readings. Typically, current reading between the electrodes is in micro-amp scale. On

this scale, the internal resistance of the meter is very high, which would alter the current reading. The correction factor can be calculated from measured resistance between the electrodes and internal resistance of the meter. While electrical current caused by corrosion was not detected during this project, future investigations at the Key Royale Bridge may make use of collected resistance data to determine correction factor.

Figure 85–Electrical resistance was measured using Nilsson model 400 soil resistance meter

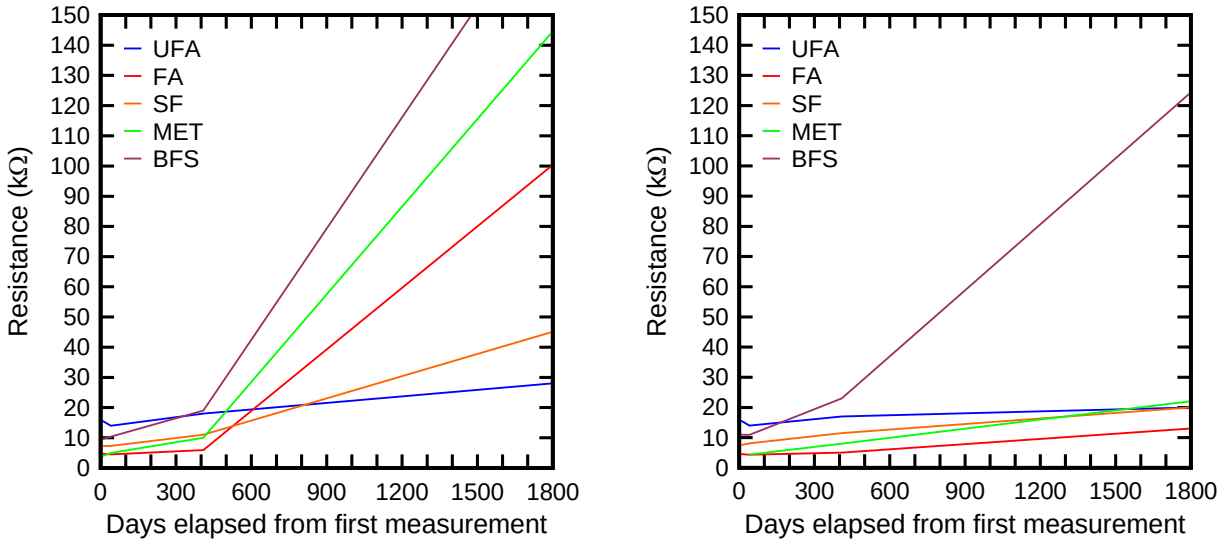

(a) (b)

Figure 86–Resistance between S1 and S2 electrodes for (a) bent 3 piles (b) bent 4 piles

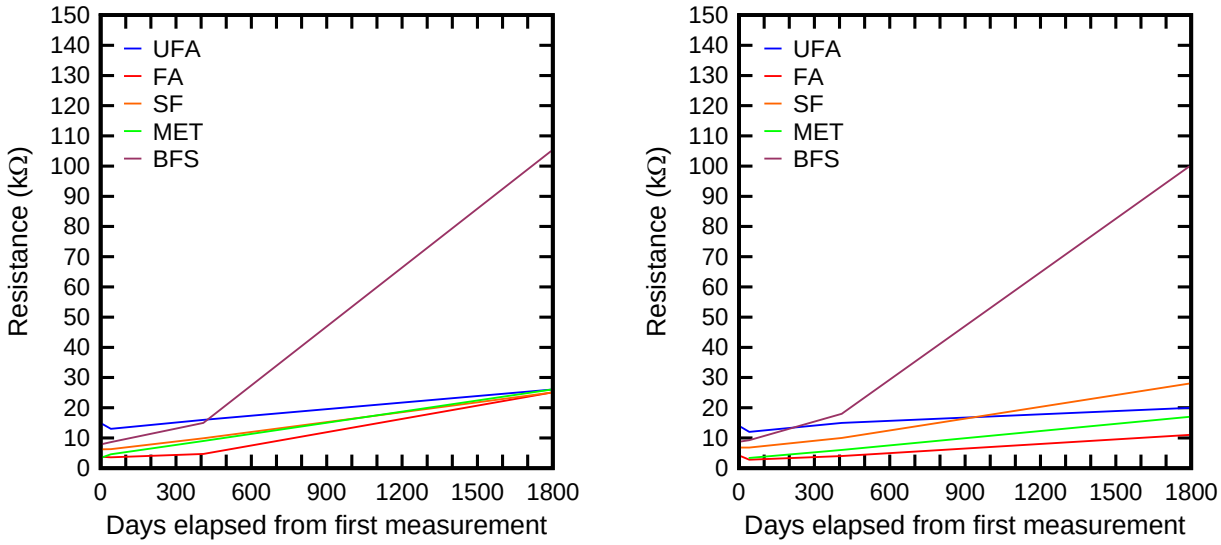

(a) (b)

Figure 87–Resistance between S1 and T1 electrodes for (a) bent 3 piles (b) bent 4 piles

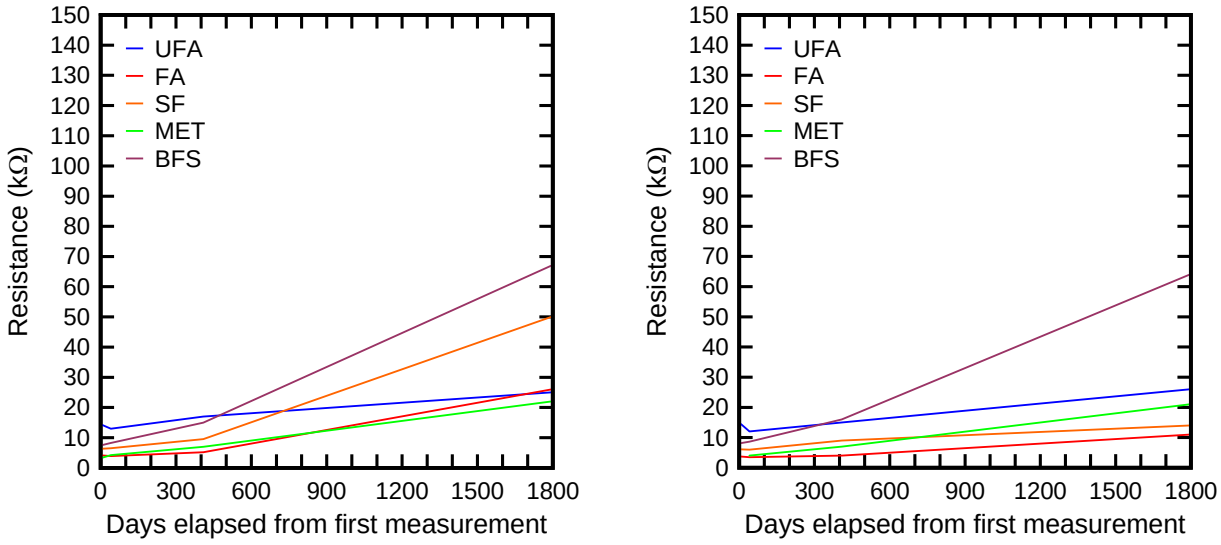

(a) (b)

Figure 88–Resistance between S2 and T2 electrodes for (a) bent 3 piles (b) bent 4 piles

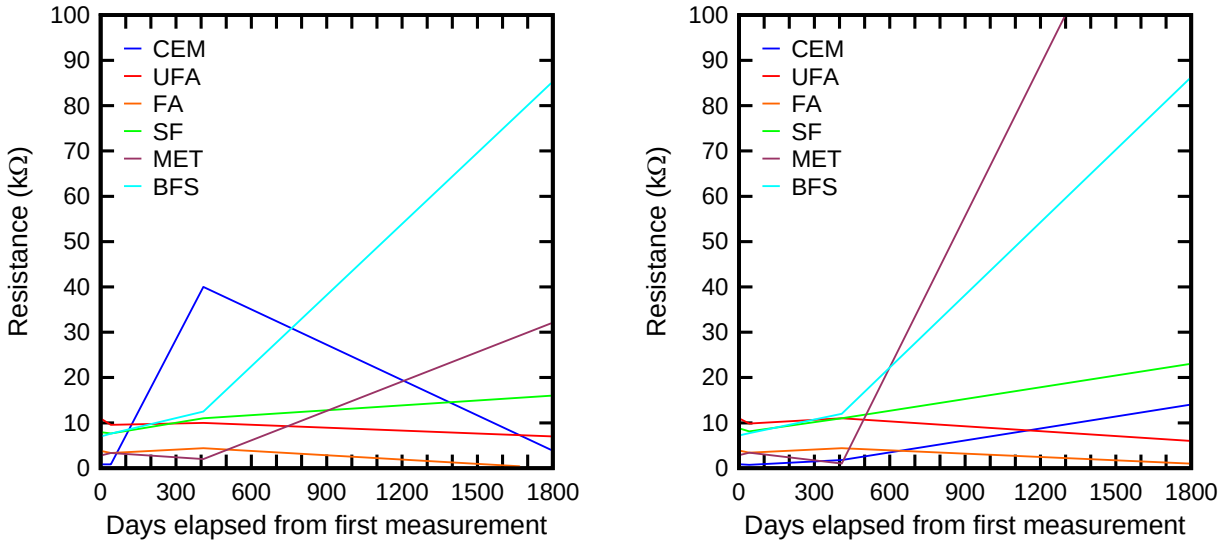

(a) (b)

Figure 89–Resistance between durability segment electrodes (a) S1 and S2 (b) S1 and S3

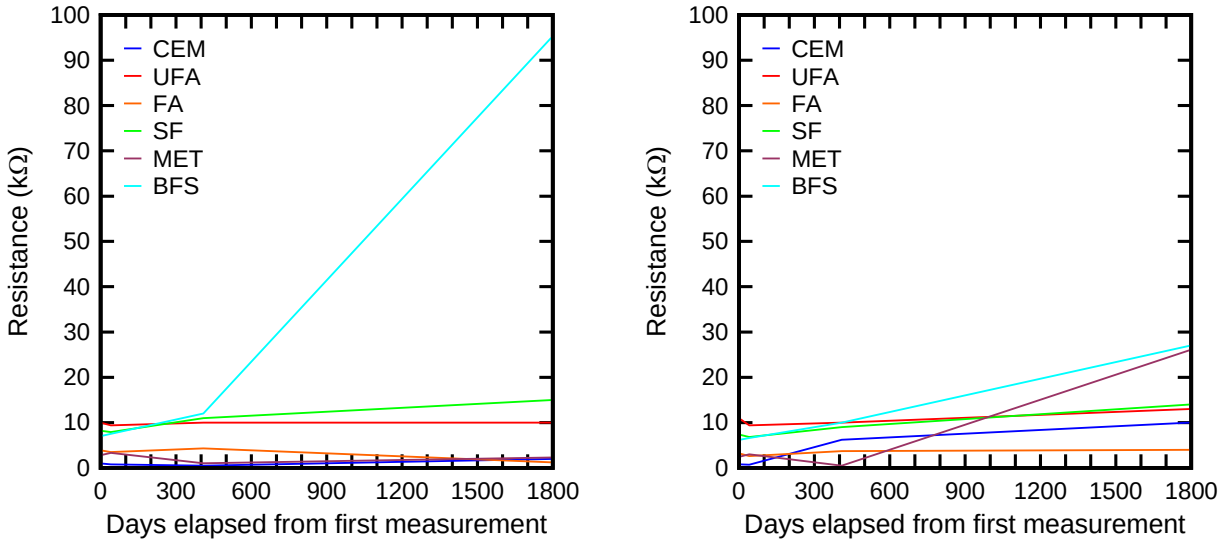

(a) (b)

Figure 90–Resistance between durability segment electrodes (a) S2 and S3 (b) S1 and T1

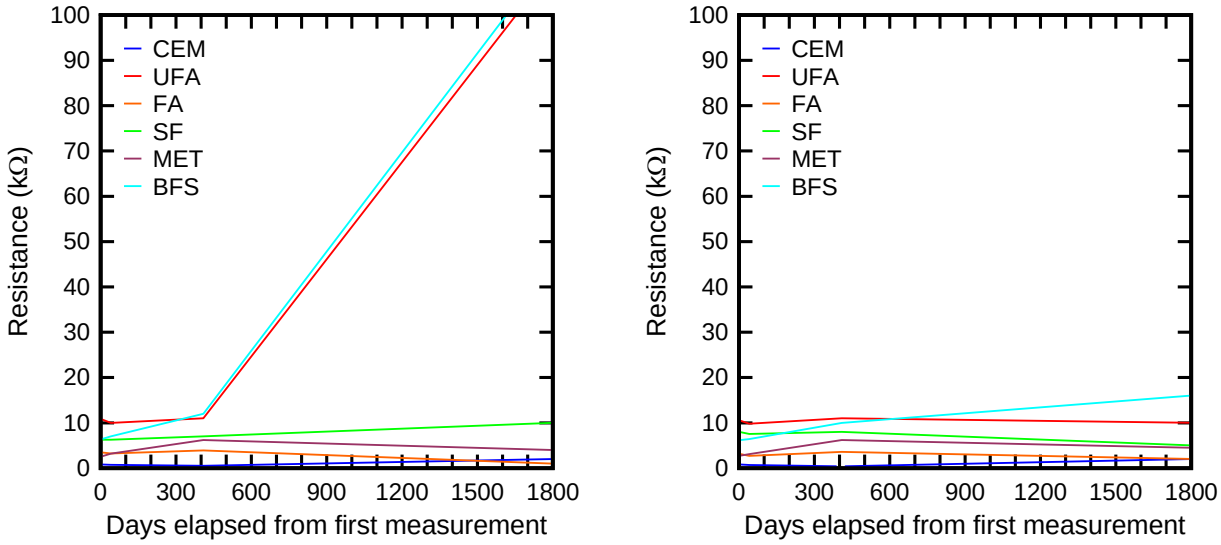

(a) (b)

Figure 91–Resistance between durability segment electrodes (a) S2 and T2 (b) S3 and T3

9.5 Electrical Current Measurement

Electrical current was measured between the steel electrodes within each of the piles in bents 3 and 4. Current flow, driven by a different potential in each internal electrode, is expected when corrosion has initiated. Prior to initiation, the electrical potential of each of the electrodes should be similar and any measured current would be an artifact of the formation of microcells within the cement matrix as hydration proceeded unevenly due to the random distribution of concrete particles.

Although corrosion was not yet apparent, the flow of electrical current between the S1 and S2 electrodes in bent 3 and 4 piles was measured to obtain a baseline value to compare to current flow once corrosion initiation had occurred. As indicated in Figure 92, current has stabilized near zero amps as time has progressed. Current flow early in the life of the structure was probably caused by the formation of microcells within the pile as hydration proceeded; with hydration largely complete, the current declined to near zero.

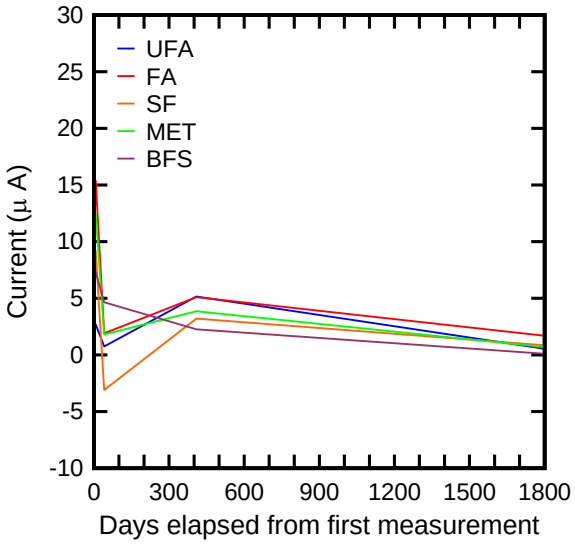

Figure 92–Electrical current flow between S1 and S2 electrodes in bent 3 and bent 4 piles

The flow of current between steel electrodes within the durability segments was also measured. Current between electrodes S1 and S2, shown in became smaller over time for all durability segments, indicating that each electrode had similar potentials. Current flow between S2 and S3 were less than 5 μA with the notable exception of FA, which had a current flow of 26 μA. The FA durability segment also had a higher current flow at 14 μA between S1 and S3 than any other durability segment; the next highest current flow was 6.6 μA in the MET durability segment. This indicates that there was a notable difference in potentials between the S3 electrode and the other two electrodes in the FA durability segment. It seems unlikely that corrosion has initiated given that the electrodes in the CEM durability segment, which would be expected to show corrosion first, show no indication of corrosion.

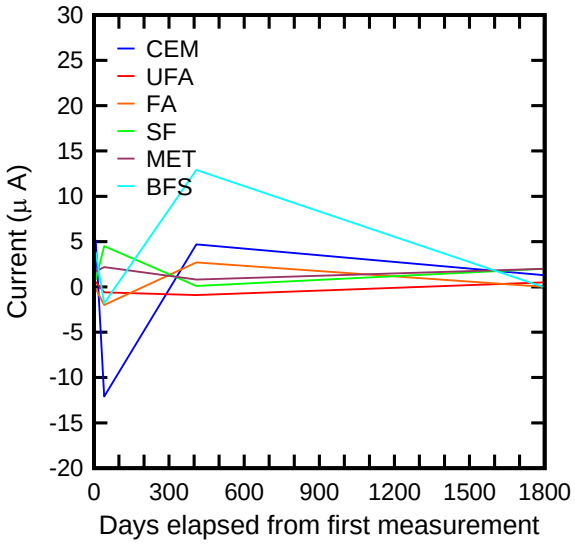

Figure 93–Electrical current flow between S1 and S2 electrodes in durability segments

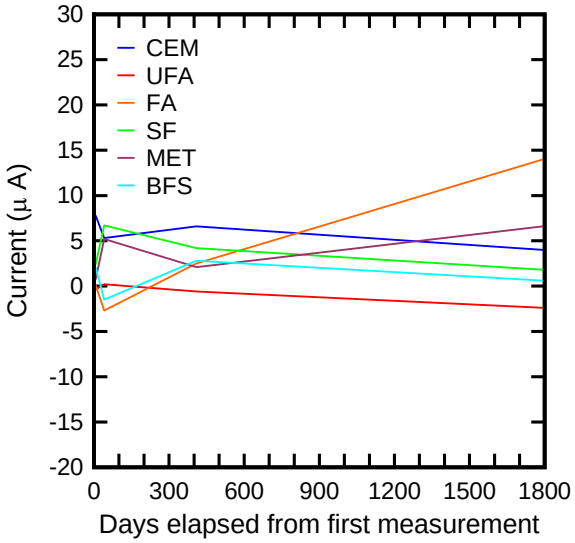

Figure 94–Electrical current flow between S1 and S3 electrodes in durability segments

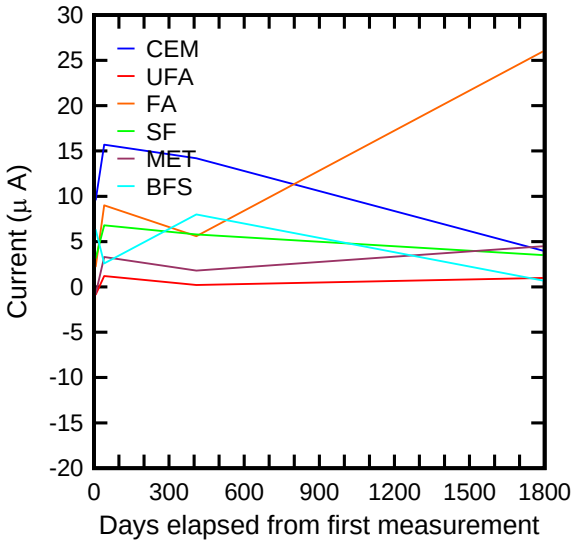

Figure 95–Electrical current flow between S2 and S3 electrodes in durability segments

10 Surface Resistivity

Surface resistivity measurement was carried out on the project bridge over a five-year period. The first measurements were taken soon after the bridge was completed in May 2007. Subsequent measurements were taken in June 2007, June 2008, and November 2011. Future measurements are expected to occur at five-year intervals. The next measurements are anticipated to occur in 2017.

The electrical resistivity of concrete is directly related to the density and interconnectedness of the paste pore structure. For this reason, resistivity is also related to the permeability and diffusivity of ions in concrete. Resistivity, therefore, provides a convenient method of estimating the rate at which chloride ions will penetrate a concrete mixture. As the permeability of a sample increases, the surface resistivity decreases. The use of SCM results in a more dense paste structure, which leads to a higher surface resistivity. The surface resistivity test is nondestructive, easy, and quick, making it ideal for field work.

Surface resistivity was measured using a Wenner linear 4-probe array with 2-in. probe spacing (Figure 96). Measurements were taken with the array placed in a horizontal orientation as shown in Figure 97. These were taken at the same locations on the pile faces as half-cell potential measurements. As with the half-cell potential measurements, initial measurements were made along one face of each pile while later measurements were made along all four faces of each pile. Some pile faces, especially those covered with burlap during curing, did not produce stable resistivity values. The irregular surface created by the burlap made establishing contact between the probes and the concrete.

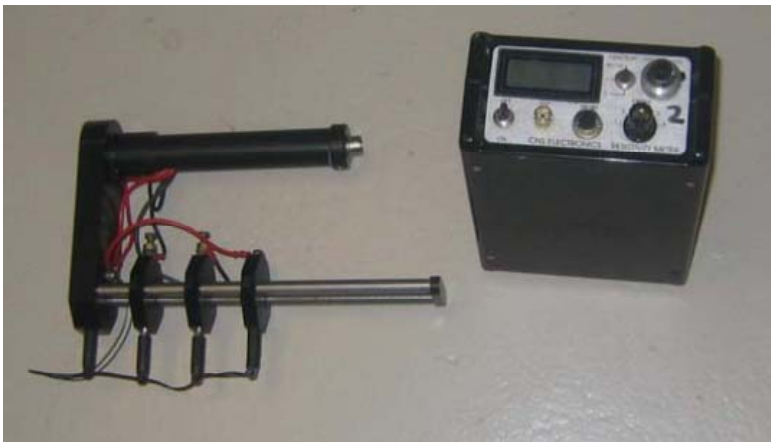

Figure 96–Wenner linear four-probe array and display

Figure 97–Surface resistivity readings were taken on the bridge piles.

Results from Presuel-Moreno et al. (2010) were incorporated into the analysis of the surface resistivity measurements. This research illustrated the difficulty of obtaining meaningful surface resistivity measurements from relatively dry concrete, such as that in the Key Royale Bridge piles. Lacking moisture in the pore structure, surface resistivity measurements of the dry concrete measures the resistivity of the concrete, not the interconnectedness of the pore structure. For this reason, surface resistivity measurements taken from the dry areas of the piles were judged to be invalid data and discarded from the analysis.

Figure 98 was created using measurements taken from the top of the marine growth. This area of the pile was saturated with seawater even at low tide, providing an electrolyte solution to conduct electric current produced by the Wenner probe and enabling the measurement of the continuity of the concrete pore structure. Measurements were taken on the same face of each pile as the half-cell potential measurements of the prestress strand, shown in Figure 55. Each plotted data point represents the average of all four piles containing the given SCM. As shown in the figure, surface resistivity increased with time for all pile mixtures as was expected. Piles containing UFA had the highest resistivity both initially and as time progressed. The surface resistivity of the FA pile had the lowest surface resistivity, which was also expected because the other four mixture designs each contained FA plus an additional SCM. Initially, the piles containing BFS had a low surface resistivity, reflecting the slower reaction rate of that SCM.

November 2011 surface resistivity measurements of piles containing SCM were higher than those of all other piles with the exception of the UFA piles. Piles containing SF or MET had lower surface resistivity than expected, particularly at early ages. MET and especially SF have small particles with high specific surface areas; these pozzolans were expected to react quickly to reduce the continuity of the concrete pore system.

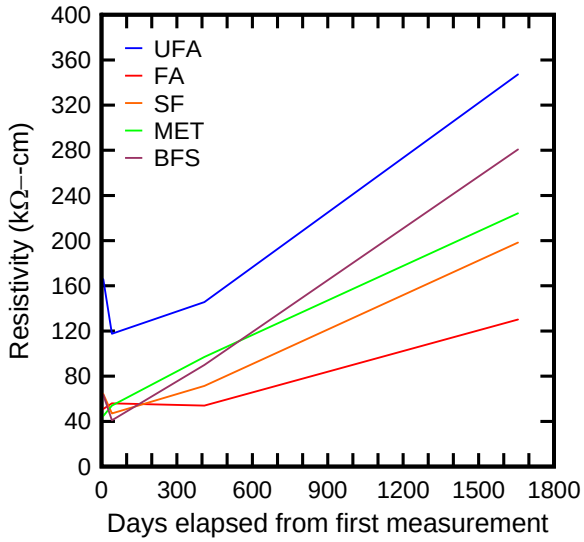

Figure 98–Surface resistivity in bridge piles measured at increasing ages

11 Chloride Diffusion

11.1 Selection of Coring Locations

Coring locations were selected in consultation with personnel at the University of Florida, University of South Florida, Florida Atlantic University, and SMO. The decision was made to obtain eight 2-in. diameter cores from each of the six fender piles at the west side of the non-navigable channel. Figure 99 shows the typical extraction layout; actual measurements varied slightly due to coring rig placement and as-built conditions and are provided in the appendix.

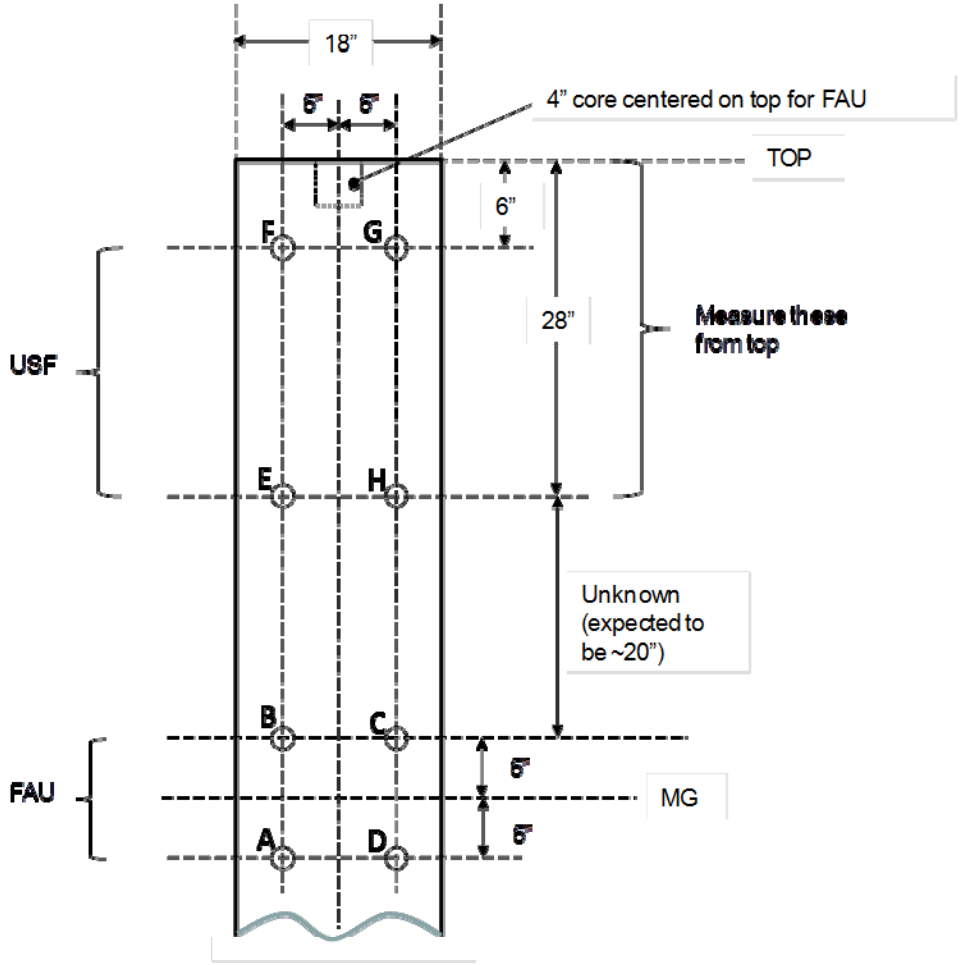

Figure 99–Typical locations of 2-in. diameter cores taken from fender piles

11.2 Results of chloride analysis

Diffusion coefficients calculated from the fender pile chloride profiles are summarized in Figure 100. In this plot, the vertical axis represents the coring location relative to the marine

growth line while the horizontal axis represents the diffusion coefficient. Diffusion coefficients and coring location data are presented in Table 29 through Table 34.

In general, diffusion coefficients were lower for cores taken higher along the pile face. In addition, the CEM diffusion coefficients are nearly an order of magnitude higher near the MGL. Others have also found that diffusion coefficients can be sensitive to the position from which the core is taken (Tang and Andersen 2000, Sagüés et al. 2001, Tang, L. 2003, and Cannon et al. 2006, Vivas et al. 2007). The silica fume concrete mixture also showed more sensitivity to location than the other piles with the exception of CEM; below the MGL, diffusion coefficients were twice those from higher elevations on the pile. Vivas et al. (2007) found that this ratio ranged from 0.63 to 4.35 depending on the age and concrete type.

Although the diffusion coefficients for the MET pile appear high, they are consistent with those obtained from cores extracted by others from this bridge (Table 3, Presuel Moreno et al., 2010). Diffusion coefficients were higher for the MET cores than any others as a group.

Chloride concentrations between 0.75 in. and 1.5 in. below the surface were analyzed to provide a supplemental assessment of the chloride resistance of the different mixtures. Only the cores closest to the MGL were included in the analysis (total of 24 points); cores higher along the pile were excluded to avoid the sensitivity of the diffusion coefficient to the position. Results are given in Figure 101 and Figure 102. From Figure 101, it is apparent that the CEM cores have chloride levels that are well above those of the other cores. Figure 102 shows the same data but with the scale expanded. As expected, the UFA and three of the four SF cores had very low chloride levels. The chloride levels in the FA cores were higher than most of the others in Figure 102; this is logical given the slow pozzolanic reaction of the fly ash. MET chloride levels were unexpectedly high and it is not clear why this is the case. Chloride levels in the BFS piles were below those of the FA binary mixture and were comparable to those of the SF piles.

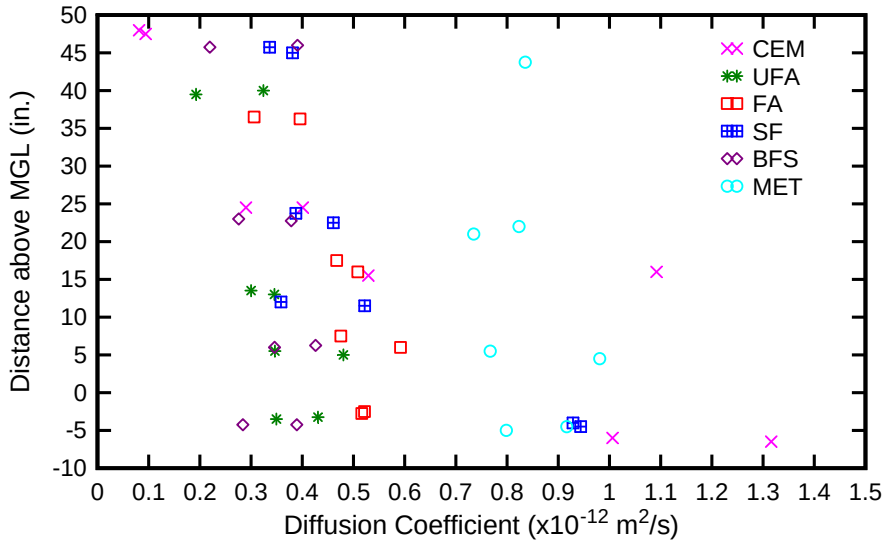

Figure 100–Diffusion coefficients and coring locations

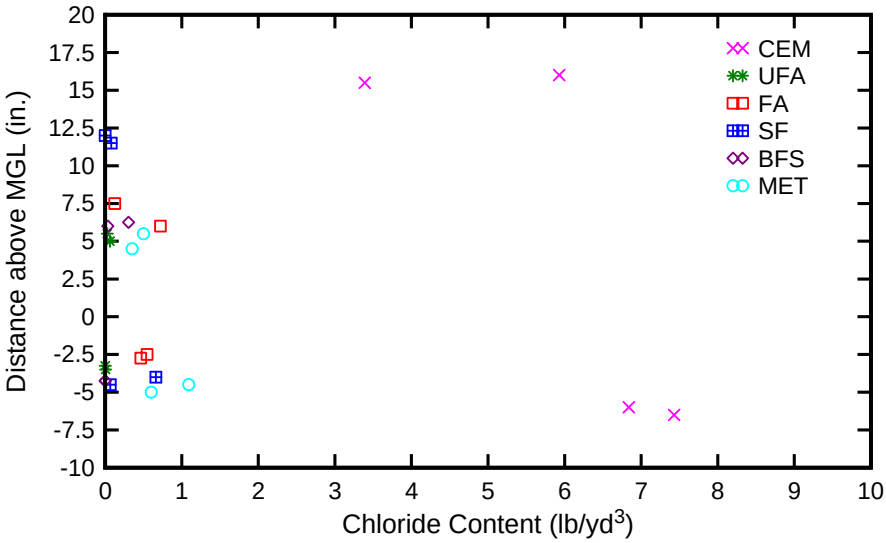

Figure 101–Coring locations and averaged measured chloride content at more than ¾” depth

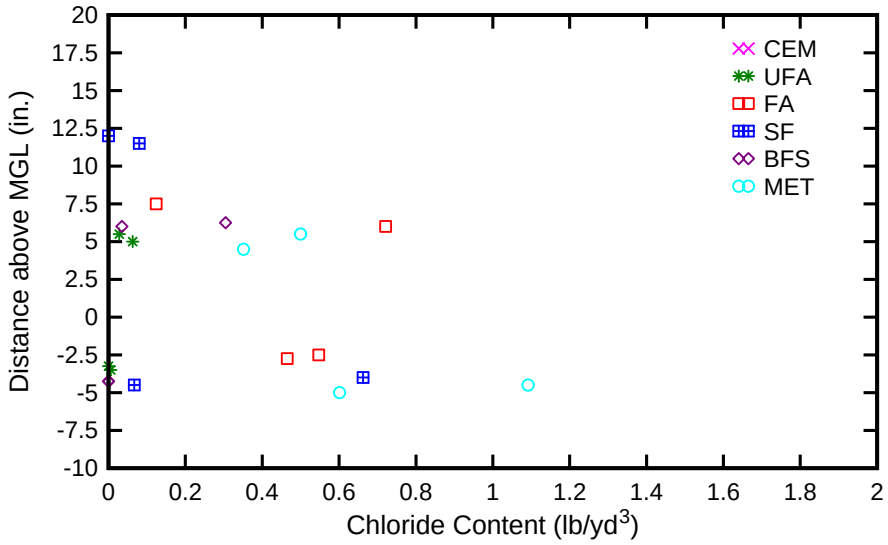

Figure 102–Coring locations and average measured chloride content at more than ¾" depth (excluding CEM)

Table 29–Diffusion coefficients for fender pile 1 (CEM)

Core	Distance above MGL (in)	D_{app} (x 10^{-12} m^2/s)	C_s (lb/yd^3)	C_o (lb/yd^3)
1-A	-6	1.006	22.70	0.22
1-B	15.5	0.529	22.55	0.05
1-C	16	1.092	20.01	0.21
1-D	-6.5	1.316	21.73	0.67
1-E	24.5	0.290	11.35	0.37
1-F	47.5	0.094	7.86	0.23
1-G	48	0.081	5.83	0.19
1-H	24.5	0.401	12.71	0.20

Table 30–Diffusion coefficients for fender pile 2 (UFA)

Core	Distance above MGL (in)	D_{app} (x 10^{-12} m^2/s)	C_s (lb/yd^3)	C_o (lb/yd^3)
2-A	-3.5	0.350	36.49	0.19
2-B	5.5	0.346	44.22	0.19
2-C	5	0.480	41.39	0.18
2-D	-3.25	0.431	31.57	0.26
2-E	13	0.346	26.74	0.28
2-F	39.5	0.192	8.87	0.17
2-G	40	0.324	7.44	0.19
2-H	13.5	0.300	22.73	0.16

Table 31–Diffusion coefficients for fender pile 3 (FA)

Core	Distance above MGL (in)	D_{app} (x 10^{-12} m^2/s)	C_s (lb/yd^3)	C_o (lb/yd^3)
3-A	-2.5	0.522	38.71	0.18
3-B	6	0.592	32.61	0.19
3-C	7.5	0.475	32.17	0.20
3-D	-2.75	0.516	40.86	0.21
3-E	16	0.509	19.25	0.16
3-F	36.25	0.396	8.46	0.17
3-G	36.5	0.306	11.16	0.19
2-H	17.5	0.467	18.89	0.17

Table 32–Diffusion coefficients for fender pile 4 (SF)

Core	Distance above MGL (in)	D_{app} (x 10^{-12} m^2/s)	C_s (lb/yd^3)	C_o (lb/yd^3)
4-A	-4.5	0.944	29.89	0.43
4-B	12	0.359	39.15	0.49
4-C	11.5	0.522	25.70	0.44
4-D	-4	0.929	26.08	0.42
4-E	23.75	0.388	14.65	0.42
4-F	45.75	0.336	10.26	0.45
4-G	45	0.381	9.38	0.38
4-H	22.5	0.461	14.15	0.49

Table 33–Diffusion coefficients for fender pile 5 (BFS)

Core	Distance above MGL (in)	D_{app} (x 10^{-12} m^2/s)	C_s (lb/yd^3)	C_o (lb/yd^3)
5-A	-4.25	0.284	42.65	0.31
5-B	6	0.346	49.31	0.28
5-C	6.25	0.426	44.34	0.28
5-D	-4.25	0.389	35.03	0.34
5-E	23	0.276	27.69	0.31
5-F	45.75	0.219	18.51	0.28
5-G	46	0.391	18.29	0.31
5-H	22.75	0.378	25.19	0.30

Table 34–Diffusion coefficients for fender pile 6 (MET)

Core	Distance above MGL (in)	D_{app} (x 10^{-12} m^2/s)	C_s (lb/yd^3)	C_o (lb/yd^3)
6-A	-4.5	0.917	29.28	0.18
6-B	5.5	0.767	29.14	0.18
6-C	4.5	0.981	23.60	0.18
6-D	-5	0.798	30.48	0.22
6-E	22	0.823	7.15	0.16
6-F	43.75	1.785	6.72	0.21
6-G	43.75	0.836	9.54	0.23
6-H	21	0.735	10.19	0.25

12 Summary and Conclusions

This report describes the five-year evaluation of the Key Royale Bridge substructure. Innovative Bridge Research and Construction (IBRC) funding was secured by the Florida Department of Transportation (FDOT) to evaluate the implementation of highly reactive supplementary cementitious materials into the construction of the Key Royale Bridge. Five different supplementary cementitious materials (SCM) were used to create the concrete mixtures used to construct the bridge and fender piles. Non-destructive evaluation techniques were used to allow monitoring under realistic exposure conditions at real time. Corrosion sensors were embedded in the bridge piles for continuous or periodic monitoring. Removable fender piles were also installed with the same mixtures. In addition, durability segments were constructed using the same concrete and prestressing strand as the fender piles. These segments were hung from the fender piles for consistent exposure conditions and instrumented with corrosion sensors for long-term corrosion monitoring. Conclusions are as follows:

- Half-cell potential measurements of the pile prestressing steel were taken using a copper-copper sulfate electrode (CSE). ASTM C876-09 was used as a guide for interpretation. Voltage measurements taken during the five year monitoring period remained consistent. No evidence of corrosion in the prestressing steel was indicated.
- Half-cell potential measurements were taken using CSE to evaluate the corrosion of steel and titanium electrodes embedded within the bridge piles and durability segments. Voltage measurements indicated that corrosion initiation had not occurred.
- Surface resistivity measurements were taken using a Wenner 4-probe linear array. Measurements indicated that surface resistivity increased with increasing concrete age.
- The six fender piles in bent 3 were cored to obtain diffusion coefficients for the six different concrete mixture designs used in the fender piles. Eight cores were taken from each of the piles. Two cores were taken from each of four elevations along the pile face.
- Diffusion coefficients were determined for each of the cores taken from the fender piles. The diffusion coefficients (x 10^{-13} m^2/s) ranged from 0.81 to 17.85. Coefficients for CEM had a range of 0.81 to 13.16. Coefficients for UFA had a range of 1.92 to 4.31. Coefficients for FA had a range of 3.06 to 5.92. Coefficients for SF had a range of 3.36 to 9.44. Coefficients for BFS had a range of 2.19 to 4.26. Coefficients for MET had a range of 7.67 to 17.85.

13 Future Inspection Plan

The Key Royale Bridge project was intended to involve long-term corrosion monitoring. With removable durability segments and fender piles, future research may be conducted to determine the continued effects of aging and chloride penetration on the different concrete mixtures used.

It is recommended that future inspections of the Key Royale Bridge similar to those conducted in this report be performed at five year intervals. Site visits should be performed in September or April so that measurement conditions are consistent with those of previous measurements. Future inspections are recommended for September 2017, 2022, and at five year intervals thereafter. Detailed descriptions of the different tests that were performed may be found in Appendix I of this report.

The time required to perform the measurements presented in this report may exceed the time available for a site visit. If this occurs, certain testing should be given priority. Measuring the half-cell potential of the pile prestressing strand using a CSE is the most important of the measurements to obtain. Obtaining these measurements should be possible within one day. Half-cell potential measurements may then be compared with previous measurements; the initiation of corrosion in the prestressing steel will probably be apparent from a voltage decrease near the MGL. To shorten the process, measurements may be limited to just those within four feet of the MGL.

Beyond measuring half-cell potentials of the pile prestressing steel, measuring the electrical activity within the pile and durability segment internal electrodes is the most important task of a site inspection. Care must be taken to ensure that the internal electrodes and internal electrode leads have not begun corroding. As of the most recent measurements (April 2012), there were indications that corrosion of the leads had initiated. Indications of malfunctioning internal electrodes must be recorded so that future visits can omit measurements of those electrodes.

In September 2017, the six durability segments should be removed and tested. A coring plan must be developed to obtain a reasonable number of cores from each segment. These cores must be taken from regions of the durability segment that were under water, near the MGL, and near the top of the segment where chloride exposure was limited. Cores must be taken

immediately after the durability segments are removed; it is recommended that a coring rig be established adjacent to the bridge. Durability segments must then be transported to the FDOT SMO for further evaluation.

In September 2022, the twelve fender piles should be removed and tested. Piles should be cut at the mud line using a pile "beaver". The six fender piles in bent 4 are undamaged by coring; these may be used in three-point flexural testing to evaluate the remaining flexural capacity within the pile. Cannon et al. (2006) performed a similar investigation on piles removed during the St. Georges Bridge replacement. Cores taken from the submerged zone must be obtained near the bottom of the pile to avoid influencing flexural testing. As with the durability segments, cores from the submerged zone must be taken immediately after the pile is removed from the water.

14 References

AASHTO, "*AASHTO LRFD Bridge Design Specifications*," 3rd Edition, American Association of State and Highway Transportation Officials, Washington, 2004.

AASHTO T 259-80 (1993). "Standard Method of Test for Resistance of Concrete to Chloride Ion Penetration." American Association of States Highway and Transportation Officials.

AASHTO T 260-97 (2001) "Sampling and Testing for Chloride Ion in concrete and Concrete Raw Materials." American Association of States Highway and Transportation Officials.

AASHTO T 277-86 (1990). "Rapid Determination of the Chloride Permeability of Concrete." American Association of States Highway and Transportation Officials.

ACI Committee 222, "Protection of Metals in Concrete Against Corrosion (ACI 222R-01)," American Concrete Institute, Farmington Hills, MI, 41 pp.

ACI Committee 232.1R, "Report on the use of Raw or Processed Natural Pozzolans in Concrete (ACI 232.1R-00)," American Concrete Institute, Farmington Hills, MI, 29 pp.

ACI Committee 232.2R, "Use of Fly Ash in Concrete (ACI 232.2R-03)," American Concrete Institute, Farmington Hills, MI, 41 pp.

ACI Committee 233, "Slag Cement in Concrete and Mortar (ACI 233R-03)," American Concrete Institute, Farmington Hills, MI, 18 pp.

ACI Committee 234, "Guide for the Use of Silica Fume in Concrete (ACI 234R-06)," American Concrete Institute, Farmington Hills, MI, 63 pp.

ACI Committee 363, 1992, "State-of-the-Art Report on High-Strength Concrete (ACI 363R-92) (Reapproved 1997)," American Concrete Institute.

American Coal Ash Association, "Fly Ash Facts for Highway Engineers," Federal Highway Administration Report FHWA-IF-03-019, June 13, 2003, 76 pp.

Assouli, B, Ballivy, G., and Rivard, P. (2008). "Influence of Environmental Parameters on Application of Standard ASTM C876-91: Half Cell Potential Measurements." *Corrosion Engineering, Science and Technology*, 43(1), 91-96.

ASTM C 39 "Compressive Strength of Cylindrical Concrete Specimens." ASTM International, West Conshohocken, PA, 2001, 7 pp.

ASTM C 78 "Flexural Strength of Concrete (Using Simple Beam with Third-Point Loading)." ASTM International, West Conshohocken, PA, 2002, 3 pp.

ASTM C114 “Standard Test Methods for Chemical Analysis of Hydraulic Cement.” ASTM International, West Conshohocken, PA, 2011, 32 pp.

ASTM C157 “Standard Test Method for Length Change of Hardened Hydraulic-Cement Mortar and Concrete.” ASTM International, West Conshohocken, PA, 2008, 7 pp.

ASTM C 469 “Static Modulus of Elasticity and Poisson’s Ratio of Concrete in Compression.” ASTM International, West Conshohocken, PA, 2000, 5 pp.

ASTM C496 “Standard Test Method for Splitting Tensile Strength of Cylindrical Concrete Specimens.” ASTM International, West Conshohocken, PA, 2011, 5 pp.

ASTM C512 “Creep of Concrete in Compression.” ASTM International, West Conshohocken, PA, 1999, 4 pp.

ASTM C642 “Standard Test Method for Density, Absorption, and Voids in Hardened Concrete.” ASTM International, West Conshohocken, PA, 2006, 3 pp.

ASTM C876, “Standard Test Method for Half-Cell Potentials of Uncoated Reinforcing Steel in Concrete.” ASTM International, West Conshohocken, PA, 2009, 7 pp.

ASTM C989 “Standard Specification for Slag Cement for Use in Concrete and Mortars.” ASTM International, West Conshohocken, PA, 2006, 8 pp.

ASTM C1012 “Standard Test Method for Length Change of Hydraulic Cement Mortars Exposed to a Sulfate Solution.” ASTM International, West Conshohocken, PA, 2004, 7 pp.

ASTM C1152 “Standard Test Method for Acid-Soluble Chloride in Mortar and Concrete.” ASTM International, West Conshohocken, PA, 2004, 7 pp.

ASTM C 1202. “Standard Test Method for Electrical Indication of Concrete’s Ability to Resist Chloride Ion Penetration.” ASTM International, West Conshohocken, PA, 2005, 7 pp.

ASTM C1293 “Standard Test Method for Determination of Length Change of Concrete Due to Alkali-Silica Reaction.” ASTM International, West Conshohocken, PA, 2005, 7 pp.

ASTM C1585 “Standard Test Method for Measurement of Rate of Absorption of Water by Hydraulic-Cement Concretes.” ASTM International, West Conshohocken, PA, 2004, 6 pp.

Badogiannis, E., Kakali, G., Dimopoulou, G., Chaniotakis, E., Tsivilis, S. (2005). “Metakaolin as a Main Cement Constituent. Exploitation of Poor Greek Kaolins,” *Cement and Concrete Composite*s, 27, pp. 197-203.

Bágel, L. (1998). ”Strength and pore structure of ternary blended cement mortars containing blast furnace slag and silica fume,” *Cement and Concrete Research*, 28 (7), pp. 1011-1022

Bai, J., Wild, S., Ware, J. A., Saber, B. B. (2003). “The Use of Neural Networks to Predict Workability of Concrete Incorporating Metakaolin and Fly Ash,” *Advances in Engineering Software*, 34, pp. 663-669.

Berube, M. A., Duchesne, J. and Frenette, J. (1998). “Influence of Storage Conditions and Concrete Composition on the Effectiveness of Different Silica Fume Against ASR.” *Proceedings of the 6th CANMET/ACI International Conference on Fly Ash, Silica Fume, Slag and Natural Pozzolans in Concrete, Supplementary Book*, pp. 1127-1147.

Bleszynski, R., Hooton, R. D., Thomas, M. D. A., and Rogers, C.A. (2002). “Durability of ternary blend concrete with silica fume and blast-furnace slag: Laboratory and outdoor exposure site studies.” *ACI Materials Journal*, 99(5), pp. 499-508.

Boral Material Technologies (2003). “Boral Micron 3, A Highly Reactive Pozzolan”

Broomfield, J. and Millard, S. (2002). “Measuring concrete resistivity to assess corrosion rates.” A report from The Concrete Society/Institute of Corrosion liaison committee, Current Practice Sheet (128), pp. 37-39.

Buil, M., and Acker, P. (1985). “Creep of a silica fume concrete.” *Cement and Concrete Research,* 15(3), pp. 463-466.

Cannon, E., Lewinger, C., Abi, C., Hamilton, H.R. (2006). “St. George Island Bridge Pile Testing” Final Report No. BD545, Florida Department of Transportation.

Chini, A.R., Muszynski, L.C., Hicks, J. (2003). “Determination of Acceptance Permeability Characteristics for Performance-Related Specifications for Portland Cement Concrete,” Florida Department of Transportation, Final Report No. BC 354-41.

Costa, A. and Appleton, J. (1998). “Chloride Penetration Into Concrete in Marine Environment – Part I: Main Parameters Affecting Chloride Penetration.” *Materials and Structure*s, 32(5), pp. 252-259

Dehuai, W. and Zhaoyuan, C. (1997). “On Predicting Compressive Strengths of Mortars with Ternary Blends of Cement, GGBFS and Fly Ash.” *Cement and Concrete Research*, 27(4), pp. 487-493.

Domone, P. L. and Soutsos, M. N. (1995). "Properties of High-Strength Concrete Mixes Containing PFA and GGBFS," *Magazine of Concrete Research*, 47(173), pp. 355-367.

Douglas, E. and Pouskouleli, G. (1991). "Prediction of Compressive Strength of Mortars Made with Portland Cement -Blast-Furnace Slag - Fly Ash Blends." *Cement and Concrete Research*, 21(4), pp. 523-534.

Elahi, A., Basheer, P.A.M., Nanukuttan, S.V., and Khan, Q.U.Z. (2009). "Mechanical and Durability Properties of High Performance Concretes Containing Supplementary Cementitious Materials." *Construction and Building Materials,* 24, pp. 292-299.

Elsener, B., Andrade, C., Gulikers, J., Polder, R., and Raupach, M. (2003). "Half-cell Potential Measurements – Potential Mapping on Reinforced Concrete Structures." Materials and Structures, 36(5), pp. 461-471.

Erdem T.K., Kirca O., (2008). "Use of Binary and Ternary Blends in High Strength Concrete", *Construction and Building Materials*, 22, pp. 1477-1483.

FDOT "Florida Department of Transportation Standard Specification for Road and Bridge Construction," Florida Department of Transportation, 2011.

FDOT "Florida Department of Transportation Structures Design Guidelines." Florida Department of Transportation, January 2011.

FM 5-516 "Florida Test Method for Determining Low-Levels of Chloride in Concrete and Raw Materials," Florida Department of Transportation, revised June 14, 2005.

FM 5-578 "Florida Test Method for Concrete Resistivity as an Electrical Indicator of Permeability," Florida Department of Transportation, January 27, 2004.Florida Department of Transportation (FDOT).

Francois, R., Arliguie, G., Bardy, D. (1993). "Electrode Potential Measurements of Concrete Reinforcement for Corrosion Evaluation." *Cement and Concrete Researc*h, 24(3), pp. 401-412.

Gowers, K.R. and Millard, S.G. (1999). "Measurement of Concrete Resistivity for Assessment of Corrosion Severity of Steel Using Wenner Technique." *ACI Materials Journal*, 96(5), pp. 536-541.

Haque, M.N. and Chulilung, T. (1990). "Strength Development of Slag and Ternary Blend Concrete," *Cement and Concrete Research,* 20(1), pp. 120-130.

Hooton, R.D.,Thomas, M.D.A. and Stanish, K. (2001). "Prediction of Chloride Penetration in Concrete." Final Report No. FHWA/RD-00/142, Federal Highway Administration.

Hughes, B.P., Soleit, A.K.O. and Brierly, R.W. (1985). "New Technique for Determining the Electrical Resistivity of Concrete." *Magazine of Concrete Research*, 37(133), 243-248.

Isaia, G. C., Gastaldini, A. L. G., and Moraes, R. (2003). "Physical and Pozzolanic Action of Mineral Additions on the Mechanical Strength of High-Performance Concrete," *Cement and Concrete Composites*, 25(1), pp 69-76.

Jones, M. R., Dhir, R. K., and Magee, B. J. (1997). "Concrete Containing Ternary Blended Binders: Resistance to Chloride Ingress and Carbonation." *Cement and Concrete Research,* 27(6), pp 825-831.

Jones, M. R., McCarthy, A., Booth, A. P. P. G. (2006). "Characteristics of the Ultrafine Component of Fly Ash," *Fuel*, 85, pp. 2250-2259.

Justice, J.M., Kennison, L.H., Mohr, B.J., Beckwith, S.L., McCormick, L.E., Wiggins, B., Zhang, Z.Z., and Kurtis, K.E. "Comparison of Two Metakaolins and a Silica Fume Used as Supplementary Cementitious Materials." *Pro. Seventh International Symposium on Utilization of High-Strength/High Performance Concrete*, Washington DC, June 20-24, 2005.

Khan, M. I. and Lynsdale, C. J. (2002). "Strength, Permeability, and Carbonation of High-Performance Concrete." *Cement and Concrete Research*, 32(1), pp. 123-131.

Khan, M. I., Lynsdale, C. J., and Waldron, P. (2000). "Porosity and Strength of PFA/SF/OPC Ternary Blended Paste," *Cement and Concrete Research*, 30(8), pp. 1225-1229.

Kim, H.S., Lee, S.H., Moon, H.Y. (2006). "Strength Properties and Durability Aspects of High Strength Concrete Using Korean Metakaolin." *Construction and Building Materials* 21, pp. 1229-1237.

Khatri, R. P., and Sirivivatnanon V. (1995). "Effect of Different Supplementary Cementitious Materials on Mechanical Properties of High Performance Concrete." *Cement and Concrete Research*, 25(1), pp 209-220.

Koch, G. H., Brongers, M.P.H., Thompson, N.G., Virmani, Y.P., Payer, J.H. (2006). "Corrosion Costis and Preventive Strategies in the United States." Federal Highway Administration Report FHWA RD-01-156, 12 pp.

Kurdowski, W., and Nocum-Wezelik, W. (1983). "The tricalcium Silicate Hydration in the Presence of Active Silica." Cement and Concrete Research, 13(1) pp.341-348.

Lane, D. S. and Ozyildirim, C. (1999). "Preventive Measures for Alkali-Silica Reactions (Binary and Ternary Systems)." *Cement and Concrete Research*, 29(8), pp 1281-1288.

Leelalerkiet V., Kyung, J.W., Ohtsu, M., and Yokota, M. (2004). "Analysis of Half-Cell Potential Measurement for Corrosion of Reinforced Concrete," *Construction and Building Materials*, 18(3), pp. 155-162.

Li, G. and Zhao, X. (2002). "Properties of Concrete Incorporating Fly Ash and Ground Granulated Blast-Furnace Slag." Cement and Concrete Composites, 25(3), pp 293-299.

Lohtia, R.P., Nautiyal, B.D., and Jain, O.P. (1976). "Creep of Fly Ash Concrete." *Journal of The American Concrete Institute,* 73(8), pp. 469-472.

Long, G., Wang, X., and Xie, Y. (2002). "Very-High-Performance Concrete With Ultrafine Powders," Cement and Concrete Research, 32(4), pp. 601-605.

Mehta, R. K. and Gjoerv O. E., (1982). "Properties of Portland Cement Concrete Containing Fly Ash and Condense Silica-Fume." Cement and Concrete Research, 12(5), pp. 587-595.

Menendez, G., Bonavetti, V., and Irassar, E. F. (2003). "Strength Development of Ternary Blended Cement with Limestone Filler and Blast-Furnace Slag," *Cement and Concrete Composites*, 25(1), pp. 61-67.

Mindess, S., Young, J. F., and Darwin, D. Concrete, Second Edition, Pearson Education, Inc., Upper Saddle River, New Jersey, 2003, 644 pp.

Monfore, G.E. (1968). "The Electrical Resistivity of Concrete." *Journal of the PCA Research and Development Laboratories*, 10(2), pp. 35-48.

Morris, W., Moreno, E.I. and Sagües, A.A. (1996). "Practical Evaluation of Resistivity of Concrete in Test CylindersUsing a Wenner Array Probe." *Cement and Concrete Research*, 26(12), pp. 1779-1787.

Moser, R., Holland, B., Kahn, L., Singh, P., Kurtis, K. (2010). "Durability of Precast Prestressed Concrete Piles in Marine Environment: Reinforcement Corrosion and Mitigation – Part 1." Georgia Institute of Technology.

Naito, C., Jones, L., Hodgson, S.E. (2010). "Inspection Methods & Techniques to Determine Non Visible Corrosion of Prestressing Strands in Concrete Bridge Components – Task 3 – Forensic Evaluation and Rating Methodology." Pennsylvania Department of Transportation Bureau of Planning and Research Project.

Nehdi, M. L. (2001). "Ternary and Quaternary Cements for Sustainable Development," *Concrete International*, American Concrete Institute, 4, pp. 35-42.

Nehdi, M.L. and Sumner, J. (2002). "Optimization of Ternary Cementitious Mortar Blends Using Factorial Experimental Plans," *Materials and Structures*, 35(252 SPEC), pp. 495-503.

Neville, A. M. (1995) "Properties of Concrete." Fourth Edition, Pearson Education.

NT BUILD 492 (1999). "Concrete, mortar and cement-based repair materials: Chloride Migration Coefficient from Non-Steady-State Migration Experiments." Nordtest Method.

Polder, R., Andrade, C., Elsener, B., Ø. Vennesland, Gulikers, J., Weidert, R., and Raupach, M. (2001) "Test Methods for On Site Measurement of Resistivity of Concrete – Recommendations." *Materials and Structures*, 33(12), pp. 603-611.

Popovics, S. (1993). "Portland Cement-Fly Ash-Silica Fume Systems in Concrete." *Advanced Cement Based Materials*, 1(12), pp 83-91.

Presuel-Moreno, F., Suares, A., Liu, Y. (2010) "Characterization of New and Old Concrete Structures Using Surface Resistivity Measurements." Final Report No. BD546, Florida Department of Transportation.

Roske, Edward K. (2007), "Implementation of highly reactive pozzolans in the Key Royale bridge replacement," M.S. Thesis, University of Florida.

Roske, E., Nash, T., Hamilton, H.R. (2008). "Development of Concrete Mixtures Containing Highly Reactive Pozzolans for Improved Durability in Florida Environments." Final Report No. BD545-64, Florida Department of Transportation.

Sagüés, A.A., Kranc, S.C., Presuel-Moreno, F., Rey, D., Torres-Acosta, A. and Yao, L. (2001). "Corrosion Forecasting for 75-Year Durability Design of Reinforced Concrete." Final Report No. BA 502, Florida Department of Transportation.

Sandberg, P., Tang, L., and Andersen, A. (1998). "Recurrent Studies of Chloride Ingress in Uncracked Marine Concrete at Various Exposure Times and Elevations." Cement and Concrete Research, 28(10), pp. 1489-1503.

Shehata, M. H. and Thomas, D. A. (2002), "Use of Ternary Blends Containing Silica Fume and Fly Ash to Suppress Expansion Due to Alkali-Silica Reaction in Concrete." Cement and Concrete Research, 32(3), pp 341-349.

Shekarchi, M., Rafiee, A., Layssi, H. (2009) "Long-term Chloride Diffusion in Silica Fume Concrete in Harsh Marine Climates." *Cement and Concrete Composites* 31, 769-775.

Smith, J.L., Virmani, Y.P. (2000). "Materials and Methods for Corrosion Control of Reinforced and Prestressed Concrete Structures in New Construction." Report No. FHWA-RD-00-081, Federal Highway Administration.

Sohanghpurwala, A.A. (2006). "Manual on Service Life of Corrosion-Damaged Reinforced Concrete Bridge Superstructure Elements." NCHRP Report No. 558.

Stanish, K.D., Hooton, R.D., Thomas, M.D.A. (1997). "Testing the Chloride Penetration Resistance of Concrete: A Literature Review." *Prediction of Chloride Penetration in Concrete*, Report No. DTFH61-97-R-00022, Federal Highway Administration

Streicher, P.E and Alexander, M.G. (1995). "A Chloride Conduction Test for Concrete." *Cement and Concrete Research*, 25(6), 1284-1294.

Tang, L. and Andersen, A. (2000). "Chloride ingress data from five years field exposure in a Swedish marine environment". Proceedings of the 2nd International RILEM Workshop on Testing and Modeling the Chloride Ingress into Concrete, Paris, 11-12, pp. 105-119.

Tang, L. (2003). "Chloride Ingress in Concrete Exposed to Marine Environment–Field data up to 10 years exposure". SP Swedish National Testing and Research Institute Building Technology and Mechanics. SP REPORT 2003:16.

Thomas, M. D. A., Shehata, M. H., Shashiprakash, S. G., Hopkins, D. S., and Cail., K. (1999)."Use of Ternary Cementitious Systems Containing Silica Fume and Fly Ash in Concrete," *Cement and Concrete Research*, 29(8), pp. 1207-1214.

Thomas, M. D. A., Scott, A. C. N. (2010). "Sustainable Concrete in a Marine Environment," *Proceedings of Honouree Sessions, Second International Conference on Sustainable Construction Materials and Technologies*, June 28-June 30, 2010.

Van Etten, N., Vivas, E., Nash, T., Hamilton, H.R. (2009). "Durability and Mechanical Properties of Ternary Blend Concretes." Final Report No. BD545-35, Florida Department of Transportation.

Vivas, E., Boyd, A., and Hamilton III, H. R. (2007). "Permeability of Concrete – Comparison of Conductivity and Diffusion Methods," Florida Department of Transportation, Final Report No. BC 354-41, 227 pp.

Whiting, D. and Mohamad, N. (2003). “Electrical Resistivity of Concrete-A Literature Review.” Portland Cement Association, R&D Serial No. 2457.

Zongjin, L., Ding, Z. (2003). “Property Improvement of Portland Cement by Incorporating with Metakaolin and Slag,” *Cement and Concrete Research*, 33, pp. 579-584.

Appendix A–Pile Construction

Construction Drawings

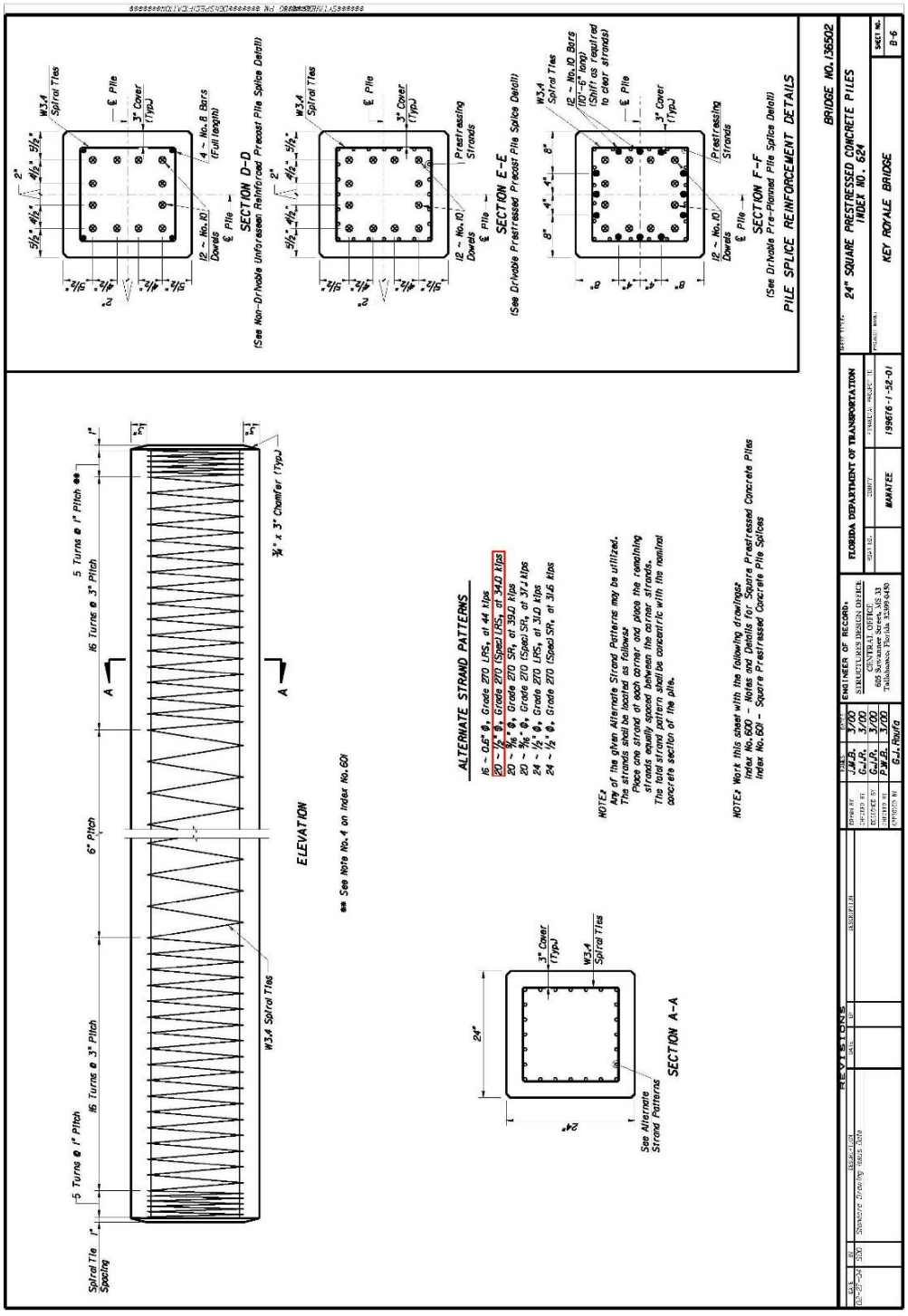

24 in square prestress pile

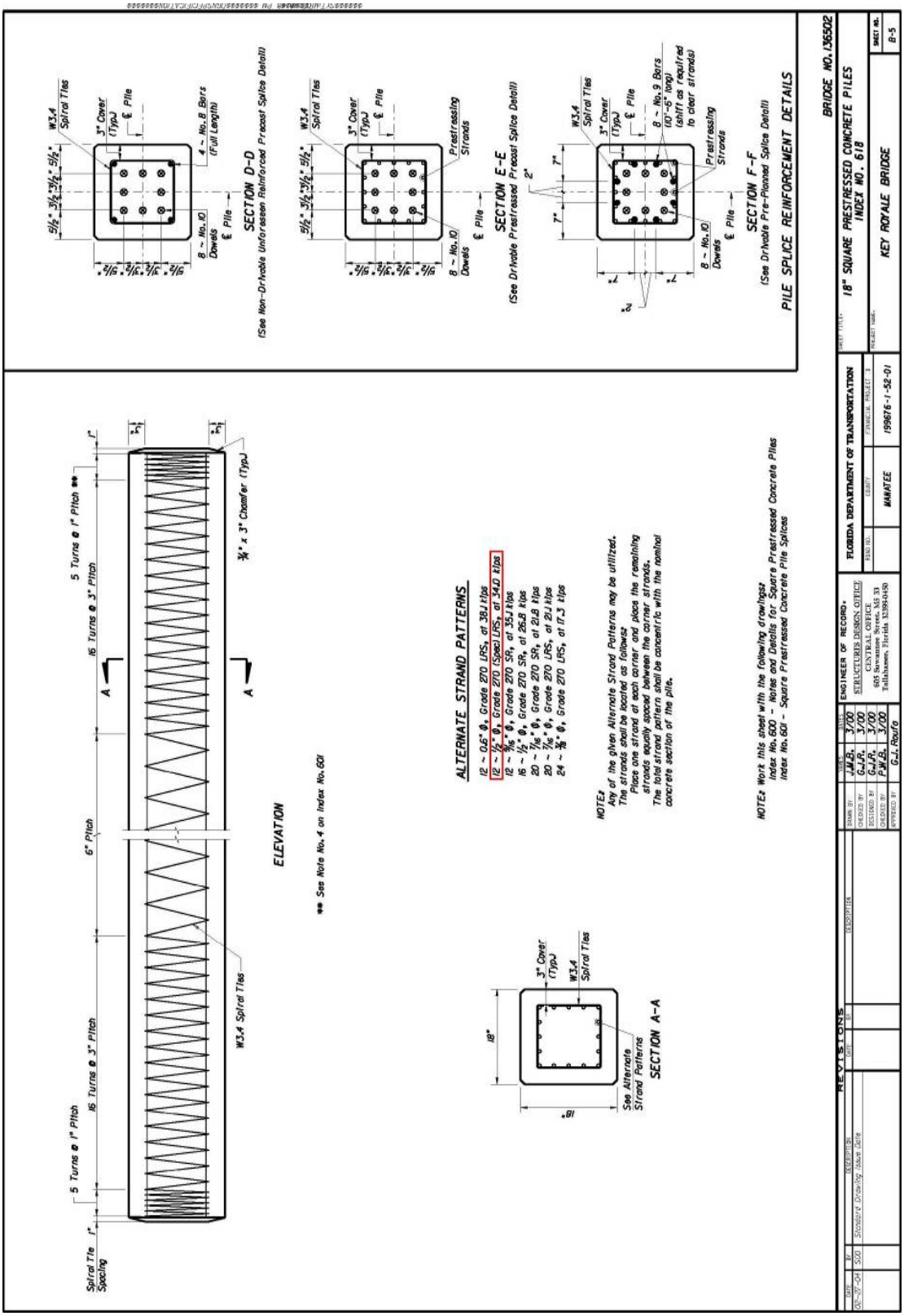

18 in square prestress pile

Pile Location Key

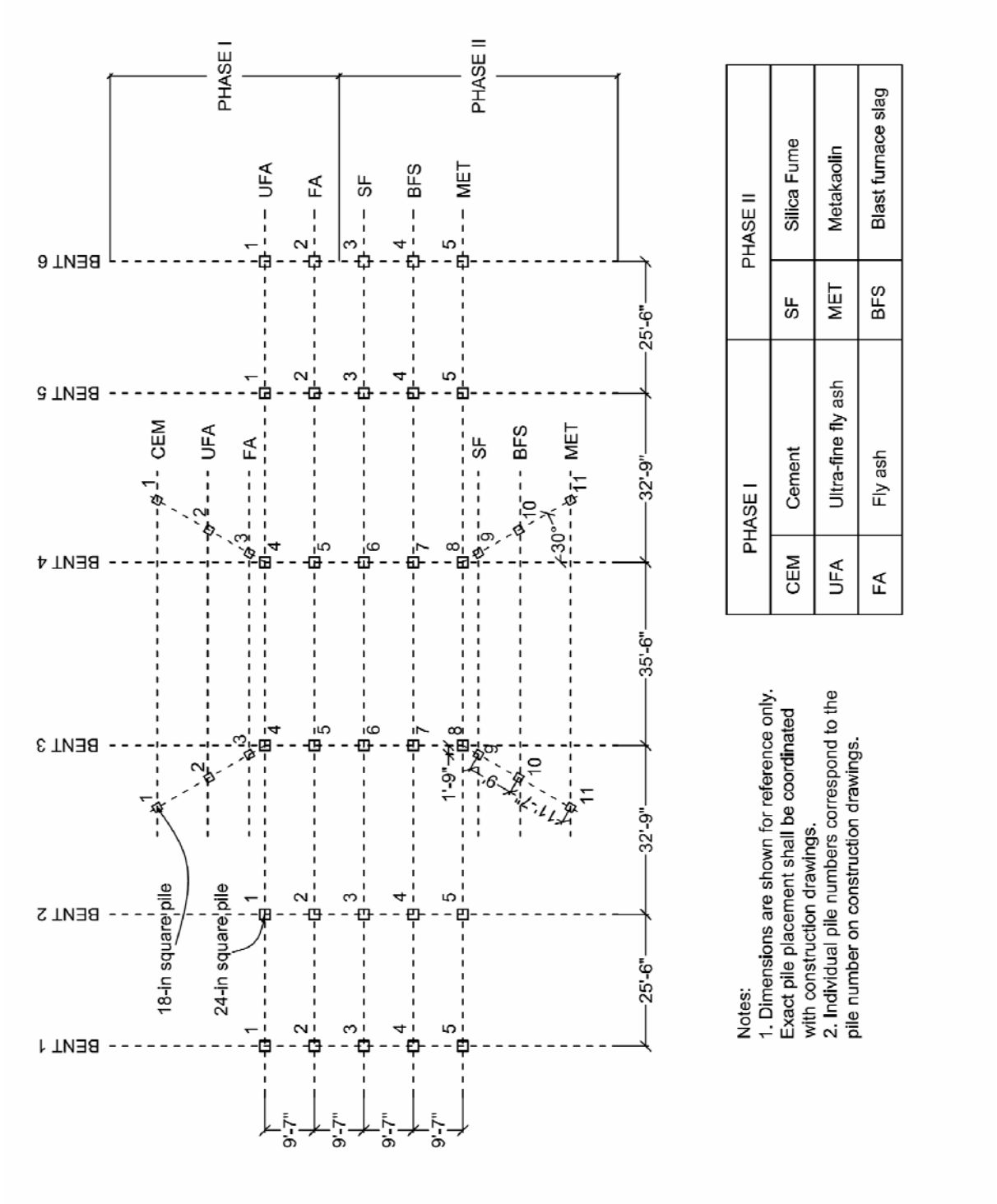

PHASE I		PHASE II	
CEM	Cement	SF	Silica Fume
UFA	Ultra-fine fly ash	MET	Metakaolin
FA	Fly ash	BFS	Blast furnace slag

Notes:
1. Dimensions are shown for reference only. Exact pile placement shall be coordinated with construction drawings.
2. Individual pile numbers correspond to the pile number on construction drawings.

PHASE I

24-in. bridge piles					
Pile Label	Job #	Date	Serial #	Length	Driving Date
UFA 1	B1349	6606	VV2	70-ft	09/08/06
UFA 2	B1349	6606	VV4	85-ft	09/06/06
UFA 3*	B1349	6606	VV6	85-ft	08/31/06
UFA 4*	B1349	6606	VV5	85-ft	08/28/06
UFA 5	B1349	6606	VV3	85-ft	09/12/06
UFA 6	B1349	6606	VV1	70-ft	09/14/06
FA1	B1349	62306	VV7	70-ft	09/08/06
FA2	B1349	62306	VV9	85-ft	09/06/06
FA3*	B1349	62306	VV12	85-ft	09/07/06
FA4*	B1349	62306	VV11	85-ft	08/28/06
FA5	B1349	62306	VV10	85-ft	09/12/06
FA6	B1349	62306	VV8	70-ft	09/14/06
18-in. fender piles					
UFA 3F	B1349	6906	VV1	45-ft	12/14/06
UFA 4F	B1349	6906	VV2	45-ft	12/15/06
FA 3F	B1349	61606	VV8	45-ft	12/14/06
FA 4F	B1349	61606	VV9	45-ft	12/15/06
CEM 3F	B1349	61606	VV5	45-ft	12/14/06
CEM 4F	B1349	61606	VV6	45-ft	12/15/06

* Contain Smart Pile Sensors

PHASE II

24-in. bridge piles					
Pile Label	Job #	Date	Serial #	Length	Driving Date
SF 1	B1349	92906	VV13	70-ft	01/19/07
SF 2	B1349	92906	VV15	85-ft	01/18/07
SF 3*	B1349	92906	VV16	85-ft	01/16/07
SF 4*	B1349	92906	VV17	85-ft	01/11/07
SF 5	B1349	92906	VV18	85-ft	01/23/07
SF 6	B1349	92906	VV14	70-ft	01/24/07
BFS 1	B1349	10606	VV19	70-ft	01/19/07
BFS 2	B1349	10606	VV21	85-ft	01/18/07
BFS 3*	B1349	10606	VV23	85-ft	01/16/07
BFS 4*	B1349	10606	VV24	85-ft	01/11/07
BFS 5	B1349	10606	VV22	85-ft	01/23/07
BFS 6	B1349	10606	VV20	70-ft	01/24/07
MET 1	B1349	101306	VV25	70-ft	01/19/07
MET 2	B1349	101306	VV29	85-ft	01/18/07
MET 3*	B1349	101306	VV27	85-ft	01/16/07
MET 4*	B1349	101306	VV28	85-ft	01/11/07
MET 5	B1349	101306	VV30	85-ft	01/23/07
MET 6	B1349	101306	VV26	70-ft	01/24/07
18-in. fender piles					
SF 3F	B1349	92906	VV10	45-ft	01/25/07
SF 4F	B1349	92906	VV12	45-ft	01/26/07
BFS 3F	B1349	10606	VV13	45-ft	01/25/07
BFS 4F	B1349	10606	VV15	45-ft	01/26/07
MET 3F	B1349	101306	VV16	45-ft	01/25/07
MET 4F	B1349	101306	VV18	45-ft	01/26/07

* Contain Smart Pile Sensors

Precast Plant Documentation

Precast plant documents are summarized below. For each bridge and fender pile, strand stress, strand type, date of construction, and strand releasing pattern are shown. The ticket for each concrete buggy is also included. The ticket shows the actual quantity of each material that was used for each specified concrete mixture. The ticket number indicates the number of the concrete buggy used in the casting of specified mixture piles. One ticket is assigned to each concrete buggy.

Fender Piles – Mixture CEM

Strand Stress Summary	
Date	06/15/06
Bed No.	22
Ambient Temp.	88 degree (F)
Cable Type	½ Special 7W 270LR ASTM A416
Final Tension	35466
+2.5%	36072
-2.5%	34579

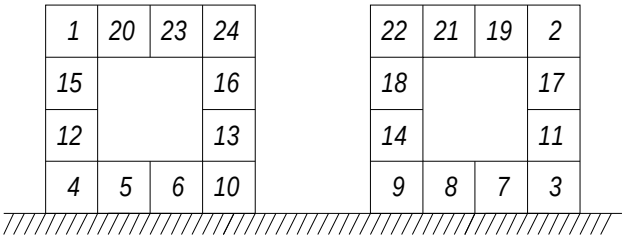

Stressing pattern for fender piles – Mixture CEM

Date: 06/16/06	Ticket: 3		
Material	Producer	Quantity	%MC
Sand 3	Pit No. 36-491	4,180 lbf	2.7
67 Granite 2	GA553	9,320 lbf	2.1
Cement 2	Suwannee American	4,815 lbf	N/A
Water	Local	1,116 lbf	
Air Ent.	Daravair 1000 (Grace)	10 Fluid oz	
Water Reducer	WRDA 60 (Grace)	145 Fluid oz	
Superplasticizer	ADVA 540 (Grace)	115 Fluid oz	
W/C Ratio	0.30		

Date: 06/16/06	Ticket: 4		
Material	Producer	Quantity	%MC
Sand 3	Pit No. 36-491	4,100 lbf	2.7
67 Granite 2	GA553	9,340 lbf	2.1
Cement 2	Suwannee American	4,810 lbf	N/A
Water	Local	1,148 lbf	
Air Ent.	Daravair 1000 (Grace)	10 Fluid oz	
Water Reducer	WRDA 60 (Grace)	145 Fluid oz	
Superplasticizer	ADVA 540 (Grace)	115 Fluid oz	
W/C Ratio	0.30		

Bridge Piles – Mixture UFA

Strand Stress Report	
Date	06/05/06
Bed No.	`18N
Ambient Temp.	82 degree (F)
Cable Type	½ Special 7W 270LR ASTM A416
Final Tension	34426
+2.5%	35287
-2.5%	33565

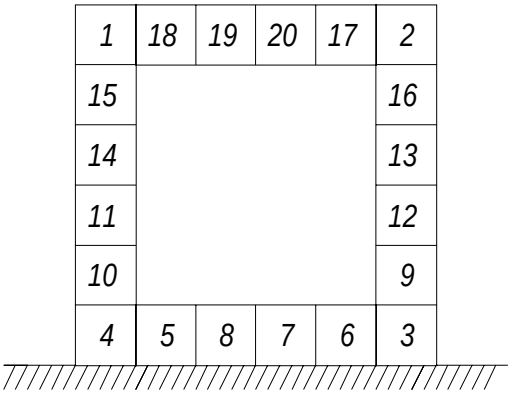

Stressing pattern for bridge piles – Mixture UF

Date: 06/06/06	Ticket 1		
Material	Producer	Quantity	%MC
Sand 3	Pit No. 36-491	4,180 lbf	2.5
78 Granite	GA553	9,360 lbf	2.5
Fly Ash	ISG	925 lbf	N/A
Cement 2	Suwannee American	3,325 lbf	
Water	Local	1,032 lbf	
Air Ent.	Daravair 1000 (Grace)	10 Fluid oz	
Water Reducer	WRDA 60 (Grace)	145 Fluid oz	
Superplasticizer	ADVA 540 (Grace)	105 Fluid oz	
Fly Ash	ISG	625 lbf	
W/C Ratio	0.29		

Date: 06/06/06	Ticket 2		
Material	Producer	Quantity	%MC
Sand 3	Pit No. 36-491	4,160 lbf	2.5
78 Granite	GA553	9,380 lbf	2.5
Fly Ash	ISG	900 lbf	N/A
Cement 2	Suwannee American	3,340 lbf	
Water	Loca	1,066 lbf	
Air Ent.	Daravair 1000 (Grace)	10 Fluid oz	
Water Reducer	WRDA 60 (Grace)	145 Fluid oz	
Superplasticizer	ADVA 540 (Grace)	115 Fluid oz	
Fly Ash	ISG	625 lbf	
W/C Ratio	0.29		

Date: 06/06/06	Ticket 3		
Material	Producer	Quantity	%MC
Sand 3	Pit No. 36-491	4,160 lbf	2.5
78 Granite	GA553	9,400 lbf	2.5
Fly Ash	ISG	930 lbf	N/A
Cement 2	Suwannee American	3,330 lbf	
Water	Local	1,112 lbf	
Air Ent.	Daravair 1000 (Grace)	10 Fluid oz	
Water Reducer	WRDA 60 (Grace)	145 Fluid oz	
Superplasticizer	ADVA 540 (Grace)	115 Fluid oz	
Fly Ash	ISG	625 lbf	
W/C Ratio	0.30		

Date: 06/06/06	Ticket: 4		
Material	Actual		%MC
Sand 3	Pit No. 36-491	4,140 lbf	2.5
78 Granite	GA553	9,400 lbf	2.5
Fly Ash	ISG	935 lbf	
Cement 2	Suwannee American	3,345 lbf	
Water	Local	1,104 lbf	
Air Ent.	Daravair 1000 (Grace)	10 Fluid oz	N/A
Water Reducer	WRDA 60 (Grace)	145 Fluid oz	
Superplasticizer	ADVA 540 (Grace)	115 Fluid oz	
Fly Ash	ISG	625 lbf	
W/C Ratio	0.29		

Date: 06/06/06	Ticket: 5		
Material	Actual		%MC
Sand 3	Pit No. 36-491	4,140 lbf	2.5
78 Granite	GA553	9,360 lbf	2.5
Fly Ash	ISG	920 lbf	
Cement 2	Suwannee American	3,320 lbf	
Water	Local	1,078 lbf	
Air Ent.	Daravair 1000 (Grace)	10 Fluid oz	N/A
Water Reducer	WRDA 60 (Grace)	145 Fluid oz	
Superplasticizer	ADVA 540 (Grace)	115 Fluid oz	
Fly Ash	ISG	625 lbf	
W/C Ratio	0.29		

Date: 06/06/06	Ticket: 6		
Material	Actual		%MC
Sand 3	Pit No. 36-491	4,100 lbf	2.5
78 Granite	GA553	9,420 lbf	2.5
Fly Ash	ISG	920 lbf	
Cement 2	Suwannee American	3,325 lbf	
Water	Local	1,084 lbf	
Air Ent.	Daravair 1000 (Grace)	10 Fluid oz	N/A
Water Reducer	WRDA 60 (Grace)	145 Fluid oz	
Superplasticizer	ADVA 540 (Grace)	115 Fluid oz	
Fly Ash	ISG	625 lbf	
W/C Ratio	0.29		

Date: 06/06/06	Ticket: 7		
Material	Actual		%MC
Sand 3	Pit No. 36-491	4,140 lbf	2.5
78 Granite	GA553	9,400 lbf	2.5
Fly Ash	ISG	875 lbf	N/A
Cement 2	Suwannee American	3,320 lbf	
Water	Local	1,086 lbf	
Air Ent.	Daravair 1000 (Grace)	10 Fluid oz	
Water Reducer	WRDA 60 (Grace)	145 Fluid oz	
Superplasticizer	ADVA 540 (Grace)	115 Fluid oz	
Fly Ash	ISG	625 lbf	
W/C Ratio	0.29		

Date: 06/06/06	Ticket: 8		
Material	Actual		%MC
Sand 3	Pit No. 36-491	4,240 lbf	2.5
78 Granite	GA553	9,400 lbf	2.5
Fly Ash	ISG	910 lbf	N/A
Cement 2	Suwannee American	3,330 lbf	
Water	Local	1,076 lbf	
Air Ent.	Daravair 1000 (Grace)	10 Fluid oz	
Water Reducer	WRDA 60 (Grace)	145 Fluid oz	
Superplasticizer	ADVA 540 (Grace)	115 Fluid oz	
Fly Ash	ISG	625 lbf	
W/C Ratio	0.29		

Date: 06/06/06	Ticket: 9		
Material	Actual		%MC
Sand 3	Pit No. 36-491	4,100 lbf	2.5
78 Granite	GA553	9,380 lbf	2.5
Fly Ash	ISG	885 lbf	N/A
Cement 2	Suwannee American	3,335 lbf	
Water	Local	1,084 lbf	
Air Ent.	Daravair 1000 (Grace)	10 Fluid oz	
Water Reducer	WRDA 60 (Grace)	145 Fluid oz	
Superplasticizer	ADVA 540 (Grace)	115 Fluid oz	
Fly Ash	ISG	625 lbf	
W/C Ratio	0.29		

Date: 06/06/06	Ticket: 10		
Material	Actual		%MC
Sand 3	Pit No. 36-491	4,160 lbf	2.5
78 Granite	GA553	9,460 lbf	2.5
Fly Ash	ISG	930 lbf	N/A
Cement 2	Suwannee American	3,340 lbf	
Water	Local	1,074 lbf	
Air Ent.	Daravair 1000 (Grace)	10 Fluid oz	
Water Reducer	WRDA 60 (Grace)	145 Fluid oz	
Superplasticizer	ADVA 540 (Grace)	115 Fluid oz	
Fly Ash	ISG	625 lbf	
W/C Ratio	0.29		

Date: 06/06/06	Ticket: 11		
Material	Actual		%MC
Sand 3	Pit No. 36-491	4,160 lbf	2.5
78 Granite	GA553	9,380 lbf	2.5
Fly Ash	ISG	930 lbf	N/A
Cement 2	Suwannee American	3,320 lbf	
Water	Local	1,080 lbf	
Air Ent.	Daravair 1000 (Grace)	10 Fluid oz	
Water Reducer	WRDA 60 (Grace)	145 Fluid oz	
Superplasticizer	ADVA 540 (Grace)	115 Fluid oz	
Fly Ash	ISG	625 lbf	
W/C Ratio	0.29		

Date: 06/06/06	Ticket: 12		
Material	Actual		%MC
Sand 3	Pit No. 36-491	4,120 lbf	2.5
78 Granite	GA553	9,420 lbf	2.5
Fly Ash	ISG	930 lbf	N/A
Cement 2	Suwannee American	3,330 lbf	
Water	Local	1,078 lbf	
Air Ent.	Daravair 1000 (Grace)	10 Fluid oz	
Water Reducer	WRDA 60 (Grace)	145 Fluid oz	
Superplasticizer	ADVA 540 (Grace)	115 Fluid oz	
Fly Ash	ISG	625 lbf	
W/C Ratio	0.29		

Date: 06/06/06	Ticket: 13		
Material	Actual		%MC
Sand 3	Pit No. 36-491	4,960 lbf	2.5
78 Granite	GA553	11,280 lbf	2.5
Fly Ash	ISG	1,100 lbf	N/A
Cement 2	Suwannee American	4,035 lbf	
Water	Local	1,346 lbf	
Air Ent.	Daravair 1000 (Grace)	12 Fluid oz	
Water Reducer	WRDA 60 (Grace)	170 Fluid oz	
Superplasticizer	ADVA 540 (Grace)	140 Fluid oz	
Fly Ash	ISG	750 lbf	
W/C Ratio	0.3		

Date: 06/06/06	Ticket: 14		
Material	Actual		%MC
Sand 3	Pit No. 36-491	4,940 lbf	2.5
78 Granite	GA553	11,220 lbf	2.5
Fly Ash	ISG	1,110 lbf	N/A
Cement 2	Suwannee American	3,985 lbf	
Water	Local	1,328 lbf	
Air Ent.	Daravair 1000 (Grace)	12 Fluid oz	
Water Reducer	WRDA 60 (Grace)	170 Fluid oz	
Superplasticizer	ADVA 540 (Grace)	140 Fluid oz	
Fly Ash	ISG	750 lbf	
W/C Ratio	0.29		

Fender Piles – Mixture UFA

Strand Stress Report	
Date	06/08/06
Bed No.	22
Ambient Temp.	94 degree (F)
Cable Type	½ Special 7W 270LR ASTM A416
Final Tension	35466
+2.5%	36072
-2.5%	34579

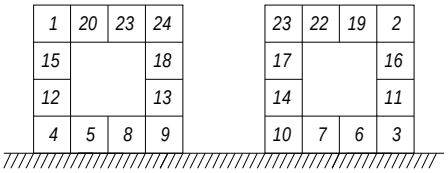

Stressing pattern for fender piles – Mixture UFA

Date: 06/09/06	Ticket: 1		
Material	Producer	Quantity	%MC
Sand 3	Pit No. 36-491	4,080 lbf	0.9
78 Granite	GA553	9,420 lbf	2.5
Fly Ash	ISG	880 lbf	N/A
Cement 2	Suwannee American	3,325 lbf	
Water	Local	1,154 lbf	
Air Ent.	Daravair 1000 (Grace)	10 Fluid oz	
Water Reducer	WRDA 60 (Grace)	145 Fluid oz	
Superplasticizer	ADVA 540 (Grace)	115 Fluid oz	
Fly Ash	ISG	625 lbf	
W/C Ratio	0.29		

Date: 06/09/06	Ticket: 2		
Material	Producer	Quantity	%MC
Sand 3	Pit No. 36-491	4,140 lbf	0.9
78 Granite	GA553	9,440 lbf	2.5
Fly Ash	ISG	890 lbf	N/A
Cement 2	Suwannee American	3,320 lb	
Water	Local	1,108 lbf	
Air Ent.	Daravair 1000 (Grace)	10 Fluid oz	
Water Reducer	WRDA 60 (Grace)	145 Fluid oz	
Superplasticizer	ADVA 540 (Grace)	115 Fluid oz	
Fly Ash	ISG	625 lbf	
W/C Ratio	0.28		

Bridge Piles – Mixture FA

Strand Stress Report	
Date	06/21/06
Bed No.	18n
Ambient Temp.	94 degree (F)
Cable Type	½ Special 7W 270LR ASTM A416
Final Tension	34426
+2.5%	35287
-2.5%	33565

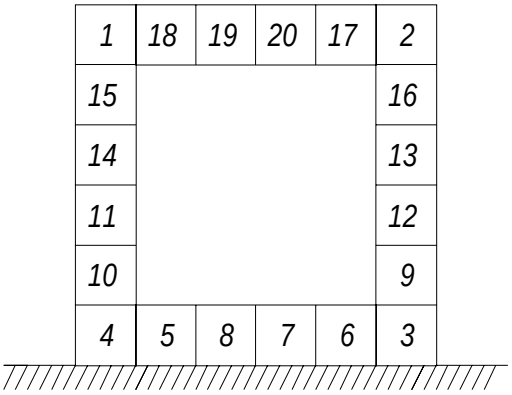

Stressing pattern for bridge piles – Mixture FA

Date: 06/23/06	Ticket: 1		
Material	Producer	Quantity	%MC
Sand 3	Pit No. 36-491	4,360 lbf	2.8
78 Granite	GA553	8,600 lbf	1.9
Fly Ash	ISG	920 lbf	N/A
Cement 2	Suwannee American	4,070 lbf	
Water	Local	1,242 lbf	
Air Ent.	Daravair 1000 (Grace)	5 Fluid oz	
Water Reducer	WRDA 60 (Grace)	85 Fluid oz	
Superplasticizer	ADVA 540 (Grace)	165 Fluid oz	
W/C Ratio	0.31		

Date: 06/23/06	Ticket: 2		
Material	Producer	Quantity	%MC
Sand 3	Pit No. 36-491	5,360 lbf	2.8
78 Granite	GA553	12,220 lbf	2.5
Fly Ash	ISG	1,130 lbf	N/A
Cement 2	Suwannee American	5,170 lbf	
Water	Local	1,410 lbf	
Air Ent.	Daravair 1000 (Grace)	13 Fluid oz	
Water Reducer	WRDA 60 (Grace)	185 Fluid oz	
Superplasticizer	ADVA 540 (Grace)	150 Fluid oz	
W/C Ratio	0.30		

Date: 06/23/06	Ticket: 3		
Material	Producer	Quantity	%MC
Sand 3	Pit No. 36-491	5,360 lbf	2.8
78 Granite	GA553	12,200 lbf	2.5
Fly Ash	ISG	1,155 lbf	N/A
Cement 2	Suwannee American	5,130 lbf	
Water	Local	1,422 lbf	
Air Ent.	Daravair 1000 (Grace)	13 Fluid oz	
Water Reducer	WRDA 60 (Grace)	185 Fluid oz	
Superplasticizer	ADVA 540 (Grace)	210 Fluid oz	
W/C Ratio	0.30		

Date: 06/23/06	Ticket: 4		
Material	Producer	Quantity	%MC
Sand 3	Pit No. 36-491	5,420 lbf	2.8
78 Granite	GA553	12,240 lbf	2.5
Fly Ash	ISG	1,170 lbf	N/A
Cement 2	Suwannee American	5,130 lbf	
Water	Local	1,428 lbf	
Air Ent.	Daravair 1000 (Grace)	13 Fluid oz	
Water Reducer	WRDA 60 (Grace)	185 Fluid oz	
Superplasticizer	ADVA 540 (Grace)	210 Fluid oz	
W/C Ratio	0.30		

Date: 06/23/06	Ticket: 5		
Material	Producer	Quantity	%MC
Sand 3	Pit No. 36-491	5,360 lbf	2.8
78 Granite	GA553	12,180 lbf	2.5
Fly Ash	ISG	1,130 lbf	N/A
Cement 2	Suwannee American	5,130 lbf	
Water	Local	1,440 lbf	
Air Ent.	Daravair 1000 (Grace)	13 Fluid oz	
Water Reducer	WRDA 60 (Grace)	185 Fluid oz	
Superplasticizer	ADVA 540 (Grace)	275 Fluid oz	
W/C Ratio	0.30		

Date: 06/23/06	Ticket: 6		
Material	Producer	Quantity	%MC
Sand 3	Pit No. 36-491	5,460 lbf	2.8
78 Granite	GA553	12,180 lbf	2.5
Fly Ash	ISG	1,145 lbf	N/A
Cement 2	Suwannee American	5,130 lbf	
Water	Local	1,438 lbf	
Air Ent.	Daravair 1000 (Grace)	13 Fluid oz	
Water Reducer	WRDA 60 (Grace)	185 Fluid oz	
Superplasticizer	ADVA 540 (Grace)	275 Fluid oz	
W/C Ratio	0.30		

Date: 06/23/06	Ticket: 7		
Material	Producer	Quantity	%MC
Sand 3	Pit No. 36-491	5,440 lbf	2.8
78 Granite	GA553	12,240 lbf	2.5
Fly Ash	ISG	1,155 lbf	N/A
Cement 2	Suwannee American	5,125 lbf	
Water	Local	1,428 lbf	
Air Ent.	Daravair 1000 (Grace)	13 Fluid oz	
Water Reducer	WRDA 60 (Grace)	185 Fluid oz	
Superplasticizer	ADVA 540 (Grace)	275 Fluid oz	
W/C Ratio	0.30		

Date: 06/23/06	Ticket: 8		
Material	Producer	Quantity	%MC
Sand 3	Pit No. 36-491	5,440 lbf	2.8
78 Granite	GA553	12,200 lbf	2.5
Fly Ash	ISG	1,130 lbf	N/A
Cement 2	Suwannee American	5,130 lbf	
Water	Local	1,424 lbf	
Air Ent.	Daravair 1000 (Grace)	13 Fluid oz	
Water Reducer	WRDA 60 (Grace)	185 Fluid oz	
Superplasticizer	ADVA 540 (Grace)	275 Fluid oz	
W/C Ratio	0.30		

Date: 06/23/06	Ticket: 9		
Material	Producer	Quantity	%MC
Sand 3	Pit No. 36-491	5,480 lbf	2.8
78 Granite	GA553	12,180 lb	2.5
Fly Ash	ISG	1,155 lbf	N/A
Cement 2	Suwannee American	5,125 lbf	
Water	Local	1,404 lbf	
Air Ent.	Daravair 1000 (Grace)	13 Fluid oz	
Water Reducer	WRDA 60 (Grace)	185 Fluid oz	
Superplasticizer	ADVA 540 (Grace)	275 Fluid oz	
W/C Ratio	0.30		

Date: 06/23/06	Ticket: 10		
Material	Producer	Quantity	%MC
Sand 3	Pit No. 36-491	5,460 lbf	2.8
78 Granite	GA553	12,200 lbf	2.5
Fly Ash	ISG	1,130 lbf	N/A
Cement 2	Suwannee American	5,135 lbf	
Water	Local	1,478 lbf	
Air Ent.	Daravair 1000 (Grace)	13 Fluid oz	
Water Reducer	WRDA 60 (Grace)	185 Fluid oz	
Superplasticizer	ADVA 540 (Grace)	275 Fluid oz	
W/C Ratio	0.31		

Fender Piles – Mixture FA

Strand Stress Report	
Date	06/15/06
Bed No.	22
Ambient Temp.	88 degree (F)
Cable Type	½ Special 7W 270LR ASTM A416
Final Tension	35465
+2.5%	36072
-2.5%	34579

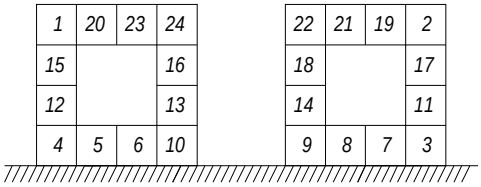

Stressing pattern for fender piles – Mixture FA

Date: 06/16/06	Ticket: 1		
Material	Producer	Quantity	%MC
Sand 3	Pit No. 36-491	4,120 lbf	2.7
78 Granite	GA553	9,380 lbf	2.1
Fly Ash	ISG	910 lbf	N/A
Cement 2	Suwannee American	3,935 lbf	
Water	Local	1,120 lbf	
Air Ent.	Daravair 1000 (Grace)	10 Fluid oz	
Water Reducer	WRDA 60 (Grace)	145 Fluid oz	
Superplasticizer	ADVA 540 (Grace)	115 Fluid oz	
W/C Ratio	0.29		

Date: 06/16/06	Ticket: 2		
Material	Pit No. 36-491	Quantity	%MC
Sand 3	GA553	4,160 lbf	2.7
78 Granite	ISG	9,340 lbf	2.1
Fly Ash	Suwannee American	970 lbf	N/A
Cement 2	Local	3,945 lbf	
Water	Daravair 1000 (Grace)	1,150 lbf	
Air Ent.	WRDA 60 (Grace)	10 Fluid oz	
Water Reducer	ADVA 540 (Grace)	145 Fluid oz	
Superplasticizer	Adva 540	115 Fluid oz	
W/C Ratio	0.30		

Bridge Piles – Mixture SF

Strand Stress Summary	
Date	09/27/06
Bed No.	18N
Ambient Temp.	86 degree (F)
Cable Type	½ Special 7W 270LR ASTM A416
Final Tension	34426
+2.5%	35287
-2.5%	33565

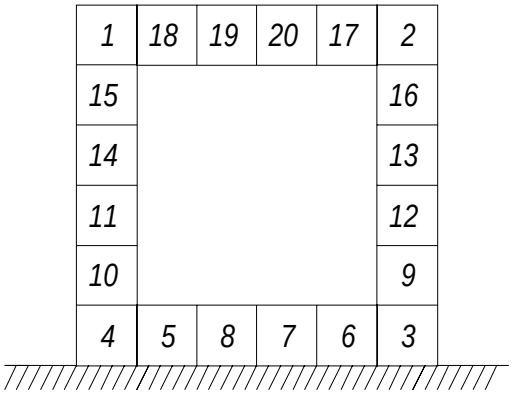

Stressing pattern for bridge piles – Mixture SF

Date: 09/29/06	Ticket: 1		
Material	Producer	Quantity	%MC
Sand 3	Pit No. 36-491	5,280 lbf	1.4
67 Granite 2	GA553	12,180 lbf	2.5
Silica Fume	Force 10000D (Grace)	520 lbf	N/A
Fly Ash	ISG	1,135 lbf	
Cement 3	Suwannee American	4,610 lbf	
Water	Local	1,512 lbf	
Water Reducer	WRDA 60 (Grace)	185 Fluid oz	
Superplasticizer	ADVA 540 (Grace)	280 Fluid oz	
W/C Ratio	0.30		

Date: 09/29/06	Ticket: 2		
Material	Producer	Quantity	%MC
Sand 3	Pit No. 36-491	5,280 lbf	1.4
67 Granite 2	GA553	12,200 lbf	2.5
Silica Fume	Force 10000D (Grace)	515 lbf	N/A
Fly Ash	ISG	1,165 lbf	
Cement 3	Suwannee American	4,605 lbf	
Water	Local	1,500 lbf	
Water Reducer	WRDA 60 (Grace)	185 Fluid oz	
Superplasticizer	ADVA 540 (Grace)	280 Fluid oz	
W/C Ratio	0.30		

Date: 09/29/06	Ticket: 3		
Material	Producer	Quantity	%MC
Sand 3	Pit No. 36-491	5,400 lbf	1.4
67 Granite 2	GA553	12,200 lbf	2.5
Silica Fume	Force 10000D (Grace)	520 lbf	N/A
Fly Ash	ISG	1,135 lbf	
Cement 3	Suwannee American	4,605 lbf	
Water	Local	1,516 lbf	
Water Reducer	WRDA 60 (Grace)	185 Fluid oz	
Superplasticizer	ADVA 540 (Grace)	280 Fluid oz	
W/C Ratio	0.30		

Date: 09/29/06	Ticket: 4		
Material	Producer	Quantity	%MC
Sand 3	Pit No. 36-491	5,340 lbf	1.4
67 Granite 2	GA553	12,180 lbf	2.5
Silica Fume	Force 10000D (Grace)	515 lbf	N/A
Fly Ash	ISG	1,165 lbf	
Cement 3	Suwannee American	4,610 lbf	
Water	Local	1,558 lbf	
Water Reducer	WRDA 60 (Grace)	185 Fluid oz	
Superplasticizer	ADVA 540 (Grace)	280 Fluid oz	
W/C Ratio	0.32		

Date: 09/29/06	Ticket: 5		
Material	Producer	Quantity	%MC
Sand 3	Pit No. 36-491	5,30 lbf	1.4
67 Granite 2	GA553	12,220 lbf	2.5
Silica Fume	Force 10000D (Grace)	515 lbf	N/A
Fly Ash	ISG	1,155 lbf	
Cement 3	Suwannee American	4,645 lbf	
Water	Local	1,530 lbf	
Water Reducer	WRDA 60 (Grace)	185 Fluid oz	
Superplasticizer	ADVA 540 (Grace)	280 Fluid oz	
W/C Ratio	0.30		

Date: 09/29/06	Ticket: 6		
Material	Producer	Quantity	%MC
Sand 3	Pit No. 36-491	5,340 lbf	1.4
67 Granite 2	GA553	12,180 lbf	2.5
Silica Fume	Force 10000D (Grace)	515 lbf	N/A
Fly Ash	ISG	1,135 lbf	
Cement 3	Suwannee American	4,605 lbf	
Water	Local	1,552 lbf	
Water Reducer	WRDA 60 (Grace)	185 Fluid oz	
Superplasticizer	ADVA 540 (Grace)	280 Fluid oz	
W/C Ratio	0.31		

Date: 09/29/06	Ticket: 7		
Material	Producer	Quantity	%MC
Sand 3	Pit No. 36-491	5,400 lbf	1.4
67 Granite 2	GA553	12,220 lbf	2.5
Silica Fume	Force 10000D (Grace)	520 lbf	N/A
Fly Ash	ISG	1,135 lbf	
Cement 3	Suwannee American	4,605 lbf	
Water	Local	1,524 lbf	
Water Reducer	WRDA 60 (Grace)	185 Fluid oz	
Superplasticizer	ADVA 540 (Grace)	280 Fluid oz	
W/C Ratio	0.30		

Date: 09/29/06	Ticket: 8		
Material	Producer	Quantity	%MC
Sand 3	Pit No. 36-491	5,400 lbf	1.4
67 Granite 2	GA553	12,240 lbf	2.5
Silica Fume	Force 10000D (Grace)	515 lbf	N/A
Fly Ash	ISG	1,175 lbf	
Cement 3	Suwannee American	4,605 lbf	
Water	Local	1,520 lbf	
Water Reducer	WRDA 60 (Grace)	185 Fluid oz	
Superplasticizer	ADVA 540 (Grace)	280 Fluid oz	
W/C Ratio	0.30		

Date: 09/29/06	Ticket: 9		
Material	Producer	Quantity	%MC
Sand 3	Pit No. 36-491	5,380 lbf	1.4
67 Granite 2	GA553	12,200 lbf	2.5
Silica Fume	Force 10000D (Grace)	515 lbf	N/A
Fly Ash	ISG	1,175 lbf	
Cement 3	Suwannee American	4,610 lbf	
Water	Local	1,502 lbf	
Water Reducer	WRDA 60 (Grace)	185 Fluid oz	
Superplasticizer	ADVA 540 (Grace)	280 Fluid oz	
W/C Ratio	0.30		

Date: 09/29/06	Ticket: 10		
Material	Producer	Quantity	%MC
Sand 3	Pit No. 36-491	5,260 lbf	1.4
67 Granite 2	GA553	12,220 lbf	2.5
Silica Fume	Force 10000D (Grace)	515 lbf	N/A
Fly Ash	ISG	1,180 lbf	
Cement 3	Suwannee American	4,605 lbf	
Water	Local	1,504 lbf	
Water Reducer	WRDA 60 (Grace)	185 Fluid oz	
Superplasticizer	ADVA 540 (Grace)	280 Fluid oz	
W/C Ratio	0.30		

Fender Piles – Mixture SF

Strand Stress Summary	
Date	09/26/06
Bed No.	21
Ambient Temp.	88 degree (F)
Cable Type	½ Special 7W 270LR ASTM A416
Final Tension	35134
+2.5%	36012
-2.5%	34256

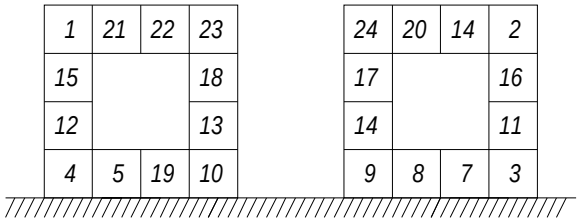

Stressing pattern for fender piles – Mixture SF

Date: 09/29/06	Ticket: 1		
Material	Producer	Quantity	%MC
Sand 3	Pit No. 36-491	5,360 lbf	1.4
67 Granite 2	GA553	12,200 lbf	2.5
Silica Fume	Force 10000D (Grace)	515 lbf	N/A
Fly Ash	ISG	1,130 lbf	
Cement 3	Suwannee American	4,625 lbf	
Water	Local	1,516 lbf	
Water Reducer	WRDA 60 (Grace)	165 Fluid oz	
Superplasticizer	ADVA 540 (Grace)	280 Fluid oz	
W/C Ratio	0.30		

Date: 09/29/06	Ticket: 2		
Material	Producer	Quantity	%MC
Sand 3	Pit No. 36-491	4,880 lbf	1.4
67 Granite 2	GA553	11,260 lbf	2.5
Silica Fume	Force 10000D (Grace)	475 lbf	N/A
Fly Ash	ISG	1,045 lbf	
Cement 3	Suwannee American	4,250 lbf	
Water	Local	1,398 lbf	
Water Reducer	WRDA 60 (Grace)	170 Fluid oz	
Superplasticizer	ADVA 540 (Grace)	255 Fluid oz	
W/C Ratio	0.30		

Bridge Piles – Mixture BFS

Strand Stress Summary	
Date	10/04/06
Bed No.	18N
Ambient Temp.	82 degree (F)
Cable Type	½ Special 7W 270LR ASTM A416
Final Tension	34426
+2.5%	35287
-2.5%	33565

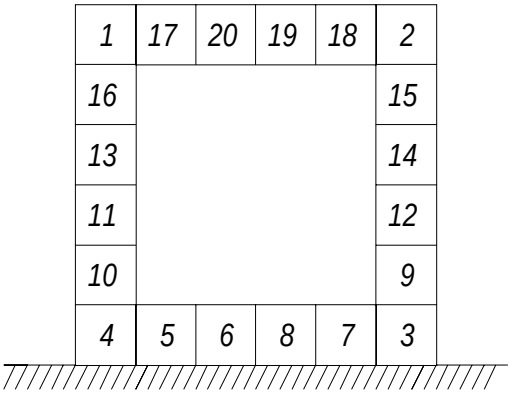

Stressing pattern for bridge piles – Mixture BFS

Date: 10/06/06	Ticket: 1		
Material	Producer	Quantity	%MC
Sand 3	Pit No. 36-491	5,320 lbf	1.4
67 Granite 2	GA553	12,300 lbf	3.3
GGBFS	Civil & Marine	2,590 lbf	N/A
Fly Ash	ISG	1,180 lbf	
Cement 3	Suwannee American	2,575 lbf	
Water	Local	1,418 lbf	
Water Reducer	WRDA 60 (Grace)	185 Fluid oz	
Superplasticizer	ADVA 540 (Grace)	280 Fluid oz	
W/C Ratio	0.30		

Date: 10/06/06	Ticket: 2		
Material	Producer	Quantity	%MC
Sand 3	Pit No. 36-491	5,260 lbf	1.4
67 Granite 2	GA553	12,360 lbf	3.3
GGBFS	Civil & Marine	2,585 lbf	N/A
Fly Ash	ISG	1,155 lbf	
Cement 3	Suwannee American	2,590 lbf	
Water	Local	1,575 lbf	
Water Reducer	WRDA 60 (Grace)	185 Fluid oz	
Superplasticizer	ADVA 540 (Grace)	280 Fluid oz	
W/C Ratio	0.33		

Date: 10/06/06	Ticket: 3		
Material	Producer	Quantity	%MC
Sand 3	Pit No. 36-491	5,360 lbf	1.4
67 Granite 2	GA553	12,340 lbf	3.3
GGBFS	Civil & Marine	2,605 lbf	N/A
Fly Ash	ISG	1,205 lbf	
Cement 3	Suwannee American	2,575 lbf	
Water	Local	1,558 lbf	
Water Reducer	WRDA 60 (Grace)	185 Fluid oz	
Superplasticizer	ADVA 540 (Grace)	280 Fluid oz	
W/C Ratio	0.32		

Date: 10/06/06	Ticket: 4		
Material	Producer	Quantity	%MC
Sand 3	Pit No. 36-491	5,320 lbf	1.4
67 Granite 2	GA553	12,320 lbf	3.3
GGBFS	Civil & Marine	2,620 lbf	N/A
Fly Ash	ISG	1,215 lbf	
Cement 3	Suwannee American	2,580 lbf	
Water	Local	1,572 lbf	
Water Reducer	WRDA 60 (Grace)	185 Fluid oz	
Superplasticizer	ADVA 540 (Grace)	280 Fluid oz	
W/C Ratio	0.32		

Date: 10/06/06	Ticket: 5		
Material	Producer	Quantity	%MC
Sand 3	Pit No. 36-491	5,340 lbf	1.4
67 Granite 2	GA553	12,260 lbf	3.3
GGBFS	Civil & Marine	2,585 lbf	N/A
Fly Ash	ISG	1,140 lbf	
Cement 3	Suwannee American	2,575 lbf	
Water	Local	1,586 lbf	
Water Reducer	WRDA 60 (Grace)	185 Fluid oz	
Superplasticizer	ADVA 540 (Grace)	280 Fluid oz	
W/C Ratio	0.33		

Date: 10/06/06	Ticket: 6		
Material	Producer	Quantity	%MC
Sand 3	Pit No. 36-491	5,260 lbf	1.4
67 Granite 2	GA553	12,260 lbf	3.3
GGBFS	Civil & Marine	2,585 lbf	N/A
Fly Ash	ISG	1,180 lbf	
Cement 3	Suwannee American	2,860 lbf	
Water	Local	1,584 lbf	
Water Reducer	WRDA 60 (Grace)	185 Fluid oz	
Superplasticizer	ADVA 540 (Grace)	280 Fluid oz	
W/C Ratio	0.31		

Date: 10/06/06	Ticket: 7		
Material	Producer	Quantity	%MC
Sand 3	Pit No. 36-491	5,260 lbf	1.4
67 Granite 2	GA553	12,260 lbf	3.3
GGBFS	Civil & Marine	2,580 lbf	N/A
Fly Ash	ISG	1,195 lbf	
Cement 3	Suwannee American	2,575 lbf	
Water	Local	1,602 lbf	
Water Reducer	WRDA 60 (Grace)	185 Fluid oz	
Superplasticizer	ADVA 540 (Grace)	280 Fluid oz	
W/C Ratio	0.33		

Date: 10/06/06	Ticket: 8		
Material	Producer	Quantity	%MC
Sand 3	Pit No. 36-491	5,320 lbf	1.4
67 Granite 2	GA553	12,260 lbf	3.3
GGBFS	Civil & Marine	2,565 lbf	N/A
Fly Ash	ISG	1,145 lbf	
Cement 3	Suwannee American	2,575 lbf	
Water	Local	1,382 lbf	
Water Reducer	WRDA 60 (Grace)	185 Fluid oz	
Superplasticizer	ADVA 540 (Grace)	280 Fluid oz	
W/C Ratio	0.30		

Date: 10/06/06	Ticket: 9		
Material	Producer	Quantity	%MC
Sand 3	Pit No. 36-491	5,340 lbf	1.4
67 Granite 2	GA553	12,260 lbf	3.3
GGBFS	Civil & Marine	2,560 lbf	N/A
Fly Ash	ISG	1,185 lbf	
Cement 3	Suwannee American	2,575 lbf	
Water	Local	1,490 lbf	
Water Reducer	WRDA 60 (Grace)	185 Fluid oz	
Superplasticizer	ADVA 540 (Grace)	280 Fluid oz	
W/C Ratio	0.31		

Date: 10/06/06	Ticket: 10		
Material	Producer	Quantity	%MC
Sand 3	Pit No. 36-491	5,300 lbf	1.4
67 Granite 2	GA553	12,300 lbf	3.3
GGBFS	Civil & Marine	2,710 lbf	N/A
Fly Ash	ISG	1,150 lbf	
Cement 3	Suwannee American	2,575 lbf	
Water	Local	1,418 lbf	
Water Reducer	WRDA 60 (Grace)	185 Fluid oz	
Superplasticizer	ADVA 540 (Grace)	280 Fluid oz	
W/C Ratio	0.29		

Fender Piles – Mixture BFS

Strand Stress Summary	
Date	10/03/06
Bed No.	22
Ambient Temp.	86degree (F)
Cable Type	½ Special 7W 270LR ASTM A416
Final Tension	35466
+2.5%	36072
-2.5%	34579

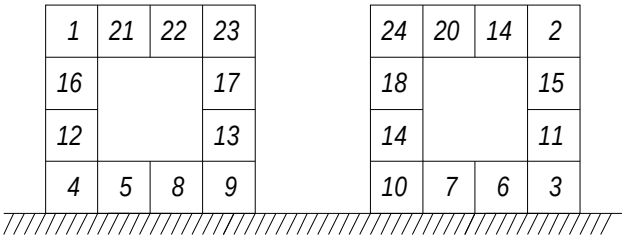

Stressing pattern for fender piles – Mxiture BFS

Date: 10/06/06	Ticket: 1		
Material	Producer	Quantity	%MC
Sand 3	Pit No. 36-491	5,340 lbf	1.4
67 Granite 2	GA553	12,280 lbf	3.3
GGBFS	Civil & Marine	2,545 lbf	N/A
Fly Ash	ISG	1,150 lbf	
Cement 3	Suwannee American	2,575 lbf	
Water	Local	1,396 lbf	
Water Reducer	WRDA 60 (Grace)	185 Fluid oz	
Superplasticizer	ADVA 540 (Grace)	280 Fluid oz	
W/C Ratio	0.30		

Date: 10/06/06	Ticket: 2		
Material	Producer	Quantity	%MC
Sand 3	Pit No. 36-491	4,100 lbf	1.4
67 Granite 2	GA553	9,480 lbf	3.3
GGBFS	Civil & Marine	1,960 lbf	N/A
Fly Ash	ISG	875 lbf	
Cement 3	Suwannee American	1,980 lbf	
Water	Local	1,120 lbf	
Water Reducer	WRDA 60 (Grace)	145 Fluid oz	
Superplasticizer	ADVA 540 (Grace)	215 Fluid oz	
W/C Ratio	0.31		

Bridge Piles – Mixture MET

Strand Stress Summary	
Date	10/11/06
Bed No.	18S
Ambient Temp.	83egree
Cable Type	½ Special 7W 270LR ASTM A416
Final Tension	34277
+2.5%	35134
-2.5%	33420

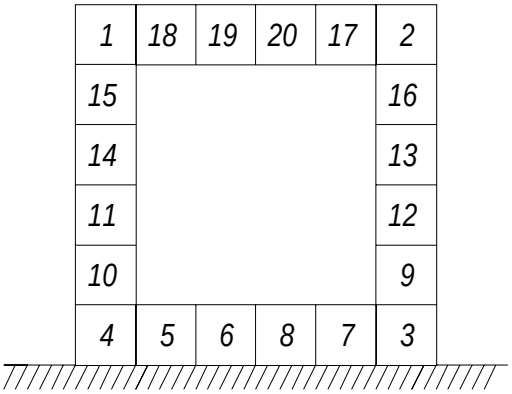

Stressing pattern for bridge piles – Mixture MET

Date: 10/13/06	Ticket: 1		
Material	Producer	Quantity	%MC
Sand 3	Pit No. 36-491	5,060 lbf	4.9
67 Granite 2	GA553	11,220 lbf	2.3
Fly Ash	ISG	1,055 lbf	N/A
Cement 2	Suwannee American	4,130 lbf	
Water	Local	1,292 lbf	
Metakaolin	Optizozz	600 lbf	
Water Reducer	WRDA 60 (Grace)	160 Fluid oz	
Superplasticizer	ADVA 540 (Grace)	255 Fluid oz	
W/C Ratio	0.31		

Date: 10/13/06	Ticket: 2		
Material	Producer	Quantity	%MC
Sand 3	Pit No. 36-491	5,140 lbf	4.9
67 Granite 2	GA553	11,240 lbf	2.3
Fly Ash	ISG	1,055 lbf	N/A
Cement 2	Suwannee American	4,130 lbf	
Water	Local	1,368 lbf	
Metakaolin	Optizozz	600 lbf	
Water Reducer	WRDA 60 (Grace)	160 Fluid oz	
Superplasticizer	ADVA 540 (Grace)	255 Fluid oz	
W/C Ratio	0.33		

Date: 10/13/06	Ticket: 3		
Material	Producer	Quantity	%MC
Sand 3	Pit No. 36-491	5,100 lbf	4.9
67 Granite 2	GA553	11,200 lbf	2.3
Fly Ash	ISG	1,075 lbf	N/A
Cement 2	Suwannee American	4,135 lbf	
Water	Local	1,432 lbf	
Metakaolin	Optizozz	600 lbf	
Water Reducer	WRDA 60 (Grace)	160 Fluid oz	
Superplasticizer	ADVA 540 (Grace)	255 Fluid oz	
W/C Ratio	0.33		

Date: 10/13/06	Ticket: 4		
Material	Producer	Quantity	%MC
Sand 3	Pit No. 36-491	5,080 lbf	4.9
67 Granite 2	GA553	11,280 lbf	2.3
Fly Ash	ISG	1,075 lbf	N/A
Cement 2	Suwannee American	4,155 lbf	
Water	Local	1,436 lb	
Metakaolin	Optizozz	600 lbf	
Water Reducer	WRDA 60 (Grace)	160 Fluid oz	
Superplasticizer	ADVA 540 (Grace)	255 Fluid oz	
W/C Ratio	0.33		

Date: 10/13/06	Ticket: 5		
Material	Producer	Quantity	%MC
Sand 3	Pit No. 36-491	5,160 lbf	4.9
67 Granite 2	GA553	11,220 lbf	2.3
Fly Ash	ISG	1,095 lbf	N/A
Cement 2	Suwannee American	4,130 lbf	
Water	Local	1,432 lbf	
Metakaolin	Optizozz	600 lbf	
Water Reducer	WRDA 60 (Grace)	160 Fluid oz	
Superplasticizer	ADVA 540 (Grace)	255 Fluid oz	
W/C Ratio	0.33		

Date: 10/13/06	Ticket: 6		
Material	Producer	Quantity	%MC
Sand 3	Pit No. 36-491	5,180 lbf	4.9
67 Granite 2	GA553	11,280 lbf	2.3
Fly Ash	ISG	1,040 lbf	N/A
Cement 2	Suwannee American	4,150 lbf	
Water	Local	1,440 lbf	
Metakaolin	Optizozz	600 lbf	
Water Reducer	WRDA 60 (Grace)	160 Fluid oz	
Superplasticizer	ADVA 540 (Grace)	255 Fluid oz	
W/C Ratio	0.33		

Date: 10/13/06	Ticket: 7		
Material	Producer	Quantity	%MC
Sand 3	Pit No. 36-491	5,200 lbf	4.9
67 Granite 2	GA553	11,260 lbf	2.3
Fly Ash	ISG	1,090 lbf	N/A
Cement 2	Suwannee American	4,130 lbf	
Water	Local	1,484 lbf	
Metakaolin	Optizozz	600 lbf	
Water Reducer	WRDA 60 (Grace)	160 Fluid oz	
Superplasticizer	ADVA 540 (Grace)	255 Fluid oz	
W/C Ratio	0.34		

Date: 10/13/06	Ticket: 8		
Material	Producer	Quantity	%MC
Sand 3	Pit No. 36-491	5,140 lbf	4.9
67 Granite 2	GA553	11,200 lbf	2.3
Fly Ash	ISG	1,045 lbf	N/A
Cement 2	Suwannee American	4,130 lbf	
Water	Local	1,444 lbf	
Metakaolin	Optizozz	600 lbf	
Water Reducer	WRDA 60 (Grace)	160 Fluid oz	
Superplasticizer	ADVA 540 (Grace)	255 Fluid oz	
W/C Ratio	0.34		

Date: 10/13/06	Ticket: 9		
Material	Producer	Quantity	%MC
Sand 3	Pit No. 36-491	5,060 lbf	4.9
67 Granite 2	GA553	11,200 lbf	2.3
Fly Ash	ISG	1,095 lbf	N/A
Cement 2	Suwannee American	4,135 lbf	
Water	Local	1,452 lbf	
Metakaolin	Optizozz	600 lbf	
Water Reducer	WRDA 60 (Grace)	160 Fluid oz	
Superplasticizer	ADVA 540 (Grace)	255 Fluid oz	
W/C Ratio	0.33		

Date: 10/13/06	Ticket: 10		
Material	Producer	Quantity	%MC
Sand 3	Pit No. 36-491	5,280 lbf	4.9
67 Granite 2	GA553	11,220 lbf	2.3
Fly Ash	ISG	1,040 lbf	N/A
Cement 2	Suwannee American	4,135 lbf	
Water	Local	1,450 lbf	
Metakaolin	Optizozz	600 lbf	
Water Reducer	WRDA 60 (Grace)	160 Fluid oz	
Superplasticizer	ADVA 540 (Grace)	255 Fluid oz	
W/C Ratio	0.34		

Date: 10/13/06	Ticket: 11		
Material	Producer	Quantity	%MC
Sand 3	Pit No. 36-491	5,240 lbf	4.9
67 Granite 2	GA553	11,300 lbf	2.3
Fly Ash	ISG	1,040 lbf	N/A
Cement 2	Suwannee American	4,130 lbf	
Water	Local	1,442 lbf	
Metakaolin	Optizozz	600 lbf	
Water Reducer	WRDA 60 (Grace)	160 Fluid oz	
Superplasticizer	ADVA 540 (Grace)	255 Fluid oz	
W/C Ratio	0.34		

Date: 10/13/06	Ticket: 12		
Material	Producer	Quantity	%MC
Sand 3	Pit No. 36-491	5,160 lbf	4.9
67 Granite 2	GA553	11,220 lbf	2.3
Fly Ash	ISG	1,090 lbf	N/A
Cement 2	Suwannee American	4,145 lbf	
Water	Local	1,436 lbf	
Metakaolin	Optizozz	600 lbf	
Water Reducer	WRDA 60 (Grace)	160 Fluid oz	
Superplasticizer	ADVA 540 (Grace)	255 Fluid oz	
W/C Ratio	0.37		

Fender Piles – Mixture MET

Strand Stress Summary	
Date	10/11/06
Bed No.	21
Ambient Temp.	81 degree (F)
Cable Type	½ Special 7W 270LR ASTM A416
Final Tension	35134
+2.5%	36012
-2.5%	34256

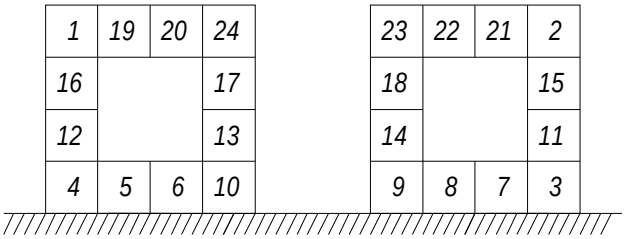

Stressing pattern for fender piles – Mixture MET

Date: 10/13/06	Ticket: 12		
Material	Producer	Quantity	%MC
Sand 3	Pit No. 36-491	5,060 lbf	4.9
67 Granite 2	GA553	11,220 lbf	2.3
Fly Ash	ISG	1,055 lbf	N/A
Cement 2	Suwannee American	4,130 lbf	
Water	Local	1,292 lbf	
Metakaolin	Optizozz	600 lbf	
Water Reducer	WRDA 60 (Grace)	160 Fluid oz	
Superplasticizer	ADVA 540 (Grace)	255 Fluid oz	
W/C Ratio	0.31		

Date: 10/13/06	Ticket: 13		
Material	Producer	Quantity	%MC
Sand 3	Pit No. 36-491	5,980 lbf	4.9
67 Granite 2	GA553	13,060 lbf	2.3
Fly Ash	ISG	1,245 lbf	N/A
Cement 2	Suwannee American	4,826 lbf	
Water	Local	1,436 lbf	
Metakaolin	Optizozz	700 lbf	
Water Reducer	WRDA 60 (Grace)	185 Fluid oz	
Superplasticizer	ADVA 540 (Grace)	300 Fluid oz	
W/C Ratio	0.30		

Appendix B–Material Testing Data

Mixture CEM

Fender pile samples taken at Durastress on: 6/16/2006

Compressive Strength of Cylinders (CEM)

Specimen	Age (days)	Comp. Strength (psi)	Average (psi)
Cylinder 1	28	6,930	6,740
Cylinder 2	28	6,640	
Cylinder 3	28	6,630	
Cylinder 4	91	7,580	7,370
Cylinder 5	91	7,430	
Cylinder 6	91	7,100	
Cylinder 7	364	8,818	8,743
Cylinder 8	364	8,705	
Cylinder 9	364	8,707	

Splitting Tensile Strength (CEM)

Specimen	Age (days)	Tens. Strength (psi)	Average (psi)
Cylinder 1	28	864	873
Cylinder 2	28	968	
Cylinder 3	28	786	
Cylinder 4	91	1,148	1,115
Cylinder 5	91	1,080	
Cylinder 6	91	1,118	
Cylinder 7	364	857	840
Cylinder 8	364	867	
Cylinder 9	364	797	

28-Day Modulus of Rupture (CEM)

Specimen	Mod. of Rupture (psi)
Beam 1	900
Beam 2	861
Beam 3	911
Beam 4	856
Beam 5	939
Average (psi)	893

Modulus of Elasticity (CEM)

Specimen		Age (days)	MOE (ksi)	Average (ksi)
Cylinder 1	Run 1	28	N/A	N/A
	Run 2	28	N/A	
	Run 3	28	N/A	
Cylinder 2	Run 1	28	N/A	
	Run 2	28	N/A	
	Run 3	28	N/A	
Cylinder 3	Run 1	91	4,734	4,686
	Run 2	91	4,850	
	Run 3	91	4,850	
Cylinder 4	Run 1	91	4,619	
	Run 2	91	4,446	
	Run 3	91	4,619	
Cylinder 5	Run 1	364	5,600	5,708
	Run 2	364	5,750	
	Run 3	364	5,700	
Cylinder 6	Run 1	364	5,650	
	Run 2	364	5,750	
	Run 3	364	5,800	

Rapid Chloride Migration Test (CEM)

Specimen	Age (days)	D_{nssm} ($x10^{-12}$ m^2 / s)	Average	STD
RMT-1	56	91.67	76.17	13.6
RMT-2	56	70.37		
RMT-3	56	66.46		
RMT-1	91	20.71	45.88	28.2
RMT-2	91	76.36		
RMT-3	91	40.56		
RMT-1	180	78.25	66.69	14.0
RMT-2	180	70.66		
RMT-3	180	51.16		

Surface Resistivity (CEM)

Specimen	Age (days)	Surface Resistivity (kΩ-cm)	Average
CEMF-1	28	12.1	12.9
CEMF-2	28	13.2	
CEMF-3	28	13.5	
CEMF-4	91	14.9	15.1
CEMF-5	91	15.2	
CEMF-6	91	15.1	
CEMF-7	364	16.4	16.9
CEMF-8	364	16.5	
CEMF-9	364	18.0	

Mixture UFA

Bridge samples taken at Durastress on: 6/6/2006

Compressive Strength of Cylinders (UFA)

Specimen	Age (days)	Comp. Strength (psi)	Average (psi)
Cylinder 1	7	4,840	4,950
Cylinder 2	7	5,040	
Cylinder 3	7	4,950	
Cylinder 4	28	7,580	7,560
Cylinder 5	28	7,580	
Cylinder 6	28	7,520	
Cylinder 7	364	N/A	N/A
Cylinder 8	364	N/A	
Cylinder 9	364	N/A	

Surface Resistivity (UFA)

Specimen	Age (days)	Surface Resistivity (kΩ-cm)	Average
UFA-1	7	5.1	5.3
UFA-2	7	5.4	
UFA-3	7	5.3	
UFA-4	28	16.8	17.0
UFA-5	28	17.4	
UFA-6	28	16.9	
UFA-7	364	N/A	N/A
UFA-8	364	N/A	
UFA-9	364	N/A	

Fender pile samples taken at Durastress on: 6/9/2006

Compressive Strength of Cylinders (UFAF)

Specimen	Age (days)	Comp. Strength (psi)	Average (psi)
Cylinder 1	28	4,710	5,910
Cylinder 2	28	6,390	
Cylinder 3	28	6,620	
Cylinder 4	91	8,230	7,550
Cylinder 5	91	8,380	
Cylinder 6	91	6,040	
Cylinder 7	364	N/A	N/A
Cylinder 8	364	N/A	
Cylinder 9	364	N/A	

Splitting Tensile Strength (UFAF)

Specimen	Age (days)	Tens. Strength (psi)	Average (psi)
Cylinder 1	28	840	843
Cylinder 2	28	790	
Cylinder 3	28	900	
Cylinder 4	91	1,010	737
Cylinder 5	91	580	
Cylinder 6	91	620	
Cylinder 7	364	N/A	N/A
Cylinder 8	364	N/A	
Cylinder 9	364	N/A	

28-Day Modulus of Rupture (UFAF)

Specimen	Mod. of Rupture (psi)
Beam 1	898
Beam 2	885
Beam 3	881
Beam 4	870
Beam 5	911
Average (psi)	889

Modulus of Elasticity (UFAF)

Specimen		Age (days)	MOE (ksi)	Average (ksi)
Cylinder 1	Run 1	28	N/A	N/A
	Run 2	28	N/A	
	Run 3	28	N/A	
Cylinder 2	Run 1	28	N/A	
	Run 2	28	N/A	
	Run 3	28	N/A	
Cylinder 3	Run 1	91	4,157	4,205
	Run 2	91	3,580	
	Run 3	91	4,042	
Cylinder 4	Run 1	91	4,619	
	Run 2	91	4,330	
	Run 3	91	4,503	
Cylinder 5	Run 1	364	N/A	N/A
	Run 2	364	N/A	
	Run 3	364	N/A	
Cylinder 6	Run 1	364	N/A	
	Run 2	364	N/A	
	Run 3	364	N/A	

Rapid Chloride Migration (UFAF)

Specimen	Age (days)	D_{nssm} ($x10^{-12}$ m^2 / s)	Average	STD
RMT-1	56	1318	1424 (Complete Penetration)	99.0
RMT-2	56	1440		
RMT-3	56	1514		
RMT-1	91	2.39	3.88	2.4
RMT-2	91	3.59		
RMT-3	91	5.66		
RMT-1	180	1.39	2.54	1.9
RMT-2	180	1.77		
RMT-3	180	4.46		

Surface Resistivity (UFAF)

Specimen	Age (days)	Surface Resistivity (kΩ-cm)	Average
UFAF-1	28	16.2	15.9
UFAF-2	28	15.8	
UFAF-3	28	15.8	
UFAF-4	91	82.9	83.0
UFAF-5	91	82.8	
UFAF-6	91	83.4	
UFAF-7	364	N/A	N/A
UFAF-8	364	N/A	
UFAF-9	364	N/A	

Mixture FA

Bridge pile samples taken at Durastress on: 6/23/2006

Compressive Strength of Cylinders (FA)

Specimen	Age (days)	Comp. Strength (psi)	Average (psi)
Cylinder 1	7	5,810	5,900
Cylinder 2	7	6,070	
Cylinder 3	7	5,810	
Cylinder 4	28	7,940	7,780
Cylinder 5	28	7,960	
Cylinder 6	28	7,450	
Cylinder 7	364	8,585	8,420
Cylinder 8	364	8,629	
Cylinder 9	364	8,045	

Surface Resistivity (FA)

Specimen	Age (days)	Surface Resistivity (kΩ-cm)	Average
FA-1	7	7.1	7.4
FA-2	7	7.4	
FA-3	7	7.8	
FA-4	28	47.3	46.2
FA-5	28	43.5	
FA-6	28	48.0	
FA-7	364	62.4	63.4
FA-8	364	65.7	
FA-9	364	62.3	

Fender pile samples taken at Durastress on: 6/16/2006

Compressive Strength of Cylinders (FAF)

Specimen	Age (days)	Comp. Strength (psi)	Average (psi)
Cylinder 1	28	6,620	6,280
Cylinder 2	28	6,140	
Cylinder 3	28	6,070	
Cylinder 4	91	8,080	8,000
Cylinder 5	91	8,010	
Cylinder 6	91	7,900	
Cylinder 7	364	8,387	8,381
Cylinder 8	364	8,541	
Cylinder 9	364	8,214	

Splitting Tensile Strength (FAF)

Specimen	Age (days)	Tens. Strength (psi)	Average (psi)
Cylinder 1	28	798	780
Cylinder 2	28	735	
Cylinder 3	28	808	
Cylinder 4	91	1,183	1,143
Cylinder 5	91	1,117	
Cylinder 6	91	1,130	
Cylinder 7	364	1,034	1,050
Cylinder 8	364	1,086	
Cylinder 9	364	1,031	

28-Day Modulus of Rupture (FAF)

Specimen	Mod. of Rupture (psi)
Beam 1	887
Beam 2	789
Beam 3	902
Beam 4	821
Beam 5	884
Average (psi)	857

Modulus of Elasticity (FAF)

Specimen		Age (days)	MOE (ksi)	Average (ksi)
Cylinder 1	Run 1	28	N/A	N/A
	Run 2	28	N/A	
	Run 3	28	N/A	
Cylinder 2	Run 1	28	N/A	
	Run 2	28	N/A	
	Run 3	28	N/A	
Cylinder 3	Run 1	91	4,157	4,301
	Run 2	91	4,561	
	Run 3	91	4,099	
Cylinder 4	Run 1	91	4,215	
	Run 2	91	4,388	
	Run 3	91	4,388	
Cylinder 5	Run 1	364	4,950	5,183
	Run 2	364	5,250	
	Run 3	364	5,250	
Cylinder 6	Run 1	364	5,100	
	Run 2	364	5,250	
	Run 3	364	5,300	

Rapid Chloride Migration (FAF)

Specimen	Age (days)	D_{nssm} ($x10^{-12}$ m^2 / s)	Average	STD
RMT-1	56	116.1	127.2	11.8
RMT-2	56	125.7		
RMT-3	56	139.6		
RMT-1	91	77.06	58.36	17.1
RMT-2	91	54.56		
RMT-3	91	43.44		
RMT-1	180	45.64	44.43	12.5
RMT-2	180	31.34		
RMT-3	180	56.32		

Surface Resistivity (FAF)

Specimen	Age (days)	Surface Resistivity (kΩ-cm)	Average
FAF-1	28	12.5	11.5
FAF-2	28	10.4	
FAF-3	28	11.8	
FAF-4	91	36.6	38.2
FAF-5	91	39.7	
FAF-6	91	38.3	
FAF-7	364	74.4	74.9
FAF-8	364	75.4	
FAF-9	364	74.8	

Mixture SF

Bridge pile samples taken at Durastress on: 9/29/2006

Compressive Strength of Cylinders (SF)

Specimen	Age (days)	Comp. Strength (psi)	Average (psi)
Cylinder 1	7	6,600	6,720
Cylinder 2	7	6,630	
Cylinder 3	7	6,910	
Cylinder 4	28	7,550	8,050
Cylinder 5	28	8,150	
Cylinder 6	28	8,450	
Cylinder 7	364	9,960	9,840
Cylinder 8	364	9,916	
Cylinder 9	364	9,643	

Surface Resistivity (SF)

Specimen	Age (days)	Surface Resistivity (kΩ-cm)	Average
SF-1	7	19.0	18.9
SF-2	7	20.0	
SF-3	7	17.7	
SF-4	28	83.4	83.0
SF-5	28	84.9	
SF-6	28	80.7	
SF-7	364	221.4	222.3
SF-8	364	223.0	
SF-9	364	222.6	

Fender pile samples taken at Durastress on: 9/29/2006

Compressive Strength of Cylinders (SFF)

Specimen	Age (days)	Comp. Strength (psi)	Average (psi)
Cylinder 1	28	5,760	6,200
Cylinder 2	28	6,630	
Cylinder 3	28	6,210	
Cylinder 4	91	9,070	8,860
Cylinder 5	91	8,820	
Cylinder 6	91	8,670	
Cylinder 7	364	9,345	9,296
Cylinder 8	364	9,274	
Cylinder 9	364	9,270	

Splitting Tensile Strength (SFF)

Specimen	Age (days)	Tens. Strength (psi)	Average (psi)
Cylinder 1	28	598	513
Cylinder 2	28	469	
Cylinder 3	28	472	
Cylinder 4	91	1,018	886
Cylinder 5	91	797	
Cylinder 6	91	843	
Cylinder 7	364	903	921
Cylinder 8	364	877	
Cylinder 9	364	983	

28-Day Modulus of Rupture (SFF)

Specimen	Mod. of Rupture (psi)
Beam 1	1,274
Beam 2	1,218
Beam 3	1,266
Beam 4	1,169
Beam 5	1,162
Average (psi)	1,218

Modulus of Elasticity (SFF)

Specimen		Age (days)	MOE (ksi)	Average (ksi)
Cylinder 1	Run 1	28	N/A	N/A
	Run 2	28	N/A	
	Run 3	28	N/A	
Cylinder 2	Run 1	28	N/A	
	Run 2	28	N/A	
	Run 3	28	N/A	
Cylinder 3	Run 1	91	5,050	5,075
	Run 2	91	4,750	
	Run 3	91	5,050	
Cylinder 4	Run 1	91	5,250	
	Run 2	91	5,150	
Cylinder 5	Run 1	364	5,250	5,242
	Run 2	364	5,350	
	Run 3	364	5,350	
Cylinder 6	Run 1	364	5,050	
	Run 2	364	5,250	
	Run 3	364	5,200	

Rapid Chloride Migration (SFF)

Specimen	Age (days)	D_{nssm} ($x10^{-12}$ m^2 / s)	Average	STD
RMT-1	56	141.2	137.5	5.2
RMT-2	56	133.8		
RMT-1	91	37.26	46.10	11.1
RMT-2	91	42.55		
RMT-3	91	58.49		
RMT-1	180	6.10	7.15	1.1
RMT-2	180	7.10		
RMT-3	180	8.25		

Surface Resistivity (SFF)

Specimen	Age (days)	Surface Resistivity (kΩ-cm)	Average
SFF-1	28	71.3	95.9
SFF-2	28	141.9	
SFF-3	28	74.7	
SFF-4	91	130.8	129.9
SFF-5	91	132.2	
SFF-6	91	126.7	
SFF-7	364	226.9	225.2
SFF-8	364	226.0	
SFF-9	364	222.6	

Mixture MET

Bridge pile samples taken at Durastress on: 10/13/2006

Compressive Strength of Cylinders (MET)

Specimen	Age (days)	Comp. Strength (psi)	Average (psi)
Cylinder 1	7	5,570	5,740
Cylinder 2	7	6,610	
Cylinder 3	7	5,480	
Cylinder 4	28	6,070	6,550
Cylinder 5	28	6,790	
Cylinder 6	28	6,770	
Cylinder 7	364	8,992	9,166
Cylinder 8	364	8,993	
Cylinder 9	364	9,512	

Surface Resistivity (MET)

Specimen	Age (days)	Surface Resistivity (kΩ-cm)	Average
META-1	7	11.8	11.8
META-2	7	12.4	
META-3	7	11.2	
META-4	28	24.8	24.0
META-5	28	23.6	
META-6	28	23.7	
META-7	364	85.7	83.5
META-8	364	84.2	
META-9	364	80.5	

Fender pile samples taken at Durastress on: 10/13/2006

Compressive Strength of Cylinders (METF)

Specimen	Age (days)	Comp. Strength (psi)	Average (psi)
Cylinder 1	28	6,070	6,520
Cylinder 2	28	6,720	
Cylinder 3	28	6,770	
Cylinder 4	91	7,530	7,580
Cylinder 5	91	7,560	
Cylinder 6	91	7,650	
Cylinder 7	364	9,036	9,287
Cylinder 8	364	9,081	
Cylinder 9	364	9,745	

Splitting Tensile Strength (METF)

Specimen	Age (days)	Tens. Strength (psi)	Average (psi)
Cylinder 1	28	695	738
Cylinder 2	28	820	
Cylinder 3	28	698	
Cylinder 4	91	490	631
Cylinder 5	91	742	
Cylinder 6	91	662	
Cylinder 7	364	946	999
Cylinder 8	364	941	
Cylinder 9	364	1,110	

28-Day Modulus of Rupture (METF)

Specimen	Mod. of Rupture (psi)
Beam 1	889
Beam 2	1,011
Beam 3	881
Beam 4	932
Beam 5	953
Average (psi)	933

Modulus of Elasticity (METF)

Specimen		Age (days)	MOE (ksi)	Average (ksi)
Cylinder 1	Run 1	28	3,930	3,310
	Run 2	28	3,810	
	Run 3	28	3,750	
Cylinder 2	Run 1	28	2,770	
	Run 2	28	2,830	
	Run 3	28	2,770	
Cylinder 3	Run 1	91	5,300	4,583
	Run 2	91	5,400	
Cylinder 4	Run 1	91	4,050	
	Run 2	91	3,700	
	Run 3	91	3,700	
Cylinder 5	Run 1	364	4,600	4,767
	Run 2	364	4,750	
	Run 3	364	4,750	
Cylinder 6	Run 1	364	4,800	
	Run 2	364	4,850	
	Run 3	364	4,850	

Rapid Chloride Migration (METF)

Specimen	Age (days)	D_{nssm} ($x10^{-12}$ m^2 / s)	Average	STD
RMT-1	56	57.99	49.57	18.6
RMT-2	56	62.47		
RMT-3	56	28.25		
RMT-1	91	106.0	95.95	14.1
RMT-2	91	85.95		
RMT-1	180	12.22	15.73	3.1
RMT-2	180	17.11		
RMT-3	180	17.85		

Surface Resistivity (METF)

Specimen	Age (days)	Surface Resistivity (kΩ-cm)	Average
METAF-1	28	24.8	24.0
METAF-2	28	23.6	
METAF-3	28	23.7	
METAF-4	91	30.4	27.3
METAF-5	91	25.8	
METAF-6	91	25.8	
METAF-7	364	81.8	84.3
METAF-8	364	86.3	
METAF-9	364	84.8	

Mixture BFS

Bridge pile samples taken at Durastress on: 10/06/2006

Compressive Strength of Cylinders (BFS)

Specimen	Age (days)	Comp. Strength (psi)	Average (psi)
Cylinder 1	7	4,750	5,090
Cylinder 2	7	3,810	
Cylinder 3	7	6,690	
Cylinder 4	28	6,730	7,570
Cylinder 5	28	8,210	
Cylinder 6	28	7,770	
Cylinder 7	364	10,682	10,609
Cylinder 8	364	10,664	
Cylinder 9	364	10,480	

Surface Resistivity (BFS)

Specimen	Age (days)	Surface Resistivity (kΩ-cm)	Average
BFS-1	7	46.7	48.7
BFS-2	7	50.5	
BFS-3	7	48.8	
BFS-4	28	91.0	71.9
BFS-5	28	80.9	
BFS-6	28	43.9	
BFS-7	364	256.0	259.4
BFS-8	364	260.3	
BFS-9	364	261.8	

Fender pile samples taken at Durastress on: 10/06/2006

Compressive Strength of Cylinders (BFSF)

Specimen	Age (days)	Comp. Strength (psi)	Average (psi)
Cylinder 1	28	8,500	8,870
Cylinder 2	28	9,050	
Cylinder 3	28	9,060	
Cylinder 4	91	9,980	10,060
Cylinder 5	91	10,250	
Cylinder 6	91	9,950	
Cylinder 7	364	10,904	10,614
Cylinder 8	364	10,588	
Cylinder 9	364	10,349	

Splitting Tensile Strength (BFSF)

Specimen	Age (days)	Tens. Strength (psi)	Average (psi)
Cylinder 1	28	915	821
Cylinder 2	28	888	
Cylinder 3	28	661	
Cylinder 4	91	802	713
Cylinder 5	91	667	
Cylinder 6	91	671	
Cylinder 7	364	1,051	1,041
Cylinder 8	364	1,050	
Cylinder 9	364	1,021	

28-Day Modulus of Rupture (BFSF)

Specimen	Mod. of Rupture (psi)
Beam 1	1,237
Beam 2	1,214
Beam 3	1,231
Beam 4	1,334
Beam 5	1,297
Average (psi)	1,262

Modulus of Elasticity (BFSF)

Specimen		Age (days)	MOE (ksi)	Average (ksi)
Cylinder 1	Run 1	28	3,640	3,859
	Run 2	28	3,700	
	Run 3	28	3,580	
Cylinder 2	Run 1	28	4,160	
	Run 2	28	4,100	
	Run 3	28	3,980	
Cylinder 3	Run 1	91	5,500	5,500
	Run 2	91	5,350	
Cylinder 4	Run 1	91	5,600	
	Run 2	91	5,550	
Cylinder 5	Run 1	364	5,250	5,208
	Run 2	364	5,150	
	Run 3	364	5,350	
Cylinder 6	Run 1	364	5,100	
	Run 2	364	5,200	
	Run 3	364	5,200	

Rapid Chloride Migration (BFSF)

Specimen	Age (days)	D_{nssm} ($x10^{-12}$ m^2 / s)	Average	STD
RMT-1	56	122.3	118.4	5.4
RMT-2	56	114.6		
RMT-1	180	2.75	2.59	0.7
RMT-2	180	3.22		
RMT-3	180	1.80		

Surface Resistivity (BFSF)

Specimen	Age (days)	Surface Resistivity (kΩ-cm)	Average
BFSF-1	28	52.0	51.5
BFSF-2	28	51.6	
BFSF-3	28	50.9	
BFSF-4	91	104.1	92.2
BFSF-5	91	89.3	
BFSF-6	91	83.3	
BFSF-7	364	262.0	258.6
BFSF-8	364	256.8	
BFSF-9	364	258.1	

Appendix C–Durability Segment

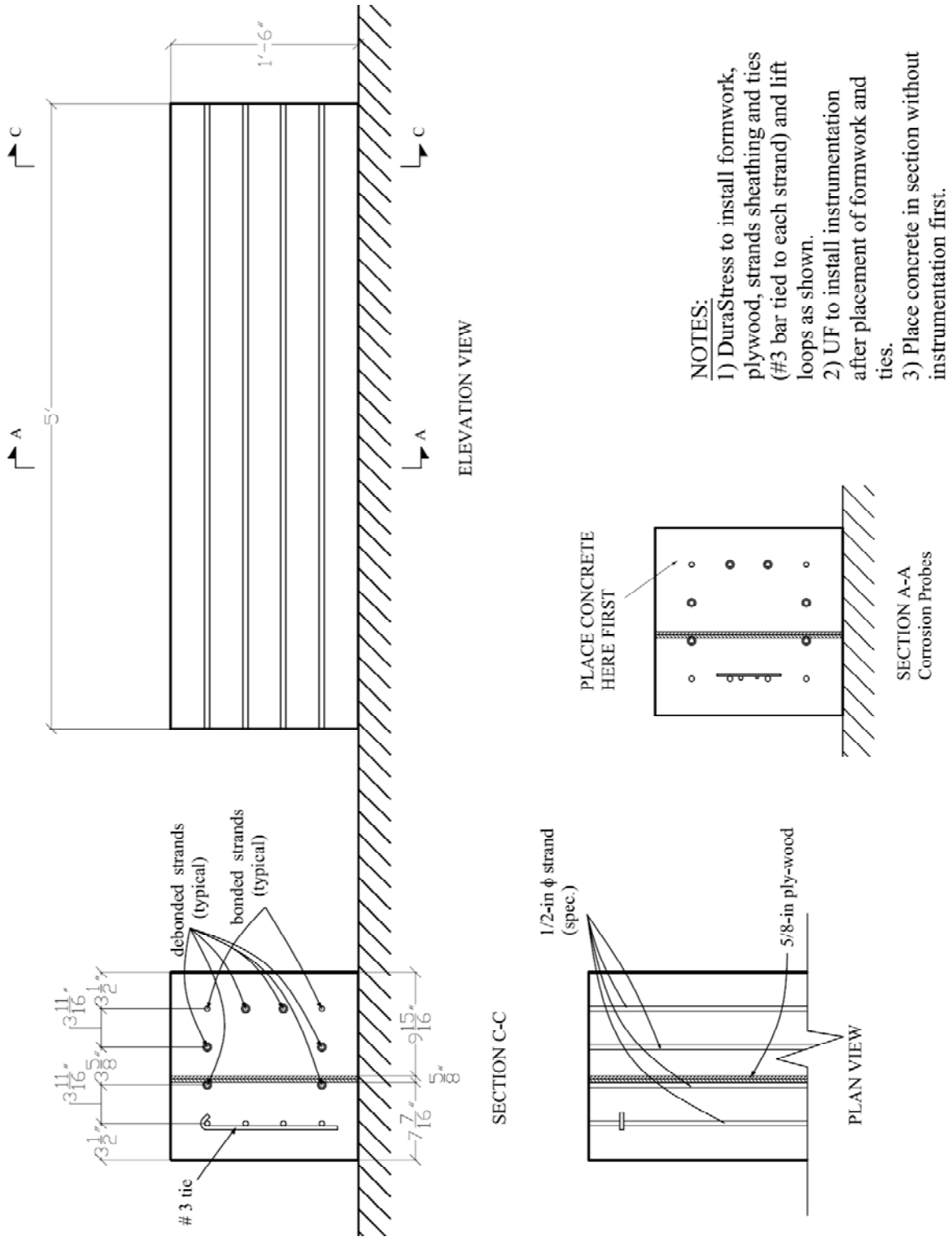

Construction of the durability segment

Thermocouple

Thermocouple

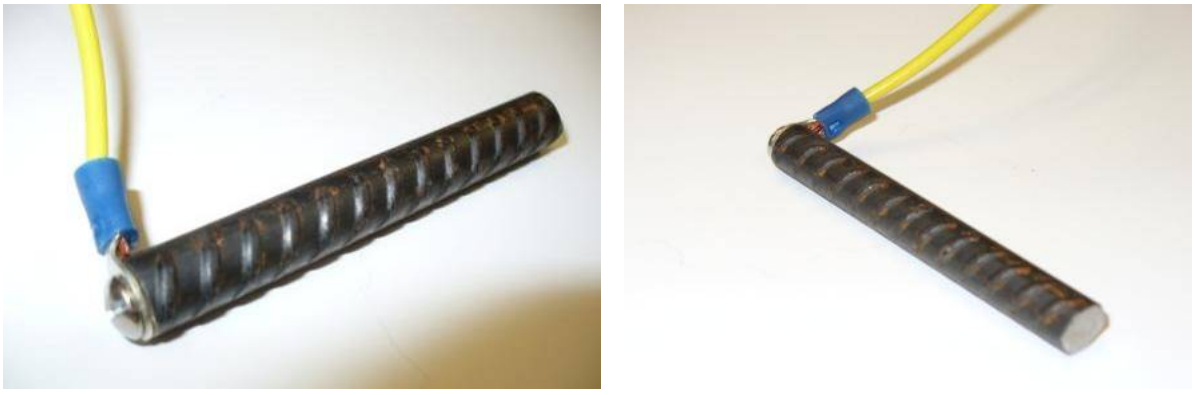

Steel corrosion probe – drilled, tapped and connected with #14 stranded copper wire with other end smoothed

Steel probe – connection with the wire is protected using scotch kote and 2 or 3 layers of the heat shrinks

Steel probe – epoxy is placed at the both ends, such that 2-in. length of the probe is exposed to the corrosion action

Titanium corrosion probe with 2-in. length of the probe exposed to the corrosion action

Appendix D–Covermeter Data

Covermeter Data Sheet 24" Pile

Project: IBRC **Tested By:** C.Ferraro, A. Doyle

Date: June, 29 2006 **Pile Name:** B1349 70

V V 7 62306

End Measurements: Top of Pile

Finish Face	Strand #	1	2	3	4	5	6
	Depth to Strand (in)	3.5	3.5	3.625	3.625	3.75	3.625
Finish Face + 90°	Strand #	1	2	3	4	5	6
	Depth to Strand (in)	3.375	3.375	3.25	3.125	3.125	3.0
Finish Face + 180°	Strand #	1	2	3	4	5	6
	Depth to Strand (in)	3.25	3.25	3.375	3.375	3.25	3.25
Finish Face + 270°	Strand #	1	2	3	4	5	6
	Depth to Strand (in)	3.375	3.375	3.625	3.625	3.375	3.75

End Measurements: Bottom of Pile

Finish Face	Strand #	1	2	3	4	5	6
	Depth to Strand (in)	3.375	3.5	3.5	3.5	3.5	3.625
Finish Face - 90°	Strand #	1	2	3	4	5	6
	Depth to Strand (in)	3.5	3.5	3.5	3.375	3.25	3.25
Finish Face - 180°	Strand #	1	2	3	4	5	6
	Depth to Strand (in)	3.25	3.375	3.25	3.25	3.25	3.5
Finish Face - 270°	Strand #	1	2	3	4	5	6
	Depth to Strand (in)	3.25	3.375	3.375	3.375	3.5	3.625

Note: The strands are measured from the clockwise direction at the top of the pile but, counterclockwise direction from the bottom of the pile to ensure consistancy

Covermeter Data Sheet

Project: IBRC | **Tested By:** C.Ferraro, A. Doyle

Date: June, 29 2006 | **Pile Name:** B1349 70 V V 7 62306

Covermeter Measurements: 20 from top of pile

Finish Face	Strand #	1	2	3	4	5	6
	Depth to Strand (in)	3.45	3.15	3.05	3.10	3.35	3.70
Finish Face + 90°	Strand #	1	2	3	4	5	6
	Depth to Strand (in)	3.25	2.95	2.95	3	3.15	3.45
Finish Face + 180°	Strand #	1	2	3	4	5	6
	Depth to Strand (in)	**	**	**	**	**	**
Finish Face + 270°	Strand #	1	2	3	4	5	6
	Depth to Strand (in)	3.25	3.05	2.95	2.95	3.1	3.5

Covermeter Measurements: Center of pile

Finish Face	Strand #	1	2	3	4	5	6
	Depth to Strand (in)	3.45	3.2	3.05	3.15	3.3	3.7
Finish Face + 90°	Strand #	1	2	3	4	5	6
	Depth to Strand (in)	3.35	2.9	2.9	2.9	2.9	3.45
Finish Face + 180°	Strand #	1	2	3	4	5	6
	Depth to Strand (in)	**	**	**	**	**	**
Finish Face + 270°	Strand #	1	2	3	4	5	6
	Depth to Strand (in)	3.20	2.90	2.90	2.80	2.80	3.15

Covermeter Measurements: 20' from bottom of pile

Finish Face	Strand #	1	2	3	4	5	6
	Depth to Strand (in)	3.35	2.9	2.9	2.9	2.9	3.5
Finish Face + 90°	Strand #	1	2	3	4	5	6
	Depth to Strand (in)	3.3	2.95	2.85	2.85	2.9	3.15
Finish Face + 180°	Strand #	1	2	3	4	5	6
	Depth to Strand (in)	**	**	**	**	**	**
Finish Face + 270°	Strand #	1	2	3	4	5	6
	Depth to Strand (in)	3.15	2.95	2.95	2.95	2.95	3.35

** Not accessible

Covermeter Data Sheet 24" Pile

Project: IBRC **Tested By:** C.Ferraro, A. Doyle

Date: June, 29 2006 **Pile Name:** B1349 70

V V 8 62306

End Measurements: Top of Pile

Finish Face	Strand #	1	2	3	4	5	6
	Depth to Strand (in)	3.375	3.375	3.375	3.5	3.5	3.375
Finish Face + 90°	Strand #	1	2	3	4	5	6
	Depth to Strand (in)	3.625	3.5	3.5	3.5	3.25	3.25
Finish Face + 180°	Strand #	1	2	3	4	5	6
	Depth to Strand (in)	3.5	3.375	3.25	3.25	3.25	3.25
Finish Face + 270°	Strand #	1	2	3	4	5	6
	Depth to Strand (in)	3.25	3.25	3.375	3.375	3.5	3.625

End Measurements: Bottom of Pile

Finish Face	Strand #	1	2	3	4	5	6
	Depth to Strand (in)	3.375	3.375	3.375	3.375	3.375	3.5
Finish Face - 90°	Strand #	1	2	3	4	5	6
	Depth to Strand (in)	3.5	3.5	3.375	3.375	3.25	3.125
Finish Face - 180°	Strand #	1	2	3	4	5	6
	Depth to Strand (in)	3.375	3.5	3.5	3.5	3.5	3.5
Finish Face - 270°	Strand #	1	2	3	4	5	6
	Depth to Strand (in)	3.25	3.375	3.375	3.5	3.375	3.5

Note: The strands are measured from the clockwise direction at the top of the pile but, counterclockwise direction from the bottom of the pile to ensure consistancy

Covermeter Data Sheet

Project: IBRC | **Tested By:** C.Ferraro, A. Doyle

Date: June, 29 2006 | **Pile Name:** B1349 70 V V 8 62306

Covermeter Measurements: 15' from top of pile

Finish Face	Strand #	1	2	3	4	5	6
	Depth to Strand (in)	3.3	3.1	3.0	3.1	3.2	3.4
Finish Face + 90°	Strand #	1	2	3	4	5	6
	Depth to Strand (in)	3.35	3.15	3.0	3.0	3.0	3.25
Finish Face + 180°	Strand #	1	2	3	4	5	6
	Depth to Strand (in)	**	**	**	**	**	**
Finish Face + 270°	Strand #	1	2	3	4	5	6
	Depth to Strand (in)	3.3	2.9	2.8	2.75	2.75	3.1

Covermeter Measurements: Center of pile

Finish Face	Strand #	1	2	3	4	5	6
	Depth to Strand (in)	3.4	3.5	2.95	3.1	3.25	2.5
Finish Face + 90°	Strand #	1	2	3	4	5	6
	Depth to Strand (in)	3.35	3.0	3.0	3.0	3.0	3.35
Finish Face + 180°	Strand #	1	2	3	4	5	6
	Depth to Strand (in)	**	**	**	**	**	**
Finish Face + 270°	Strand #	1	2	3	4	5	6
	Depth to Strand (in)	3.45	3.1	3.1	3.1	3.1	3.3

Covermeter Measurements: 15' from bottom of pile

Finish Face	Strand #	1	2	3	4	5	6
	Depth to Strand (in)	3.75	3.55	3.45	3.45	3.55	3.65
Finish Face + 90°	Strand #	1	2	3	4	5	6
	Depth to Strand (in)	3.45	3.0	3.0	3.0	3.0	3.0
Finish Face + 180°	Strand #	1	2	3	4	5	6
	Depth to Strand (in)	**	**	**	**	**	**
Finish Face + 270°	Strand #	1	2	3	4	5	6
	Depth to Strand (in)	3.25	3.25	3.1	3.05	3.1	3.25

** Not accessible

Covermeter Data Sheet 24" Pile

Project: IBRC **Tested By:** C.Ferraro, A. Doyle

Date: June, 29 2006 **Pile Name:** B1349 70

V V 9 62306

End Measurements: Top of Pile

Finish Face	Strand #	1	2	3	4	5	6
	Depth to Strand (in)	3.25	3.375	3.375	3.25	3.375	3.375
Finish Face + 90°	Strand #	1	2	3	4	5	6
	Depth to Strand (in)	3.5	3.5	3.5	3.375	3.375	3.25
Finish Face + 180°	Strand #	1	2	3	4	5	6
	Depth to Strand (in)	3.375	3.5	3.5	3.375	3.375	3.375
Finish Face + 270°	Strand #	1	2	3	4	5	6
	Depth to Strand (in)	3.25	3.25	3.375	3.375	3.5	3.5

End Measurements: Bottom of Pile

Finish Face	Strand #	1	2	3	4	5	6
	Depth to Strand (in)	3.5	3.375	3.375	3.375	3.375	3.5
Finish Face - 90°	Strand #	1	2	3	4	5	6
	Depth to Strand (in)	3.5	3.375	3.375	3.375	3.375	3.25
Finish Face - 180°	Strand #	1	2	3	4	5	6
	Depth to Strand (in)	3.375	3.5	3.5	3.5	3.5	3.625
Finish Face - 270°	Strand #	1	2	3	4	5	6
	Depth to Strand (in)	3.25	3.375	3.375	3.5	3.5	3.625

Note: The strands are measured from the clockwise direction at the top of the pile but, counterclockwise direction from the bottom of the pile to ensure consistancy

Covermeter Data Sheet

Project: IBRC | **Tested By:** C.Ferraro, A. Doyle

Date: June 29, 2006 | **Pile Name:** B1349 70 V V 9 62306

Covermeter Measurements: 15' from top of pile

Finish Face	Strand #	1	2	3	4	5	6
	Depth to Strand (in)	3.30	2.95	2.95	3.00	3.00	3.50
Finish Face + 90°	Strand #	1	2	3	4	5	6
	Depth to Strand (in)	3.30	2.80	2.70	2.70	2.70	3.50
Finish Face + 180°	Strand #	1	2	3	4	5	6
	Depth to Strand (in)	**	**	**	**	**	**
Finish Face + 270°	Strand #	1	2	3	4	5	6
	Depth to Strand (in)	3.45	2.85	2.90	3.00	3.10	3.40

Covermeter Measurements: Center of pile

Finish Face	Strand #	1	2	3	4	5	6
	Depth to Strand (in)	3.50	3.00	3.00	3.10	3.15	3.65
Finish Face + 90°	Strand #	1	2	3	4	5	6
	Depth to Strand (in)	3.35	2.80	2.75	2.65	2.60	3.40
Finish Face + 180°	Strand #	1	2	3	4	5	6
	Depth to Strand (in)	**	**	**	**	**	**
Finish Face + 270°	Strand #	1	2	3	4	5	6
	Depth to Strand (in)	3.40	2.95	2.95	3.10	3.20	3.60

Covermeter Measurements: 15' from bottom of pile

Finish Face	Strand #	1	2	3	4	5	6
	Depth to Strand (in)	3.45	3.00	3.00	3.05	3.05	3.60
Finish Face + 90°	Strand #	1	2	3	4	5	6
	Depth to Strand (in)	3.50	3.00	2.90	2.85	2.85	3.70
Finish Face + 180°	Strand #	1	2	3	4	5	6
	Depth to Strand (in)	**	**	**	**	**	**
Finish Face + 270°	Strand #	1	2	3	4	5	6
	Depth to Strand (in)	3.20	2.80	2.85	2.90	3.00	3.60

** Not accessible

Covermeter Data Sheet 24" Pile

Project: IBRC **Tested By:** C.Ferraro, A. Doyle

Date: June, 29 2006 **Pile Name:** B1349 70

V V 10 62306

End Measurements: Top of Pile

Finish Face	Strand #	1	2	3	4	5	6
	Depth to Strand (in)	3.5	3.375	3.375	3.25	3.375	3.375
Finish Face + 90°	Strand #	1	2	3	4	5	6
	Depth to Strand (in)	3.5	3.5	3.5	3.375	3.375	3.25
Finish Face + 180°	Strand #	1	2	3	4	5	6
	Depth to Strand (in)	3.375	3.5	3.5	3.375	3.375	3.375
Finish Face + 270°	Strand #	1	2	3	4	5	6
	Depth to Strand (in)	3.25	3.25	3.375	3.375	3.5	3.5

End Measurements: Bottom of Pile

Finish Face	Strand #	1	2	3	4	5	6
	Depth to Strand (in)	3.375	3.375	3.375	3.375	3.375	3.375
Finish Face - 90°	Strand #	1	2	3	4	5	6
	Depth to Strand (in)	3.5	3.5	3.5	3.375	3.25	3.125
Finish Face - 180°	Strand #	1	2	3	4	5	6
	Depth to Strand (in)	3.375	3.375	3.375	3.375	3.375	3.375
Finish Face - 270°	Strand #	1	2	3	4	5	6
	Depth to Strand (in)	3.125	3.25	3.25	3.325	3.5	3.5

Note: The strands are measured from the clockwise direction at the top of the pile but, counterclockwise direction from the bottom of the pile to ensure consistancy

Covermeter Data Sheet

Project: IBRC | **Tested By:** C.Ferraro, A. Doyle

Date: June 29, 2006 | **Pile Name:** B1349 70 V V 10 62306

Covermeter Measurements: 15' from top of pile

Finish Face	Strand #	1	2	3	4	5	6
	Depth to Strand (in)	3.60	3.20	3.20	3.15	3.15	3.55
Finish Face + 90°	Strand #	1	2	3	4	5	6
	Depth to Strand (in)	3.20	2.80	2.75	2.70	2.65	3.10
Finish Face + 180°	Strand #	1	2	3	4	5	6
	Depth to Strand (in)	**	**	**	**	**	**
Finish Face + 270°	Strand #	1	2	3	4	5	6
	Depth to Strand (in)	3.15	2.75	2.75	2.80	2.90	3.30

Covermeter Measurements: Center of pile

Finish Face	Strand #	1	2	3	4	5	6
	Depth to Strand (in)	3.40	2.90	2.95	3.00	2.95	3.45
Finish Face + 90°	Strand #	1	2	3	4	5	6
	Depth to Strand (in)	3.35	2.90	2.80	2.70	2.60	3.50
Finish Face + 180°	Strand #	1	2	3	4	5	6
	Depth to Strand (in)	**	**	**	**	**	**
Finish Face + 270°	Strand #	1	2	3	4	5	6
	Depth to Strand (in)	3.40	3.00	3.00	2.95	2.95	3.35

Covermeter Measurements: 15' from bottom of pile

Finish Face	Strand #	1	2	3	4	5	6
	Depth to Strand (in)	3.20	2.75	2.85	2.80	2.85	3.30
Finish Face + 90°	Strand #	1	2	3	4	5	6
	Depth to Strand (in)	3.45	2.85	2.75	2.70	2.65	3.75
Finish Face + 180°	Strand #	1	2	3	4	5	6
	Depth to Strand (in)	**	**	**	**	**	**
Finish Face + 270°	Strand #	1	2	3	4	5	6
	Depth to Strand (in)	3.60	3.15	3.00	2.90	2.90	3.50

** Not accessible

Covermeter Data Sheet 24" Pile

Project: IBRC **Tested By:** C.Ferraro, A. Doyle

Date: June, 29 2006 **Pile Name:** B1349 70

V V 11 62306

End Measurements: Top of Pile

Finish Face	Strand #	1	2	3	4	5	6
	Depth to Strand (in)	3.375	3.5	3.5	3.5	3.5	3.5
Finish Face + 90°	Strand #	1	2	3	4	5	6
	Depth to Strand (in)	3.625	3.625	3.5	3.5	3.375	3.25
Finish Face + 180°	Strand #	1	2	3	4	5	6
	Depth to Strand (in)	3.375	3.5	3.5	3.25	3.25	3.25
Finish Face + 270°	Strand #	1	2	3	4	5	6
	Depth to Strand (in)	3.25	3.25	3.375	3.375	3.5	3.625

End Measurements: Bottom of Pile

Finish Face	Strand #	1	2	3	4	5	6
	Depth to Strand (in)	3.5	3.5	3.5	3.5	3.375	3.375
Finish Face - 90°	Strand #	1	2	3	4	5	6
	Depth to Strand (in)	3.5	3.5	3.375	3.5	3.5	3.375
Finish Face - 180°	Strand #	1	2	3	4	5	6
	Depth to Strand (in)	3.625	3.625	3.625	3.5	3.5	3.625
Finish Face - 270°	Strand #	1	2	3	4	5	6
	Depth to Strand (in)	3.5	3.5	3.375	3.375	3.5	3.5

Note: The strands are measured from the clockwise direction at the top of the pile but, counterclockwise direction from the bottom of the pile to ensure consistancy

Covermeter Data Sheet

Project: IBRC | **Tested By:** C.Ferraro, A. Doyle

Date: June 29, 2006 | **Pile Name:** B1349 70 V V 9 62306

Covermeter Measurements: 15' from top of pile

Finish Face	Strand #	1	2	3	4	5	6
	Depth to Strand (in)	3.60	3.25	3.20	3.05	3.15	3.65
Finish Face + 90°	Strand #	1	2	3	4	5	6
	Depth to Strand (in)	3.65	3.00	2.85	2.70	2.65	3.05
Finish Face + 180°	Strand #	1	2	3	4	5	6
	Depth to Strand (in)	**	**	**	**	**	**
Finish Face + 270°	Strand #	1	2	3	4	5	6
	Depth to Strand (in)	3.5	2.95	2.90	3.00	3.25	3.70

Covermeter Measurements: Center of pile

Finish Face	Strand #	1	2	3	4	5	6
	Depth to Strand (in)	3.75	3.25	3.20	3.15	3.25	3.75
Finish Face + 90°	Strand #	1	2	3	4	5	6
	Depth to Strand (in)	3.35	2.70	2.65	2.50	2.40	3.05
Finish Face + 180°	Strand #	1	2	3	4	5	6
	Depth to Strand (in)	**	**	**	**	**	**
Finish Face + 270°	Strand #	1	2	3	4	5	6
	Depth to Strand (in)	3.35	3.10	3.10	3.10	3.15	3.60

Covermeter Measurements: 15' from bottom of pile

Finish Face	Strand #	1	2	3	4	5	6
	Depth to Strand (in)	3.25	3.00	3.10	3.15	3.25	3.85
Finish Face + 90°	Strand #	1	2	3	4	5	6
	Depth to Strand (in)	3.65	3.20	3.05	2.95	2.85	3.35
Finish Face + 180°	Strand #	1	2	3	4	5	6
	Depth to Strand (in)	**	**	**	**	**	**
Finish Face + 270°	Strand #	1	2	3	4	5	6
	Depth to Strand (in)	3.25	2.75	2.70	2.75	2.85	3.35

** Not accessible

Covermeter Data Sheet 24" Pile

Project: IBRC	**Tested By:**	C.Ferraro, A. Doyle	
Date: June, 29 2006	**Pile Name:**	B1349	70
		V V 12	62306

End Measurements: Top of Pile

Finish Face	Strand #	1	2	3	4	5	6
	Depth to Strand (in)	3.375	3.375	3.375	3.375	3.375	3.375
Finish Face + 90°	Strand #	1	2	3	4	5	6
	Depth to Strand (in)	3.625	3.5	3.375	3.375	3.25	3.25
Finish Face + 180°	Strand #	1	2	3	4	5	6
	Depth to Strand (in)	3.5	3.5	3.375	3.375	3.375	3.5
Finish Face + 270°	Strand #	1	2	3	4	5	6
	Depth to Strand (in)	3.125	3.25	3.375	3.375	3.5	3.625

End Measurements: Bottom of Pile

Finish Face	Strand #	1	2	3	4	5	6
	Depth to Strand (in)	3.375	3.375	3.375	3.375	3.5	3.5
Finish Face - 90°	Strand #	1	2	3	4	5	6
	Depth to Strand (in)	3.5	3.5	3.375	3.5	3.5	3.375
Finish Face - 180°	Strand #	1	2	3	4	5	6
	Depth to Strand (in)	3.625	3.625	3.625	3.5	3.5	3.625
Finish Face - 270°	Strand #	1	2	3	4	5	6
	Depth to Strand (in)	3.5	3.5	3.375	3.375	3.5	3.5

Note: The strands are measured from the clockwise direction at the top of the pile but, counterclockwise direction from the bottom of the pile to ensure consistancy

Covermeter Data Sheet

Project: IBRC | **Tested By:** C.Ferraro, A. Doyle

Date: June 29, 2006 | **Pile Name:** B1349 70 V V 9 62306

Covermeter Measurements: 15' from top of pile

Finish Face	Strand #	1	2	3	4	5	6
	Depth to Strand (in)	3.60	3.25	3.20	3.05	3.15	3.65
Finish Face + 90°	Strand #	1	2	3	4	5	6
	Depth to Strand (in)	3.65	3.00	2.85	2.70	2.65	3.05
Finish Face + 180°	Strand #	1	2	3	4	5	6
	Depth to Strand (in)	**	**	**	**	**	**
Finish Face + 270°	Strand #	1	2	3	4	5	6
	Depth to Strand (in)	3.5	2.95	2.90	3.00	3.25	3.70

Covermeter Measurements: Center of pile

Finish Face	Strand #	1	2	3	4	5	6
	Depth to Strand (in)	3.75	3.25	3.20	3.15	3.25	3.75
Finish Face + 90°	Strand #	1	2	3	4	5	6
	Depth to Strand (in)	3.35	2.70	2.65	2.50	2.40	3.05
Finish Face + 180°	Strand #	1	2	3	4	5	6
	Depth to Strand (in)	**	**	**	**	**	**
Finish Face + 270°	Strand #	1	2	3	4	5	6
	Depth to Strand (in)	3.35	3.10	3.10	3.10	3.15	3.60

Covermeter Measurements: 15' from bottom of pile

Finish Face	Strand #	1	2	3	4	5	6
	Depth to Strand (in)	3.25	3.00	3.10	3.15	3.25	3.85
Finish Face + 90°	Strand #	1	2	3	4	5	6
	Depth to Strand (in)	3.65	3.20	3.05	2.95	2.85	3.35
Finish Face + 180°	Strand #	1	2	3	4	5	6
	Depth to Strand (in)	**	**	**	**	**	**
Finish Face + 270°	Strand #	1	2	3	4	5	6
	Depth to Strand (in)	3.25	2.75	2.70	2.75	2.85	3.35

** Not accessible

Appendix E–Bridge Pile Corrosion Data

Tables below are the surface resistivity and external surface potential readings of the prestressing strands collected from all the bridge piles except bent 1 and 6 piles. Total of 10 surface potential readings and 9 surface resistivity readings were taken from each pile. Locations 0 to 8 indicate the locations along each pile where the readings were taken. Location 8 is at the top of marine growth and location 0 is right below the pile cap. Due to the high tide water, location 8 and 7 readings were not able to obtain. Since the readings were taken from location 8 up to location 1 at every 1 foot increment, the distance between location 1 and 0 varies. Three sets of readings are included, which were taken on three specific dates shown in the table.

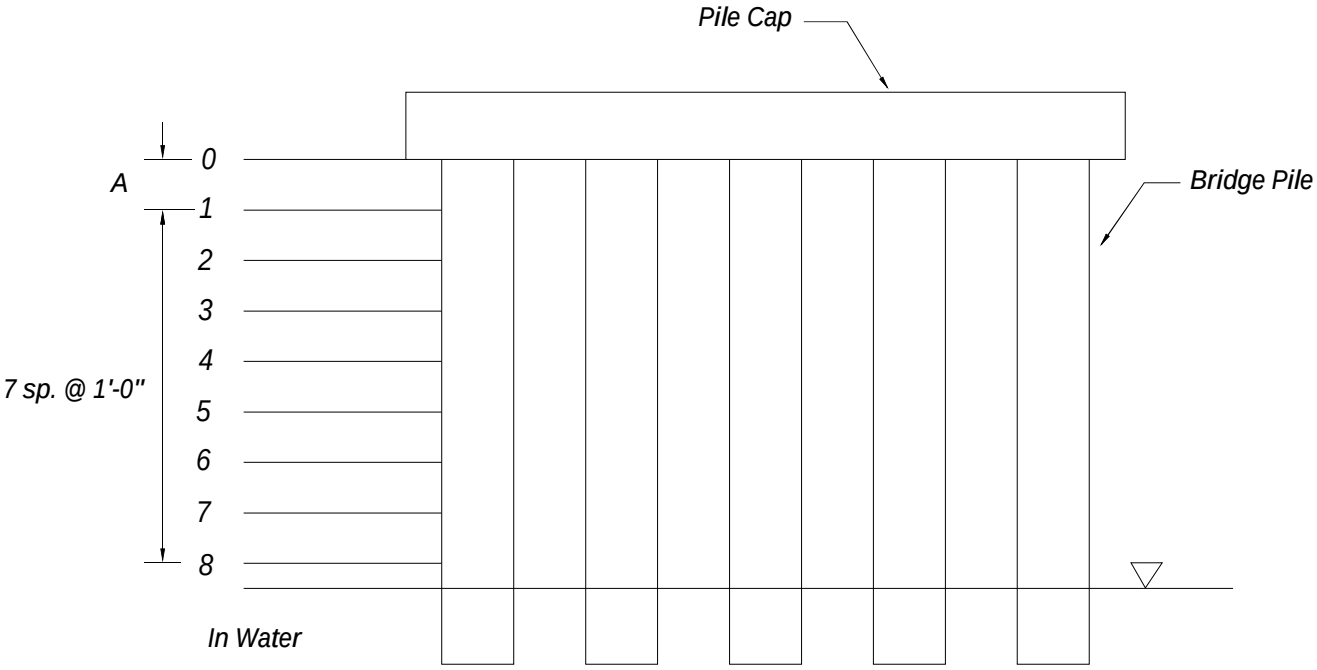

Surface resistivity and external potentials measuring locations along the pile

Bent 2 electrical potential data

Location	UFA			FA			SF			BFS			MET		
	Potential(mV)			Potential(mV)			Potential(mV)			Potential(mV)			Potential(mV)		
	5/8/07	6/26/07	6/29/08	5/8/07	6/26/07	6/29/08	5/8/07	6/26/07	6/29/08	5/8/07	6/26/07	6/29/08	5/8/07	6/26/07	6/29/08
0	-171	-178	-119	-403	79	-129	-243	-403	-112	-29	-192	-106	-354	-345	-146
1	-49	-94	-61	-157	73	-87	-104	-157	-39	-152	-140	-76	-289	-291	-120
2	-13	-63	-14	-165	70	-93	-113	-165	-75	-147	-125	-56	-210	-237	-93
3	-34	-78	-22	-77	-138	-104	-146	-160	-101	-148	-142	-62	-219	-240	-120
4	-49	-95	-57	-97	-150	-117	-183	-182	-122	-171	-162	-102	-235	-227	-139
5	-117	-165	-63	-119	-173	-157	-193	-223	-167	-189	-188	-113	-307	-302	-160
6	-244	-309	-221	-160	-220	-220	-247	-297	-242	-269	-253	-196	-355	-347	-255
7	-426	-521	-302	-350	-347	-282	-470	-525	-346	-490	-435	-311	N/A	-500	-319
in water	-549	-542	-515	-461	-438	-414	-571	-560	-511	-568	-533	-460	-551	-534	-455

Bent 2 electrical potential data

Location	UFA					FA				
	Potential(mV)					Potential(mV)				
	9/6/11	4/2/12 (N)	4/2/12(S)	4/2/12(E)	4/2/12(W)	9/6/11	4/2/12 (N)	4/2/12(S)	4/2/12(E)	4/2/12(W)
0	NA	NA	NA	NA	NA	NA	NA	NA	NA	NA
1	-102	-46	-70	-78		-165	-82	-82	-81	-80
2	-81	-40	-56	-62		-119	-77	-60	-73	-80
3	-80	-52	-63	-96		-124	-100	-88	-91	-60
4	-92	-85	-110	-118		-124	-144	-84	-137	-117
5	-146	-160	-195	-220		-161	-220	-126	-225	-183
6	-373	-210	-240	-244		-238	-272	-155	-186	-243
7	-449	-318	-302	-280		-331	-318	-223	-304	-294
in water	-449	-459	NA	NA		-415	-406	NA	NA	NA

Bent 2 electrical potential data

Location	SF					BFS				
	Potential(mV)					Potential(mV)				
	9/6/11	4/2/12 (N)	4/2/12(S)	4/2/12(E)	4/2/12(W)	9/6/11	4/2/12 (N)	4/2/12(S)	4/2/12(E)	4/2/12(W)
0	NA	NA	NA	NA	NA	NA	NA	NA	NA	NA
1	-81	-22	-36	-60	-62	-95	-60	-76	-55	-81
2	-88	-60	-47	-64	-65	-87	-62	-77	-48	-87
3	-154	-77	-60	-83	-84	-94	-76	-60	-52	-85

4	-177	-108	-91	-104	-119	-110	-112	-89	-100	-72
5	-189	-154	-164	-228	-212	-158	-185	-171	-188	-127
6	-290	-224	-278	-285	-291	-261	-264	-284	-250	-160
7	-419	-357	-357	-350	-384	-385	-369	-371	-420	-268
in water	-464	-472	NA	NA	NA	-421	-432	NA	NA	NA

Bent 2 electrical potential data

Location	MET				
	Potential(mV)				
	9/6/11	4/2/12 (N)	4/2/12(S)	4/2/12(E)	4/2/12(W)
0	NA	NA	NA	NA	NA
1	-155	-66	-79	-56	-52
2	-154	-67	-79	-54	-88
3	-120	-95	-78	-60	NA
4	-138	-115	-88	-94	NA
5	-183	-224	-165	-182	-120
6	-271	-281	-242	-242	-268
7	-223	-310	-310	-288	-290
in water	-446	-444	NA	NA	NA

Bent 2 surface resistivity (SR) data

Location	UFA			FA			SF			BFS			MET		
	S.R.(kΩ)			S.R.(kΩ)			S.R.(kΩ)			S.R.(kΩ)			S.R.(kΩ)		
	5/8/07	6/26/07	6/29/08	5/8/07	6/26/07	6/29/08	5/8/07	6/26/07	6/29/08	5/8/07	6/26/07	6/29/08	5/8/07	6/26/07	6/29/08
0	204	218	242	90	53	118	79	90	58	83	78	166	40	128	72
1	187	228	255	73	51	101	73	73	64	80	78	71	34	44	71
2	151	176	193	76	57	123	70	76	81	88	82	67	35	44	71
3	194	195	215	58	56	86	75	82	55	91	96	64	34	59	63
4	184	210	191	64	57	85	75	78	56	94	99	64	41	51	71
5	180	225	232	58	60	76	88	97	56	87	102	63	43	59	67
6	198	206	198	54	58	72	80	83	56	85	94	63	44	52	70
7	166	N/A	125	56	58	68	56	44	56	57	82	62	N/A	25	60

Bent 2 surface resistivity (SR) data

Location	UFA				FA				SF			
	S.R.(kΩ)				S.R.(kΩ)				S.R.(kΩ)			
	11/28/11(N)	11/28/11(S)	11/28/11(E)	11/28/11(W)	11/28/11(N)	11/28/11(S)	11/28/11(E)	11/28/11(W)	11/28/11(N)	11/28/11(S)	11/28/11(E)	11/28/11(W)
0	NA	NA	NA	NA	NA	NA	NA	NA	NA	NA	NA	NA
1	398	461	413	379	127	104	164	126	222	258	268	NA
2	357	425	439	329	119	126	162	115	277	214	292	NA
3	377	389	430	289	107	121	166	127	229	216	368	NA
4	351	409	451	349	124	120	144	117	246	244	270	NA
5	460	376	403	312	127	120	171	113	274	252	268	NA
6	360	406	461	334	129	115	158	136	247	212	289	NA
7	328	338	395	311	139	125	169	120	206	219	262	NA

Bent 2 surface resistivity (SR) data

Location	BFS				MET			
	S.R.(kΩ)				S.R.(kΩ)			
	11/28/11(N)	11/28/11(S)	11/28/11(E)	11/28/11(W)	11/28/11(N)	11/28/11(S)	11/28/11(E)	11/28/11(W)
0	NA	NA	NA	NA	NA	NA	NA	NA
1	352	324	357	313	211	283	280	315
2	310	298	397	272	252	180	290	233
3	352	302	432	248	229	180	290	373
4	388	250	406	293	207	190	248	NA
5	353	260	411	317	293	193	273	234
6	363	285	372	298	278	199	292	NA
7	308	230	NA	200	194	135	206	NA
8	NA	NA	NA	NA	NA	103	81	NA

Bent 3 electrical potential data

Location	UFA			FA			SF			BFS			MET		
	Potential(mV)			Potential(mV)			Potential(mV)			Potential(mV)			Potential(mV)		
	5/8/07	6/26/07	6/29/08	5/8/07	6/26/07	6/29/08	5/8/07	6/26/07	6/29/08	5/8/07	6/26/07	6/29/08	5/8/07	6/26/07	6/29/08
0	-140	-236	-140	-193	-279	-122	-401	-344	-136	-335	-435	-159	-332	-301	-134
1	-85	-124	-85	-179	-208	-114	-266	-223	-66	-256	-172	-113	-256	-232	-82
2	-38	-104	-72	-173	-197	-118	-205	-180	-53	-174	-121	-57	-213	-208	-65
3	-42	-106	-74	-210	-225	-129	-219	-166	-44	-218	-102	-60	-221	-195	-87
4	-69	-115	-95	-213	-237	-137	-219	-158	-55	-85	-106	-85	-216	-204	-99
5	-112	-163	-150	-239	-247	-148	-239	-205	-108	-107	-146	-142	-209	-251	-97
6	-227	-274	-157	-256	-306	-243	-248	-253	-227	-189	-258	-198	-259	-314	-173
7	-302	-348	-276	-320	-389	-329	-307	-404	-385	-354	-409	-317	-365	-380	-207
8	-394	-431	-317	-383	-468	-336	-457	-504	-466	-506	-527	-425	-448	-472	-311
in water	-394	-510	-468	-514	-482	-375	-603	-601	-558	-603	-602	-519	-574	-537	-420

Bent 3 electrical potential data

Location	UFA					FA				
	Potential(mV)					Potential(mV)				
	9/6/11	4/2/12 (N)	4/2/12(S)	4/2/12(E)	4/2/12(W)	9/6/11	4/2/12 (N)	4/2/12(S)	4/2/12(E)	4/2/12(W)
0	NA	NA	NA	NA	NA	NA	NA	NA	NA	NA
1	-75	-70	-74	-76	-50	-100	-54	-58	-55	-27
2	-45	-30	-69	-63	-38	-94	-45	-62	-64	-27
3	-52	-30	-92	-60	-60	-123	-68	-77	-65	-54
4	-94	-66	-165	-80	-80	-161	-91	-95	-104	-75
5	-132	-147	-214	-168	-148	-205	-186	-156	-158	-100
6	-247	-260	-255	-253	-215	-276	-285	-244	-242	-203
7	-297	-276	-291	-292	-239	-292	-272	-237	-279	-257
8	NA	NA	NA	NA	NA	-311	NA	NA	NA	NA
in water	-331	-373				-324	-276			

Bent 3 electrical potential data

Location	SF					BFS				
	Potential(mV)					Potential(mV)				
	9/6/11	4/2/12 (N)	4/2/12(S)	4/2/12(E)	4/2/12(W)	9/6/11	4/2/12 (N)	4/2/12(S)	4/2/12(E)	4/2/12(W)
0	NA	NA	NA	NA	NA	NA	NA	NA	NA	NA

1	-76	-77	-75	-52	-41	-128	-106	-68	-69	-80
2	-48	-90	-56	-61	-104	-102	-101	-170	-79	-76
3	-48	-84	-80	-80	-102	-101	-99	-120	-88	-67
4	-108	-109	-85	-102	-94	-124	-92	-148	-189	-97
5	-169	-175	-140	-225	-150	-169	-156	-194	-233	-145
6	-233	-280	-239	-307	-198	-256	-283	-263	-280	-248
7	-302	-350	-346	-349	-220	-32	-324	-327	-306	-313
in water	-324	-360				-447	-453			

Bent 3 electrical potential data

Location	MET				
	Potential(mV)				
	9/6/11	4/2/12 (N)	4/2/12(S)	4/2/12(E)	4/2/12(W)
0					
1	-67	-39		-10	-13
2	-71	-57		-42	-57
3	-105	-99	-67	-47	-55
4	-136	-165	-104	-96	-133
5	-207	-185	-160	-187	-146
6	-256	-251	-186	-255	-231
7	-272	-250	-238	-283	-276
in water	-298	-317			

Bent 3 surface resistivity (SR) data

Location	UFA			FA			SF			BFS			MET		
	S.R.(kΩ)			S.R.(kΩ)			S.R.(kΩ)			S.R.(kΩ)			S.R.(kΩ)		
	5/8/07	6/26/07	6/29/08	5/8/07	6/26/07	6/29/08	5/8/07	6/26/07	6/29/08	5/8/07	6/26/07	6/29/08	5/8/07	6/26/07	6/29/08
0	246	124	252	60	62	53	88	73	N/A	89	69	123	39	52	N/A
1	216	183	239	50	50	34	89	65	130	87	71	117	45	47	139
2	229	172	254	54	50	35	85	89	109	85	75	115	37	59	132
3	266	184	238	54	43	50	89	59	72	76	78	143	45	53	125
4	307	184	211	56	50	62	72	73	109	88	76	151	39	50	137
5	280	200	254	54	49	62	65	65	103	74	79	133	51	58	121
6	257	193	214	61	52	55	59	75	112	76	76	145	43	45	51
7	289	164	229	62	56	69	73	73	89	88	65	144	45	46	51
8	279	145	N/A	61	50	N/A	70	64	N/A	81	54	120	38	36	N/A

Bent 3 surface resistivity (SR) data

Location	UFA				FA				SF			
	S.R.(kΩ)				S.R.(kΩ)				S.R.(kΩ)			
	11/28/11(N)	11/28/11(S)	11/28/11(E)	11/28/11(W)	11/28/11(N)	11/28/11(S)	11/28/11(E)	11/28/11(W)	11/28/11(N)	11/28/11(S)	11/28/11(E)	11/28/11(W)
0	NA	NA	NA	NA	NA	NA	NA	NA	NA	NA	NA	NA
1	369	412	443	NA	118	100	157	NA	210	200	NA	265
2	347	385	468	NA	120	120	166	NA	254	234	NA	298
3	318	372	415	NA	121	108	150	130	220	185	NA	291
4	330	422	436	318	121	117	141	111	210	185	217	220
5	364	378	382	342	118	135	147	113	235	187	248	294
6	358	354	461	334	130	192	173	123	204	234	204	237
7	329	356	407	298	136	138	169	116	196	190	189	266
8	NA	NA	NA	NA	NA	NA	NA	NA	166	157	NA	208

Bent 3 surface resistivity (SR) data

Location	BFS				MET			
	S.R.(kΩ)				S.R.(kΩ)			
	11/28/11(N)	11/28/11(S)	11/28/11(E)	11/28/11(W)	11/28/11(N)	11/28/11(S)	11/28/11(E)	11/28/11(W)
0	NA	NA	NA	NA	NA	NA	NA	NA
1	320	255	NA	355	270	200	NA	310
2	287	236	NA	256	269	163	162	353
3	295	243	298	398	308	145	227	261
4	313	276	281	376	254	160	198	224
5	257	253	304	344	256	208	233	280
6	287	264	291	348	273	294	241	273
7	259	236	265	354	212	218	201	261

Bent 4 electrical potential data

Location	UFA			FA			SF			BFS			MET		
	Potential(mV)			Potential(mV)			Potential(mV)			Potential(mV)			Potential(mV)		
	5/8/07	6/26/07	6/29/08	5/8/07	6/26/07	6/29/08	5/8/07	6/26/07	6/29/08	5/8/07	6/26/07	6/29/08	5/8/07	6/26/07	6/29/08
0	-196	-423	-165	-275	-350	-194	-241	-224	-110	-361	-230	-101	-255	-250	-90
1	-145	-207	-130	-196	-246	-155	-163	-173	-89	-141	-126	-71	-226	-211	-71
2	-101	-171	-117	-221	-261	-162	-132	-168	-87	-138	-110	-53	-191	-165	-69
3	-88	-170	-133	-231	-265	-173	-125	-134	-102	-116	-129	-67	-191	-197	-87
4	-122	-203	-170	-262	-306	-186	-127	-172	-120	-129	-162	-76	-199	-271	-87
5	-164	-271	-233	-259	-323	-227	-149	-221	-139	-221	-228	-109	-209	-230	-143
6	-264	-367	-322	-304	-397	328	-182	-316	-218	-291	-289	-257	-223	-291	-247
7	-348	-490	-376	-369	-470	-365	-349	-479	-345	-530	-494	-358	-318	-354	-308
8	-521	N/A	N/A	-457	N/A	N/A	-448	-553	N/A	-592	-566	N/A	-414	-379	N/A
in water	-569	-549	-472	-578	-560	-446	-550	-560	-442	-627	-616	-519	-553	-475	-385

Bent 4 electrical potential data

Location	UFA					FA				
	Potential(mV)					Potential(mV)				
	9/6/11	4/2/12 (N)	4/2/12(S)	4/2/12(E)	4/2/12(W)	9/6/11	4/2/12 (N)	4/2/12(S)	4/2/12(E)	4/2/12(W)
0	NA	NA	NA	NA	NA	NA	NA	NA	NA	NA
1	-79	-47	-61	-70	-46	-71	-100	-100	-101	-100
2	-89	-30	-75	-72	-48	-61	-107	-118	-105	-101
3	-65	-69	-85	-81	-40	-69	-131	-130	-101	-75
4	-90	-132	-214	-78	-143	-102	-202	-170	-119	-111
5	-150	-130	-232	-160	-161	-120	-270	-236	-185	-250
6	-310	-163	-260	-236	-197	-166	-275	-280	-261	-260
7	-314	-194	-290	-250	-244	-248	-274	-260	-238	-272
8	NA	NA	NA	NA	NA	-276	NA	NA	NA	NA
in water	-369	-305	NA	NA	NA	-276	-323	NA	NA	NA

Bent 4 electrical potential data

Location	SF					BFS				
	Potential(mV)					Potential(mV)				
	9/6/11	4/2/12 (N)	4/2/12(S)	4/2/12(E)	4/2/12(W)	9/6/11	4/2/12 (N)	4/2/12(S)	4/2/12(E)	4/2/12(W)
0	NA	NA	NA	NA	NA	NA	NA	NA	NA	NA

1	-97	-44	-47	-15	-28	-111	-101	-76	-86	-87
2	-106	-50	-41	-47	-36	-104	-90	-80	-78	-77
3	-101	-51	-50	-53	-41	-118	-101	-81	-85	-80
4	-127	-94	-57	-73	-44	-133	-120	-84	-103	-110
5	-185	-172	-124	-127	-31	-164	-190	-156	-205	-132
6	-299	-232	-278	-230	-152	-282	-272	-258	-271	-195
7	-398	-262	-284	-243	-170	-370	-360	-322	-281	-236
in water	-543	-303	NA	NA	NA	-427	-459	NA	NA	NA

Bent 4 electrical potential data

Location	MET				
	Potential(mV)				
	9/6/11	4/2/12 (N)	4/2/12(S)	4/2/12(E)	4/2/12(W)
0	NA	NA	NA	NA	NA
1	-56	-52	-32	-30	-22
2	-77	-70	-40	-27	-45
3	-121	-93	-44	-39	-55
4	-177	-145	-80	-44	-126
5	-230	-229	-176	-50	-185
6	-284	-251	-210	-223	-191
7	-326	-255	-232	-250	-228
in water	-330	-192	NA	NA	NA

Bent 4 surface resistivity (SR) data

Location	UFA			FA			SF			BFS			MET		
	S.R.(kΩ)			S.R.(kΩ)			S.R.(kΩ)			S.R.(kΩ)			S.R.(kΩ)		
	5/8/07	6/26/07	6/29/08	5/8/07	6/26/07	6/29/08	5/8/07	6/26/07	6/29/08	5/8/07	6/26/07	6/29/08	5/8/07	6/26/07	6/29/08
0	223	202	N/A	64	52	N/A	88	81	N/A	87	89	143	77	52	78
1	254	237	297	76	57	56	112	77	115	103	89	141	48	48	77
2	245	239	296	72	53	48	118	77	123	97	88	139	48	56	76
3	259	226	296	75	54	47	85	70	110	103	87	138	51	64	75
4	269	212	198	62	54	44	109	81	39	109	88	138	52	50	74
5	280	195	138	63	60	72	140	87	39	108	93	137	40	42	73
6	268	197	147	64	48	41	97	76	39	99	96	136	43	36	73
7	243	90	148	59	60	40	93	49	39	97	39	65	47	31	69
8	N/A	N/A	N/A	N/A	N/A	N/A	77	29	N/A	73	25	N/A	39	N/A	N/A

Bent 4 surface resistivity (SR) data

Location	UFA				FA				SF			
	S.R.(kΩ)				S.R.(kΩ)				S.R.(kΩ)			
	11/28/11(N)	11/28/11(S)	11/28/11(E)	11/28/11(W)	11/28/11(N)	11/28/11(S)	11/28/11(E)	11/28/11(W)	11/28/11(N)	11/28/11(S)	11/28/11(E)	11/28/11(W)
0	NA	NA	NA	NA	NA	NA	NA	NA	NA	NA	NA	NA
1	336	369	388	NA	120	141	151	NA	267	242		259
2	328	366	416	350	120	139	153	135	238	257	247	270
3	302	378	369	392	123	111	148	142	220	227	320	273
4	326	367	382	387	124	130	159	107	212	218	257	294
5	389	312	359	332	117	127	144	135	215	232	239	290
6	426	370	445	435	142	131	153	115	228	255	227	248
7	385 NA	328* NA	411 NA	357 NA	129 NA	145 127	138 NA	NA NA	195 NA	182 NA	205 NA	272 NA

Bent 4 surface resistivity (SR) data

Location	BFS				MET			
	S.R.(kΩ)				S.R.(kΩ)			
	11/28/11(N)	11/28/11(S)	11/28/11(E)	11/28/11(W)	11/28/11(N)	11/28/11(S)	11/28/11(E)	11/28/11(W)
0	NA	NA	NA	NA	NA	NA	NA	NA
1	339	324	NA	412	272	152	NA	260
2	352	330	423	432	302	202	NA	286
3	354	294	399	405	262	162	185	218
4	338	273	369	422	282	NA	232	252
5	350	266	301	430	223	156	208	243
6	348	331	286	413	215	208	202	251
7	327	302	255	364	178	NA	224	211

Bent 5 electrical potential data

Location	UFA			FA			SF			BFS			MET		
	Potential(mV)			Potential(mV)			Potential(mV)			Potential(mV)			Potential(mV)		
	5/8/07	6/26/07	6/29/08	5/8/07	6/26/07	6/29/08	5/8/07	6/26/07	6/29/08	5/8/07	6/26/07	6/29/08	5/8/07	6/26/07	6/29/08
0	-251	-236	-353	-305	-310	-139	-242	-287	-104	-307	-269	-175	-431	-419	-250
1	-66	-93	-76	-142	-192	-81	-161	-178	-75	-222	-184	-114	-345	-341	-183
2	-63	-71	-26	-117	-184	-97	-143	-178	-80	-163	-170	-95	-310	-291	-174
3	-41	-78	-43	-125	-195	-108	-133	-178	-94	-175	-165	-98	-292	-292	-154
4	-51	-81	-45	-135	-214	-124	-132	-186	-98	-223	-214	-115	-279	-292	-167
5	-126	-182	-88	-159	-248	-132	-204	-260	-156	-302	-286	-171	-321	-359	-225
6	-287	-331	-268	-258	-350	-249	-252	-367	-235	-410	-394	-216	-417	-444	-351
7	-398	-410	-395	-395	-420	-346	-453	-534	-402	-584	-553	-404	-576	-538	-460
8	-535	N/A	N/A	-499	N/A	N/A	N/A	N/A	N/A	N/A	N/A	N/A	N/A	N/A	N/A
in water	-543	-519	-495	-515	-499	-407	-561	-560	-502	-632	-625	-577	-643	-626	-599

Bent 5 electrical potential data

Location	UFA					FA				
	Potential(mV)					Potential(mV)				
	9/6/11	4/2/12 (N)	4/2/12(S)	4/2/12(E)	4/2/12(W)	9/6/11	4/2/12 (N)	4/2/12(S)	4/2/12(E)	4/2/12(W)
0	NA	NA	NA	NA	NA	NA	NA	NA	NA	NA
1	-113	-160	-102	-80	-50	-119	-101	-74	-41	-99
2	-73	-133	-98	-63	-42	-111	-48	-84	-62	-70
3	-66	-63	-110	-60	-44	-117	-82	-112	-102	-86
4	-130	-80	-155	-82	-120	-111	-156	-125	-116	-180
5	-233	-92	-238	-190	-223	-248	-266	-198	-181	-262
6	-378	-185	-270	-249	-230	-289	-260	-308	-276	-294
7	NA	-324	-345	-297	-382	NM	-300	-360	-305	-342
in water	-475	-464				-390	-389			

Bent 5 electrical potential data

Location	SF					BFS				
	Potential(mV)					Potential(mV)				
	9/6/11	4/2/12 (N)	4/2/12(S)	4/2/12(E)	4/2/12(W)	9/6/11	4/2/12 (N)	4/2/12(S)	4/2/12(E)	4/2/12(W)
0	NA	NA	NA	NA	NA	NA	NA	NA	NA	NA
1	-72	-51	-62	-70	-77	-115	-212	-70	-71	-70

2	-72	-45	-44	-56	-59	-111	-365	-60	-79	-61
3	-79	-60	-56	-114	-132	-112	-360	-66	-102	-80
4	-114	-75	-139	-134	-141	-131	-280	-108	-152	-120
5	-187	-170	-219	-227	-175	-179	-267	-188	-182	-230
6	-267	-250	-272	-241	-285	-313	-282	-261	-232	-249
7	NA	-345	-283	-300	-338	NA	-314	-320	-332	-350
in water	-469	-450				-467	-445			

Bent 5 electrical potential data

Location	MET				
	Potential(mV)				
	9/6/11	4/2/12 (N)	4/2/12(S)	4/2/12(E)	4/2/12(W)
0	NA	NA	NA	NA	NA
1	-143	-120	-112	-95	-74
2	-147	-108	-110	-83	-81
3	-144	-125	-90	-90	-97
4	-177	-133	-90	-113	-136
5	-269	-237	-132	-230	-247
6	-404	-294	-214	-285	-293
7	NA	-372	-245	-335	-351
in water	-517	-485			

Bent 5 surface resistivity (SR) data

Location	UFA			FA			SF			BFS			MET		
	S.R.(kΩ)			S.R.(kΩ)			S.R.(kΩ)			S.R.(kΩ)			S.R.(kΩ)		
	5/8/07	6/26/07	6/29/08	5/8/07	6/26/07	6/29/08	5/8/07	6/26/07	6/29/08	5/8/07	6/26/07	6/29/08	5/8/07	6/26/07	6/29/08
0	104	-168	141	34	36	N/A	73	83	N/A	76	75	140	35	42	N/A
1	202	226	160	39	50	152	52	75	220	77	102	165	41	42	153
2	175	154	190	44	55	150	68	75	221	90	83	163	40	47	140
3	204	170	197	36	35	150.6	79	72	219	75	82	161	35	42	156
4	191	168	207	47	38	50.2	65	60	219	79	64	160	35	42	152
5	201	180	208	47	44	49.7	65	69	221	69	94	160	36	52	147
6	184	148	212	50	29	14	77	77	215	83	92	141	41	48	145
7	175	168	211	46	44	104	69	51	87	51	60	N/A	37	44	132
8	17	N/A	164	24	N/A	N/A	N/A	N/A	N/A	N/A	N/A	N/A	N/A	N/A	N/A

Bent 5 surface resistivity (SR) data

Location	UFA				FA				SF			
	S.R.(kΩ)				S.R.(kΩ)				S.R.(kΩ)			
	11/28/11(N)	11/28/11(S)	11/28/11(E)	11/28/11(W)	11/28/11(N)	11/28/11(S)	11/28/11(E)	11/28/11(W)	11/28/11(N)	11/28/11(S)	11/28/11(E)	11/28/11(W)
0	NA	NA	NA	NA	NA	NA	NA	NA	NA	NA	NA	NA
1	369	428	513	418	110	117	155	115	217	208	219	220
2	308	435	519	356	145	119	122	105	227	243	234	210
3	382	446	491	389	117	118	154	133	228	202	240	271
4	309	429	500	387	112	116	130	131	210	239	246	257
5	308	368	454	369	119	105	132	108	263	197	208	256
6	402	431	454	489	119	123	150	122	228	245	207	259
7	377	341	428	338	117	122	133	104	248	181	211	230

Bent 5 surface resistivity (SR) data

Location	BFS				MET			
	S.R.(kΩ)				S.R.(kΩ)			
	11/28/11(N)	11/28/11(S)	11/28/11(E)	11/28/11(W)	11/28/11(N)	11/28/11(S)	11/28/11(E)	11/28/11(W)
0	NA	NA	NA	NA	NA	NA	NA	NA
1	303	268	252	351	229	251	297	350
2	340	277	260	397	289	161	318	272
3	325	260	285	400	303	NA	222	308
4	338	259	283	365	308	201	291	245
5	289	238	287	380	235	161	292	248
6	313	267	281	432	275	189	290	270
7	277	222	205	382	183	137	212	225

Corrosion Data – Bent 3

Tables below are the corrosion data collected from the embedded corrosion electrodes in the bent 3 and 4 piles. The subscript 1 and 2 indicate the top pair of corrosion electrodes in layer 1 and lower pair of corrosion electrodes in layer 2. For example, potential reading S_1-R means the surface external potential of top steel electrode in layer 1 or electrical resistance reading S_2–T_2 means the electrical resistance between steel and titanium electrodes in layer 2. Multimeter polarity for each reading us also included. S(+)R(-) means the steel electrode needs to be connected to the positive terminal of the multimeter and external reference electrode needs to be connected to negative terminal of the multimeter. Pile mixtures can be determined from bridge foundation plan (Figure 11). External reference electrode contact locations are described in the corrosion monitoring section.

Electrical potential data (mV) (T– titanium, S – steel, R – Reference Electrode)

Pile Mixture	S_1 - R				S_2 - R			
	5/16/07	6/26/07	6/29/08	4/2/2012	5/16/07	6/26/07	6/29/08	4/2/2012
UFA	-64	-35	-59	-67	-184	-226	-129	-102
FA	-101	-143	-42	46	-96	-196	-140	-70
SF	-72	-137	-30	-58	-203	-208	-131	-119
META	-110	-129	-11	50	-122	-165	-90	12
BFS	-473	-555	-65	-38	-688	-755	-203	-100
Multimeter polarity	S(+) R(-)							

Electrical potential data (mV)

Pile Mixture	S_1 - T_1					S_2 - T_2				
	5/16/07	6/26/07	6/29/08	9/7/2011	4/2/2012	5/16/07	6/26/07	6/29/08	9/7/2012	4/2/2012
UFA	-21	-13	-17	-46	-12	-26.1	-34	-30	-14	-12
FA	-17.8	35.9	-21	-17	-33	-1.4	3.7	-2	-24	-33
SF	-67.8	28	-19	-33	-25	-223.4	213	-30	27	-25
META	-83	-64	-62	NA	38	-101	-4	-20	NA	38
BFS	-170	-173	-203	-15	-12	-99.8	-100	-19	-45	-12
Multimeter polarity	T(+) R(-)									

Electrical potential data (mV)

Pile Mixture	T_1 - R				T_2 - R			
	5/16/07	6/26/07	6/29/08	4/2/2012	5/16/07	6/26/07	6/29/08	4/2/2012
UFA	-45	-29	-34	-57	-185	-171	-98	-85
FA	-83	-107	-15	-4	-88	-188	-123	-90
SF	-134	-163	-11	-24	-380	-421	-162	-130
META	-27	-67	-56	40	-227	-162	-68	0
BFS	-314	-387	-37	--53	-587	-660	-223	-117
Multimeter polarity	S(+) T(-)							

Electrical potential data (mV) with reference electrode in water

Pile Mixture	S_1 - R				S_2 - R				T_1 - R				T_2 - R			
	5/16/07	6/26/07	6/29/08	4/2/2012	5/16/07	6/26/07	6/29/08	4/2/2012	5/16/07	6/26/07	6/29/08	4/2/2012	5/16/07	6/26/07	6/29/08	4/2/2012
UFA	-352	-358	-316	-234	-258	-320	-265	-182	-330	-343	-298	-22	-228	-265	-236	-158
FA	-314	-351	-232	-554	-227	-247	-183	-89	-298	-306	-211	-135	-228	-256	-181	-114
SF	-445	-507	-433	-346	-311	-413	-334	-249	-514	-536	-416	-315	-534	-625	-365	-260
META	-431	-448	-312	-205	-300	-355	-236	-139	-349	-382	-249	-166	-401	-346	-215	-126
BFS	-908	-982	-456	-261	-784	-901	-390	-230	-740	-810	-420	-273	-684	-801	-409	-219
Multimeter polarity	S(+) R(-)								S(+) T(-)							

Electrical current data (μA) (S-Steel)

Pile Mixture	S_1 - S_2			
	5/16/07	6/25/07	6/29/08	4/2/2012
UFA	2.7	0.5	4.8	0.3
FA	10.1	2	5	2.4
SF	11.5	0.9	0.6	1.0
META	14.7	6	1.5	0.6
BFS	10.3	1.1	-0.7	0.1
Multimeter polarity	S_1(+) S_2(-)			

Electrical resistance data (kΩ) (S – Steel, T – Titanium)

Pile Mixture	S_1 - S_2				S_1 - T_1				S_2 - T_2			
	5/16/07	6/26/07	6/29/08	4/2/2012	5/16/07	6/26/07	6/29/08	4/2/2012	5/16/07	6/26/07	6/29/08	4/2/2012
UFA	16	14	18	28	15	13	16	26	14.5	13	17	25
FA	4.8	4.5	5.9	100	3.8	3.6	4.7	25	4.2	3.9	5.2	26
SF	7.2	7.3	11	45	6.2	6.3	9.9	25	6.3	6.5	9.5	50
META	3.7	4.95	10	144	3.35	4.6	9	26	3.2	4.2	7	22
BFS	9.3	10.35	19	189	7.8	8.6	15	105	7.4	8.25	15	67

Corrosion Data – Bent 4

Electrical potential data (mV) (T– titanium, S – steel, R – Reference Electrode) (a)

Pile Mixture	S_1 - R				S_2 - R			
	5/16/07	6/26/07	6/29/08	4/2/2012	5/16/07	6/26/07	6/29/08	4/2/2012
UFA	-125	-100	-68	-126	-269	-229	-154	-94
FA	-163	-118	-48	-13	-126	-211	-185	110
SF	-115	-95	-18	39	-162	-198	-82	60
META	N/A	-123	-19	225	N/A	-156	-23	-65
BFS	-458	-491	-24	-24	-764	-787	-167	-116
Multimeter polarity	S(+) R(-)							

Electrical potential data (mV) (b)

Pile Mixture	S_1 - T_1					S_2 - T_2				
	5/16/07	6/26/07	6/29/08	9/7/2011	4/2/2012	5/16/07	6/26/07	6/29/08	9/7/2011	4/2/2012
UFA	-38	-24	-18	-11	-64	-98	17	31	-13	-64
FA	3.3	-2	-17	-30	-20	-12.7	-39	-32	-1	-20
SF	-40.2	-42	-43	-51	26	-64.8	-67	-42	-13	26
META	N/A	-41	-40	-11	0	N/A	2	-40	3	0
BFS	31.6	17	-4	NA	22	76	81	78	NA	22
Multimeter polarity	S(+) T(-)									

Electrical potential data (mV) (c)

Pile Mixture	T_1 - R				T_2 - R			
	5/16/07	6/26/07	6/29/08	4/2/2012	5/16/07	6/26/07	6/29/08	4/2/2012
UFA	-89	-77	-52	-94	-171	-248	-184	-84
FA	-165	-124	-36	-2	-121	-172	-138	-95
SF	-82	-59	-85	63	-84	-174	-10	62
META	N/A	-42	20	250	N/A	-184	-138	-141
BFS	-463	-573	-32	-7	-854	-878	-251	-111
Multimeter polarity	T(+) R(-)							

Electrical potential data (mV) with reference electrode in water

Pile Mixture	S_1 - R				S_2 - R				T_1 - R				T_2 - R			
	5/16/07	6/26/07	6/29/08	4/2/2012	5/16/07	6/26/07	6/29/08	4/2/2012	5/16/07	6/26/07	6/29/08	4/2/2012	5/16/07	6/26/07	6/29/08	4/2/2012
UFA	-523	-469	-361	-214	-479	-382	-289	-139	-490	-445	-343	-183	-382	-399	-319	-127
FA	-452	-410	-295	-184	-344	-361	-262	-142	-461	-404	-278	-160	-333	-318	-230	-128
SF	-477	-174	-351	-196	-439	-131	-292	-159	-444	-143	-250	-170	-376	-71	-305	-128
META	N/A	-400	-301	-127	N/A	-147	-272	-120	N/A	-192	-260	-131	N/A	-303	-229	-175
BFS	-899	-750	-436	-330	-920	-956	-416	-296	-871	-895	-432	-316	-997	-1034	-494	-290
Multimeter polarity	S(+) R(-)								T(+) R(-)							

Electrical current data (μA) (S-Steel)

Pile Mixture	S_1 - S_2			
	5/16/07	6/26/07	6/29/08	4/2/2012
UFA	3.5	1	5.5	0.8
FA	26.4	1.8	5.2	1
SF	12.1	-7.1	5.8	0.7
META	N/A	-2.4	6.2	0.8
BFS	5.4	8.2	5.2	0.1
Multimeter polarity	S_1(+) S_2(-)			

Electrical resistance data (kΩ) (S – Steel, T – Titanium)

Pile Mixture	S_1 - S_2				S_1 - T_1				S_2 - T_2			
	5/16/07	6/26/07	6/29/08	4/2/2012	5/16/07	6/26/07	6/29/08	4/2/2012	5/16/07	6/26/07	6/29/08	4/2/2012
UFA	16	14	17	20	14	12	15	20	15	12	15	26
FA	4.6	4.35	5	13	4.2	2.8	4	11	3.8	3.5	4	11
SF	7.4	8.1	11.5	20	6.8	6.8	10	28	6.1	6	9	14
META	N/A	4.4	8	22	N/A	3.35	6	17	N/A	4	7	21
BFS	11	10.9	23	124	8.7	9.25	18	100	8	8.6	16	64

Appendix F–Durability Segment Corrosion Data

Tables below are the corrosion data collected from the embedded corrosion electrodes in the durability segments. The subscript 1, 2 and 3 indicate the top, middle and lower pair of corrosion electrodes (). Durability segments and bridge piles used same table as template for collecting corrosion data. Durability segment corrosion data is similar to bridge pile data. Each durability segments contains three sets of corrosion electrodes instead of two in bridge piles.

Electrical potential data (mV) (T – titanium, S – steel, R – Reference Electrode)

Pile Mixture	S_1 - R				S_2 - R				S_3 - R			
	5/7/07	6/25/07	6/29/08	4/2/2012	5/7/07	6/25/07	6/29/08	4/2/2012	5/7/07	6/25/07	6/29/08	4/2/2012
CEM	-15	-172	-125	-130	-71	-205	-114	-247	-80	-210	-263	-220
UFA	17	-171	-188	-49	-67	-174	-182	-78	-47	-196	-161	-138
FA	-22	-220	-238	-140	-82	-228	-259	-165	-121	-251	-197	-82
SF	3	-152	-148	-178	-58	-213	-132	-308	-101	-132	-302	-336
META	-10	-154	-169	-139	-143	-163	-175	-190	-120	-182	-188	-239
BFS	-54	-127	-135	-32	-153	-147	-17	-135	-90	-120	-152	-169
Multimeter polarity	S(+) R(-)											

Electrical potential data (mV)

Pile Mixture	T_1 - R				T_2 - R				T_3 - R			
	5/7/07	6/25/07	6/29/08	4/2/2012	5/7/07	6/25/07	6/29/08	4/2/2012	5/7/07	6/25/07	6/29/08	4/2/2012
CEM	14	-231	-45	-154	-38	-127	-132	-250	-73	-153	-177	-190
UFA	-19	-89	-140	-50	-20	-139	-170	-76	-41	-211	-140	-92
FA	-35	-281	-128	-164	-44	-202	-173	-183	-246	-122	-112	-220
SF	11	-178	-88	-103	-55	-96	-67	-130	-40	-92	-156	-120
META	-9	-127	-120	-148	-103	-107	-128	-183	-96	-154	-133	-172
BFS	-78	-139	-115	-118	-93	-211	-196	-166	-90	-177	-195	-135
Multimeter Polarity	T(+) R(-)											

Electrical potential data (mV)

Pile	S_1 - T_1	S_2 - T_2	S_3 - T_3

Mixture	5/7/07	6/25/07	6/29/08	9/7/2011	4/2/2012	5/7/07	6/25/07	6/29/08	9/7/2011	4/2/2012	5/7/07	6/25/07	6/29/08	9/7/2011	4/2/2012
CEM	-25	56	-60	3	6	-51	-29	24	24	-3	-34	-54	-56	-9	-17
UFA	-36	-67	-28	-7	-17	-60	-27	25	6	8	-15	28	-10	-24	-7
FA	7.6	-47	-98	-59	-43	-62.9	115	-84	-45	-13	124.5	23	-82	-24	-79
SF	-5	13	-56	48	-92	-14	-84	-23	-127	-134	-56	-69	-131	-158	-156
META	-27	-24	-35	83	16	-38	-52	-41	76	15	-39	-27	-68	-64	-56
BFS	37	11	-15	32	19	0	68	219	94	49	71	58	43	55	0
Multimeter Polarity	S(+) T(-)														

Electrical potential data (mV) with reference electrode in water

Pile Mixture	S_1 - R				S_2 - R				S_3 - R			
	5/7/07	6/25/07	6/29/08	4/2/2012	5/7/07	6/25/07	6/29/08	4/2/2012	5/7/07	6/25/07	6/29/08	4/2/2012
CEM	-58	-90	-97	-291	-99	-112	-73	-292	-90	-114	-221	-262
UFA	-104	-157	-181	-124	-109	-148	-163	-105	-90	-175	-166	-168
FA	-121	-203	-227	-202	-127	-194	-251	-220	-138	-219	-187	-127
SF	-120	-176	-165	-281	-119	-197	-161	-340	-137	-118	-316	-375
META	-127	-147	-170	-215	-167	-151	-182	-182	-102	-172	-195	-190
BFS	-139	-94	-13	-132	-144	-103	-105	-162	-138	-72	-73	-137
Multimeter polarity	S(+) R(-)											

Electrical potential data (mV) with reference electrode in water

Pile Mixture	T_1 - R				T_2 - R				T_3 - R			
	5/7/07	6/25/07	6/29/08	4/2/2012	5/7/07	6/25/07	6/29/08	4/2/2012	5/7/07	6/25/07	6/29/08	4/2/2012
CEM	-31	-153	-22	-276	-33	-33	-94	-294	-66	-60	-139	-239
UFA	-67	-83	-149	-130	-63	-124	-183	-100	-74	-197	-149	-118
FA	-127	-261	-121	-234	-62	-169	-160	-223	263	-97	-100	-271
SF	-113	-215	-105	-224	-102	-100	-131	-177	-84	-116	-175	-165
META	-163	-122	-127	-215	-166	-95	-136	-203	-171	-143	-136	-259
BFS	-113	-96	-4	-90	-108	-141	-114	-151	-99	-132	-115	-172
Multimeter polarity	T(+) R(-)											

Electrical resistance data (kΩ)

Pile	S_1 - S_2	S_2 - S_3	S_1 - S_3

Mixture	5/7/07	6/25/07	6/29/08	4/2/2012	5/7/07	6/25/07	6/29/08	4/2/2012	5/7/07	6/25/07	6/29/08	4/2/2012
CEM	0.87	0.85	40	4	0.97	0.78	0.5	2	0.89	0.73	1.8	14
UFA	11	9.55	10	7	10	9.4	10	10	11	9.85	11	6
FA	3.8	3.35	4.4	0.013	3.9	3.5	4.3	1.2	3.9	3.4	4.4	1
SF	7.95	7.65	11	16	8.2	7.9	11	15	8.8	8.1	11	23
META	2.75	3.35	2	32	2.8	3.3	1	2.3	2.85	3.4	1	155
BFS	6.95	7.6	12.5	85	7	7.5	12	95	7.2	7.7	12	86

Electrical resistance data (kΩ)

Pile Mixture	S_1 - T_1				S_2 - T_2				S_3 - T_3			
	5/7/07	6/25/07	6/29/08	4/2/2012	5/7/07	6/25/07	6/29/08	4/2/2012	5/7/07	6/25/07	6/29/08	4/2/2012
CEM	0.78	0.7	6.2	10	0.83	0.74	0.5	2	0.82	0.69	0.4	2
UFA	11	9.4	10	13	10.9	10	11	110	10.6	9.8	11	10
FA	3.2	2.6	3.7	4	3.5	3.25	3.9	1	3.2	2.7	3.6	2
SF	7.35	6.8	9	14	6.3	6.25	7	10	8	7.55	8	5
META	2.4	3	0.5	26	2.5	3.2	6.2	4	2.7	3.1	6.2	4.5
BFS	6.15	6.6	10	27	6.3	7	12	113	6.15	6.4	10	16

Electrical Current data (μA)

Pile Mixture	S_1 - S_2				S_2 - S_3				S_1 - S_3			
	5/7/07	6/25/07	6/29/08	4/2/2012	5/7/07	6/25/07	6/29/08	4/2/2012	5/7/07	6/25/07	6/29/08	4/2/2012
CEM	8.8	-12.1	4.7	1.3	8.3	15.7	14.2	4	8.3	5.3	6.6	4
UFA	0.8	-0.6	-0.9	0.5	-1.3	1.2	0.2	1	-0.5	0.2	-0.6	-2.4
FA	0.2	-2	2.7	0	0.8	9	5.6	26	0.7	-2.7	2.5	14
SF	0	4.5	0.1	2	2.4	6.8	5.8	3.5	1.5	6.7	4.2	1.8
META	1.6	2.2	0.8	2	-1.6	3.3	1.8	4.5	-0.2	5.2	2.1	6.6
BFS	5	-1.8	12.9	0	7.1	2.6	8	0.7	2.8	-1.5	2.8	
Multimeter Polarity	S_1(+) S_2(-)				S_2(+) S_3(-)				S_1(+) S_3(-)			

Appendix G–Chloride Profile Data

Slice number	Depth at center of slice (in.)
1	0.125
2	0.375
3	0.625
4	0.875
5	1.125
6	1.375

		Results (lb/yd^3)				Average	
		A	**B**	**C**	**Range**	**ppm**	**lb/yd^3**
FP1A	1	31.194			0.0000	8208.9	31.194
	2	21.075	20.771	20.877	0.3040	5502.0	20.908
	3	12.456	12.202	12.061	0.3950	3221.0	12.240
	4	10.750	10.450	10.108	0.6420	2746.3	10.436
	5	7.585	7.190	7.402	0.3950	1945.4	7.392
	6	3.344	3.310	3.382	0.0720	880.4	3.345
	7	1.737	1.733	1.744	0.0110	457.4	1.738
	Co	0.217	0.209	0.224	0.0150	57.0	0.217
FP1B	1	24.932			0.0000	6561.1	24.932
	2	18.510	18.734	18.856	0.3460	4921.1	18.700
	3	11.757	11.913	11.237	0.6760	3062.0	11.636
	4	5.582	5.624	5.681	0.0990	1481.3	5.629
	5	3.439	3.481	3.488	0.0490	913.0	3.469
	6	1.201	1.227	1.212	0.0260	319.3	1.213
	7	0.372	0.395	0.376	0.0230	100.3	0.381
	Co	0.061	0.046	0.038	0.0230	12.7	0.048
FP1C	1	26.463			0.0000	6963.9	26.463
	2	16.705	15.983	16.420	0.7220	4307.7	16.369
	3	14.455	14.394	14.676	0.2820	3818.0	14.508
	4	10.051	10.047	10.553	0.5060	2688.7	10.217
	5	5.316	4.849	5.335	0.4860	1359.6	5.167
	6	3.181	2.842	3.063	0.3390	797.0	3.029
	7	1.216	1.197	1.193	0.0230	316.3	1.202
	Co	0.194	0.209	0.228	0.0340	55.4	0.210
FP1D	1	32.011			0.0000	8423.9	32.011
	2	19.437	19.471	19.589	0.1520	5131.3	19.499
	3	14.436	14.676	14.178	0.4980	3797.4	14.430
	4	11.541	11.860	11.769	0.3190	3085.1	11.723
	5	7.296	7.364	7.190	0.1740	1916.7	7.283
	6	5.206	5.309	5.377	0.1710	1394.0	5.297
	7	3.181	2.884	3.279	0.3950	819.6	3.115
	Co	0.676	0.669	0.673	0.0070	177.0	0.673

		Results (lb/yd^3)				Average	
		A	**B**	**C**	**Range**	**ppm**	**lb/yd^3**
FP1E	1	14.550			0.0000	3828.9	14.550
	2	8.736	9.147	8.379	0.7680	2303.7	8.754
	3	4.442	4.655	4.655	0.2130	1206.3	4.584
	4	1.885	1.927	1.934	0.0490	504.0	1.915
	5	0.661	0.654	0.665	0.0110	173.7	0.660
	6	0.247	0.217	0.228	0.0300	60.7	0.231
	7	0.217	0.209	0.205	0.0120	55.4	0.210
	Co	0.369	0.369	0.376	0.0070	97.7	0.371
FP1F	1	11.666			0.0000	3070.0	11.666
	2	4.803	4.894	4.811	0.0910	1272.6	4.836
	3	1.132	1.132	1.129	0.0030	297.6	1.131
	4	0.350	0.353	0.357	0.0070	93.0	0.353
	5	0.217	0.209	0.209	0.0080	55.7	0.212
	6	0.243	0.198	0.243	0.0450	60.0	0.228
	7	0.220	0.186	0.217	0.0340	54.6	0.208
	Co	0.232	0.220	0.243	0.0230	61.0	0.232
FP1G	1	9.306			0.0000	2448.9	9.306
	2	3.412	3.507	3.401	0.1060	905.3	3.440
	3	0.695	0.695	0.741	0.0460	186.9	0.710
	4	0.289	0.262	0.236	0.0530	69.0	0.262
	5	0.198	0.209	0.217	0.0190	54.7	0.208
	6	0.190	0.224	0.201	0.0340	53.9	0.205
	7	0.182	0.190	0.209	0.0270	51.0	0.194
	Co	0.160	0.198	0.205	0.0450	49.4	0.188
FP1H	1	15.272			0.0000	4018.9	15.272
	2	10.382	9.857	10.089	0.5250	2660.4	10.109
	3	6.152	6.357	5.616	0.7410	1589.9	6.042
	4	3.036	2.774	3.097	0.3230	781.3	2.969
	5	0.806	0.836	0.817	0.0300	215.7	0.820
	6	0.239	0.236	0.266	0.0300	65.0	0.247
	7	0.220	0.217	0.217	0.0030	57.4	0.218
	Co	0.186	0.198	0.205	0.0190	51.7	0.196

		Results (lb/yd^3)				Average	
		A	**B**	**C**	**Range**	**ppm**	**lb/yd^3**
FP2A	1	26.691	26.691		0.0000	7023.9	26.691
	2	20.596	20.505	20.307	0.2890	5386.7	20.469
	3	2.196	2.155	2.291	0.1360	582.6	2.214
	4	0.209	0.205	0.213	0.0080	55.0	0.209
	5	0.171	0.152	0.144	0.0270	41.0	0.156
	6	0.152	0.160	0.152	0.0080	40.7	0.155
	Co	0.179	0.194	0.198	0.0190	50.1	0.190
FP2B	1	32.209	32.338		0.1290	8493.0	32.274
	2	24.666	24.856	24.860	0.1940	6524.7	24.794
	3	2.204	2.413	2.440	0.2360	619.0	2.352
	4	0.224	0.224	0.247	0.0230	61.0	0.232
	5	0.201	0.217	0.201	0.0160	54.3	0.206
	6	0.209	0.220	0.220	0.0110	56.9	0.216
	Co	0.190	0.194	0.186	0.0080	50.0	0.190
FP2C	1	29.864	29.891		0.0270	7862.5	29.878
	2	29.423	29.085	29.150	0.3380	7689.3	29.219
	3	6.255	6.034	5.985	0.2700	1603.0	6.091
	4	0.365	0.376	0.380	0.0150	98.3	0.374
	5	0.156	0.175	0.160	0.0190	43.1	0.164
	6	0.179	0.160	0.179	0.0190	45.4	0.173
	Co	0.182	0.182	0.186	0.0040	48.2	0.183
FP2D	1	22.553	22.906		0.3530	5981.4	22.730
	2	21.421	21.493	21.519	0.0980	5652.0	21.478
	3	3.059	3.203	3.165	0.1440	826.9	3.142
	4	0.239	0.213	0.255	0.0420	62.0	0.236
	5	0.198	0.171	0.209	0.0380	50.7	0.193
	6	0.163	0.148	0.141	0.0220	39.6	0.151
	Co	0.258	0.262	0.270	0.0120	69.3	0.263

		Results (lb/yd^3)				Average	
		A	**B**	**C**	**Range**	**ppm**	**lb/yd^3**
FP2E	1	19.779	19.935		0.1560	5225.5	19.857
	2	14.113	13.988	14.125	0.1370	3704.0	14.075
	3	2.561	2.455	2.466	0.1060	656.3	2.494
	4	0.304	0.331	0.315	0.0270	83.3	0.317
	5	0.194	0.190	0.194	0.0040	50.7	0.193
	6	0.224	0.228	0.224	0.0040	59.3	0.225
	Co	0.281	0.266	0.285	0.0190	73.0	0.277
FP2F	1	6.376	6.255		0.1210	1662.0	6.316
	2	2.569	2.569	2.569	0.0000	676.1	2.569
	3	0.566	0.524	0.551	0.0420	143.9	0.547
	4	0.213	0.209	0.228	0.0190	57.0	0.217
	5	0.171	0.171	0.171	0.0000	45.0	0.171
	6	0.163	0.171	0.160	0.0110	43.3	0.165
	Co	0.167	0.179	0.167	0.0120	45.0	0.171
FP2G	1	5.761	5.719		0.0420	1510.5	5.740
	2	3.310	3.165	3.059	0.2510	836.3	3.178
	3	1.212	1.205	1.193	0.0190	316.7	1.203
	4	0.384	0.384	0.372	0.0120	100.0	0.380
	5	0.160	0.160	0.163	0.0030	42.4	0.161
	6	0.160	0.160	0.182	0.0220	44.0	0.167
	Co	0.182	0.198	0.190	0.0160	50.0	0.190
FP2H	1	16.610	16.564		0.0460	4365.0	16.587
	2	11.123	11.073	11.419	0.3460	2948.7	11.205
	3	0.790	0.787	0.806	0.0190	209.0	0.794
	4	0.198	0.179	0.213	0.0340	51.8	0.197
	5	0.152	0.190	0.160	0.0380	44.0	0.167
	6	0.201	0.179	0.175	0.0260	48.7	0.185
	Co	0.160	0.163	0.160	0.0030	42.4	0.161

		Results (lb/yd^3)				Average	
		A	**B**	**C**	**Range**	**ppm**	**lb/yd^3**
FP3A	1	29.667	29.545		0.1220	7791.1	29.606
	2	23.989	24.058	24.069	0.0800	6326.0	24.039
	3	9.371	9.679	9.310	0.3690	2487.7	9.453
	4	1.790	1.759	1.794	0.0350	468.7	1.781
	5	0.228	0.190	0.213	0.0380	55.4	0.210
	6	0.194	0.171	0.148	0.0460	45.0	0.171
	Co	0.179	0.163	0.182	0.0190	46.0	0.175
FP3B	1	25.289			0.0000	6655.0	25.289
	2	20.748	20.680	20.330	0.4180	5417.4	20.586
	3	10.180	10.446	10.157	0.2890	2700.3	10.261
	4	1.843	1.858	1.828	0.0300	485.0	1.843
	5	0.711	0.695	0.699	0.0160	184.6	0.702
	6	0.217	0.205	0.163	0.0540	51.3	0.195
	Co	0.186	0.205	0.186	0.0190	50.6	0.192
FP3C	1	24.312			0.0000	6397.9	24.312
	2	19.847	19.551	19.551	0.2960	5171.0	19.650
	3	6.768	6.874	6.874	0.1060	1799.6	6.839
	4	0.756	0.775	0.182	0.5930	150.3	0.571
	5	0.175	0.186	0.182	0.0110	47.6	0.181
	6	0.186	0.163	0.179	0.0230	46.3	0.176
	Co	0.190	0.198	0.205	0.0150	52.0	0.198
FP3D	1	31.544			0.0000	8301.1	31.544
	2	24.286	24.411	24.339	0.1250	6406.7	24.345
	3	11.001	10.860	10.435	0.5660	2833.0	10.765
	4	1.585	1.571	1.600	0.0290	417.2	1.585
	5	0.213	0.217	0.198	0.0190	55.1	0.209
	6	0.418	0.141	0.156	0.2770	62.7	0.238
	Co	0.220	0.209	0.213	0.0110	56.3	0.214

		Results (lb/yd^3)				Average	
		A	**B**	**C**	**Range**	**ppm**	**lb/yd^3**
FP3E	1	14.444			0.0000	3801.1	14.444
	2	12.430	12.757	12.779	0.3490	3330.4	12.655
	3	3.808	3.967	3.872	0.1590	1021.7	3.882
	4	0.897	0.904	0.889	0.0150	236.0	0.897
	5	0.281	0.270	0.258	0.0230	71.0	0.270
	6	0.179	0.171	0.175	0.0080	46.1	0.175
	Co	0.167	0.156	0.152	0.0150	41.7	0.158
FP3F	1	6.281			0.0000	1652.9	6.281
	2	4.784	5.145	5.434	0.6500	1347.6	5.121
	3	0.844	0.813	0.825	0.0310	217.7	0.827
	4	0.433	0.456	0.426	0.0300	115.4	0.438
	5	0.175	0.179	0.171	0.0080	46.1	0.175
	6	0.182	0.198	0.186	0.0160	49.6	0.189
	Co	0.160	0.163	0.182	0.0220	44.3	0.168
FP3G	1	8.204			0.0000	2158.9	8.204
	2	5.586	5.559	5.567	0.0270	1466.0	5.571
	3	0.597	0.627	0.604	0.0300	160.4	0.609
	4	0.220	0.205	0.220	0.0150	56.6	0.215
	5	0.171	0.201	0.171	0.0300	47.6	0.181
	6	0.182	0.171	0.163	0.0190	45.3	0.172
	Co	0.182	0.182	0.198	0.0160	49.3	0.187
FP3H	1	13.821			0.0000	3637.1	13.821
	2	12.795	12.608	12.814	0.2060	3352.4	12.739
	3	3.013	2.922	3.086	0.1640	791.3	3.007
	4	0.255	0.232	0.247	0.0230	64.4	0.245
	5	0.148	0.137	0.129	0.0190	36.3	0.138
	6	0.156	0.141	0.171	0.0300	41.1	0.156
	Co	0.163	0.179	0.179	0.0160	45.7	0.174

		Results (lb/yd^3)				Average	
		A	**B**	**C**	**Range**	**ppm**	**lb/yd^3**
FP4A	1	23.366	23.446		0.0800	6159.5	23.406
	2	16.724	16.830	17.514	0.7900	4479.6	17.023
	3	9.777	9.732	9.743	0.0450	2566.0	9.751
	4	0.627	0.600	0.604	0.0270	160.6	0.610
	5	0.369	0.334	0.323	0.0460	90.0	0.342
	6	0.467	0.452	0.445	0.0220	119.6	0.455
	Co	0.414	0.437	0.445	0.0310	113.7	0.432
FP4B	1	29.306	28.743		0.5630	7638.0	29.025
	2	17.218	17.438	17.708	0.4900	4593.3	17.455
	3	3.070	3.158	3.055	0.1030	814.3	3.094
	4	0.395	0.403	0.395	0.0080	104.6	0.398
	5	0.452	0.471	0.467	0.0190	121.9	0.463
	6	0.437	0.418	0.437	0.0190	113.3	0.431
	Co	0.490	0.498	0.494	0.0080	130.0	0.494
FP4C	1	26.281	25.943		0.3380	6871.6	26.112
	2	23.226	23.203	23.036	0.1900	6093.4	23.155
	3	4.108	4.112	4.020	0.0920	1073.7	4.080
	4	0.680	0.661	0.684	0.0230	177.6	0.675
	5	0.437	0.410	0.429	0.0270	111.9	0.425
	6	0.369	0.384	0.410	0.0410	102.0	0.388
	Co	0.426	0.452	0.426	0.0260	114.4	0.435
FP4D	1	19.916	19.980		0.0640	5249.5	19.948
	2	18.278	18.153	18.175	0.1250	4790.0	18.202
	3	12.130	12.141	11.962	0.1790	3178.3	12.078
	4	2.314	2.451	2.428	0.1370	631.0	2.398
	5	0.399	0.414	0.395	0.0190	106.0	0.403
	6	0.437	0.437	0.433	0.0040	114.6	0.436
	Co	0.418	0.433	0.418	0.0150	111.3	0.423

		Results (lb/yd^3)				Average	
		A	**B**	**C**	**Range**	**ppm**	**lb/yd^3**
FP4E	1	10.792	10.792		0.0000	2840.0	10.792
	2	7.535	7.452	8.143	0.6910	2028.9	7.710
	3	0.954	0.950	0.939	0.0150	249.4	0.948
	4	0.422	0.407	0.433	0.0260	110.7	0.421
	5	0.369	0.353	0.369	0.0160	95.7	0.364
	6	0.414	0.429	0.479	0.0650	116.0	0.441
	Co	0.414	0.429	0.426	0.0150	111.3	0.423
FP4F	1	7.718	7.592		0.1260	2014.5	7.655
	2	4.507	4.389	4.621	0.2320	1185.7	4.506
	3	0.977	0.977	0.980	0.0030	257.4	0.978
	4	0.517	0.467	0.513	0.0500	131.3	0.499
	5	0.407	0.433	0.429	0.0260	111.3	0.423
	6	0.437	0.429	0.410	0.0270	111.9	0.425
	Co	0.441	0.441	0.452	0.0110	117.0	0.445
FP4G	1	7.087	6.962		0.1250	1848.6	7.025
	2	4.959	4.233	4.712	0.7260	1219.6	4.635
	3	0.935	0.946	0.969	0.0340	250.0	0.950
	4	0.407	0.407	0.418	0.0110	108.1	0.411
	5	0.445	0.452	0.479	0.0340	120.7	0.459
	6	0.384	0.380	0.388	0.0080	101.1	0.384
	Co	0.376	0.407	0.369	0.0380	101.1	0.384
FP4H	1	10.268	10.629		0.3610	2749.6	10.449
	2	8.569	8.531	8.656	0.1250	2259.3	8.585
	3	1.387	1.383	1.376	0.0110	363.7	1.382
	4	0.562	0.593	0.566	0.0310	151.0	0.574
	5	0.445	0.471	0.448	0.0260	119.6	0.455
	6	0.452	0.452	0.452	0.0000	118.9	0.452
	Co	0.467	0.524	0.464	0.0600	127.6	0.485

		Results (lb/yd^3)				Average	
		A	**B**	**C**	**Range**	**ppm**	**lb/yd^3**
FP5A	1	31.152	30.776		0.3760	8148.4	30.964
	2	14.672	14.611	14.995	0.3840	3884.0	14.759
	3	2.120	2.622	2.516	0.5020	636.7	2.419
	4	0.300	0.296	0.293	0.0070	78.0	0.296
	5	0.274	0.266	0.258	0.0160	70.0	0.266
	6	0.266	0.220	0.262	0.0460	65.6	0.249
	Co	0.304	0.308	0.304	0.0040	80.4	0.305
FP5B	1	36.013	36.309		0.2960	9516.1	36.161
	2	21.945	22.158	21.478	0.6800	5752.7	21.860
	3	2.348	2.443	2.318	0.1250	623.6	2.370
	4	0.391	0.372	0.391	0.0190	101.2	0.385
	5	0.217	0.213	0.201	0.0160	55.4	0.210
	6	0.224	0.247	0.224	0.0230	61.0	0.232
	Co	0.266	0.304	0.270	0.0380	73.7	0.280
FP5C	1	32.657	33.087		0.4300	8650.5	32.872
	2	23.419	23.587	23.537	0.1680	6188.0	23.514
	3	3.466	3.492	3.089	0.4030	881.3	3.349
	4	0.954	0.961	0.996	0.0420	255.4	0.970
	5	0.494	0.490	0.502	0.0120	130.4	0.495
	6	0.285	0.274	0.285	0.0110	74.0	0.281
	Co	0.270	0.274	0.289	0.0190	73.1	0.278
FP5D	1	25.791	25.988		0.1970	6813.0	25.890
	2	17.476	17.047	17.343	0.4290	4549.6	17.289
	3	2.698	2.421	2.462	0.2770	665.0	2.527
	4	0.293	0.312	0.285	0.0270	78.1	0.297
	5	0.312	0.312	0.327	0.0150	83.4	0.317
	6	0.285	0.277	0.289	0.0120	74.6	0.284
	Co	0.327	0.338	0.346	0.0190	88.7	0.337

		Results (lb/yd^3)				Average	
		A	**B**	**C**	**Range**	**ppm**	**lb/yd^3**
FP5E	1	20.216	19.958		0.2580	5286.1	20.087
	2	9.318	9.223	9.238	0.0950	2436.8	9.260
	3	1.835	1.759	1.680	0.1550	462.6	1.758
	4	0.315	0.304	0.319	0.0150	82.3	0.313
	5	0.281	0.262	0.270	0.0190	71.3	0.271
	6	0.262	0.277	0.274	0.0150	71.3	0.271
	Co	0.312	0.308	0.296	0.0160	80.4	0.305
FP5F	1	13.023	12.928		0.0950	3414.6	12.976
	2	5.160	4.853	4.742	0.4180	1294.3	4.918
	3	0.980	0.984	0.996	0.0160	259.6	0.987
	4	0.281	0.281	0.270	0.0110	73.0	0.277
	5	0.228	0.258	0.247	0.0300	64.3	0.244
	6	0.266	0.266	0.247	0.0190	68.3	0.260
	Co	0.285	0.289	0.277	0.0120	74.6	0.284
FP5G	1	13.881	14.288		0.4070	3706.4	14.085
	2	7.334	7.676	7.706	0.3720	1992.6	7.572
	3	2.371	2.489	2.535	0.1640	648.7	2.465
	4	1.129	1.129	1.136	0.0070	297.7	1.131
	5	0.893	0.893	0.893	0.0000	235.0	0.893
	6	0.289	0.270	0.270	0.0190	72.7	0.276
	Co	0.293	0.319	0.308	0.0260	80.7	0.307
FP5H	1	18.745	18.954		0.2090	4960.4	18.850
	2	11.461	11.544	11.484	0.0830	3025.4	11.496
	3	1.961	1.976	1.953	0.0230	516.7	1.963
	4	1.140	1.155	1.125	0.0300	300.0	1.140
	5	0.464	0.456	0.452	0.0120	120.4	0.457
	6	0.289	0.312	0.296	0.0230	78.7	0.299
	Co	0.285	0.315	0.300	0.0300	78.9	0.300

		Results (lb/yd^3)				Average	
		A	**B**	**C**	**Range**	**ppm**	**lb/yd^3**
FP6A	1	21.660			0.0000	5700.0	21.660
	2	22.443	22.561	22.466	0.1180	5918.4	22.490
	3	10.974	10.712	10.287	0.6870	2804.6	10.658
	4	3.576	2.907	3.116	0.6690	842.0	3.200
	5	0.421	0.414	0.433	0.0190	111.2	0.423
	6	0.198	0.160	0.217	0.0570	50.4	0.192
	Co	0.182	0.175	0.182	0.0070	47.3	0.180
FP6B	1	21.987			0.0000	5786.1	21.987
	2	20.144	20.193	20.045	0.1480	5296.7	20.127
	3	9.397	9.363	9.318	0.0790	2463.0	9.359
	4	1.653	1.653	1.649	0.0040	434.6	1.652
	5	0.209	0.213	0.209	0.0040	55.4	0.210
	6	0.175	0.163	0.171	0.0120	44.6	0.170
	Co	0.179	0.190	0.175	0.0150	47.7	0.181
FP6C	1	14.991			0.0000	3945.0	14.991
	2	23.864	23.454	23.313	0.5510	6195.7	23.544
	3	7.828	8.280	7.927	0.4520	2108.3	8.012
	4	1.186	1.193	1.186	0.0070	312.7	1.188
	5	0.194	0.205	0.190	0.0150	51.7	0.196
	6	0.194	0.182	0.205	0.0230	51.0	0.194
	Co	0.175	0.182	0.167	0.0150	46.0	0.175
FP6D	1	22.032			0.0000	5797.9	22.032
	2	23.651	24.107	23.727	0.4560	6270.6	23.828
	3	8.903	8.459	8.523	0.4440	2270.6	8.628
	4	1.991	2.052	1.984	0.0680	528.7	2.009
	5	0.243	0.224	0.239	0.0190	61.9	0.235
	6	0.201	0.182	0.167	0.0340	48.2	0.183
	Co	0.220	0.213	0.228	0.0150	58.0	0.220

		Results (lb/yd^3)				Average	
		A	**B**	**C**	**Range**	**ppm**	**lb/yd^3**
FP6E	1	5.233			0.0000	1377.1	5.233
	2	5.388	5.476	5.578	0.1900	1442.3	5.481
	3	2.592	2.519	2.535	0.0730	670.7	2.549
	4	0.372	0.388	0.380	0.0160	100.0	0.380
	5	0.167	0.175	0.209	0.0420	48.3	0.184
	6	0.160	0.160	0.175	0.0150	43.4	0.165
	Co	0.160	0.171	0.160	0.0110	43.1	0.164
FP6F	1	4.210			0.0000	1107.9	4.210
	2	4.951	5.388	5.107	0.4370	1354.9	5.149
	3	21.022	1.930	2.227	19.0920	2208.7	8.393
	4	0.308	0.285	0.258	0.0500	74.6	0.284
	5	0.171	0.163	0.152	0.0190	42.6	0.162
	6	0.163	0.163	0.182	0.0190	44.6	0.169
	Co	0.198	0.217	0.213	0.0190	55.1	0.209
FP6G	1	7.387			0.0000	1943.9	7.387
	2	6.395	6.186	6.639	0.4530	1686.0	6.407
	3	3.827	3.724	4.131	0.4070	1024.7	3.894
	4	0.836	0.840	0.832	0.0080	220.0	0.836
	5	0.239	0.236	0.224	0.0150	61.3	0.233
	6	0.186	0.201	0.186	0.0150	50.3	0.191
	Co	0.236	0.224	0.220	0.0160	59.6	0.227
FP6H	1	7.681			0.0000	2021.3	7.681
	2	7.285	6.984	6.912	0.3730	1858.0	7.060
	3	3.363	3.211	3.504	0.2930	884.0	3.359
	4	0.513	0.536	0.502	0.0340	136.1	0.517
	5	0.182	0.190	0.186	0.0080	48.9	0.186
	6	0.171	0.179	0.205	0.0340	48.7	0.185
	Co	0.243	0.255	0.258	0.0150	66.3	0.252

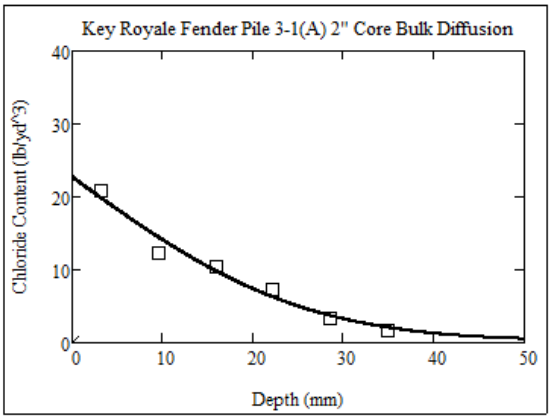

Diffusion(m^2/sec)	1.006E-12	**Background(lb/yd^3)**	0.217
Surface(lb/yd^3)	22.700	**R^2 Value**	0.9832

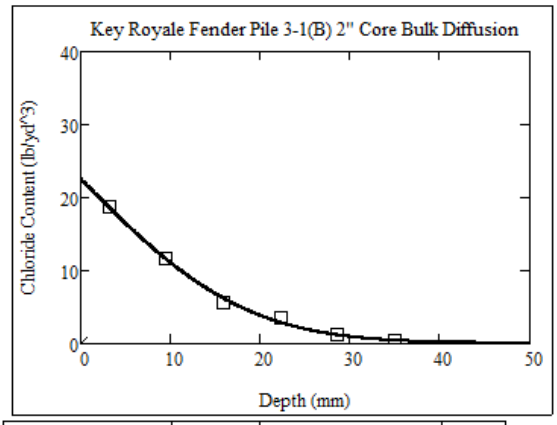

Diffusion(m^2/sec)	5.290E-13	**Background(lb/yd^3)**	0.048
Surface(lb/yd^3)	22.548	**R^2 Value**	0.9986

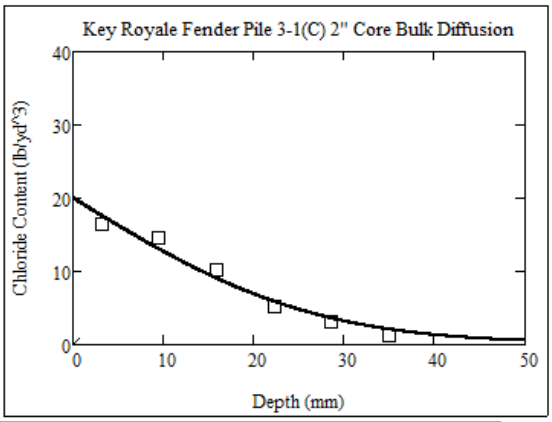

Diffusion(m^2/sec)	1.092E-12	**Background(lb/yd^3)**	0.210
Surface(lb/yd^3)	20.012	**R^2 Value**	0.9836

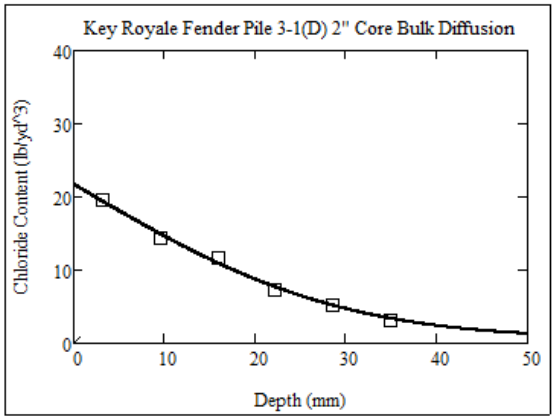

Diffusion(m^2/sec)	1.316E-12	**Background(lb/yd^3)**	0.673
Surface(lb/yd^3)	21.730	**R^2 Value**	0.9971

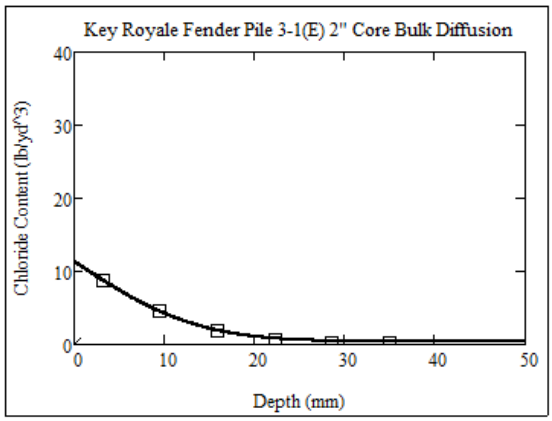

Diffusion(m^2/sec)	2.899E-13	**Background(lb/yd^3)**	0.371
Surface(lb/yd^3)	11.345	**R^2 Value**	0.9996

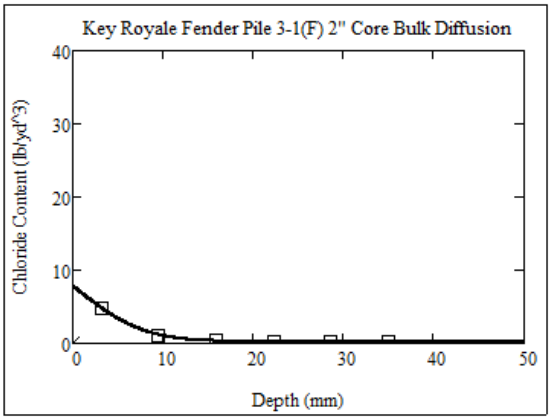

Diffusion(m^2/sec)	9.394E-14	**Background(lb/yd^3)**	0.232
Surface(lb/yd^3)	7.858	**R^2 Value**	0.9999

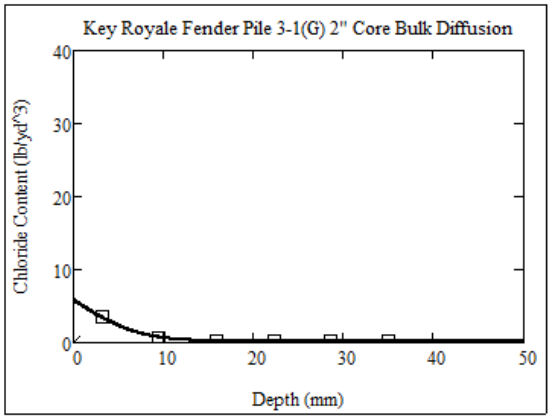

Diffusion(m^2/sec)	8.119E-14	**Background(lb/yd^3)**	0.188
Surface(lb/yd^3)	5.828	**R^2 Value**	0.9999

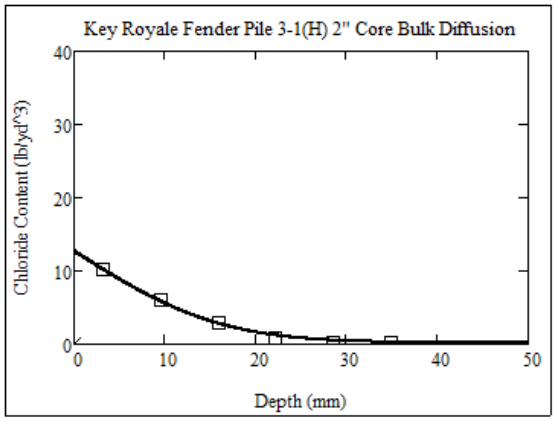

Diffusion(m^2/sec)	4.010E-13	**Background(lb/yd^3)**	0.196
Surface(lb/yd^3)	12.706	**R^2 Value**	0.9986

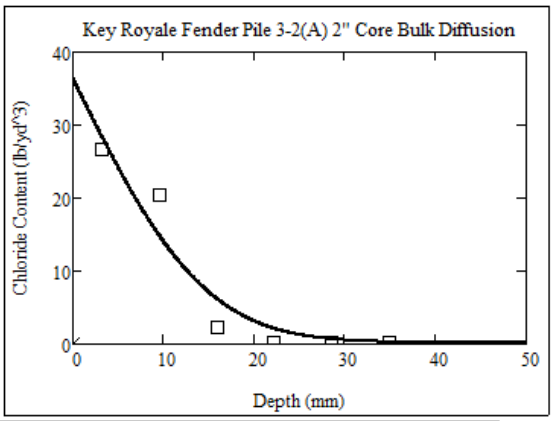

Diffusion(m^2/sec)	3.495E-13	**Background(lb/yd^3)**	0.190
Surface(lb/yd^3)	36.492	**R^2 Value**	0.9635

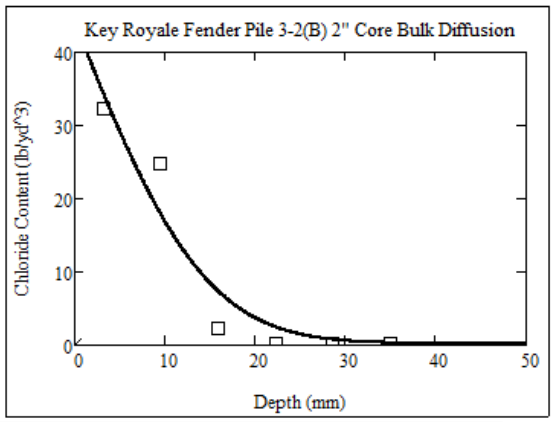

Diffusion(m^2/sec)	3.464E-13	**Background(lb/yd^3)**	0.190
Surface(lb/yd^3)	44.219	**R^2 Value**	0.9618

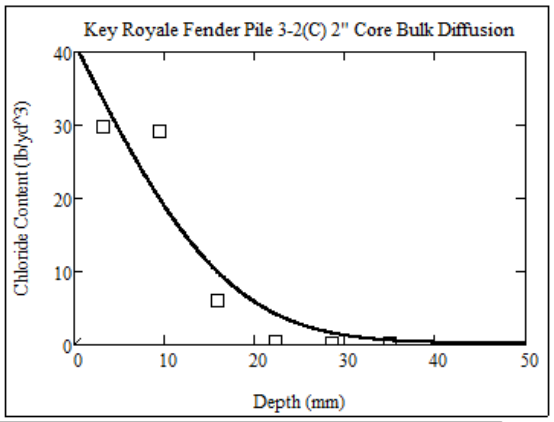

Diffusion(m^2/sec)	4.802E-13	**Background(lb/yd^3)**	0.183
Surface(lb/yd^3)	41.388	**R^2 Value**	0.9376

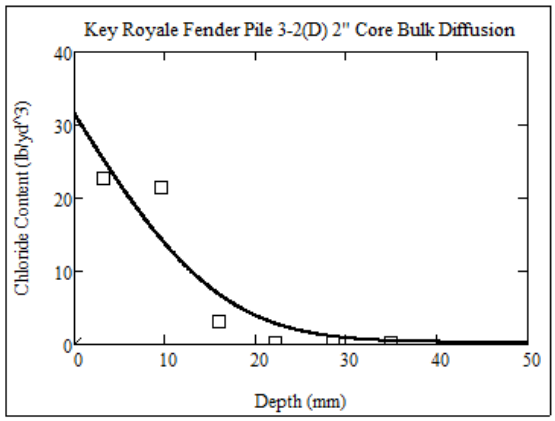

Diffusion(m^2/sec)	4.307E-13	**Background(lb/yd^3)**	0.263
Surface(lb/yd^3)	31.566	**R^2 Value**	0.9364

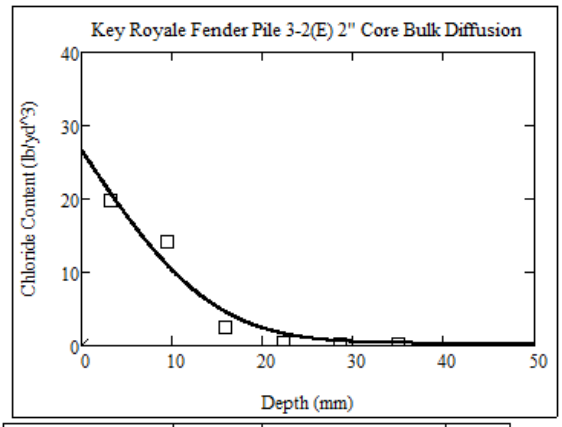

Diffusion(m^2/sec)	3.455E-13	**Background(lb/yd^3)**	0.277
Surface(lb/yd^3)	26.735	**R^2 Value**	0.9777

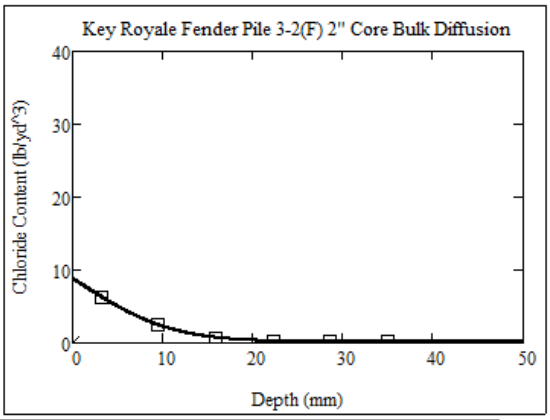

Diffusion(m^2/sec)	1.923E-13	**Background(lb/yd^3)**	0.171
Surface(lb/yd^3)	8.874	**R^2 Value**	0.9994

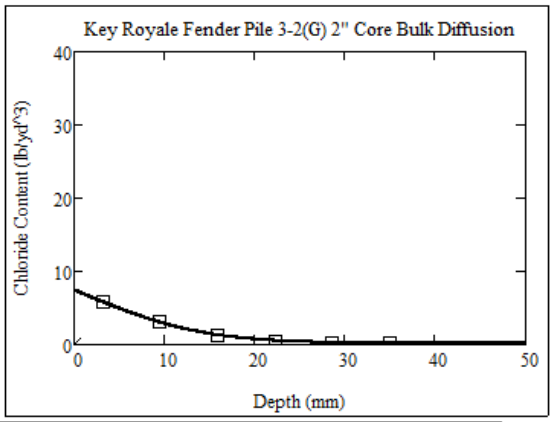

Diffusion(m^2/sec)	3.240E-13	**Background(lb/yd^3)**	0.190
Surface(lb/yd^3)	7.443	**R^2 Value**	0.9990

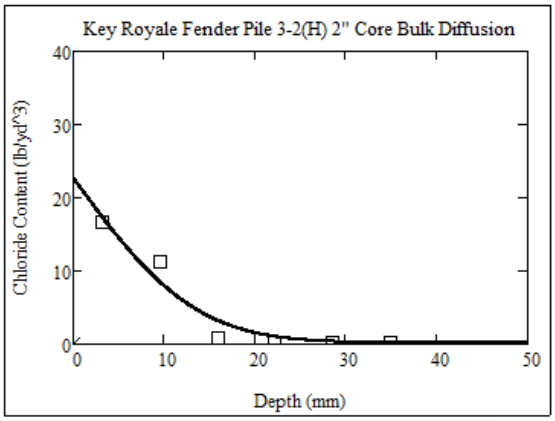

Diffusion(m^2/sec)	2.999E-13	**Background(lb/yd^3)**	0.161
Surface(lb/yd^3)	22.727	**R^2 Value**	0.9730

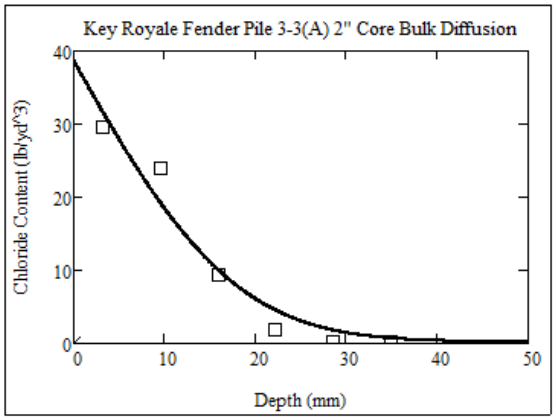

Diffusion(m^2/sec)	5.216E-13	**Background(lb/yd^3)**	0.175
Surface(lb/yd^3)	38.714	**R^2 Value**	0.9789

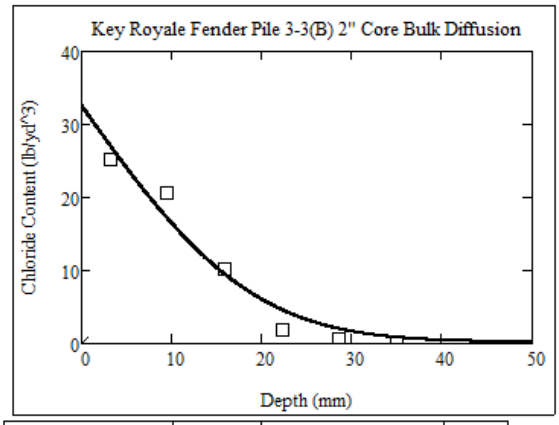

Diffusion(m^2/sec)	5.917E-13	**Background(lb/yd^3)**	0.192
Surface(lb/yd^3)	32.613	**R^2 Value**	0.9800

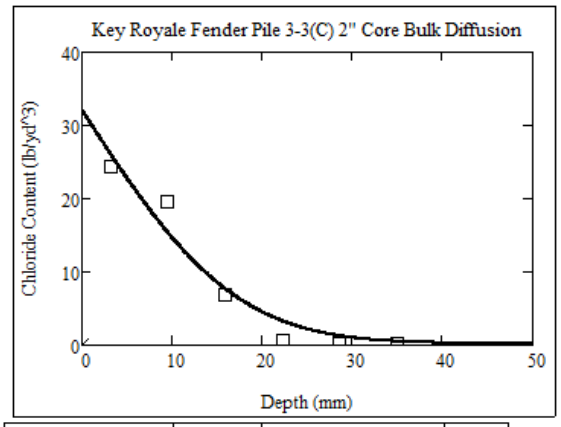

Diffusion(m^2/sec)	4.752E-13	**Background(lb/yd^3)**	0.198
Surface(lb/yd^3)	32.165	**R^2 Value**	0.9751

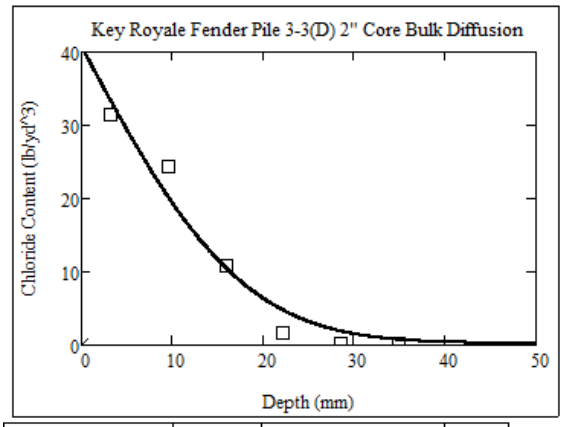

Diffusion(m^2/sec)	5.161E-13	**Background(lb/yd^3)**	0.214
Surface(lb/yd^3)	40.855	**R^2 Value**	0.9835

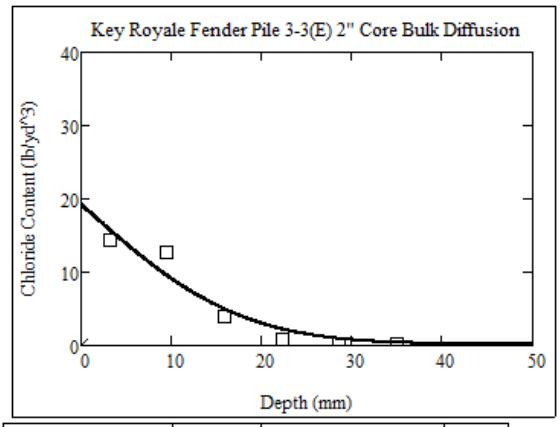

Diffusion(m^2/sec)	5.085E-13	**Background(lb/yd^3)**	0.158
Surface(lb/yd^3)	19.246	**R^2 Value**	0.9657

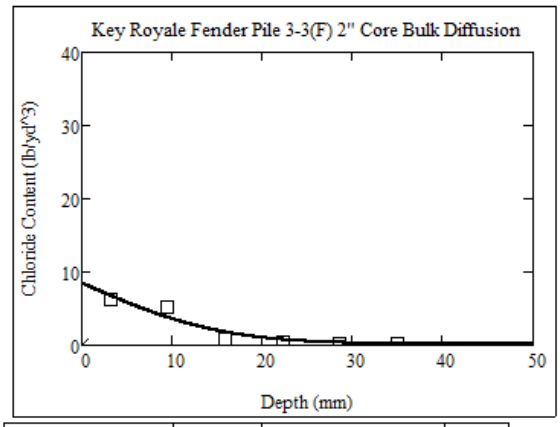

Diffusion(m^2/sec)	3.957E-13	**Background(lb/yd^3)**	0.168
Surface(lb/yd^3)	8.460	**R^2 Value**	0.9607

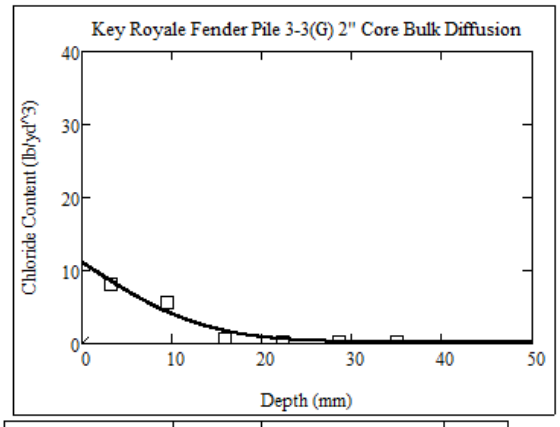

Diffusion(m^2/sec)	3.059E-13	**Background(lb/yd^3)**	0.187
Surface(lb/yd^3)	11.159	**R^2 Value**	0.9752

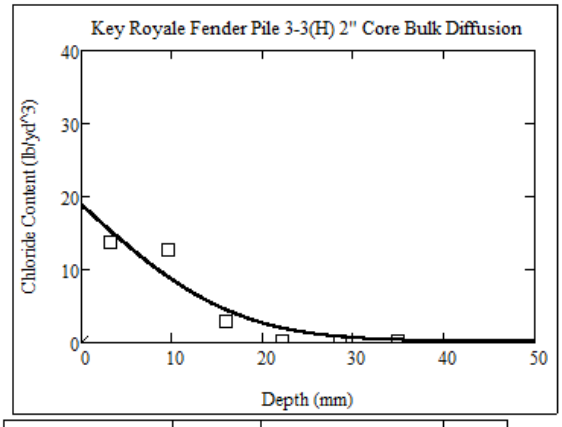

Diffusion(m^2/sec)	4.672E-13	**Background(lb/yd^3)**	0.174
Surface(lb/yd^3)	18.885	**R^2 Value**	0.9499

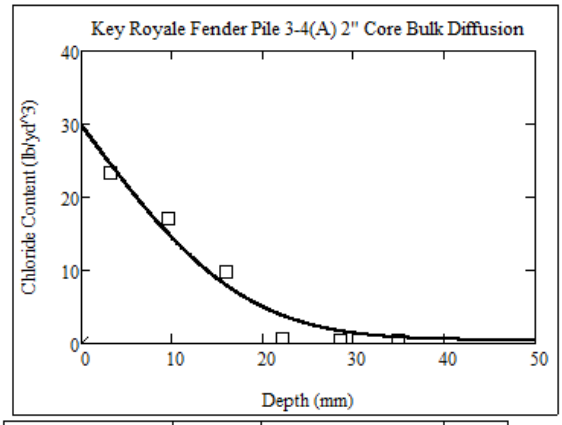

Diffusion(m^2/sec)	6.437E-13	**Background(lb/yd^3)**	0.432
Surface(lb/yd^3)	29.885	**R^2 Value**	0.9813

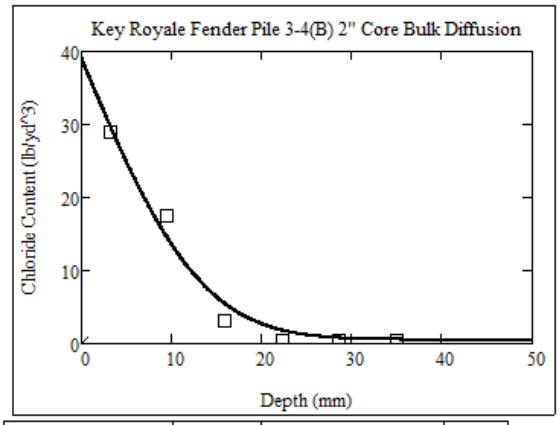

Diffusion(m^2/sec)	3.585E-13	**Background(lb/yd^3)**	0.494
Surface(lb/yd^3)	39.152	**R^2 Value**	0.9889

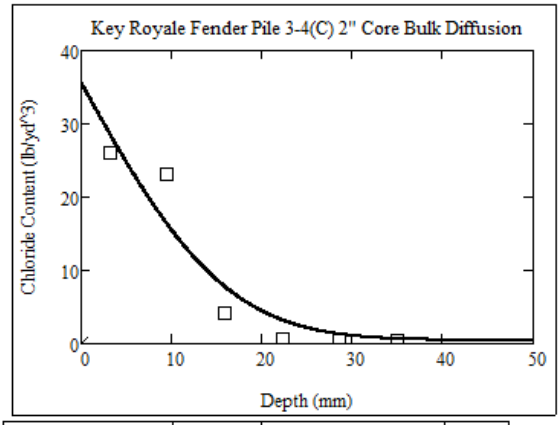

Diffusion(m^2/sec)	5.218E-13	**Background(lb/yd^3)**	0.435
Surface(lb/yd^3)	35.696	**R^2 Value**	0.9502

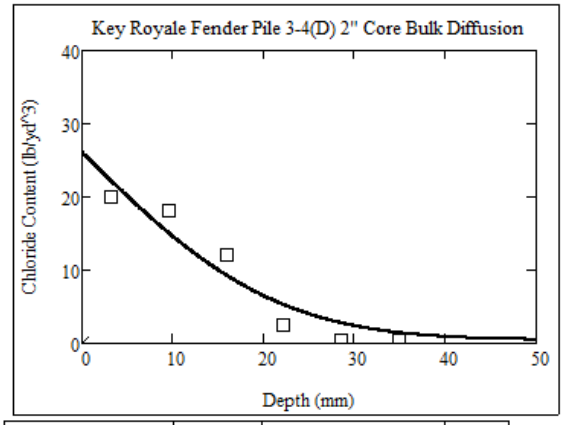

Diffusion(m^2/sec)	9.288E-13	**Background(lb/yd^3)**	0.423
Surface(lb/yd^3)	26.078	**R^2 Value**	0.9568

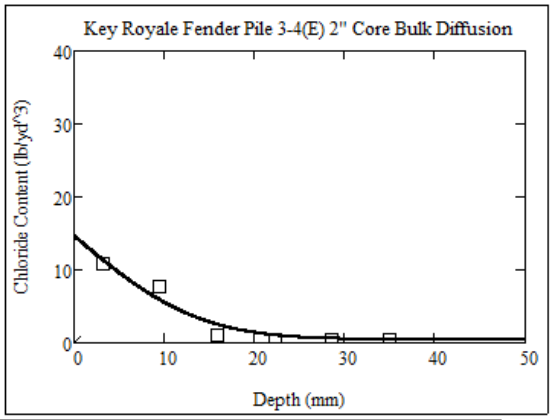

Diffusion(m^2/sec)	3.876E-13	**Background(lb/yd^3)**	0.423
Surface(lb/yd^3)	14.651	**R^2 Value**	0.9702

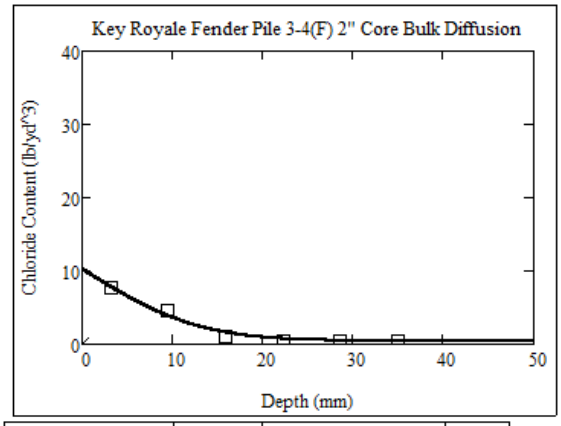

Diffusion(m^2/sec)	3.362E-13	**Background(lb/yd^3)**	0.445
Surface(lb/yd^3)	10.260	**R^2 Value**	0.9908

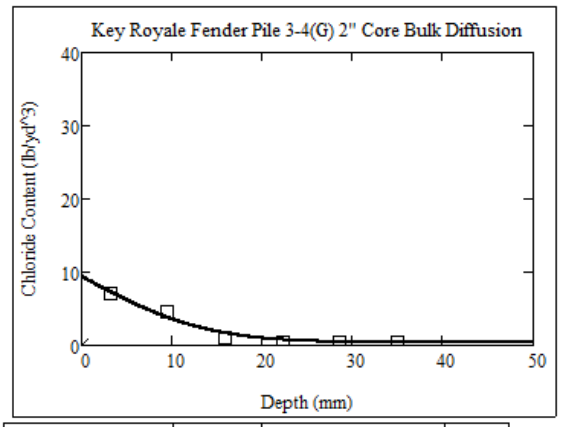

Diffusion(m^2/sec)	3.809E-13	**Background(lb/yd^3)**	0.384
Surface(lb/yd^3)	9.378	**R^2 Value**	0.9830

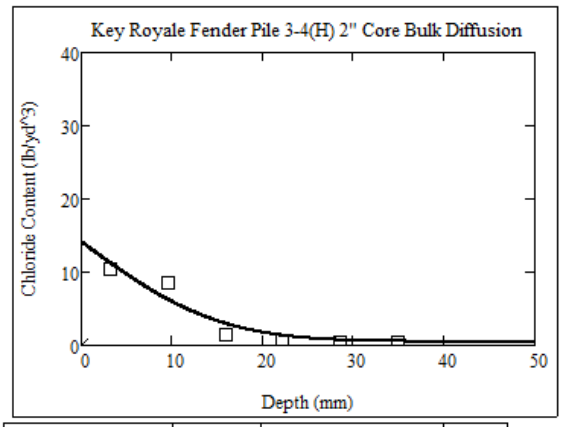

Diffusion(m^2/sec)	4.605E-13	**Background(lb/yd^3)**	0.485
Surface(lb/yd^3)	14.151	**R^2 Value**	0.9573

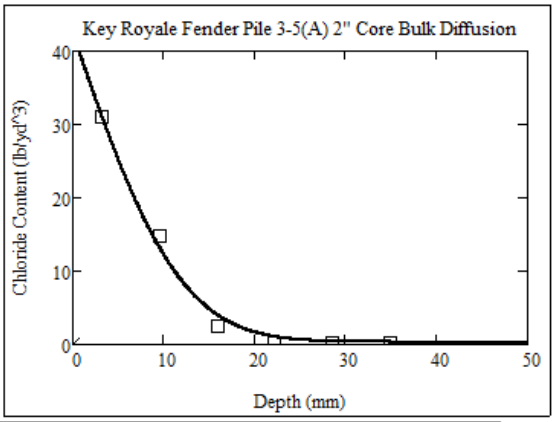

Diffusion(m^2/sec)	2.839E-13	**Background(lb/yd^3)**	0.305
Surface(lb/yd^3)	42.651	**R^2 Value**	0.9968

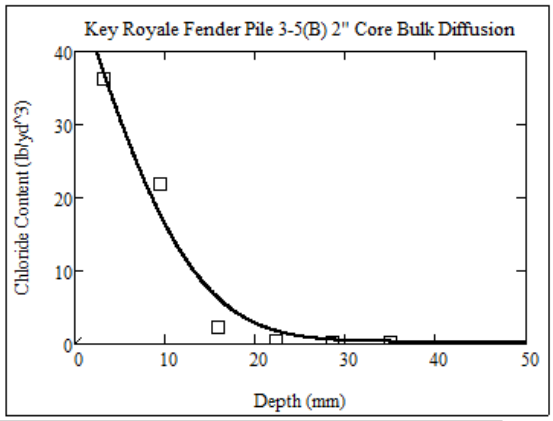

Diffusion(m^2/sec)	3.458E-13	**Background(lb/yd^3)**	0.280
Surface(lb/yd^3)	49.314	**R^2 Value**	0.9850

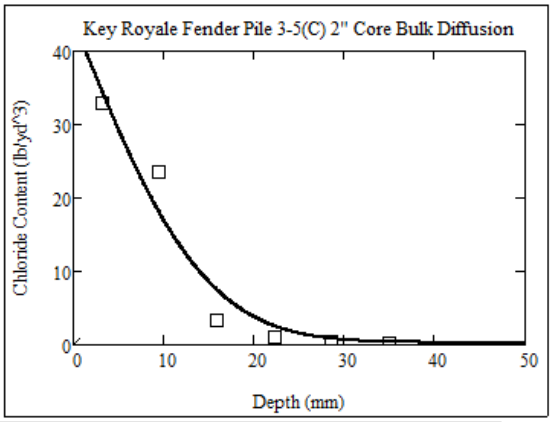

Diffusion(m^2/sec)	4.260E-13	**Background(lb/yd^3)**	0.278
Surface(lb/yd^3)	44.343	**R^2 Value**	0.9746

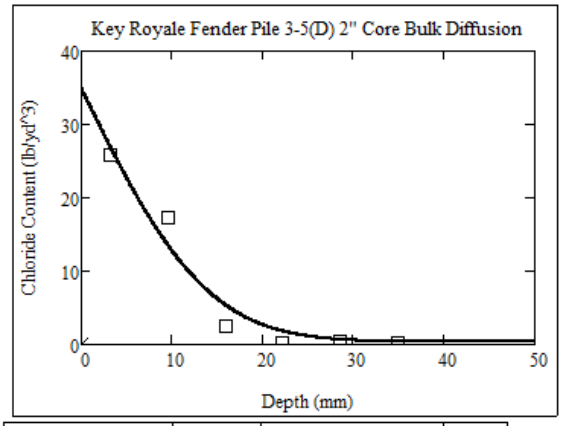

Diffusion(m^2/sec)	3.891E-13	**Background(lb/yd^3)**	0.337
Surface(lb/yd^3)	35.029	**R^2 Value**	0.9803

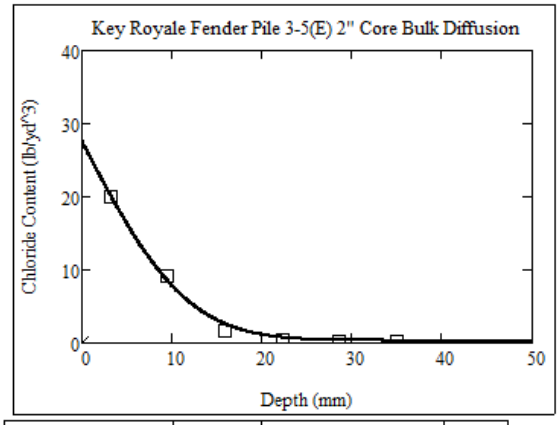

Diffusion(m^2/sec)	2.758E-13	**Background(lb/yd^3)**	0.305
Surface(lb/yd^3)	27.689	**R^2 Value**	0.9980

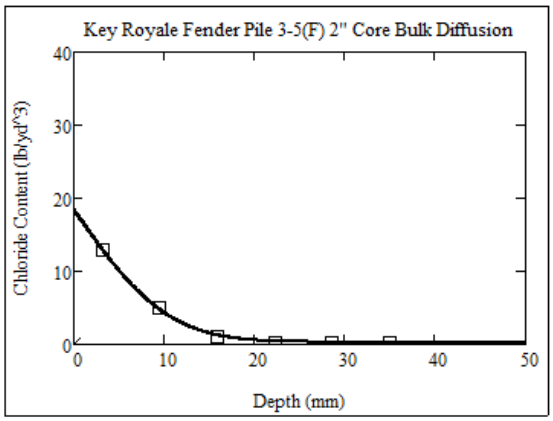

Diffusion(m^2/sec)	2.194E-13	**Background(lb/yd^3)**	0.284
Surface(lb/yd^3)	18.512	**R^2 Value**	0.9997

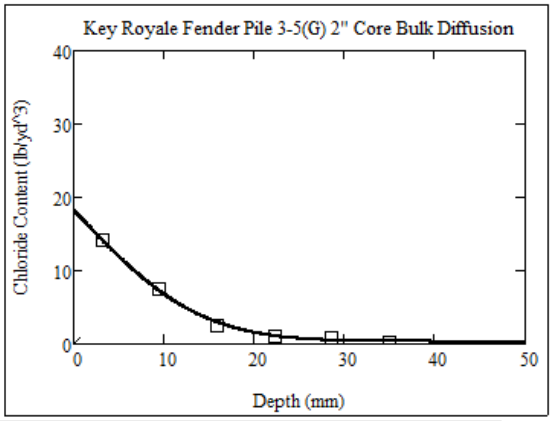

Diffusion(m^2/sec)	3.907E-13	**Background(lb/yd^3)**	0.307
Surface(lb/yd^3)	18.292	**R^2 Value**	0.9982

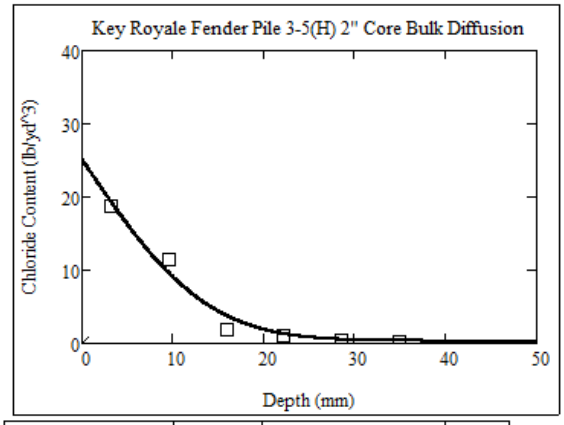

Diffusion(m^2/sec)	3.784E-13	**Background(lb/yd^3)**	0.300
Surface(lb/yd^3)	25.185	**R^2 Value**	0.9884

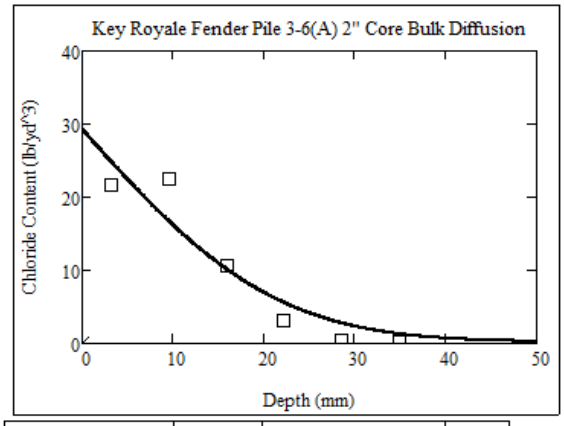

Diffusion(m^2/sec)	9.165E-13	**Background(lb/yd^3)**	0.180
Surface(lb/yd^3)	29.282	**R^2 Value**	0.9487

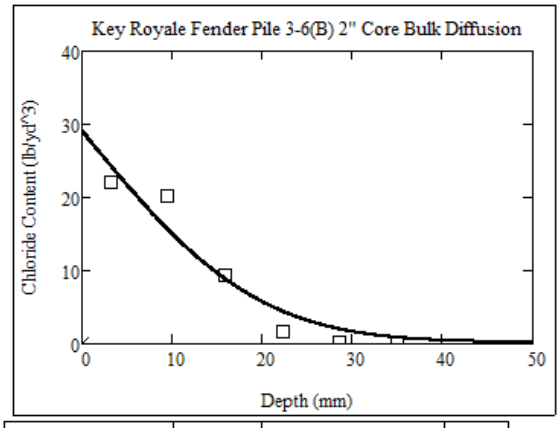

Diffusion(m^2/sec)	7.671E-13	**Background(lb/yd^3)**	0.181
Surface(lb/yd^3)	29.138	**R^2 Value**	0.9647

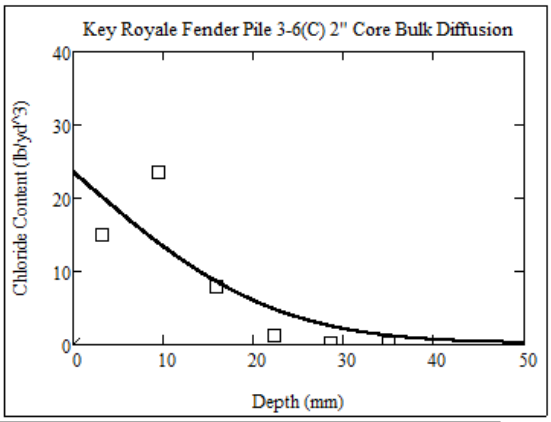

Diffusion(m^2/sec)	9.809E-13	**Background(lb/yd^3)**	0.175
Surface(lb/yd^3)	23.603	**R^2 Value**	0.8365

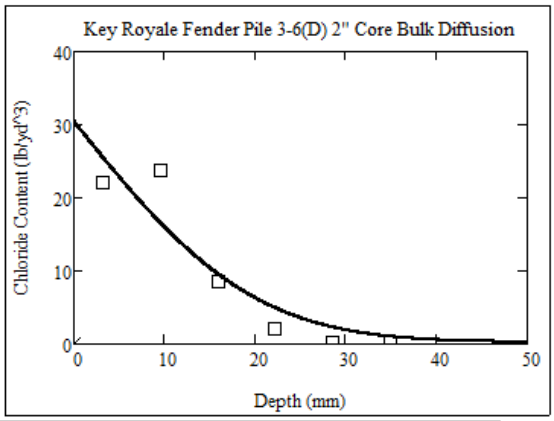

Diffusion(m^2/sec)	7.984E-13	**Background(lb/yd^3)**	0.220
Surface(lb/yd^3)	30.475	**R^2 Value**	0.9343

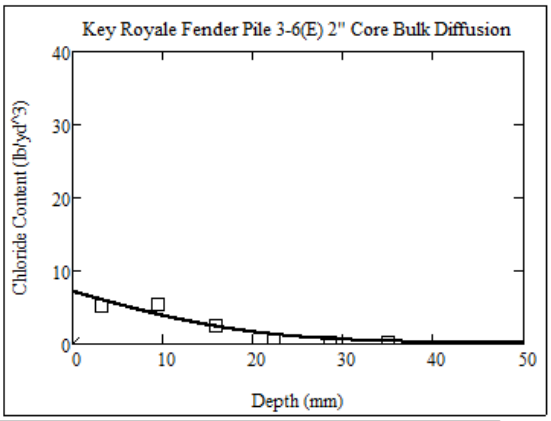

Diffusion(m^2/sec)	8.232E-13	**Background(lb/yd^3)**	0.164
Surface(lb/yd^3)	7.150	**R^2 Value**	0.9381

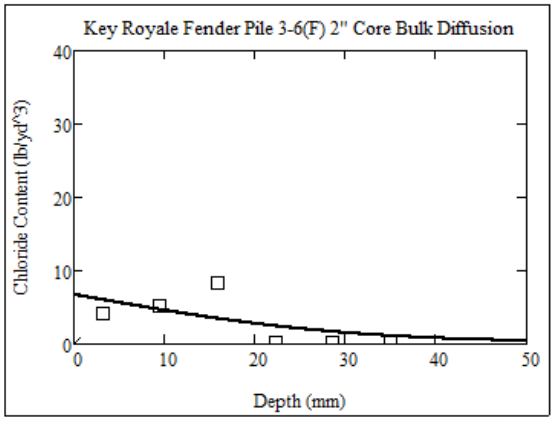

Diffusion(m^2/sec)	1.785E-12	**Background(lb/yd^3)**	0.209
Surface(lb/yd^3)	6.716	**R^2 Value**	0.6332

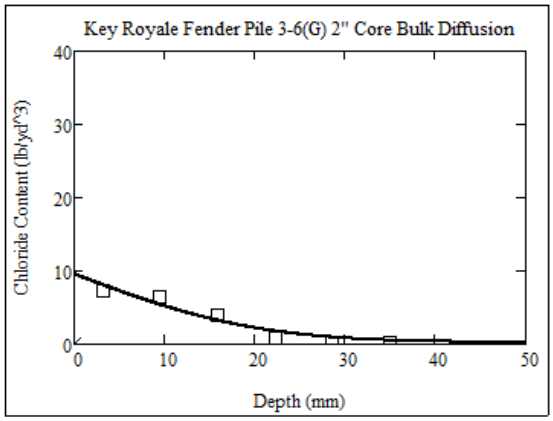

Diffusion(m^2/sec)	8.355E-13	**Background(lb/yd^3)**	0.227
Surface(lb/yd^3)	9.543	**R^2 Value**	0.9692

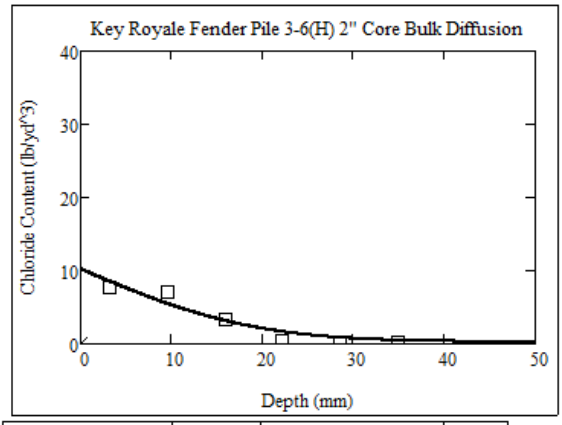

Diffusion(m^2/sec)	7.348E-13	**Background(lb/yd^3)**	0.252
Surface(lb/yd^3)	10.194	**R^2 Value**	0.9612

Appendix H–Application of Epoxy Protection at Fender Pile Coring Site

4” diameter cores were taken from the top of the six fender piles at the west side of the channel in the Key Royale Bridge. These cores were intended for further research projects outside the scope of the current research. After the cores were extracted, Quikrete was applied to patch the hole and prevent chloride intrusion into the top of the pile. There was concern that the patch would be insufficient to seal the piles and an alternative epoxy patch was supplemented.

(a)

(b)

Core extraction from top of fender piles (a) taking cores (b) applying Quikrete

The epoxy patch was developed to be rapidly implementable in the field. It was based on the epoxy cap used to seal the durability segments (Figure 46 and Figure 47) but with modifications to construct the formwork. The process for the capping operation is provided below.

Equipment required (for 6 caps):

1. SikaDur 32 Hi-Mod epoxy: (2) 2 gallon kits
2. Sika Paddle for mixing epoxy
3. ~100 lbf all-purpose well-graded kiln dried sand
4. (9) 5-gallon buckets
5. (12) 24” pipe clamps
6. (6) 18” long 1x6 (no curves in wood)

7. (6) 22” long 1x6 (no curves in wood)
8. (1) roll of Gorilla tape
9. (2) packages of rope caulk
10. Fresh water
11. Towels

Process

1. Clean pile surface using towels with fresh water. Allow to surface dry.
2. Apply Gorilla tape to form boards to enable facilitation of form removal after hardening.
3. Attach (2) 22” form boards to two opposite sides of each of (3) piles using (2) pipe hangers for each pile. The sides were chosen based on the geometry of the piles and the wales.
4. Attach (2) 18” form boards to each of (3) piles using (2) pipe hangers. These form boards attach to the two sides of the pile not covered by the 22” long 1x6 boards.
5. Use rope caulk to create a bead between the form boards and the pile top. This prevents leakage.
6. Mix preparation: place 1.33 gallons of sand in each of (3) 5-gal. buckets/
7. Place 2 gal. of Sikadur component “A” in clean 5-gal. bucket. Add 2-gal of Sikadur component B to this bucket. Mix with Sika Paddle for ~1 minute until components are mixed.
8. Place 2/3 gal. into each of two separate clean 5-gal. buckets. There should now be (3) 5-gal. buckets each containing 2/3 gallon of epoxy.
9. Place contents of each of (3) buckets with sand into each of (3) buckets containing epoxy.
10. Use Sika Paddle to mix each bucket of epoxy and sand. After ~ 1min of mixing, place contents of bucket into form.
11. Smooth epoxy mixture within form to form a dome shape. Ensure that mixture flows through entire form to provide at least ¾” of cover. Place each bucket as they are mixed; form a “bucket brigade” to ensure that each mixture is delivered as soon as it is mixed.
12. Wait for at least four hours until epoxy has cured sufficiently. Epoxy should not leak from form system.
13. Carefully remove formwork. Remove pipe hangers first; use mallet to “pop” form boards free; they should come loose easily.
14. Repeat this process for additional (3) piles; an additional (3) 5-gallon buckets shall be required for each (3) piles.

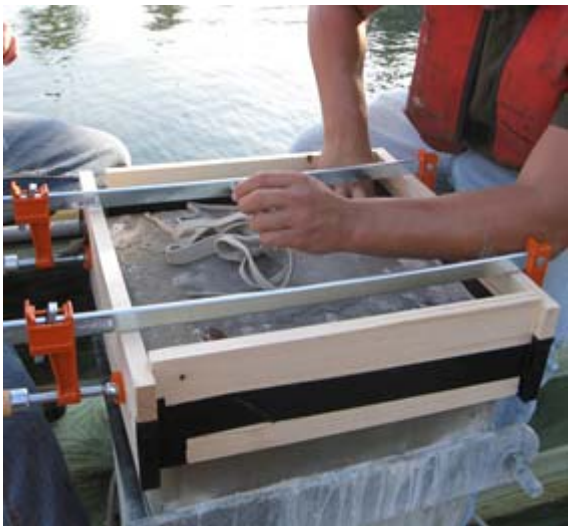

(a)

(b)

Installing form for epoxy retention (a) sealing concrete-tape interface with rope caulk (b) finished form

(a)

(b)

Ready for pour (a) finished form with caulk (b) mixing epoxy

(a) (b)

After initial cure (a) remove form work (b) finished product

Appendix I–Long-Term Monitoring Plan for Key Royale Bridge

Recommended Return Interval

The initial recommendation from this project was for measurements to be performed at 5-year intervals. Measurements should be performed either in late spring (May) or early fall (September) to increase the probability that temperatures during measurements are consistent. The last measurements were performed in 2012, indicating that future measurements should be performed in 2017 and 2022.

Personnel Required (minimum):

Boat operator
#1 Technician (to operate measurement equipment)
#2 Technician (to record measurements

Equipment required:

1. Water resistant digital multimeter (2 identical units if feasible)
2. Copper sulfate electrodes (bring 3+ in case of erratic performance)
3. Connecting wires, alligator clips, and banana clips for multimeter
4. Wenner linear four-probe array and display
5. Scotch-Kote
6. #8 stainless sheet metal screws
7. Electric (battery) screwdriver
8. Duct tape
9. Pliers
10. Scissors
11. Hammer
12. Chisel or small crowbar
13. Fine sandpaper
14. Screw tap (to remove damaged screws)
15. Wire cutters/strippers
16. Phillips head screwdriver
17. Measuring tape
18. Digital camera with adequate flash capability
19. Extra batteries for camera
20. Data recording sheets
21. Scratch paper
22. Clipboard
23. Pieces of chalk (3+) or paint pens
24. Rags
25. Towels

26. Potable water

Measurement Tasks:

1. Bridge Piles: external corrosion potential of prestressing strand
2. Bridge Piles: surface resistivity
3. Bridge Piles: corrosion potential between steel and titanium electrodes
4. Bridge Piles: external corrosion potential of steel and titanium electrodes
5. Bridge Piles: electrical current reading of steel electrodes
6. Bridge Piles: electrical resistance reading of steel and titanium electrodes
7. Durability Segments: external corrosion potential of steel and titanium electrodes
8. Durability Segments: corrosion potential between steel and titanium electrodes
9. Durability Segments: electrical current reading of steel electrodes
10. Durability Segments: electrical resistance reading of steel and titanium electrodes

Measurement Procedures

The procedures listed below are for performing a complete set of measurements. Some of the procedures labeled "combination task" combine measurements to reduce the time required to perform measurements. Time estimates are provided for each task with the intent that a measurement plan would be formulated based on the amount of time that may be spent at the bridge. Where time constraints restrict the number of measurements that may be taken, half-cell potentials for the bridge piles should receive priority.

<u>Bridge pile external corrosion potential of prestressing strand</u>

1. Set up multimeter. Multimeter must be set to record "mV". Two wires are required. Both wires must have banana plugs on one end. One wire must have alligator clips; the other must have a water resistant plug end (to mate with the reference probe). Place banana plug end of the probe connecting wire into the "COM" port and the alligator connecting wire into the "V" port.
2. Attach reference electrode to the water resistant plug.
3. Establish a boat position to enable measurements to be taken at a specific pile.
4. Remove screws attaching the electrical box cover to electrical box (box with wires connected to prestress strand). If necessary, use a screw tap, pliers, etc. to remove screws.
5. Remove box cover and store carefully.
6. Set up electrical connection at the electrical box. Verify that both lead wires in the electrical box are clean and free of excess corrosion or debris. Use sandpaper if required to clean wire surfaces.
7. Test electrical connection at electrical box. Turn on multimeter. Attach alligator clip to one of the electrical box wires and place reference electrode in the water. Record stable reading. Place alligator clip on other wire and repeat measurement. Both measurements must be within ~2mV of each other. Otherwise, clean the electrical box wires. If this still doesn't yield stable readings, switch reference electrodes and repeat measurements. If this doesn't work, trim off exposed wire and remove ~1 cm of insulation and repeat measurements. This

process works best with two people; one holding the multimeter and connecting alligator clips and the other dipping the electrode in the water. This can be done with one person with the other person marking the pile.

8. Assuming both wires produce acceptable measurements, choose one for taking the potential readings on the face of the pile.
9. Determine which pile face is to be used for measurement.
10. Remove any potentially confusing or misleading markings from pile using alcohol, cotton balls, and rags.
11. Mark a measurement point that corresponds to position "1". This is to be placed at the location of dimension "a" as indicated in the initial report. Place the reference point off-center.
12. Mark measurement locations at 12" o.c. below measurement point "1". These must extend to the waterline. Do not place markings underwater.
13. Draw a ~2" diameter circle at the center of the pile face at each measurement location. This serves as a "target" for placing the electrode against the pile.
14. Take half-cell readings using the CuSO4 references. Start at the junction between the bent and pile (position "0") and proceed down the pile. The reference electrode must be rewetted after every two or three measurements or every time readings are erratic. The measurements will proceed more quickly using two people. Person one has the multimeter and clipboard, person two uses the electrode and calls out when readings are to be taken. The recorder must tell the person holding the electrode if readings are erratic and that the electrode must be rewetted.
15. Readings within the marine growth zone must be taken on exposed concrete. If necessary, take readings slightly off center. If marine growth is pervasive, use the hammer and chisel to remove enough growth to take measurements.
16. Repeat this process for each of 20 pilings. Bents 3 and 4 should be analyzed at low tide; bents 2 and 5 should be analyzed at medium to high tide due to boat draft issues. A decision about whether the tide is too low or not must be made in consultation with the boat operator or FDOT representative on board.
17. Time Estimation: Maximum: 5 min. for boat positioning, 5 min. for electrical box removal, 10 min. to perform measurements (20 min. per pile or 400 min. total). Minimum: 5 min. for boat positioning, 3 min. for electrical box removal, 7 min to perform measurements (15 min. per pile or 300 min. total). Total time range: 300-400 min. (5 to 7 hours).

Bridge pile surface resistivity

1. Set up Wenner array for use. Connect appropriate cables to Wenner array, display unit, and soil resistance meter.
2. Establish a boat position to enable measurements to be taken at a specific pile.
3. Steps 5 through 7 below shall be omitted if external corrosion potential readings have been taken before determining surface resistivity.
4. Determine which pile face is to be used for measurement.
5. Measurements must be made using two people. One person positions the array against the pile, holds it in place, and lets the recorder know that the array is in position; the second person verifies that readings are stable and records the resistance.

6. Place the array longitudinally against the pile just above the marine growth line such that the four points of the probe are in contact with the pile face. The probe must be centered in the pile face.
7. Wait for 3 to 5 seconds until a stable reading is obtained. A negative, unstable, or obviously erroneous reading indicates that there are problems with the instrument or probe array, which need to be addressed before proceeding. A reading is considered unstable if it drifts by more than 1 kΩ-cm.
8. Repeat this process for each of 20 pilings. Bents 3 and 4 should be analyzed at low tide; bents 2 and 5 should be analyzed at medium to high tide due to boat draft issues. A decision about whether the tide is too low or not must be made in consultation with the boat operator or FDOT representative on board.
9. Time estimation: 5 min. for boat positioning, 5 min. to perform measurements (10 min), total time of 10 to 15 min. per pile. Total time range: 200-300 min (3 to 5 hours)

Bridge pile corrosion potential between steel and titanium electrodes

1. This task may be done in conjunction with task (6). See task (6a) for alternate instructions.
2. Set up multimeter. Multimeter must be set to record "mV". Two wires are required. Both wires must have banana plugs on one end and alligator clips on the other end.
3. Establish a boat position to enable measurements to be taken at a specific pile.
4. If not done before, remove screws attaching electrical box cover to electrical box (embedded box connected to titanium and steel electrodes). If necessary, use a screw tap, pliers, etc. to remove screws.
5. Remove box cover and store carefully.
6. There are two pairs of wires in the box, one pair from each hole.
7. Verify that all four lead wires in the electrical box are clean and free of excess corrosion or debris. Use sandpaper if required to clean wire surfaces.
8. 8. Pull the top pair of wires out and remove protective coating if present. There should be a black and white wire.
9. Attach one alligator clip to each wire in the top pair. The multimeter wire clipped to the black wire (steel layer 2 electrode) must be plugged into the positive (red) terminal in the multimeter, the multimeter wire clipped to the white wire (titanium layer 2 electrode) must be plugged into the negative terminal of the multimeter.
10. Record the reading once it has stabilized.
11. Disconnect the alligator clips from the top two wires.
12. Attach one alligator clip to each wire in the bottom pair. The multimeter wire clipped to the yellow wire (steel layer 1 electrode) must be plugged into the positive (red) terminal in the multimeter, the multimeter wire clipped to the white wire (titanium layer 1 electrode) must be plugged into the negative terminal of the multimeter. Note that some of the yellow wires are white wires with a yellow shrink wrap.
13. Record the reading once it has stabilized.
14. Disconnect the alligator clips from the bottom two wires.
15. Repeat this process for each of 10 pilings. Tidal conditions are not relevant to this measurement.
16. Time estimation: 5 min. for boat positioning, 5 min. to 10 min to perform measurements, total time of 10 to 15 min. per pile. Total time: 100-150 min (2 hours).

Bridge pile external corrosion potential of steel and titanium electrodes

1. Set up multimeter. Multimeter must be set to record "mV". Two wires are required. Both wires must have banana plugs on one end. One wire must have alligator clips; the other must have a water resistant plug end (to mate with the reference probe). Place banana plug end of the probe connecting wire into the "COM" port and the alligator connecting wire into the "V" port.
2. Attach reference electrode to the water resistant plug.
3. Establish a boat position to enable measurements to be taken at a specific pile.
4. If not already done, remove screws attaching electrical box cover to electrical box (embedded box connected to titanium and steel electrodes). If necessary, use a screw tap, pliers, etc. to remove screws.
5. Remove box cover and store carefully.
6. Mark the height where the two pairs of measurements are to be taken. Mark off-center.
7. Draw a ~2" diameter circle at the center of the pile face at each measurement location. This serves as a "target" for placing the electrode against the pile.
8. There are two pairs of wires in the box, one pair from each hole. Pull the wires out and remove protective coating if present.
9. Attach the alligator clip to the white wire (titanium) from the top pair. Dip the electrode in the water and verify that the reading is stable. If reading is not stable, clean the wire. If this still doesn't yield stable readings, switch reference electrodes and repeat measurement. If this doesn't work, trim off exposed wire and remove ~1 cm of insulation and repeat measurements. Record the reading as layer 2 titanium in water.
10. Take half-cell reading using the CuSO4 references. This measurement must be taken at the bottom target. The reference electrode must be rewetted if readings are erratic. The measurements will proceed more quickly using two people. Person one has the multimeter and clipboard, person two uses the electrode and calls out when readings are to be taken. The recorder must tell the person holding the electrode if readings are erratic and that the electrode must be rewetted. Record as layer 2 titanium.
11. Remove the alligator from the white wire.
12. Attach the alligator clip to the black wire (steel) from the top pair. Dip the electrode in the water and verify that the reading is stable. If reading is not stable, clean the wire. If this still doesn't yield stable readings, switch reference electrodes and repeat measurement. If this doesn't work, trim off exposed wire and remove ~1 cm of insulation and repeat measurements. Record the reading as layer 2 steel in water.
13. Take half-cell reading using the CuSO4 references. This measurement must be taken at the bottom target. The reference electrode must be rewetted if readings are erratic. Record as layer 2 steel.
14. Remove the alligator from the black wire.
15. Attach the alligator clip to the white wire (titanium) from the bottom pair. Dip the electrode in the water and verify that the reading is stable. If reading is not stable, clean the wire. If this still doesn't yield stable readings, switch reference electrodes and repeat measurement. If this doesn't work, trim off exposed wire and remove ~1 cm of insulation and repeat measurements. Record the reading as layer 1 titanium in water.

16. Take half-cell reading using the CuSO4 references. This measurement must be taken at the top target. The reference electrode must be rewetted if readings are erratic. Record as layer 1 titanium.
17. Remove the alligator from the black wire.
18. Attach the alligator clip to the white wire (titanium) from the bottom pair. Dip the electrode in the water and verify that the reading is stable. If reading is not stable, clean the wire. If this still doesn't yield stable readings, switch reference electrodes and repeat measurement. If this doesn't work, trim off exposed wire and remove ~1 cm of insulation and repeat measurements. Record the reading as layer 1 steel in water.
19. Take half-cell reading using the CuSO4 references. This measurement must be taken at the top target. The reference electrode must be rewetted if readings are erratic. Record as layer 1 steel.
20. Remove the alligator from the yellow wire.
21. Repeat this process for each of 10 pilings. Tidal conditions may be relevant to this measurement.
22. Time estimation: 5 min. for boat positioning, 10 min. to 20 min to perform measurements, total time of 15 to 25 min. per pile. Total time: 150-250 min (3-4 hours).

Bridge pile electrical current reading of steel electrodes

1. Set up multimeter. Multimeter must be set to record "μA". Two wires are required. Both wires must have banana plugs on one end and alligator clips on the other end.
2. Establish a boat position to enable measurements to be taken at a specific pile.
3. If not done before, remove screws attaching electrical box cover to electrical box (embedded box connected to titanium and steel electrodes). If necessary, use a screw tap, pliers, etc. to remove screws.
4. Remove box cover and store carefully.
5. There are two pairs of wires in the box, one pair from each hole.
6. Verify that all four lead wires in the electrical box are clean and free of excess corrosion or debris. Use sandpaper if required to clean wire surfaces.
7. Attach one alligator clip to the black wire in the top pair. The multimeter wire clipped to the black wire (steel layer 2 electrode) must be plugged into the negative (COM) terminal in the multimeter.
8. Attach the other alligator clip to the black wire in the bottom pair. This multimeter wire must be plugged into the "μA" terminal in the multimeter.
9. Record the reading once it has stabilized.
10. Disconnect the alligator clips from the two wires.
11. Repeat this process for each of 10 pilings. Tidal conditions are not relevant to this measurement.
12. Time estimation: 5 min. for boat positioning, 5 min. to 10 min to perform measurements, total time of 10 to 15 min. per pile. Total time: 100-150 min (2 hours).

Bridge pile electrical resistance reading of steel and titanium electrodes

13. 1. This task may be done in conjunction with task (3). See task (6a) for alternate instructions.

14. 2. Set up multimeter. Multimeter must be set to record "Ω". Two wires are required. Both wires must have banana plugs on one end and alligator clips on the other end. Place one banana clip into the "COM" port and the other into the "V Ω" port.
15. 3. Establish a boat position to enable measurements to be taken at a specific pile.
16. 4. If not done before, remove screws attaching electrical box cover to electrical box (embedded box connected to titanium and steel electrodes). If necessary, use a screw tap, pliers, etc. to remove screws.
17. 5. Remove box cover and store carefully.
18. 6. There are two pairs of wires in the box, one pair from each hole.
19. 7. Verify that all four lead wires in the electrical box are clean and free of excess corrosion or debris. Use sandpaper if required to clean wire surfaces.
20. 8. Pull the top pair of wires out and remove protective coating if present. There should be a black and white wire.
21. 9. Attach one alligator clip to each wire in the top pair. The polarity of the wires is not important.
22. 10. Record the reading once it has stabilized as the "S2-T2" resistance.
23. 11. Disconnect the alligator clips from the top two wires.
24. 12. Attach one alligator clip to each wire in the bottom pair. The polarity of the wires is not important.
25. 13. Record the reading once it has stabilized as the "S1-T1" resistance
26. 14. Disconnect the alligator clips from the bottom two wires.
27. 15. Attach one alligator clip to the black wire from the top pair and the yellow wire from the bottom pair. The yellow wire may be a white wire with yellow shrink wrap. The polarity of the wires is not important.
28. 16. Record the reading once it has stabilized as the "S1-S2" resistance.
29. 17. Repeat this process for each of 10 pilings. Tidal conditions are not relevant to this measurement.
30. 18. Time estimation: 5 min. for boat positioning, 5 min. to 10 min to perform measurements, total time of 10 to 15 min. per pile. Total time: 100-150 min (2 hours).

Combination task: bridge pile electrical resistance reading of steel and titanium electrodes and external corrosion potential between steel and titanium electrodes

1. Part I: Potential (part 3).
2. Set up multimeter. Multimeter must be set to record "mV". Two wires are required. Both wires must have banana plugs on one end and alligator clips on the other end.
3. Establish a boat position to enable measurements to be taken at a specific pile.
4. If not done before, remove screws attaching electrical box cover to electrical box (embedded box connected to titanium and steel electrodes). If necessary, use a screw tap, pliers, etc. to remove screws.
5. Remove box cover and store carefully.
6. There are two pairs of wires in the box, one pair from each hole.
7. Verify that all four lead wires in the electrical box are clean and free of excess corrosion or debris. Use sandpaper if required to clean wire surfaces.

8. Pull the top pair of wires out and remove protective coating if present. There should be a black and white wire.
9. Attach one alligator clip to each wire in the top pair. The multimeter wire clipped to the black wire (steel layer 2 electrode) must be plugged into the positive (red) terminal in the multimeter, the multimeter wire clipped to the white wire (titanium layer 2 electrode) must be plugged into the negative terminal of the multimeter.
10. Record the reading once it has stabilized.
11. Disconnect the alligator clips from the top two wires.
12. Attach one alligator clip to each wire in the bottom pair. The multimeter wire clipped to the yellow wire (steel layer 1 electrode) must be plugged into the positive (red) terminal in the multimeter, the multimeter wire clipped to the white wire (titanium layer 1 electrode) must be plugged into the negative terminal of the multimeter. Note that some of the yellow wires are white wires with a yellow shrink wrap.
13. Record the reading once it has stabilized.
14. Disconnect the alligator clips from the bottom two wires.
15. Part II: Resistance (part 6).
16. Set up multimeter. Multimeter must be set to record "Ω". Two wires are required. Both wires must have banana plugs on one end and alligator clips on the other end. Place one banana clip into the "COM" port and the other into the "V Ω" port.
17. Attach one alligator clip to each wire in the top pair. The polarity of the wires is not important.
18. Record the reading once it has stabilized as the "S2-T2" resistance.
19. Disconnect the alligator clips from the top two wires.
20. 20. Attach one alligator clip to each wire in the bottom pair. The polarity of the wires is not important.
21. Record the reading once it has stabilized as the "S1-T1" resistance
22. Disconnect the alligator clips from the bottom two wires.
23. Attach one alligator clip to the black wire from the top pair and the yellow wire from the bottom pair. The yellow wire may be a white wire with yellow shrink wrap. The polarity of the wires is not important.
24. Record the reading once it has stabilized as the "S1-S2" resistance.
25. Repeat this process for each of 10 pilings. Tidal conditions are not relevant to this measurement.
26. Time estimation: 5 min. for boat positioning, 10 min. to 15 min to perform measurements, total time of 15 to 20 min. per pile. Total time: 150-200 min (3-4 hours).

Durability segment external corrosion potential of steel and titanium electrodes

1. Set up multimeter. Multimeter must be set to record "mV". Two wires are required. Both wires must have banana plugs on one end. One wire must have alligator clips; the other must have a water resistant plug end (to mate with the reference probe). Place banana plug end of the probe connecting wire into the "COM" port and the alligator connecting wire into the "V" port.
2. Attach reference electrode to the water resistant plug.
3. Establish a boat position to enable measurements to be taken at a specific durability segment.

4. There are six pins on the electrical box that correspond to the six electrodes within. They are referenced “top left, top right, middle left, middle right, bottom left, bottom right”.
5. Unscrew electrical box cover. Remove “S”-shaped wire connecting three steel electrodes together. Reattach electrical box cover.
6. Mark the height where the measurements are to be taken. Mark off-center.
7. Draw a ~2” diameter circle at the center of the pile face at each measurement location. This serves as a “target” for placing the electrode against the pile.
8. Attach the alligator clip to the top left pin on the durability segment. Dip the electrode in the water and verify that the reading is stable. If reading is not stable, switch reference electrodes and repeat measurement. If this doesn’t work, repair of the connections within the electrical box may be required.
9. Take half-cell reading using the CuSO4 references. This measurement must be taken at the upper target. The reference electrode must be rewetted if readings are erratic. The measurements will proceed more quickly using two people. Person one has the multimeter and clipboard, person two uses the electrode and calls out when readings are to be taken. The recorder must tell the person holding the electrode if readings are erratic and that the electrode must be rewetted. Record as layer 1 titanium.
10. Remove the alligator from the top left pin.
11. Attach the alligator clip to the top right pin on the durability segment. Dip the electrode in the water and verify that the reading is stable.
12. Take half-cell reading using the CuSO4 references. This measurement must be taken at the upper target. Record as layer 1 steel.
13. Remove the alligator from the top right pin.
14. Attach the alligator clip to the middle left pin on the durability segment. Dip the electrode in the water and verify that the reading is stable.
15. Take half-cell reading using the CuSO4 references. This measurement must be taken at the lower target. Record as layer 2 titanium.
16. Remove the alligator from the middle left pin.
17. Attach the alligator clip to the middle right pin on the durability segment. Dip the electrode in the water and verify that the reading is stable.
18. Take half-cell reading using the CuSO4 references. This measurement must be taken at the lower target. Record as layer 2 steel.
19. Remove the alligator from the middle right pin.
20. Attach the alligator clip to the lower left pin on the durability segment. Dip the electrode in the water and verify that the reading is stable.
21. Take half-cell reading using the CuSO4 references. This measurement must be taken at the lower target. Record as layer 3 titanium.
22. Remove the alligator from the lower left pin.
23. Attach the alligator clip to the lower right pin on the durability segment. Dip the electrode in the water and verify that the reading is stable.
24. Take half-cell reading using the CuSO4 references. This measurement must be taken at the lower target. Record as layer 3 steel.
25. Remove the alligator from the lower right pin.
26. Unscrew electrical box cover. Reattach “S”-shaped wire connecting three steel electrodes together. Reattach electrical box cover.

27. Repeat this process for each of 6 segments. Tidal conditions may be relevant to this measurement.
28. Time estimation: 5 min. for boat positioning, 10 min. to 15 min to perform measurements, total time of 15 to 20 min. per segment. Total time: 75-120 min (1-2 hours).

Durability segment corrosion potential between steel and titanium electrodes

1. This task may be done in conjunction with tasks 9 and 10. See task 10a for alternate instructions.
2. Set up multimeter. Multimeter must be set to record "mV". Two wires are required. Both wires must have banana plugs on one end and alligator clips on the other end.
3. Establish a boat position to enable measurements to be taken at a specific durability segment.
4. There are six pins on the electrical box that correspond to the six electrodes within. They are referenced "top left, top right, middle left, middle right, bottom left, bottom right".
5. Unscrew electrical box cover. Remove "S"-shaped wire connecting three steel electrodes together. Reattach electrical box cover.
6. Attach one alligator clip to each pin in the top pair. The multimeter wire clipped to the left (titanium layer 1 electrode) must be plugged into the negative terminal of the multimeter; the multimeter wire clipped to the right pin (steel layer 1 electrode) must be plugged into the positive (red) terminal in the multimeter.
7. Record the reading once it has stabilized.
8. Disconnect the alligator clips from the top two pins.
9. Attach one alligator clip to each pin in the middle pair. The multimeter wire clipped to the left (titanium layer 1 electrode) must be plugged into the negative terminal of the multimeter; the multimeter wire clipped to the right pin (steel layer 2 electrode) must be plugged into the positive (red) terminal in the multimeter.
10. Record the reading once it has stabilized.
11. Disconnect the alligator clips from the middle two pins.
12. Attach one alligator clip to each pin in the bottom pair. The multimeter wire clipped to the left (titanium layer 3 electrode) must be plugged into the negative terminal of the multimeter; the multimeter wire clipped to the right pin (steel layer 3 electrode) must be plugged into the positive (red) terminal in the multimeter.
13. Record the reading once it has stabilized.
14. Disconnect the alligator clips from the bottom two pins.
15. Unscrew electrical box cover. Reattach "S"-shaped wire connecting three steel electrodes together. Reattach electrical box cover.
16. Repeat this process for each of 6 segments. Tidal conditions are not relevant to this measurement.
17. Time estimation: 5 min. for boat positioning, 5 min. to 10 min to perform measurements, total time of 10 to 15 min. per segment. Total time: 60-90 min (1-2 hours).

Durability segments electrical current reading of steel electrodes

1. This task may be done in conjunction with tasks 8 and 10. See task 10a for alternate instructions.

2. Set up multimeter. Multimeter must be set to record "μA". Two wires are required. Both wires must have banana plugs on one end and alligator clips on the other end.
3. Establish a boat position to enable measurements to be taken at a specific durability segment.
4. There are six pins on the electrical box that correspond to the six electrodes within. They are referenced "top left, top right, middle left, middle right, bottom left, bottom right".
5. Unscrew electrical box cover. Remove "S"-shaped wire connecting three steel electrodes together. Reattach electrical box cover.
6. Attach one alligator clip to the top right pin and one to the middle right pin. The wire clipped to the top right pin (steel layer 1 electrode) must be plugged into the "μA" terminal in the multimeter; the multimeter wire clipped to the middle right pin (steel layer 2 electrode) must be plugged into the negative (COM) terminal in the multimeter.
7. Record the reading as "S1-S2" once it has stabilized.
8. Disconnect the alligator clips from the two pins.
9. Attach one alligator clip to the middle right pin and one to the bottom right pin. The wire clipped to the middle right pin (steel layer 2 electrode) must be plugged into the "μA" terminal in the multimeter; the multimeter wire clipped to the bottom right pin (steel layer 3 electrode) must be plugged into the negative (COM) terminal in the multimeter.
10. Record the reading as "S2-S3" once it has stabilized.
11. Disconnect the alligator clips from the two pins.
12. Attach one alligator clip to the top right pin and one to the bottom right pin. The wire clipped to the top right pin (steel layer 1 electrode) must be plugged into the "μA" terminal in the multimeter; the multimeter wire clipped to the bottom right pin (steel layer 3 electrode) must be plugged into the negative (COM) terminal in the multimeter.
13. Record the reading as "S1-S3" once it has stabilized.
14. Disconnect the alligator clips from the two pins.
15. Unscrew electrical box cover. Reattach "S"-shaped wire connecting three steel electrodes together. Reattach electrical box cover.
16. Repeat this process for each of 6 segments. Tidal conditions are not relevant to this measurement.
17. Time estimation: 5 min. for boat positioning, 5 min. to 10 min to perform measurements, total time of 10 to 15 min. per segment. Total time: 60-90 min (1-2 hours).

<u>Durability segments electrical resistance reading of steel and titanium electrodes</u>

1. This task may be done in conjunction with tasks 8 and 9). See task (10a) for alternate instructions.
2. Set up multimeter. Multimeter must be set to record "Ω". Two wires are required. Both wires must have banana plugs on one end and alligator clips on the other end. Place one banana clip into the "COM" port and the other into the "V Ω" port.
3. Establish a boat position to enable measurements to be taken at a specific durability segment.
4. There are six pins on the electrical box that correspond to the six electrodes within. They are referenced "top left, top right, middle left, middle right, bottom left, bottom right".
5. Unscrew electrical box cover. Remove "S"-shaped wire connecting three steel electrodes together. Reattach electrical box cover.
6. Attach one alligator clip to each pin in the top pair. The polarity of the wires is not important.

7. Record the reading once it has stabilized as the “S1-T1” resistance.
8. Disconnect the alligator clips from the top two pins.
9. Attach one alligator clip to each pin in the middle pair. The polarity of the wires is not important.
10. Record the reading once it has stabilized as the “S2-T2” resistance.
11. Disconnect the alligator clips from the middle two pins.
12. Attach one alligator clip to each pin in the bottom pair. The polarity of the wires is not important.
13. Record the reading once it has stabilized as the “S3-T3” resistance.
14. Disconnect the alligator clips from the bottom two pins.
15. Attach one alligator clip to the top right pin and one to the middle right pin. The polarity of the wires is not important.
16. Record the reading as “S1-S2” once it has stabilized.
17. Disconnect the alligator clips from the two pins.
18. Attach one alligator clip to the middle right pin and one to the bottom right pin. The polarity of the wires is not important.
19. Record the reading as “S2-S3” once it has stabilized.
20. Disconnect the alligator clips from the two pins.
21. Attach one alligator clip to the top right pin and one to the bottom right pin. The polarity of the wires is not important.
22. Record the reading as “S1-S3” once it has stabilized.
23. Disconnect the alligator clips from the two pins.
24. Unscrew electrical box cover. Reattach “S”-shaped wire connecting three steel electrodes together. Reattach electrical box cover.
25. Repeat this process for each of 6 segments. Tidal conditions are not relevant to this measurement.
26. Time estimation: 5 min. for boat positioning, 10 min. to 15 min to perform measurements, total time of 15 to 20 min. per segment. Total time: 75-120 min (1-2 hours).

Combination task: durability segments corrosion potential between steel and titanium electrodes, electrical current reading of steel electrodes, and electrical resistance reading of steel and titanium electrodes (combined tasks 5.8, 5.9, and 5.10)

1. Part I: Resistance
2. Set up multimeter. Multimeter must be set to record “Ω”. Two wires are required. Both wires must have banana plugs on one end and alligator clips on the other end. Place one banana clip into the “COM” port and the other into the “V Ω” port.
3. Establish a boat position to enable measurements to be taken at a specific durability segment.
4. There are six pins on the electrical box that correspond to the six electrodes within. They are referenced “top left, top right, middle left, middle right, bottom left, bottom right”.
5. Unscrew electrical box cover. Remove “S”-shaped wire connecting three steel electrodes together. Reattach electrical box cover.

6. Attach one alligator clip to each pin in the top pair. The polarity of the wires is not important.
7. Record the reading once it has stabilized as the "S1-T1" resistance.
8. Disconnect the alligator clips from the top two pins.
9. Attach one alligator clip to each pin in the middle pair. The polarity of the wires is not important.
10. Record the reading once it has stabilized as the "S2-T2" resistance.
11. Disconnect the alligator clips from the middle two pins.
12. Attach one alligator clip to each pin in the bottom pair. The polarity of the wires is not important.
13. Record the reading once it has stabilized as the "S3-T3" resistance.
14. Disconnect the alligator clips from the bottom two pins.
15. Attach one alligator clip to the top right pin and one to the middle right pin. The polarity of the wires is not important.
16. Record the reading as "S1-S2" once it has stabilized.
17. Disconnect the alligator clips from the two pins.
18. Attach one alligator clip to the middle right pin and one to the bottom right pin. The polarity of the wires is not important.
19. Record the reading as "S2-S3" once it has stabilized.
20. Disconnect the alligator clips from the two pins.
21. Attach one alligator clip to the top right pin and one to the bottom right pin. The polarity of the wires is not important.
22. Record the reading as "S1-S3" once it has stabilized.
23. Disconnect the alligator clips from the two pins.
24. Part II: Current
25. Set up multimeter. Multimeter must be set to record "μA".
26. Attach one alligator clip to the top right pin and one to the middle right pin. The wire clipped to the top right pin (steel layer 1 electrode) must be plugged into the "μA" terminal in the multimeter; the multimeter wire clipped to the middle right pin (steel layer 2 electrode) must be plugged into the negative (COM) terminal in the multimeter.
27. Record the reading as "S1-S2" once it has stabilized.
28. Disconnect the alligator clips from the two pins.
29. Attach one alligator clip to the middle right pin and one to the bottom right pin. The wire clipped to the middle right pin (steel layer 2 electrode) must be plugged into the "μA" terminal in the multimeter; the multimeter wire clipped to the bottom right pin (steel layer 3 electrode) must be plugged into the negative (COM) terminal in the multimeter.
30. Record the reading as "S2-S3" once it has stabilized.
31. Disconnect the alligator clips from the two pins.
32. Attach one alligator clip to the top right pin and one to the bottom right pin. The wire clipped to the top right pin (steel layer 1 electrode) must be plugged into the "μA" terminal in the multimeter; the multimeter wire clipped to the bottom right pin (steel layer 3 electrode) must be plugged into the negative (COM) terminal in the multimeter.
33. Record the reading as "S1-S3" once it has stabilized.
34. Disconnect the alligator clips from the two pins.
35. Part III: Potential

36. Set up multimeter. Multimeter must be set to record "mV". Two wires are required. Both wires must have banana plugs on one end and alligator clips on the other end.
37. Establish a boat position to enable measurements to be taken at a specific durability segment.
38. There are six pins on the electrical box that correspond to the six electrodes within. They are referenced "top left, top right, middle left, middle right, bottom left, bottom right".
39. Attach one alligator clip to each pin in the top pair. The multimeter wire clipped to the left (titanium layer 1 electrode) must be plugged into the negative terminal of the multimeter; the multimeter wire clipped to the right pin (steel layer 1 electrode) must be plugged into the positive (red) terminal in the multimeter.
40. Record the reading once it has stabilized.
41. Disconnect the alligator clips from the top two pins.
42. Attach one alligator clip to each pin in the middle pair. The multimeter wire clipped to the left (titanium layer 1 electrode) must be plugged into the negative terminal of the multimeter; the multimeter wire clipped to the right pin (steel layer 2 electrode) must be plugged into the positive (red) terminal in the multimeter.
43. Record the reading once it has stabilized.
44. Disconnect the alligator clips from the middle two pins.
45. Attach one alligator clip to each pin in the bottom pair. The multimeter wire clipped to the left (titanium layer 3 electrode) must be plugged into the negative terminal of the multimeter; the multimeter wire clipped to the right pin (steel layer 3 electrode) must be plugged into the positive (red) terminal in the multimeter.
46. Record the reading once it has stabilized.
47. Disconnect the alligator clips from the bottom two pins.
48. Unscrew electrical box cover. Reattach "S"-shaped wire connecting three steel electrodes together. Reattach electrical box cover.
49. Repeat this process for each of 6 segments. Tidal conditions are not relevant to this measurement.
50. Time estimation: 5 min. for boat positioning, 15 min. to 20 min to perform measurements, total time of 20 to 25 min. per segment. Total time: 120-150 min (2-3 hours).

Visit Wrap-Up:

1. Place Skotchkote or equal on all exposed wires in piling electrical boxes.
2. Use only stainless steel screws when replacing electrical box covers.
3. Use duct tape to seal boxes with less than 3 functional screws.
4. Inventory and photograph all damaged, missing, or otherwise imperfect electrical boxes for future repair.

Appendix J–Key Royale Bridge Inspection Report

FLORIDA DEPARTMENT OF TRANSPORTATION
BRIDGE MANAGEMENT SYSTEM
Inspection Report with PDF attachment(s)

BRIDGE NUMBER: 136502
DISTRICT: 01 Bartow **INSPECTION DATE: 3/20/2012 FFOZ**

BY:	Centurion	STRUCTURE NAME:	KEY ROYALE BRIDGE
OWNER:	4 City/Municipal Hwy Agy	YEAR BUILT:	2007
MAINTAINED BY:	4 City/Municipal Hwy Agy	SECTION NO.:	13 000 000
STRUCTURE TYPE:	2 Reinf Concrete Cont. - 01 Slab	MP:	0
LOCATION:	0.3 MI E/O MARINA DRIVE	ROUTE:	00000
SERVICE TYPE ON:	5 Highway-pedestrian	FACILITY CARRIED:	KEY ROYALE DRIVE
SERV TYPE UND:	5 Waterway	FEATURE INTERSECTED:	BIMINI BAY

☐ FUNCTIONALLY OBSOLETE ☐ STRUCTURALLY DEFICIENT

TYPE OF INSPECTION:Regular NBI
DATE FIELD INSPECTION WAS PERFORMED: ABOVE WATER: 03/20/2012 UNDERWATER: 3/23/2012

SUFFICIENCY RATING: 88.1
HEALTH INDEX: 99.01

This report contains information relating to the physical security of a structure and depictions of the structure. This information is confidential and exempt from public inspection pursuant to sections 119.071(3)(a) and 119.071(3)(b), Florida Statutes. Only the cover page of this report may be inspected and copied.

REPORT ID: INSP005 (detailed) PRINTED: 07/06/2012

FLORIDA DEPARTMENT OF TRANSPORTATION
BRIDGE MANAGEMENT SYSTEM
Inspection Report with PDF attachment(s)

BRIDGE NUMBER: 136502
DISTRICT: 01 Bartow **INSPECTION DATE: 3/20/2012 FFOZ**

BY: Centurion	STRUCTURE NAME: KEY ROYALE BRIDGE
OWNER: 4 City/Municipal Hwy Agy	YEAR BUILT: 2007
MAINTAINED BY: 4 City/Municipal Hwy Agy	SECTION NO.: 13 000 000
STRUCTURE TYPE: 2 Reinf Concrete Cont. - 01 Slab	MP: 0
LOCATION: 0.3 MI E/O MARINA DRIVE	ROUTE: 00000
SERVICE TYPE ON: 5 Highway-pedestrian	FACILITY CARRIED: KEY ROYALE DRIVE
SERV TYPE UND: 5 Waterway	FEATURE INTERSECTED: BIMINI BAY

☐ THIS BRIDGE CONTAINS FRACTURE CRITICAL COMPONENTS
☐ THIS BRIDGE IS SCOUR CRITICAL
☐ THIS REPORT IDENTIFIES DEFICIENCIES WHICH REQUIRE PROMPT CORRECTIVE ACTION
☐ FUNCTIONALLY OBSOLETE ☐ STRUCTURALLY DEFICIENT

TYPE OF INSPECTION: Regular NBI
DATE FIELD INSPECTION WAS PERFORMED: ABOVE WATER: 03/20/2012 UNDERWATER: 3/23/2012

SMART FLAGS:

OVERALL NBI RATINGS:

DECK: 8 Very Good	CHANNEL: 8 Protected
SUPERSTRUCTURE: 8 Very Good	CULVERT: N N/A (NBI)
SUBSTRUCTURE: 8 Very Good	SUFF. RATING: 88.1
PERF RATING: Excellent	HEALTH INDEX: 99.01

FIELD PERSONNEL/ TITLE/ NUMBER	INITIALS
St. Clair, Clayton - Bridge Inspector (CBI #00374) (lead)	_____
Menendez, Marilyn - Assisant Bridge Inspector	_____
Hoogland, Keith - Bridge Inspector (CBI#00341)	_____
Elliott, Charles - Bridge Inspector/Diver (CBI #00363)	_____
Young, Ryan - Diver-Inspector	_____

REVIEWING BRIDGE INSPECTION SUPERVISOR:

Rhodes. Ritchie - Bridge Inspector (CBI #00209) _____

CONFIRMING REGISTERED PROFESSIONAL ENGINEER:

Fielding, Robert - Professional Engineer (PE #53156)
Centurion
1907 US Hwy 301 North, Suite 160C
Certificate of Authorization #26928
Tampa, FL 33619

SIGNATURE: _____

Date: _____

This report contains information relating to the physical security of a structure and depictions of the structure. This information is confidential and exempt from public inspection pursuant to sections 119.071(3)(a) and 119.071(3)(b), Florida Statutes. Only the cover page of this report may be inspected and copied.

REPORT ID: INSP005 (detailed) PRINTED: 07/06/2012

FLORIDA DEPARTMENT OF TRANSPORTATION
BRIDGE MANAGEMENT SYSTEM
Inspection Report with PDF attachment(s)

All Elements

DECKS ELEMENT CATEGORY: Decks/Slabs

ELEMENT/ ENV: 38/4 Bare Concrete Slab 6429 sf.

CONDITION STATE	DESCRIPTION	QUANTITY
1	The surface and underside of the deck have few repaired areas, there are few spalls/delaminations in the deck surface or underside and the only cracking is superficial or surface map cracking. The combined distressed area is 2% or less of the deck area.	6429
2	Repaired areas and/or spalls/delaminations and/or cracks exist in the deck surface or underside. The combined distressed area is more than 2% but less than 10% of the deck area.	0
3	Repaired areas and/or spalls/delaminations and/or cracks exist in the deck surface or underside. The combined area of distress is more than 10% but less than 25% of the total deck area.	0
4	Repaired areas and/or spalls/delaminations and/or cracks exist in the deck surface or underside. The combined area of distress is more than 25% but less than 50% of the total deck area.	0
5	Repaired areas and/or spalls/delaminations and/or cracks exist in the deck surface or underside. The combined area of distress is more than 50% of the total deck area.	0

ELEMENT INSPECTION NOTES:
CS1: There is a transverse crack up to 1/64in. on the deck top over each bent.

Both sidewalk top surfaces have up to 1/32in. transverse cracking and up to 1/64in. map cracking intermittently throughout.

Both fascias have vertical cracks up to 1/64in. wide, some with efflorescence intermittently throughout - NEW.

BRIDGE NUMBER: 136502
DISTRICT: 01 Bartow **INSPECTION DATE: 3/20/2012 FFOZ**

All Elements

DECKS ELEMENT CATEGORY: Joints

ELEMENT/ ENV: 301/4 Pourable Joint Seal 80 lf.

CONDITION STATE	DESCRIPTION	QUANTITY
1	The element shows minimal deterioration. Adhesion is sound with no signs of leakage. There are no cohesion cracks. The adjacent deck and/or header is sound.	80
2	Minor adhesion and/or cohesion failures may be present. Signs of seepage along the joint may be present. Joint may be slightly impacted with debris. Minor spalls in the deck and/or headers may be present adjacent to the joint.	0
3	Major adhesion and/or cohesion failures may be present. Signs or observance of leakage along the joint may be present. Joint may be heavily impacted with debris and/or stones. Major spalls may be present in the deck and/or header adjacent to the joint.	0

ELEMENT INSPECTION NOTES:

BRIDGE NUMBER: 136502
DISTRICT: 01 Bartow **INSPECTION DATE: 3/20/2012 FFOZ**

All Elements

DECKS ELEMENT CATEGORY: Railing

ELEMENT/ ENV: 333/4 Other Bridge Railing 299 lf.

CONDITION STATE	DESCRIPTION	QUANTITY
1	The element shows little or no deterioration. There may be minor cracking, corrosion and/or other minor deterioration having no affect on strength or serviceability.	299
2	Minor cracking, spalls, decay of timber portions or corrosion of metal may be present.	0
3	Deterioration is advanced. Corrosion, decay or loss of section is sufficient to warrant review to ascertain the impact on the serviceability or strength of the element.	0

ELEMENT INSPECTION NOTES:
NOTE: This element quantifies the jersey barriers with aluminum rail attached to the top face.

There are two navigational swing lights and 1in. diameter conduit attached to the outside faces of both concrete barriers in Span 3. Anchorage is unknown. Refer to Photo 1.

REPORT ID: INSP005 (detailed) PRINTED: 07/06/2012

All Elements

SUPERSTRUCTURE — ELEMENT CATEGORY: Movable

ELEMENT/ ENV: 580/4 Navigational Lights **1 ea.**

CONDITION STATE	DESCRIPTION	QUANTITY
1	Lights are operational, lenses are clean and not broken, there is no evidence of corrosion.	0
2	There is some evidence of corrosion, lights may be burned out, lens may be broken.	0
3	Lights are not operational.	1

BRIDGE NUMBER: 136502 **PAGE: 7 OF 16**
DISTRICT: 01 Bartow **INSPECTION DATE: 3/20/2012 FFOZ**

ELEMENT INSPECTION NOTES:
NOTE: This structure is not listed in the USCG Florida Bridges Over Navigable Waterways. No permit is required.

This element includes eight navigational lights attached to the top of the fender system and two navigational swing lights attached to the outside face of both concrete barriers in Span 3.

CS3: None of the navigational swing light anchors have lock washers. The lights are secure.

There is a broken pull box exposing the interior wiring for the southeast fender navigational lights on the west face, south end of Bent 4 cap. Refer to Photo 2. REPAIR

The support pole and the navigational swing light on the north side of the left barrier in Span 3 is missing - NEW. Refer to Photo 3. REPAIR. The navigational light housing/attachment is in place and secure. This condition was called in to owner at the time of this inspection.

All Elements

SUBSTRUCTURE ELEMENT CATEGORY: Substructure

ELEMENT/ ENV: 204/4 P/S Conc Column 20 ea.

CONDITION STATE	DESCRIPTION	QUANTITY
1	The element shows little or no deterioration. There may be discoloration, efflorescence, and/or superficial cracking but without affect on strength and/or serviceability.	20
2	Minor cracks, spalls and scaling may be present and there may be exposed reinforcing with no evidence of corrosion. There is no exposure of the prestress system.	0
3	Moderate cracks, spalls, scaling and some delaminations may be present. There may be minor exposure but no deterioration of the prestress system. Corrosion of non-prestressed reinforcement may be present but loss of section is incidental and does not significantly affect the strength and/or serviceability of either the element or the bridge.	0
4	Severe cracks, spalls, scaling, delaminations, and corrosion of non-prestressed reinforcement are prevalent. There may also be exposure and deterioration of the prestress system (manifested by loss of bond, broken strands or wire, failed anchorages, etc). There is sufficient concern to warrant a review to ascertain the impact on the strength and/or serviceability of either the element or the bridge.	0

ELEMENT INSPECTION NOTES:
NOTE: These piling have embedded SmartPile sensors. The channel piles have exposed sensors.

CS1: Pile 4-5 east face has one broken SmartPile housing. A repair will not be recommended. This was only used to record the pile drive.

FLORIDA DEPARTMENT OF TRANSPORTATION
BRIDGE MANAGEMENT SYSTEM
Inspection Report with PDF attachment(s)

All Elements

SUBSTRUCTURE ELEMENT CATEGORY: Substructure

ELEMENT/ ENV: 215/4 R/Conc Abutment 90 lf.

CONDITION STATE	DESCRIPTION	QUANTITY
1	The element shows little or no deterioration. There may be discoloration, efflorescence, and/or superficial cracking but without affect on strength and/or serviceability.	90
2	Minor cracks, spalls and scaling may be present but there is no exposed reinforcing or surface evidence of rebar corrosion.	0
3	Some delaminations, moderate cracks, spalls and/or scaling may be present and some reinforcing may be exposed. Corrosion of rebar may be present but loss of section is incidental and does not significantly affect the strength and/or serviceability of either the element or the bridge.	0
4	Deterioration is advanced. Corrosion of reinforcement and/or loss of concrete section is sufficient to warrant review to ascertain the impact on the strength and/or serviceability of either the element or the bridge.	0

ELEMENT INSPECTION NOTES:

BRIDGE NUMBER: 136502
DISTRICT: 01 Bartow **INSPECTION DATE: 3/20/2012 FFOZ**

All Elements

SUBSTRUCTURE ELEMENT CATEGORY: Substructure

ELEMENT/ ENV: 234/4 R/Conc Cap 172 lf.

CONDITION STATE	DESCRIPTION	QUANTITY
1	The element shows little or no deterioration. There may be discoloration, efflorescence, and/or superficial cracking but without affect on strength and/or serviceability.	172
2	Minor cracks, spalls and scaling may be present but there is no exposed reinforcing or surface evidence of rebar corrosion.	0
3	Some delaminations, moderate cracks, spalls and/or scaling may be present and some reinforcing may be exposed. Corrosion of rebar may be present but loss of section is incidental and does not significantly affect the strength and/or serviceability of either the element or the bridge.	0
4	Deterioration is advanced. Corrosion of reinforcement and/or loss of concrete section is sufficient to warrant review to ascertain the impact on the strength and/or serviceability of either the element or the bridge.	0

ELEMENT INSPECTION NOTES:
NOTE: There is 1in. diameter PVC conduits attached to the vertical face of both bridge rails in Span 3, Bent Caps 3 and 4, Pile 2-5 and 3-5 and the underside of Span 3 for the fender and swing navigational lights. Anchorage is unknown.

REPORT ID: INSP005 (detailed) PRINTED: 07/06/2012

BRIDGE NUMBER: 136502
DISTRICT: 01 Bartow **INSPECTION DATE: 3/20/2012 FFOZ**

All Elements

SUBSTRUCTURE ELEMENT CATEGORY: Substructure

ELEMENT/ ENV: 387/4 P/S Fender/Dolphin 80 lf.

CONDITION STATE	DESCRIPTION	QUANTITY
1	The element shows little or no deterioration. There may be discoloration, efflorescence, and/or superficial cracking but without affect on strength and/or serviceability.	80
2	Minor cracks and spalls may be present and there may be exposed reinforcing with no evidence of corrosion. There is no exposure of the prestress system.	0
3	Some delaminations and/or spalls may be present. There may be minor exposure but no deterioration of the prestress system. Corrosion of non-prestressed reinforcement may be present but loss of section is incidental and does not significantly affect the strength and/or serviceability of either the element or the bridge.	0
4	Delaminations, spalls and corrosion of non-prestressed reinforcement are prevalent. There may also be exposure and deterioration of the prestress system (manifested by loss of bond, broken strands or wire, failed anchorages, etc). There is sufficient concern to warrant a review to ascertain the impact on the strength and/or serviceability of either the element or the bridge.	0

ELEMENT INSPECTION NOTES:
NOTE: This structure is not listed in the USCG Florida Bridges Over Navigable Waterways. No permit is required.

The fender does not extend under the structure.

The following was noted by the underwater team:

NOTE: The fender system consists of four wings extending from both sides of Bents 3 and 4. Each section measures 20ft. with three 18in. concrete piling. The six piling on the south side at the bridge have concrete pieces attached to the back side that extend 3ft. below the marine growth. These pieces have electrical connections on them.

CS1: The lower connecting hardware has light to moderate surface corrosion.

All Elements

SUBSTRUCTURE ELEMENT CATEGORY: Substructure

ELEMENT/ ENV: 396/4 Other Abut Slope Pro 5901 sf.

CONDITION STATE	DESCRIPTION	QUANTITY
1	There is little or no deterioration. Surface defects only are in evidence. Random open joints may exist.	5901
2	There may be minor deterioration, random open joints, cracking and weathering. Mortar in joints may show minor deterioration.	0
3	Moderate to major deterioration and cracking. Major deterioration of joints. Minor settlement may be present.	0
4	Major deterioration, splitting, cracking or settlement of materials may be affecting the structural capacity of the element.	0

ELEMENT INSPECTION NOTES:
NOTE: This element quantifies the rock rubble slope protection at Abutments 1 and 6.

All Elements

CHANNEL ELEMENT CATEGORY: Channel

ELEMENT/ ENV: 290/4 Channel **1 ea.**

CONDITION STATE	DESCRIPTION	QUANTITY
1	The channel is in good condition, channel banks are protected or well vegetated, river control devices and embankment protection are not required or are in good condition.	1
2	Bank protection is in need of minor repairs, bank may be beginning to slump, minor stream bed movement may be evident or debris may be present.	0
3	Bank protection may be being eroded, bank protection may be undermined, river control devices may have severe damage or trees, brush or debris may be restricting the channel.	0
4	Bank protection has failed. River control devices have been destroyed. Stream bed aggradation, degradation or lateral movement has changed the channel to now threaten the bridge and/ or approach roadway.	0

ELEMENT INSPECTION NOTES:
CS1: The southeast seawall at the transition to the private sector has a spalling/delamination with exposed steel in the sheet pile 1ft. x 10in. x 4in. and a delamination in the cap 1ft. x 1ft. with an open joint up to 3in. leaking back fill. Refer to Photo 4. REPAIR

There is erosion 6ft. x 2ft. x 3ft. deep behind the southeast seawall at the transition to the private sector. Refer to Photo 5. REPAIR

All Elements

MISCELLANEOUS ELEMENT CATEGORY: Other Elements

ELEMENT/ ENV: 321/4 R/Conc Approach Slab 2 ea.

CONDITION STATE	DESCRIPTION	QUANTITY
1	The slab has not settled and shows no sign of deterioration other than superficial surface cracks.	2
2	Minor cracking, spalls may be present but they do not affect the ability of the slab to carry traffic. Settlement may be occurring which increases the traffic impact on the bridge.	0
3	Cracks may extend completely through the slab cross-section, but the slab does not act as if it is broken. Spalls may be heavy but they do not affect the structural integrity of the slab. Minor undermining may be present. Settlement may be occurring which increases the traffic impact on the bridge.	0
4	The slab is broken or rocks under traffic loads. Significant undermining may be present. Settlement is excessive and cannot be corrected without increasing the size of the slab.	0

ELEMENT INSPECTION NOTES:

All Elements

MISCELLANEOUS ELEMENT CATEGORY: Other Elements

ELEMENT/ ENV: 475/4 R/Conc Walls 241 lf.

CONDITION STATE	DESCRIPTION	QUANTITY
1	The element shows little or no deterioration. There may be discoloration, efflorescence, and/or superficial cracking but without affect on strength and/or serviceability. Random open joints may exist.	241
2	Minor cracks and spalls may be present but there is no exposed reinforcing or surface evidence of rebar corrosion. Open joints may be prevalent.	0
3	Some delaminations and/or spalls and/or minor settlement may be present and some reinforcing may be exposed. Corrosion of rebar may be present but loss of section is incidental and does not significantly affect the strength and/or serviceability of either the element or the bridge.	0
4	Advanced deterioration. Corrosion of reinforcement and/or loss of concrete section and/or settlement is sufficient to warrant review to ascertain the impact on the strength and/or serviceability of either the element or the bridge.	0

ELEMENT INSPECTION NOTES:
NOTE: This element quantifies the four cheek walls and the walls retaining the slope protection abutting the private sector at all four corners.

BRIDGE NUMBER: 136502 **PAGE: 16 OF 16**
DISTRICT: 01 Bartow **INSPECTION DATE: 3/20/2012 FFOZ**

STRUCTURE NOTES:

BRIDGE OWNER: CITY OF HOLMES BEACH

TRAFFIC RESTRICTION: This bridge is not posted. According to the load rating dated 11/27/2007, posting is not required.

Structure was inventoried west to east.

INSPECTION NOTES: FFOZ 3/20/2012

Sufficiency Rating Calculation Accepted by knicana-P at 2012-05-06 16:03:27
Sufficiency Rating Calculation Accepted by knicacs-P at 2012-03-31 16:26:20

LOAD CAPACITY EVALUATION:
The load rating dated 11/27/2007 applies to the current condition of this bridge.

NOTE: Divers inspected Bents 2 through 5 each with five 24in. concrete piling, fender system, slope protection and channel.

CORRECTIVE ACTION TAKEN:
The posting sign that was at the west approach has been removed. This structure does not require posting.

REPORT ID: INSP005 (detailed) PRINTED: 07/06/2012

BRIDGE INSPECTION REPORT

PREPARED FOR: FLORIDA DEPARTMENT OF TRANSPORTATION

BRIDGE OWNER: CITY OF HOLMES BEACH

INSPECTED BY:

CENTURION Consultant Group

BRIDGE NO.	136502	CONTENTS OF REPORT	INSPECTION DATE:	03/20/2012

Pontis Report

CIDR

Scour Elevation (Profile)

* Addendum (Element Notes & Photos/Sketches)

U/W Inspection Report

* Fracture Critical Data

* Load Rating Analysis Summary

*This section is not included in this report.

KEY ROYALE DRIVE OVER BIMINI BAY — 0.3 MI E/O MARINA DRIVE

BOLT Underwater Services, Inc
7930 62ND STREET NORTH, PINELLAS PARK, FL 33781

Routine Underwater Bridge Inspection Report
for
CENTURION CONSULTANT GROUP, INC.

NBI Structure No. (8): **136502**

Underwater Date (93): 03/23/12

Structure/Roadway Identification:

District (2):	01
County (3):	Manatee
Feature Intersected (6):	Key Royale Drive
Facility Carried (7):	Bimini Bay

Underwater Inspection Details:

Special Crew Hours:	3.0
Max. Depth:	9ft.
Type of Dive Insp.:	SCUBA
Type of Boat Used:	N/A
Water Type/Marine Growth:	Salt/Tidal – Barnacles/Oysters

Previous Inspection:

Lead Diver:	C.B.I. No.:	Inspection Date:
Hays, Stephen F.	00438	04/27/10

Inspection Personnel:

Field Personnel:	Title	C.B.I. No.:	Duty:	Signature:
Hoogland, Keith S.	C.B.I. Diver-Inspector	00341/Lead	Dive	KSH
Elliott, Charles W.	C.B.I. Diver-Inspector	00363	Tend	
Young, Ryan C.	Diver-Inspector		Dive	

PILING/COLUMNS
ELEMENT: 204 P/S CONCRETE — **20**: ea.

Condition State:	QTY:	Recommended Feasible Action:
CS-1	**20**	**Do Nothing**

NOTE: Piles 2-1, 2-2 and all deficiencies cleaned.

CHANNEL
ELEMENT: 290 — **1**: ea.

Condition State:	QTY:	Recommended Feasible Action:
CS-1	**1**	**Do Nothing**

FENDER SYSTEM
ELEMENT: 387 P/S CONCRETE — **80 lf.**

NOTE: The fender consists of four wings extending from both sides of Bents 3 and 4. Each section measures 20ft. with three 18in. concrete piling. The six piling on the south side at the bridge have concrete pieces attached to the back side that extend 3ft. below the marine growth. These pieces have electrical connections on them.

Condition State:	QTY:	Recommended Feasible Action:
CS-1	**80**	**Do Nothing**

The lower connecting hardware has light to moderate corrosion.

ABUTMENT SLOPE PROTECTION
ELEMENT: 396 OTHER: — **2800 sf.**

NOTE: This element quantifies the rock rubble slope protection at Abutments 1 and 6.

Condition State:	QTY:	Recommended Feasible Action:
CS-1	**2800**	**Do Nothing**

INSPECTION NOTES: Divers inspected Bents 2 through 5 each with five 24in. concrete piling, Fender System, Slope Protection and Channel.
STRUCTURE NOTES: Structure inventoried west to east.